Institute of **C**ondensed **M**atter and **N**anosciences (**IMCN**)

Molecular **C**hemistry, **M**aterials and **C**atalysis (**MOST**)

Design, synthesis and biological evaluation of compounds targeting metabolic pathways as potent anticancer agents

Thesis submitted in partial fulfillment of the requirements for the degree of Docteur en sciences

Junjie Lan

Louvain-la-Neuve

March 2022

Jury

Professor Sophie Demoustier (President)

Université catholique de Louvain (UCLouvain), Belgium

Prof. Raphaël Frédérick

Université catholique de Louvain (UCLouvain), Belgium

Prof. Michael Singleton

Université catholique de Louvain (UCLouvain), Belgium

Prof. Benjamin Elias

Université catholique de Louvain (UCLouvain), Belgium

Prof. Delphine Joseph

Université Paris-Saclay, France

Dr. Florence Mahuteau-Betzer

CNRS, France

Prof. Olivier Riant (Supervisor)

Université catholique de Louvain (UCLouvain), Belgium

Prof. Olivier Feron (Supervisor)

Université catholique de Louvain (UCLouvain), Belgium

Acknowledgments

The experience of studying abroad in last 4 years was unique and unforgettable in my life. I am truly grateful to the people who have been with me along the way and for their support, kindness, concern and help during the years.

I would like to express my sincere and deepest gratitude to my supervisors, Prof. Olivier Riant and Prof. Olivier Feron, for their excellent supervision, guidance, suggestions, encouragement, and enthusiasm during my PhD. I benefited a lot from their erudition, wisdom, rigor and persistence. I am particularly grateful for their advice on my research and excellent guidance on my thesis. I would like to express my special thanks to Prof. Weidong Pan for recommending me to study at UCLouvain and his continuous help, encouragement, and care during my PhD. I also would like to thank Prof. István E. Markó for accepting me as a PhD candidate at UCLouvain, with my sincere respect.

I would like to thank all jury members of my thesis committee: Prof. Sophie Demoustier, Prof. Michael Singleton, Prof. Benjamin Elias, Prof. Delphine Joseph (Université Paris-Saclay, France) and Dr. Florence Mahuteau-Betzer (CNRS, France), for being jury members of my PhD defense and taking their time to read and review this thesis. Thanks a lot for their patience, expertise, and guidance. My thanks also go to the jury members in my mid-term

confirmation, Prof. Raphaël Robiette and Dr. Cyril Corbet for their kind advice on the thesis.

I would like to express my special thanks to François Billard and Audrey Dejean for their attentive help to my experiments, life and daily affairs. I would like to express my special thanks to my colleagues: Corentin Lefebvre, Mathilde Quertenmont, Yonghua Tan, Gilles Marghem, Michela Maria Marchese, Nathalie Body, Marine Lefevre, Maria Shoueiry, Sarah Eeckhout, Simone Grosso, François Pierrard, Logan Salamone, Sebastian Strähler, Anne Sophie Léonard, Saroj Kumar Rout, Corentin Rasson, Audric Nagy, Sébastien Leloux, Mathieu Soetens, Antonin Desmecht, Ricky Payen, Michael Guillot.

I would like to thank my friends Yang, Lu, Hui, Xiao, Xi, Yiyi, Lei, Qian G, Yazhou, Xiao, Yonghua, Wenzhang, Bin, Qian Q, Yinghui, Cuilian, Mingxi, and many of my friends who I didn't list in Belgium and China. Thanks for their company, support and encouragement. They have helped me gain so much joy and happiness in more than four years.

Finally, I would like to express my most sincere gratitude to my families who care and support me. I am especially grateful to my parents and my grandparents, who always support me unconditionally, offer me the best education. Whenever I encounter frustration, this warm harbor is always there for me.

I would like to thank the China Scholarship Council (CSC) for their financial support, WBI for their co-funding, UCLouvain for their three months co-funding and Prof. Olivier Riant for his help.

Authors' Contributions

The author wrote and revised the thesis, carried out the experiments, recorded and analyzed the data, and interpreted the results that are presented in this thesis.

Professor Olivier Riant and Professor Olivier Feron, supervised, discussed and revised the thesis, proposed the ideas and provided financial support.

Other partners are partly involved in the thesis:

In chapter I, the biological experiments were conducted by Dr. Octavia Cadassou (UCLouvain).

In chapter II, the pHLIP part and the conjugate physicochemical property assay were recorded by Marine Deskeuvre and biological experiments were conducted by Emeline Dierge (UCLouvain).

The mass spectroscopic experiments were conducted by Mr. Raoul Rozenberg and Mr. Laurent Collard (UCLouvain). The LC-MS experiments were conducted by Dr. Esra Yildiz (UCLouvain).

Some HPLC experiments were conducted by Mr. Laurent Collard (UCLouvain).

Abbreviation

^{1}H-^{1}H COSY	^{1}H-^{1}H Correlated spectroscopy
2-HG	2-hydroxyglutaric acid
Å	Ångström
Ac	Acetyl
ACC	acetyl-CoA carboxylase
ACLY	ATP-citrate lyase
AML	Acute myeloid leukemia
AMPK	5' adenosine monophosphate-activated protein kinase
APCI	Atmospheric-pressure chemical ionization
Asc	Ascorbate
ATP	Adenosine triphosphate
AzoR	Azo reductases
BINAP	2,2′-bis(diphenylphosphino)-1,1′-binaphthyl
Bn	Benzyl
Boc	*t*-butoxycarbonyle
Bp	Boiling point
Bu	Butyl
CACT	Carnitine acylcarnitine translocase
CAI	Carboxyamidotriazole
CAIX	Carbonic anhydrase
Cat	Catalyst / catalytical
CD	Circular dichroism
COX	Cyclooxygenase
CPPs	Cell penetraing peptides
CPT1	Carnitine palmitoyltransferase I

CSC	Cancer stem cell
CT26	Murine colorectal carcinoma cell line
CYP	Cytochrome P450
Cyt-C	Cytochrome C
DAG	Diglyceride
DBU	1,8-Diazabicyclo[5.4.0]undec-7-ene
DCE	1,2-Dichloroethane
DCM	Dichloromethane
DDS	Drug delivery systems
DEAD	Diethyl azadicarboxylate
DGAT	Diacylglycerol acyltransferases
DIAD	Diisopropyl azodicarboxylate
DIBAL-H	Diisobutylaluminium hydride
DIPEA	*N*,*N*-Diisopropylethylamine
DMAP	4-dimethylaminopyridine
DMF	Dimethylformamide
DMSO	Dimethyl sulfoxide
DPPA	Diphenyl phosphoryazide
EDCI	1-Ethyl-3-(3-dimethylaminopropyl)carbodiimide salt
EDTA	Ethylene diamine tetra acetic
eq.	Equivalents
ESI	Electrospray ionization
Et	Ethyl
ETC	Electron transport chain
FA	Fatty acid
FADH2	Flavin adenine dinucleotide
FAO	Fatty acid oxidation
FAS	Fatty acid synthesis
FMN	Flavin mononucleotide
GBM	Glioblastoma
GDH	Glucose dehydrogenase
GLUT1	Glucose transporter 1
GSH	Glutathione

GT	Triglyceride
HAPs	Hypoxia activated prodrugs
HER2	Receptor tyrosine-protein kinase erbB-2
HIF-1α	Hypoxia-inducible factor 1
HK	Hexokinase
HMBC	Heteronuclear multiple bond coherence
HMQC	Heteronuclear multiple quantum coherence
HOBt	Hydroxybenzotriazole
HPLC	High-performance liquid chromatography
HRMS	High Resolution Mass Spectrometry
IDH	Isocitrate dehydrogenases
iNOS	Inducible nitric oxide synthase
***i*Pr**	Iso-propyl
LDA	Lithium diisopropylamide
LDH A/B	Lactate dehydrogenase A/B
LG	Leaving group
LiHMDS	Lithium bis(trimethylsilyl)amide
***m*-CPBA**	*meta*-Chloroperoxybenzoic acid
MCT	Monocarboxylate transporter
MDR	Multidrug resistance
Me	Methyl
MeCN	Acetonitrile
MGATs	Monoacyglycerol acyltransferases
MPC 1/2	Mitochondrial pyruvate carrier 1/2
MS	Molecular sieves
mTOR	Mammalian target of rapamycin
MW	Molecular Weight
n.d.	Not determined
NADH	Reduced nicotinamide adenine dinucleotide
NADPH	Reduced nicotinamide adenine dinucleotide phosphate
NBS	N-Bromosuccinimide
NHE	Normal hydrogen electrode
NMP	N-methyl-2-pyrrolidone

NMR	Nuclear magnetic resonance
Nu	Nucleophile
O.N.	Overnight
OCR	Oxygen consumption rate
OTf	Triflate
OXPHOS	Oxidative phosphorylation
PBS	Phosphate buffer solution
PFK	Phosphofructokinase
Ph	Phenyl
pHLIP	pH low insertion peptide
PK	Pyruvate kinase
POPC	Phosphatidylcholine
ppm	Parts per million
PTSA	*para*-Toluenesulfonic acid
PUFAs	Polyunsaturated fatty acids
Py	Pyridyl
r.t.	Room Temperature
ROS	Reactive oxygen species
SiHa	Uterus carcinoma cells
TAG	Triglyceride
TBAF	Tetrabutylammonium fluoride
TBDPS	*tert*-Butyldiphenylsilyl
TBS	*t*-butyl-dimethylsilyl
TBSOTf	Tert-butyldimethylsilyl trifluoromethanesulfonate
TCA cycle	Triacrboxylic acid cycle
TEA	Triethylamine
TFA	Trifluoroacetic acid
THF	Tetrahydrofuran
TIC	Tumor initiating cell
TLC	Thin layer chromatography
TME	Tumor Microenvironment
TMS	Trimethylsilyl
Tol	Toluene

Trp	Tryptophan
U	Enzymatic unit
UV	Ultra-violet
α-KG	α-ketoglutarate
δ	NMR shift
λ_{em}	Emission wavelength
λ_{ex}	Excitation wavelength

Contents

Abstract

Tumors reprogram metabolic pathways to support the bioenergetic, biosynthetic, and redox needs of malignant cells. There is an increasing recognition that the tumor microenvironment drives many of these alterations in the metabolic phenotype of tumor cells, thereby paving the way for the development of specific anticancer metabolism-targeting compounds. In this thesis, we designed and synthesized such inhibitors, including some in the form of prodrugs to be activated in response to the acidic or hypoxic tumor microenvironment.

In the first chapter, we designed and synthesized carboxyamidotriazole analogues to inhibit mitochondrial complex I of the oxidative phosphorylation (OXPHOS) pathway. *In vitro* cellular studies were conducted to evaluate their pharmacological activities, and preliminary structure-activity relationship analysis was obtained. Promising complex I inhibitors were further validated in 3D tumor spheroids.

In the second chapter, we designed a pH-sensitive drug delivery system by conjugating a pH-dependent peptide with lipid metabolism-targeting drugs including Etomoxir (CPT1 inhibitor) and T863 (DGAT1 inhibitor), targeting mitochondrial fatty acylCoA uptake and the last step of triglyceride synthesis, respectively. Efficacy was evaluated using liposome models and *in vitro* cellular assays.

In the third chapter, we designed and synthesized hypoxia-activated prodrugs (HAPs). Among the drugs that were modified to be specifically activated under low pO2 upon reduction of a nitro moiety (Part A), we considered COX inhibitor diclofenac repurposed recently as an inhibitor of lactate transport through MCT4 and a traditional antitumor drug tetrandrine. In Part B, a novel HAP model containing a triazene group was designed and synthesized. Mechanisms of triazene probe release by chemical reduction were studied to further gain insights on the potential use of these HAP in tumors.

Altogether, the data obtained in this thesis support the feasibility of targeting peculiarities of the tumor metabolism while sparing healthy tissues.

General Introduction

Malignant tumors represent a serious threat to human health worldwide. Cancer actually shares with cardiovascular diseases the first place on the podium of the largest killer in industrialized countries. Governments and scientists from various countries have invested a lot of human and material resources in tumor prevention and treatment research in the last decades. Despite many progresses, challenges persist for a large variety of cancers to prevent their occurrence and when diagnosed, to offer cancer patients valuable therapeutic options.

Current treatments for malignant tumors are mainly based on chemotherapy, radiotherapy, immunotherapy and surgery. Anti-cancer chemotherapy, which has undergone more than half a century of daily use in the clinic, is still an important part of cancer patients' overall treatment. Conventional chemotherapy is however like a carpet bombing with unclear targets, knocking out both tumor cells and normal cells in the body. It is only in 2001 that the small molecule imatinib mesylate was approved as the first targeted therapy to treat cancer. This tyrosine kinase inhibitor was compared to a precision guided cruise missile capable of hitting the exact cancer site. Today anticancer precision medicine consists of small drugs or antibodies targeting oncoproteins mainly resulting from mutations, overexpression or chromosomal rearrangement. The specificity of the target accounts for the

preferred activity of these drugs toward the tumor while sparing healthy tissues and thus reducing the extent of adverse effects. However, the occurrence of resistance usually limiting the effects of targeted therapies to a prolongation of patient survival of 6 to 12 months, together with the high costs of these treatments, have led scientists working in the field of medical oncology to explore other avenues. In recent years, more and more studies have confirmed that metabolic reprogramming of tumor cells could represent one such target that could still offer a reasonable level of selectivity for innovative drugs and be shared by different tumor types, thereby extending the market and thus reducing the costs for social security systems.

1. Cancer metabolism in a nutshell

Tumor metabolic reprogramming is an important feature in the process of tumor development. Firstly, tumor cells need energy to maintain intracellular functions and reductive equivalents to resist oxidative stress. Secondly, the rapid proliferation of tumor cells requires the synthesis of relevant intermediates that make up the cellular components. Tumor cells therefore require a variety of nutrients and metabolic routes to fulfil their bioenergetic and biosynthetic needs (**Figure 1-1**).

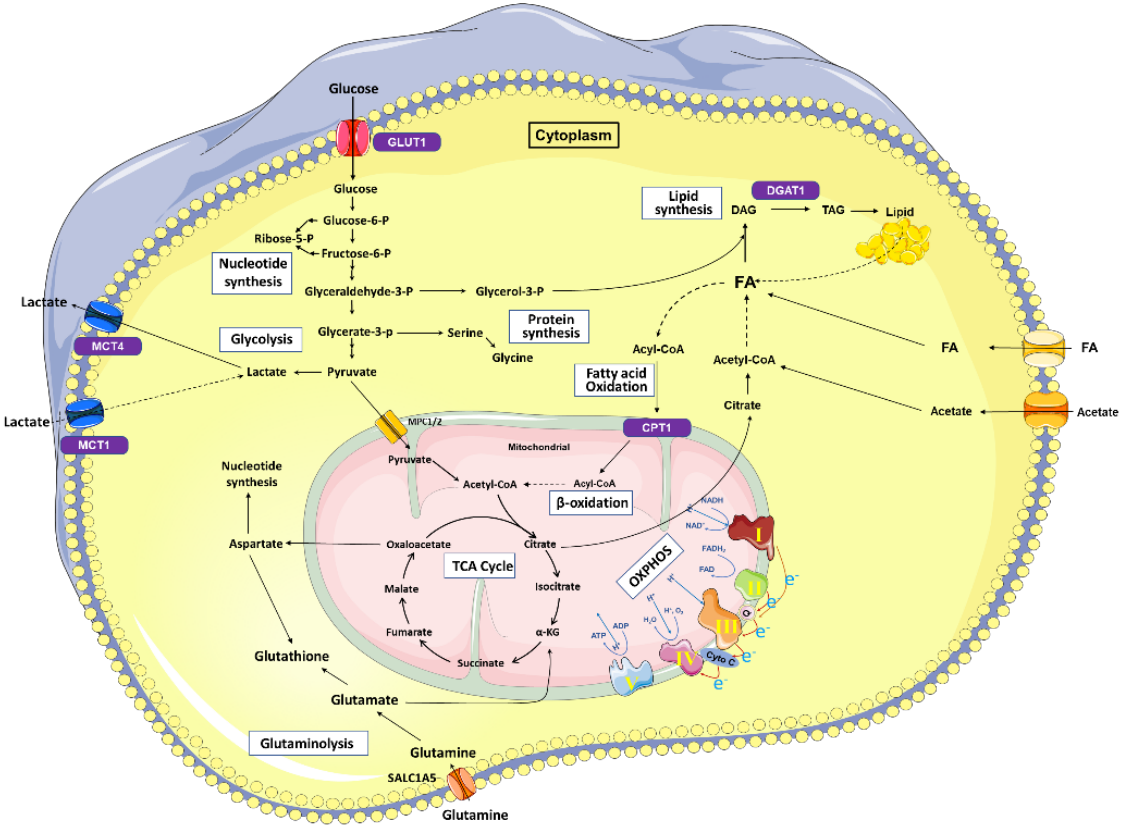

Figure 1-1 Nutrient metabolism in tumor cells[1-3]

The rearrangement of the metabolic network in tumor cells to support survival and proliferation is the consequences of mutations (i.e., oncogene-driven metabolic preferences) but is also directly dependent on the local microenvironment. Indeed, besides cancer cells, solid tumors consist of a variety of resident host cells (e.g., fibroblasts, endothelial cells, immune cells, adipocytes) embedded in an extracellular matrix and forming a complex ecosystem called the tumor microenvironment (TME). Among the major determinants of the TME are hypoxia and acidosis since uncontrolled proliferation of cancer cells leads to a situation where tumor perfusion rapidly becomes insufficient to provide O_2 (and allow mitochondria to work properly) and remove waste products such as protons (H^+), respectively. Despite angiogenesis (i.e., formation of new blood vessels), some areas within tumors will always be deficient in O_2 and acidic. Hypoxia will dictate the preferential use of glycolysis as metabolic route able to generate ATP regardless of O_2-consuming mitochondrial activity (see Heading 2 below) while oxygenated cancer cells will be more dependent on OXPHOS (see Heading 3 below) and the subset of acidic cancer cells will reprogram their bioenergetic preferences toward lipid metabolism (see Heading 4 below).

2. Glycolysis and lactate transporters

2.1. Glycolysis

Besides ATP, anaerobic glycolysis also generates biosynthetic intermediates, antioxidant molecules and nucleotide precursors through side metabolic branches such as the serine pathway and the pentose phosphate pathway. The

latter specificities are actually thought to be more critical than ATP production. In agreement with this observation, it is worth to note that cancer cells may use glycolysis (i.e., glucose to lactate) in the presence of O_2. This observation initially reported by Otto Warburg was proposed to be due to the mitochondrial dysfunction[4, 5] (**Figure 1-2**).

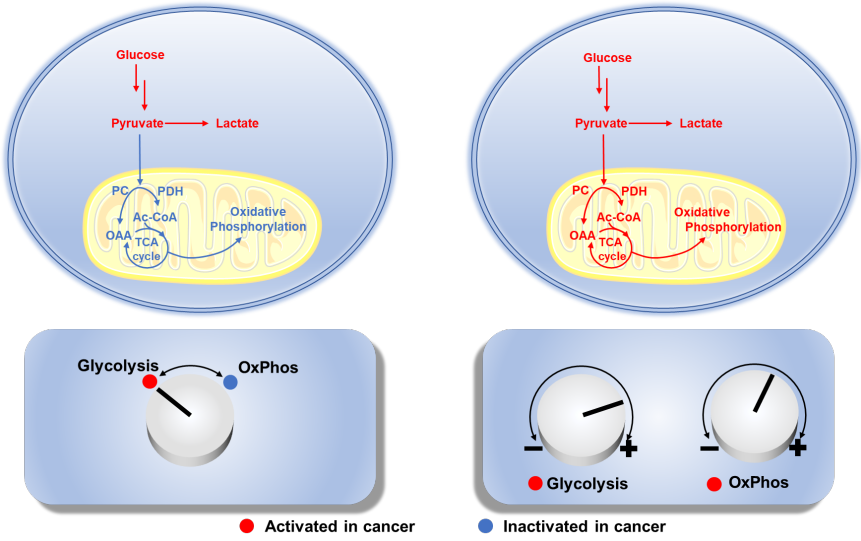

Figure 1-2 The relationship between glycolysis and oxidative phosphorylation in tumor cells [3]

Today, it is known that besides a few exceptions, mitochondria are fully functional in cancer cells and that aerobic glycolysis actually co-exists with oxidative metabolic routes involving the TCA cycle and oxidative phosphorylation (OXPHOS)[6]. In the last decade, stable isotope tracers (e.g. ^{13}C) were used to track the fate of biosynthetic fuels by analyzing downstream isotopic enrichment of labeled nutrients. Main conclusions are that (i) glucose metabolism includes not only glycolysis (with lactate as end-product), but also

mitochondrial respiration (**Figure 1-2**), (ii) mitochondrial respiration requires acetyl-CoA, which is generated not only from blood glucose but also from acetate, lactate reconversion into pyruvate (see below) and the breakdown of lipids and amino acids (**Figure 1-1**).

As mentioned above for glycolysis, besides energy, the same substrate can generate biosynthetic intermediates through the mitochondrial route. For instance, citrate derived from the mitochondrial TCA cycle serves as the starting point for the synthesis of fatty acids while aspartate, another TCA cycle may be used for purine and pyrimidine synthesis upon transamination. Another key example of how metabolism may participate in the production of critical cell component is glutamine that is needed to generate glutathione, a central actor in the cancer cell handling of excess production of reactive oxygen species (ROS).

Glycolysis has two main stages. The first one requires energy and is considered as a preparatory step. It starts with the capture of glucose in the cell through dedicated transporters of the GLUT family and continues with the "reorganization" of the 6 carbon skeleton to be efficiently cleaved. The second stage is the energy release phase, which produces ATP and NADH, and ends up with pyruvate (**Figure 1-3**). The glucose to pyruvate metabolism pathway consists of nine reactions catalyzed by several enzymes, three of them being rate-limiting, namely hexokinase (HK), phosphofructokinase (PFK), and pyruvate kinase (PK) (**Figure 1-3**).

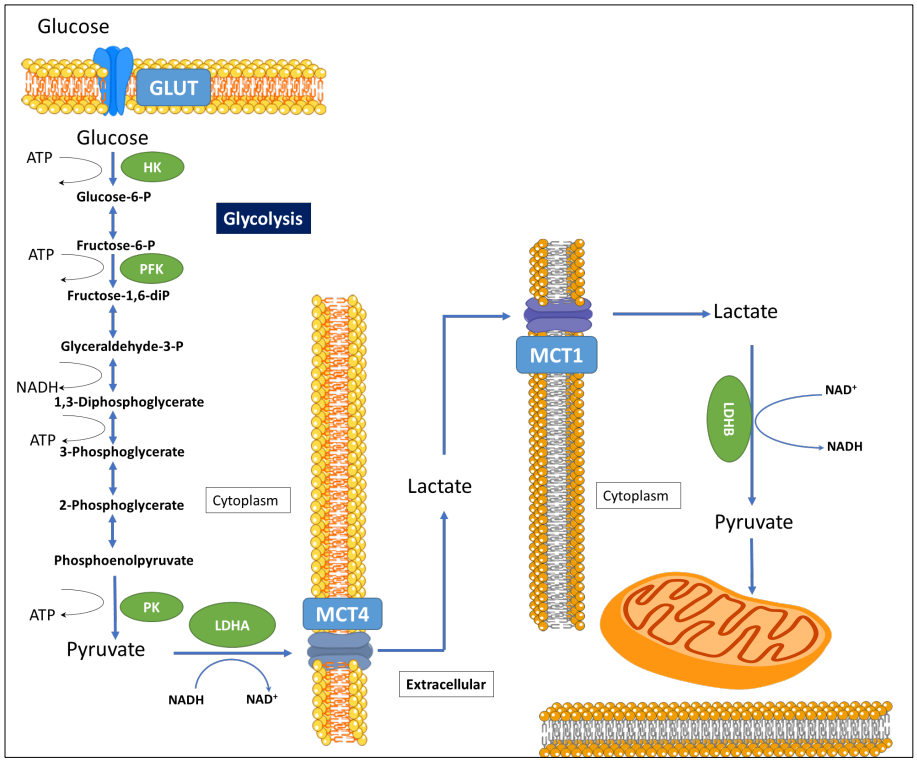

Figure 1-3 Glycolytic pathways and lactate metabolism in tumor cells[2, 3]

Pyruvate is the end-product of glycolysis and may either be transported into the mitochondria or be reduced into lactate. As a significant source of acetylCoA, pyruvate can be considered as a major TCA cycle fuel. However, in the absence of O_2, pyruvate will be reduced into lactate thereby regenerating NAD^+ to sustain the glycolytic turnover. This second option is favored by hypoxia in the response to the production of the transcription factor HIF-1α. The latter will promote the expression of lactate dehydrogenase A (LDHA) and monocarboxylate transporter protein 4 (MCT4) that support the conversion of pyruvate into lactate and importantly allows to export lactate

out of the cells (together with one proton). HIF-1α also stimulates the expression of GLUT transporters and several glycolytic enzymes. Preventing lactate efflux may thus have detrimental effects on cancer cell growth as well as blocking glycolysis when it represents the only route to generate ATP in the absence of O_2. Therefore, GLUT1, LDHA, MCT4 or one of the three rate-limiting enzymes in glycolysis have been considered as potential targets to develop anticancer strategies.

2.2. Monocarboxylate transporters

MCTs are encoded by the solute carrier 16 (SLC16) family of genes. The MCT family comprises 14 members in total, among which MCT1-4 play major roles in mammals. Glycosylated chaperone proteins are required to maintain the proper location and function of MCTs, including CD147 for MCT1/3/4 and gp70 for MCT2[7-9].

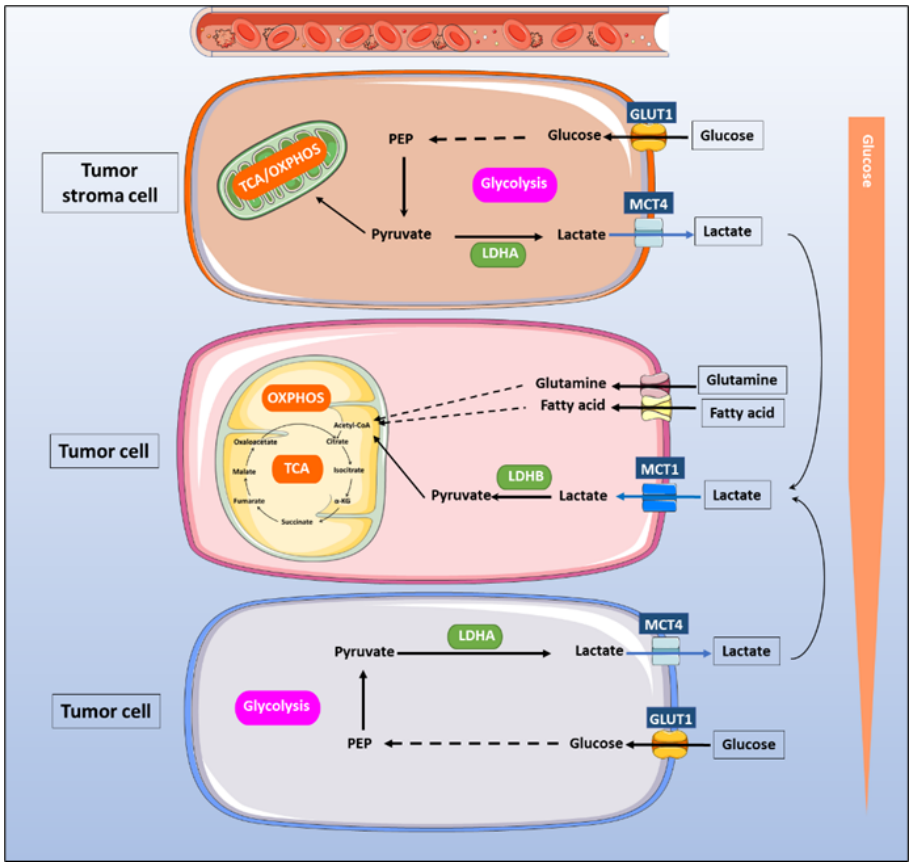

Figure 1-4 Tumor microenvironment and tumors metabolic heterogeneity[2, 10]

MCT1-4 expression varies in normal human tissues and organs depending on their function. MCT1 is widely expressed in the intestinal epithelium, cardiomyocytes, renal tubular cells and hepatocytes[11]. MCT2 expression is restricted to specific tissues, *e.g.* liver parenchyma, the proximal convoluted tubule of the kidney and neurons[12]. MCT3 is only expressed in the retinal pigment and choroid plexus epithelia of the eye[13]. MCT4 is also widely distributed in human tissues *e.g.*, white skeletal muscle fibres, astrocytes, immune cells, chondrocytes, and hypoxic cells[11] (**Table 1-1**).

Expression of MCT1 and MCT4 has been extensively studied in tumors from various origins, *e.g.*, brain cancer, breast cancer, cervix cancer, gastric cancer, lung cancer, lymphoma, oral squamous cell carcinoma, esophageal carcinoma, squamous cell skin cancer, soft tissue sarcoma[11].

Among various functions in cancer cells, MCTs control lactate exchange. MCT4 is usually considered as the main transporter to support the efflux of lactate while MCT1 can support both the export and import of lactate. In more oxidative tumor cells, lactate can indeed be captured by MCT1 and upon oxidation into pyruvate be used to support the TCA cycle and associated OXPHOS (**Figure 1-4**). Differences in Km account for these distinct capacities (**Table 1-1**). MCT4 has indeed the lowest affinity for lactate (Km= 22-28 mM) making it more prone to be activated by high concentrations as reached intracellularly in response to high glycolytic turnover[14]. In contrast, MCT1 has a higher affinity for lactate (Km=3.5 mM) and is therefore more likely to promote the import of lactate (generated by the most hypoxic cancer cells). (**Table 1-1**).

Table 1-1 The main characteristics of MCT1-4 and the related inhibitors

	chaperone	Expression in normal tissues	Expression in cancers	$K_{m\ lactate}$	Inhibitor		Refs
MCT1 (SLC 16A1)	CD147	wide range of expressions	Brian cancer, breast cancer, cervix cancer, gastric cancer, lung cancer, lymphoma, squamous cell skin cancer, soft tissue sarcoma	3.5-10 nM	7ACC2 BAY-8002 AZD3965 ARC155858 Phloretin α-cyano-4-hydroxycinnamate (CHC) lonidamine		14-19
MCT2 (SLC 16A7)	gp70	liver, kidney, testis, CNS		~0.75 nM			9, 20
MCT3 (SLC 16A8)	CD147	retina, choroid plexus		~6 nM		regulates the pH of the subretinal space	13, 20
MCT4 (SLC 16A3)	CD147	white skeletal muscle fibers, astrocytes, immune cells, chondrocytes, and hypoxic cells	breast cancer, gastric cancer, oral squamous cell carcinoma, esophagal carcinoma, lung cancer, prostate cancer, squamous cell skin cancer, soft tissue sarcoma	22-28 nM	Syrosingopine Diclofenac Bindarit AZD0095 AZ93		14, 21-26

CNS, central nervous system

Km value is a measure of the affinity of a transporter and its ligand, with a high Km value relating to low affinity

These distinct affinities of MCT1 and MCT4 for lactate actually account for a dual expression of both MCTs in tumors. Indeed, production of lactate in hypoxic cancer cells requires MCT4 to export it in the extracellular medium where after diffusion, it will be taken in charge by MCT1 expressed at the surface of more oxidative cancer cells [27] (**Figure 1-4**). Thus, MCT1 and MCT4 play vital roles in the lactate shuttle, regulating lactate influx and efflux, and thereby supporting a metabolic symbiosis between hypoxic and more oxygenated cancer cells. Glucose not consumed by oxidative cancer cells is somehow spared to reach hypoxic cancer cells in a larger extent. Of note, studies have also reported the capacity of oxidative tumor cells to force nearby stromal cells to adopt aerobic glycolysis, thereby also generating a source of lactate that can be recycled taking advantage of the MCT1/4-mediated lactate shuttling (**Figure 1-4**)[26]. Interestingly, while pharmacological inhibitors of MCT4 may directly kill hypoxic cancer cells, MCT1 may also lead to the killing of these cells by preventing lactate shuttling. The latter bystander effect may be particularly attractive considering the easier access of drug to MCT1-expressing cancer cells located at the vicinity of blood vessels.

2.2.1. MCT1 transporter

Lactate is a source of energy for oxidative cancer cells which fuels TCA cycle upon prior conversion into pyruvate. MCT1 expression in these oxidative cancer cells mainly accounts for this lactate uptake, in particular in cancer[18]. Most notably, some compounds exhibiting MCT1 inhibitory activity have

been used for research. Among them, quercetin, lonidamine, α-cyano-4-hydroxycinnamate (CHC) are usually reported as mixed inhibitors of MCT1 and MCT4, but with low affinity and poor selectivity [20, 24, 28]. Recently, more potent MCT1 inhibitors, exemplified by AR-C155858, AZD3965 and BAY-8002 have been reported with IC_{50} or K_i at nM range[15, 16, 19]. ARC155858 and AZD3965 are pyrrole pyrimidine derivatives, which exert slowly reversible inhibition of MCT1 and show no effect on MCT4[15]. Our lab also reported the capacity of 7ACC2 to inhibit lactate uptake but not lactate efflux, and eventually documented that such effect resulted from a specific inhibition of the mitochondrial pyruvate carrier MPC1 (i.e., the inhibition of lactate uptake resulting from the cytosolic accumulation of lactate and pyruvate, the latter not being able to enter mitochondria). BAY-8002 has a 5-fold selectivity to MCT1 over MCT2 and no inhibition on MCT4[16] (**Figure 1-5**).

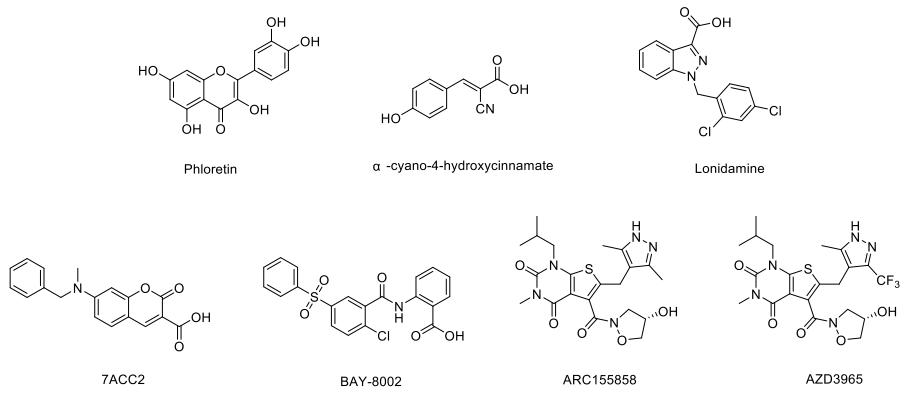

Figure 1-5 MCT1 inhibitor

To further understand the action mechanism of MCT1 inhibitors, high-resolution structures of MCTs are required. Recently, the cryo-EM structure

of the wild type (WT) human MCT1/Basigin-2 (MCT1/CD147) complex (bound to some compounds) were reported at 3.0-3.3 Å in the inward-open and outward-open two states[17]. In the structure of the MCT1, a cavity is wrapped by two subunits, and the amino acid residues make the cavity positively charged to attract molecules such as lactate (**Figure 1-6** A, B and C). The structure of human MCT1 suggests that the amino acid residues lysine 38 (Lys38), aspartate 309 (Asp309), and arginine 313 (Arg313) are of particular relevance for transporter activity and substrate binding[17]. The operation mechanism of MCT1 is through rigid-body rotation of the two domains that exposes the central substrate binding sites alternatingly to either side of the membrane (**Figure 1-6** D)[17].

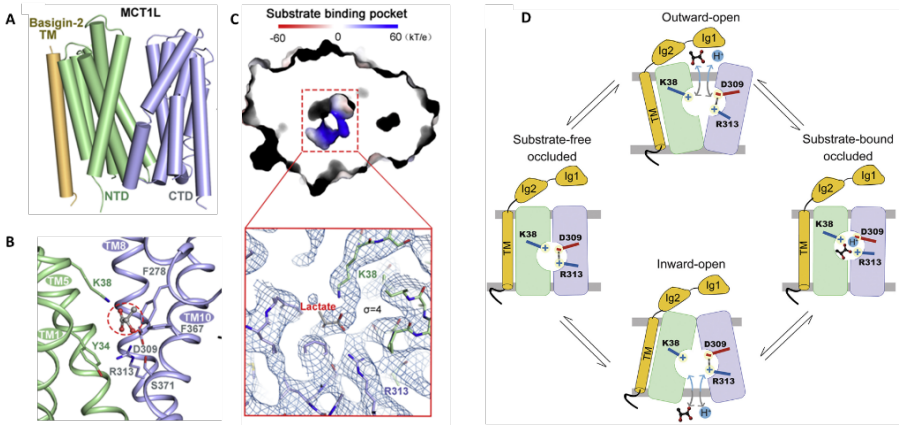

Figure 1-6 Structure of MCT1/Basigin-2 complex in the presence of L-lactate[17](A) Overall structure of outward-open MCT1; (B) Substrate-binding pocket of MCT1, (C) A central substrate binding pocket is enclosed by the two domains and opens to the extracellular side in MCT1; (D) The working mechanism of MCTs

Studies have shown that different inhibitors target different conformations of MCT1. For instance, AZD3965 and BAY-8002 compounds occupy the central

substrate binding site, locking the MCT1 protein into an outward-open conformation (**Figure 1-7**)[17].

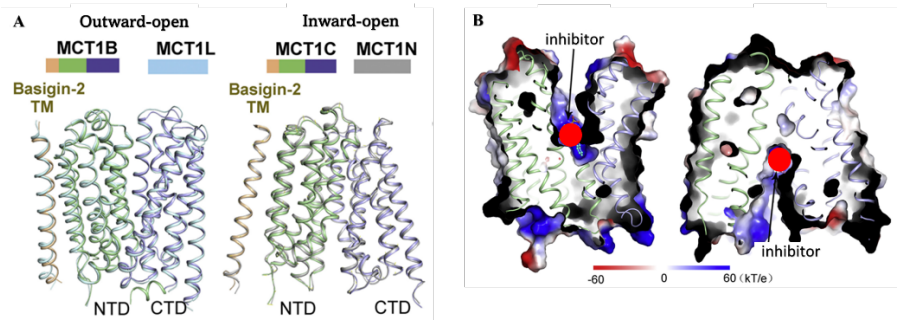

Figure 1-7 Distinct conformational states of MCT1[17] (A) Trapping MCT1 in the outward- and inward-open states under different inhibitor conditions; (B) Central binding site for the different inhibitors, show the electrostatic surface representations

2.2.2. MCT4 transporter

MCT4 is a lactate low-affinity transporter, mainly involved in lactate/H^+ efflux from glycolytic cancer cells and thus acting as a main pH regulator. MCT4 inhibition results in the intracellular accumulation of lactate and H^+, leading to the cytosolic acidification. As intracellular maintenance pH near 7.4 is essential for cell survival, knockdown of MCT4 rapidly leads to the inhibition of glycolysis, and to cell death (if cancer cells cannot switch to another metabolic route)[21]. Lactate accumulation in tumors was also reported to lead to an immunosuppressive milieu making MCT4 as a potential target to re-establish an environment more prone to the activity of anticancer immune cells[29]. Also, in cancer cells with mutations in mitochondrial NADH dehydrogenase gene mutations, MCT4 is suggested to be a biomarker and a therapeutic target to eradicate these cells and combat their associated

enhanced metastatic potential [23].

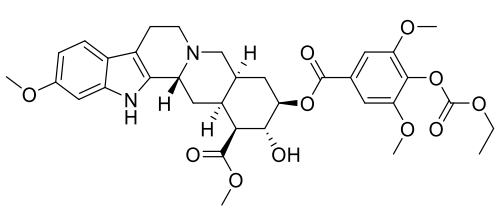

Syrosingopine

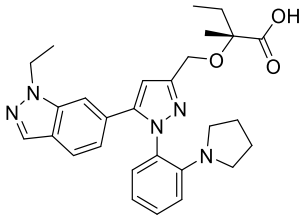

Benzopyrazole derivatives

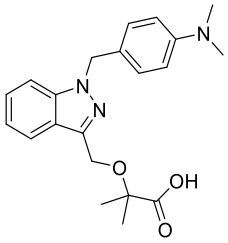

Bindarit derivative

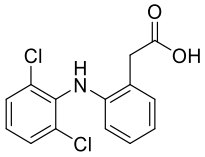

Diclofenac

Figure 1-8 MCT4 inhibitor

High-resolution structural information about MCT4 has not been reported yet, limiting the rational design of inhibitors. More conventional screening campaigns have however identified compounds endowed with MCT4 inhibitory activity. The antihypertensive drug syrosingopine has been reported to effectively block the lactate transporter including through MCT4 and exert additive effects with OXPHOS inhibitors (OXPHOSi)[30]. Parnell *et al*. reported a series of pyrazoles and indazoles, showing that acetic acid structures containing chiral centres have

inhibitory activities[22]. Mereddy *et al*. also reported in a patent, a class of indazoles (Bindarit derivatives) acting as MCT4 inhibitors[31]. Recently,

AstraZeneca reported that AZD0095 as a highly selective and potent MCT4 inhibitor (nM activity) and >1000-fold selectivity over MCT1[32]. Diclofenac is a nonsteroidal anti-inflammatory drug (NSAID) belonging to the aryl-acetic acid group that is widely used as an anti-inflammatory drug and was recently repurposed as a MCT4 inhibitor. Diclofenac was actually found to have a significantly higher affinity for MCTs than lactate in tumor cells, with non-competitive inhibition and a 10-fold higher potency of MCT4 than MCT1, while retaining the antitumor activity of effector T cells[21, 25, 33] (**Figure 1-8**). Diclofenac was used to develop a hypoxia-activated prodrug that inhibited MCT4 activity in tumor cells in the current thesis (see *Chapter III*).

3. Mitochondrial TCA cycle and OXPHOS

A primary function of mitochondria is ATP production, hence the nickname of "powerhouse of the cell". Mitochondria have however many other functions besides energy production, including biosynthetic metabolism, cell signaling, production of reactive oxygen species (ROS) and regulation of programmed cell death, all these tasks allowing cells to adapt to their environment[34]. For a long time, the significance of mitochondria in cancer metabolism has been overlooked. It was thought that cancer cells underwent aerobic glycolysis due to damaged mitochondria, a phenomenon referred to as the "Warburg effect". With the development of ^{13}C isotope tracing and other techniques, it became however clear that cancer cells may also undergo aerobic glycolysis exploiting intact mitochondria. As in healthy cells, mitochondrial respiration is required to generate energy and support biosynthesis, both being critical for the

survival and proliferation of tumor cells[35, 36]. These observations led medicinal chemists to consider the possibility to develop inhibitors of mitochondrial OXPHOS and biomass production. This is all the more relevant that many studies have demonstrated that in various tumor types, drug resistant cancer cells, metastatic cancer cells, circulating cancer cells, cancer stem cells (CSC) and tumor initiating cells (TIC) are dependent on mitochondrial respiration[6].

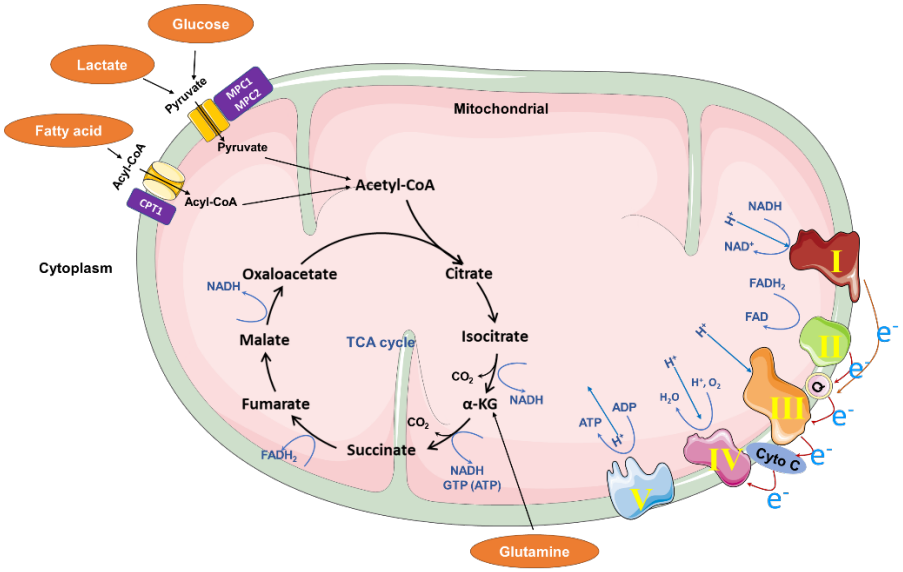

Figure 1-9 The TCA cycle and OXPHOS in mitochondrial metabolism[37]

3.1. TCA cycle

In normal cells, aerobic respiration is divided into three stages, in which the TCA cycle and OXPHOS are mainly completed in mitochondria. The TCA cycle is an enzyme catalyzed series of oxidation-reduction reactions that result in the transfer of hydride ions from carbon atoms to NAD^+ and FAD^+, leading to the formation of NADH, $FADH_2$ and CO_2 molecules together with the regeneration of intermediates to complete the cycle. NADH and $FADH_2$ store

energy as electron motive forces shunted to the electron transport chain, where they interact with complexes I and II respectively to produce ATP (**Figure 1-9**).

The unrestricted replicative potential of cancer cells requires the constant production of large amounts of biological material including nucleotides for DNA and fatty acids for biological membranes. Normal mitochondrial metabolic processes cannot meet this increased demand. It is the existence of multiple anaplerotic/cataplerotic circuitries centred on mitochondria that allow to ensure the metabolic needs of cancer cells. An important intermediate in the TCA cycle and a critical junction between catabolism and anabolism is citrate which is generated by the condensation of acetyl-CoA and oxaloacetate (**Figure 1-10**). Citrate represents one such node of flexibility in cancer cell metabolism. Citrate, in addition to being part of the TCA cycle, can be shunted into the cytoplasm and transformed into acetyl-CoA that is required for fatty acids and cholesterol production. At the same time, acetyl-CoA also directly participats to the acetylation of proteins and thus alterations in various signaling pathways and enzyme activities. In addition, citrate can also maintain NADPH levels, which essential for maintaining redox homeostasis in tumor cells. To compensate the loss of citrate and more generally of TCA cycle intermediates involves in various biosynthetic routes, cancer cells usually capture very large amounts of glutamine (**Figure 1-10**). Once inside the mitochondria, glutamine is converted to the TCA cycle intermediate α-ketoglutarate (α-KG), which promotes oxaloacetate regeneration and the

continued production of citrate as a precursor to downstream TCA cycle intermediates.

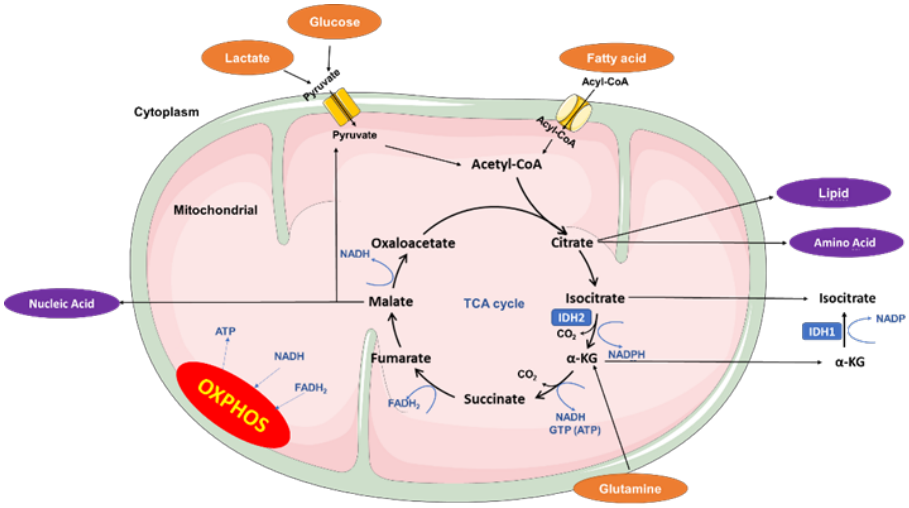

Figure 1-10 Mitochondria are the center of catabolism and biosynthesis[38]

Other major actors of the rewiring of mitochondrial metabolism in cancer cells is represented by the different isoforms of isocitrate dehydrogenases (IDH). IDH1 and IDH2 are involved in the interconversion of α-ketoglutarate (α-KG) and isocitrate (**Figure 1-10**). IDHs are the most common metabolic mutations in human cancers, occurring mainly at different arginine residues in the enzyme active site (R132 in IDH1 and R172 in IDH2), leading to the production of 2-hydroxyglutaric acid (2-HG) instead of α-KG and promoting tumorigenesis. IDHs mutations also enhance the dependence of cancer cells on OXPHOS[39]. It has been reported that AGI-6780 inhibits mutant IDH2 in AML with good efficacy, normalizing 2-HG levels, and blocking cell proliferation and differentiation[40].

3.2. Oxidative phosphorylation (OXPHOS)

Complex I and complex II are the OXPHOS entry points for the reductive equivalents produced by the TCA cycle. The electron motive force stored as NADH and $FADH_2$ is *in fine* converted into a proton motive force by the enzymes of the electron transport chain. The electrons liberated by the oxidation are transferred to ubiquinol and carried to complex III. Complex III functions to move electrons across the inner membrane, where they are transferred to cytochrome C (Cyt-C). Electrons are then carried to Complex IV, where they are used to reduce oxygen to water (**Figure 1-11**). Each complex uses the energy of electron motion to pump H^+ into the intermembrane space. The final step in aerobic respiration uses the proton gradient (resulting from H^+ accumulation in the intermembrane area) to power the phosphorylation of ADP to ATP by complex IV (**Figure 1-11**). As described earlier, aerobic respiration is slower than glycolysis, but produces more ATP, with a theroretical yield of 38 ATP molecules per glucose molecule.

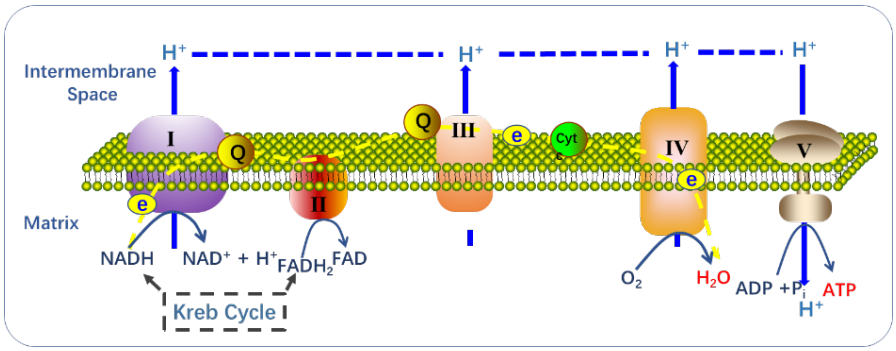

Figure 1-11 Electron transport chain (OXPHOS)[41, 42]

Given the critical role of OXPHOS in some cancer cells, there is a growing interest in developing inhibitors of OXPHOS. Still, whether the degree of mitochondrial dysregulation in tumors is sufficient to exert anticancer effects without affecting normal cells remains challenging. The search for a safe therapeutic window therefore justifies that compounds targeting one or several steps in the mitochondrial respiratory complexes are being explored. In this section, inhibitors of OXPHOS Complex I-V are briefly described (**Table 1-2**, **Figure 1-12, Figure 1-14**).

Many of OXPHOS inhibitors listed in **Table 1-2** were identified based on phenotypic assays, and their molecular targets were identified at later stage. The rational design of OXPHOS inhibitors remains challenging, given that the binding modes of current inhibitors to ETC complexes are still unknown. Their large size and flexibility, especially for complex I, make difficult the generation of high-quality cocrystal structures. The diverse structures of OXPHOS inhibitors also suggest that the mechanism of action is likely to be very diverse.

Table 1-2 Developing OXPHOS inhibitors for tumor therapy

Target	Name	Advantages	Disadvantages	Stage	Cancers	Refs
I	Metformin	targeting complex I leads to modification of the AMPK/mTOR axis, reduces cancer cell growth reduced, ATP production and energy crisis	The compound is strongly basic, with high HBL value, difficult to diffuse passively, and large dose	CT phase 1,2,3	solid tumor, prostate cancer, oral caner	43, 44, 45, 46
	Phenformin	Enhanced lipophilicity	high risk of lactic acidosis	CT phase 1	Melanoma	47
	MitoMet	Increased lipophilicity, enhanced cellular uptake, increased activity and reduced effective concentration compared to metformin		EXP		48
	HL156A	bioavailability was ~72.9%		CT phase 1	oral cancer, glioblastoma	49
	Papaverine	inhibition of complex I through binding to the rotenone-binding site	phosphodiesterase 10A (PDE10A) inhibitor	EXP		50
	SMV-32			EXP		50
	Rotenone	tool compounds for complex I inhibition		EXP		
	Fenofibrate		PPARα agonist	EXP		51
	Deguelin	selectively kills PTEN-null prostate cancer cells		EXP	prostate cancer	52
	AG311	induced cell membrane permeabilization and rapid mitochondrial membrane changes	Weak inhibition	EXP	breast cancer	53
	Mubritinib			EXP	breast cancer	54

	Me-344			Early CT phase 1	breast cancer	[55]
	BAY87-2243	reduced OCR and cellular ATP levels	serious drug side effects	CT phase 1 cancel	melanoma cells	[56]
	CAI			CT phase 1	solid tumor, gliomas	[41, 57]
	IACS-010759	favorable therapeutic window, well-tolerated		CT phase 1	AML, solid tumor	[58 59]
II	Lonidamin		inhibit MPC and MCT	CT phase 2		
	α-TOS	targets Qp or Qd sites in complex II.		EXP		[60]
	Atovaquone		Lack of selectivity	CT phase 1	nonsmall cell lung cancer	[61]
III	Antimycin A	binding to the Qi site of complex III		EXP	cervical cancer	[62]
	Neoantimycin F			EXP		[63]
IV	ADDA 5			EXP		[64]
	Oligomycin A	naturally occurring OXPHOS inhibitor that specifically targets complex V	Effective in recurrent tumors	EXP		[65]
V	Bedaquiline	stem-like cancer cells		EXP		[66]
	Apoptolidin			EXP		[67]
	Gboxin		Short half-life	EXP	glioblastoma	[68]
I, II, IV	VLX-600	cytotoxicity through iron chelation		EXP	colon carcinoma	[69]

CT: clinical trial, EXP: experiment, HLB: hydrophile-lipophile balance, MPC: mitochondrial pyruvate carrier, MCT: monocarboxylate transporter, PPARα: Peroxisome proliferator-activated receptor α

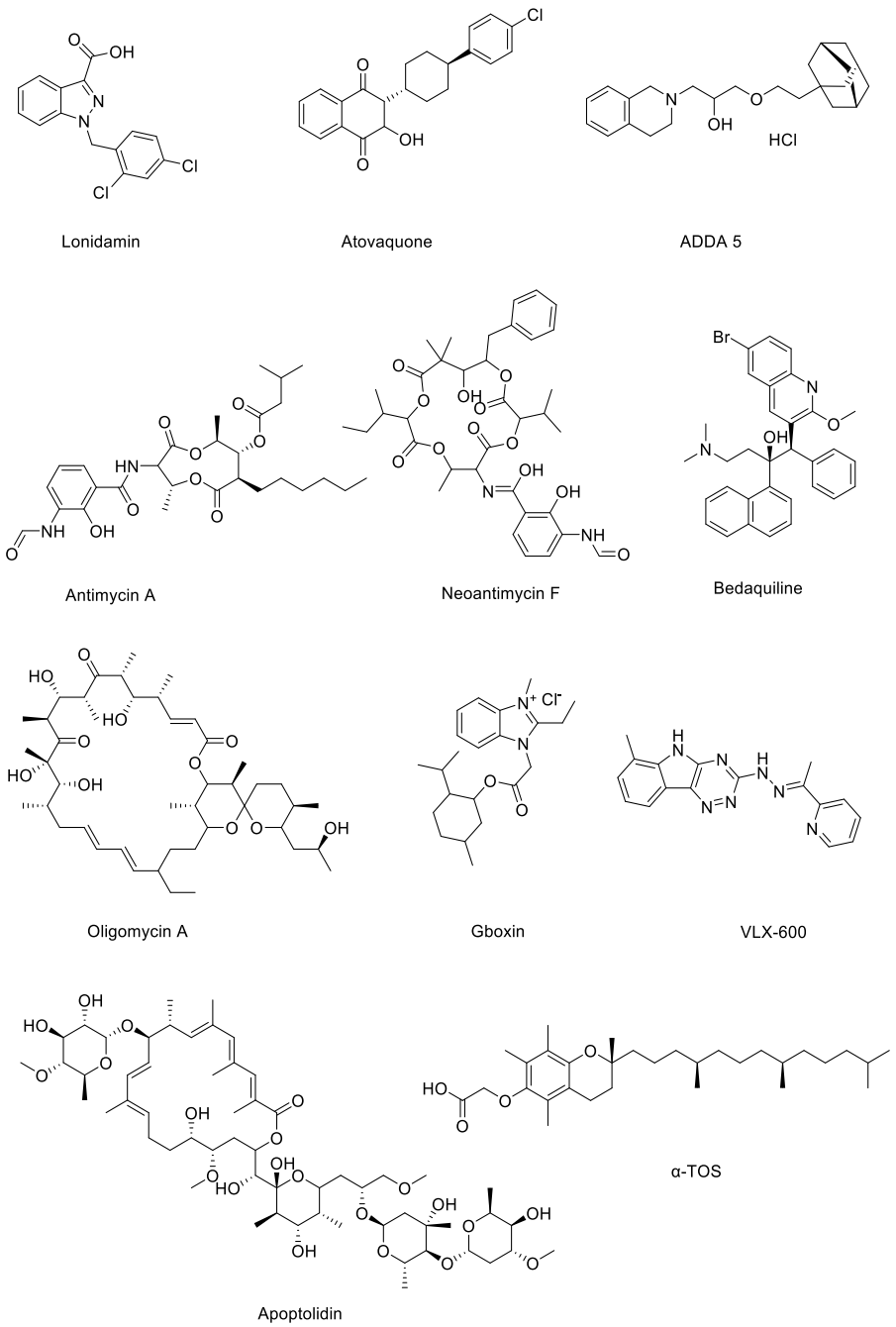

Figure 1-12 Complex II/III/IV/V inhibitor

3.3. Mitochondrial Complex I and its inhibitors

Complex I is an L-shaped assembly (**Figure 1-13**) composed of a hydrophilic peripheral arm, which contains the redox centres involved in electron transfer, and a membrane arm having the proton translocating machinery[70]. NADH is oxidized to NAD^+ at the hydrophilic arm by flavin mononucleotide (FMN), releasing a pair of electrons. Eight Fe-S clusters then transfer the electrons to ubiquinone at its binding pocket located at the interface of the 49 kDa and PSST subunits. Ubiquinone is thought to slide from the entrance of the ND1 subunit to its binding pocket[71]. Complex I is the main point of entry of electrons in the ETC and a critical target to inhibit OXPHOS in cancer cells (**Figure 1-13**). Indeed, enhanced activity of Complex I was associated with tumor formation, acquisition of resistance and promotion of metastasis (*via* increases ROS formation). Mechanistically, Complex I stimulation supports HIF1α and mammalian target of rapamycin (mTOR) signalling.

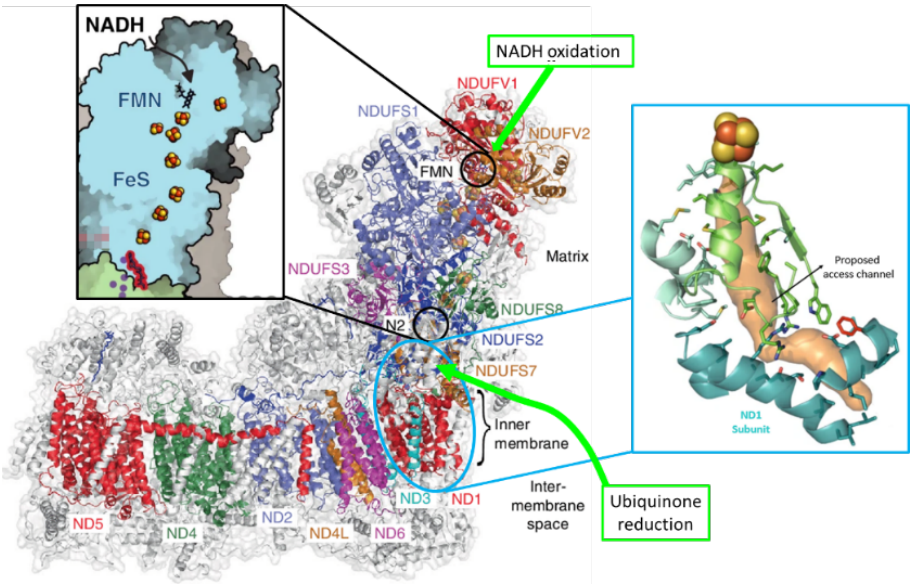

Figure 1-13 The core subunits and ubiquinone-binding site of mammalian complex I[71]

The activity of Complex I is mainly inhibited by preventing the transfer of electrons from NADH to Fe-S clusters and then to ubiquinone. Most complex I inhibitors bind in the ubiquinone pocket. Some inhibitors were also reported

to establish their binding to the entry point of the ubiquinone channel in the ND1 subunit. Mutagenesis and photoaffinity labeling experiments suggest that some inhibitors (e.g. Rotenone, AG311，Papaverine)[72] bind to different sites in this pocket[73]; IACS-010759 and Mubritinib, in particular was found to bind to residues at the entrance of the ubiquinone channel in the ND1 subunit. Metformin is thought instead to act on the Complex 1 ND3 subunit amphipathic region to produce non-competitive inhibition. For other Complex I inhibitors, the exact mechanism is unknown as for carboxamide triazole (CAI)[57]. Of note, CAI could act similarly to IACS-010759, since both compounds share a amidine-like nitrogen substitution pattern[41] (**Figure 1-14**).

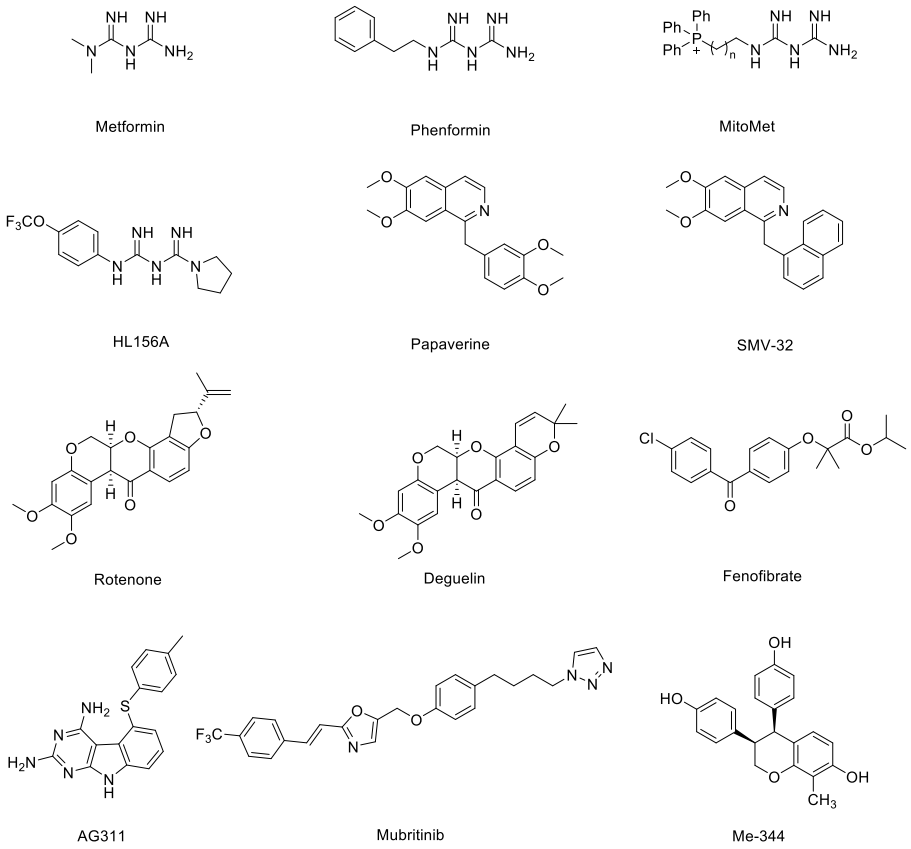

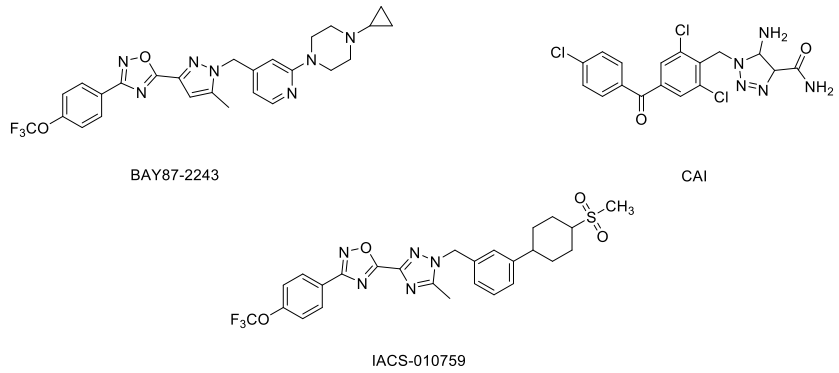

Figure 1-14 Complex I inhibitor

This structural proximities amaong CAI, BAY87-2243 and IACS-010759 were actually exploited in the current thesis to develop new complex I inhibitors (see Results section - Chapter I).

4. Fatty acid metabolism

Lipids describe many types of molecules, including fatty acids, phospholipids, triglycerides, sphingolipids, cholesterol and cholesteryl esters. They have multiple roles in cells. Firstly, lipids constitute the basic structure of plasma and organelle membranes. Secondly, they may act as second messengers to support signal transduction within the cell. Thirdly, they represent energy sources that cells can capture from the extracellular medium or mobilize from internal stores such as lipid droplets. In tumors, all these functions support growth and accounts for a profound reprogramming of lipid metabolism in cancer cells where lipid uptake, storage, oxidation and synthesis can even be observed concomitantly[74]. Targeting circuits that govern lipid metabolism (i.e., fatty acid synthesis (FAS) and fatty acid oxidation (FAO)) has therefore progressively emerged as an attractive strategy to block tumor growth. The chapter II of the Results section of in this thesis is focused on modalities aiming to alter lipid homeostasis in cancer cells.

4.1. Fatty acid synthesis and storage

In tumor cells, FA can be synthesized *de novo* from available nutrients. Glucose is the primary substrate for lipid synthesis. It is converted to pyruvate through glycolysis and enters mitochondria to form citrate. Glutamine can also be used to generate citrate from the TCA cycle. Citrate is then released into the cytoplasm to serve as a precursor for the synthesis of fatty acids. Acetyl-CoA is generated from citrate by the enzyme ATP-citrate lyase (ACLY) and then converted to malonyl-CoA by acetyl-CoA carboxylase (ACC). Acetyl-CoA and malonyl-CoA are then coupled to the acyl-carrier protein domain of the multifunctional enzyme fatty acid synthase (FAS) (**Figure 1-15**). Repeated condensations of acetyl groups generate a basic 16-carbon saturated FA: palmitic acid. Palmitic acid is further elongated and desaturated to generate the diverse spectrum of saturated and unsaturated FA in the tumor cell. Neo-synthesized FA is either used to generate specialized lipids such as phospholipids or stored into lipid droplets. The latter is thought to reduce the risk of lipotoxicity and to offer a internal reserve of FA that may be released upon the action of specific lipases[75, 76]. Monoacyglycerol acyltransferases (MGATs) and diacylglycerol acyltransferases (DGATs) catalyze two consecutive steps of enzyme reactions in the synthesis of triglycerides. Both MGAT and DGAT respresent potential targets to interfere with FA metabolism in cancer cells (**Figure 1-15**).

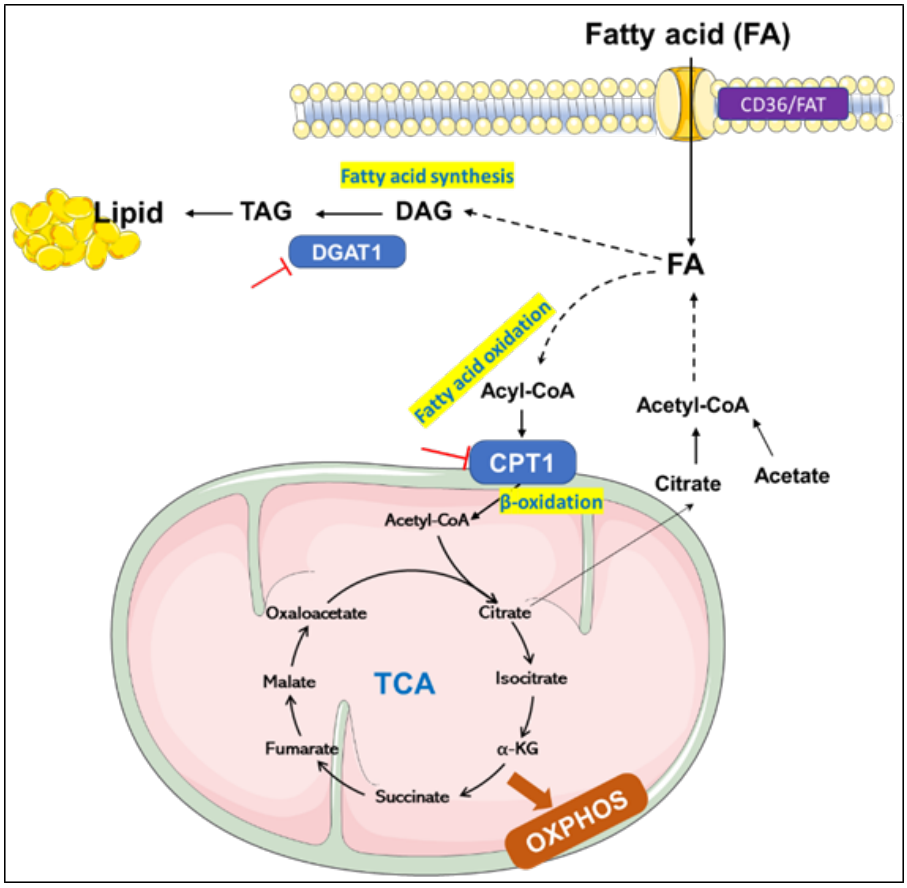

Figure 1-15 Fatty acid anabolism and catabolism[75, 76]

4.1.1. DGAT1

There are two DGAT isoenzymes, DGAT1 and DGAT2, which belong to different gene families. DGAT1 is mainly found in the gut, testes, liver and adipose tissue while DGAT2 is found primarily in the liver and adipose tissue[77]. Studies show that DGAT1 gene transcript levels are very high in most types of tumors, including ovarian, prostate, breast, liver, lung, head and neck, melanoma, pancreatic, sarcoma, cervical, thymoma, thyroid and kidney cancers[78]. Increased expression of DGAT1 in tumor cells regulates FA homeostasis. Indeed, preferred conversion of FAs to TG can prevent excessive *β*-oxidation in mitochondria and consecutive oxidative stress. Inhibition of DGAT1 by preventing lipid droplet formation therefore leads to accumulation

of FA in the cytoplasm and consecutive ROS formation and also affects membrane composition[78].

To facilitate the development of pharmacological inhibitors of DGAT1, it is vital to understand the 3D structure of this enzyme and its catalytic mechanism. Cryo-EM studies recently revealed that DGAT1 exists as a dimer (**Figure 1-16**). Each DGAT1 subunit has nine transmembrane helices, with -*N* and -*C* termini located on the cytosolic and luminal sides of the endoplasmic reticulum membrane. The transmembrane helices of DGAT1 form a large central cavity in the membrane, and the catalytic histidine residue (His415) is buried in the central cavity, providing a possibility for DGAT1 to catalyze the synthesis of TG from DAG and acyl-CoA. Acyl-CoA binds at the entrance of the cytoplasm and slips into the DGAT1 cavity *via* hydrophobic interaction. Glycerol diesters slip into the reaction chamber from hydrophobic channels within the lipid bilayer, and amino acid residues E416 and His415 in DGAT1 facilitate the acyl transfer reaction by activating the hydroxyl group on DAG[79, 80](**Figure 1-16**).

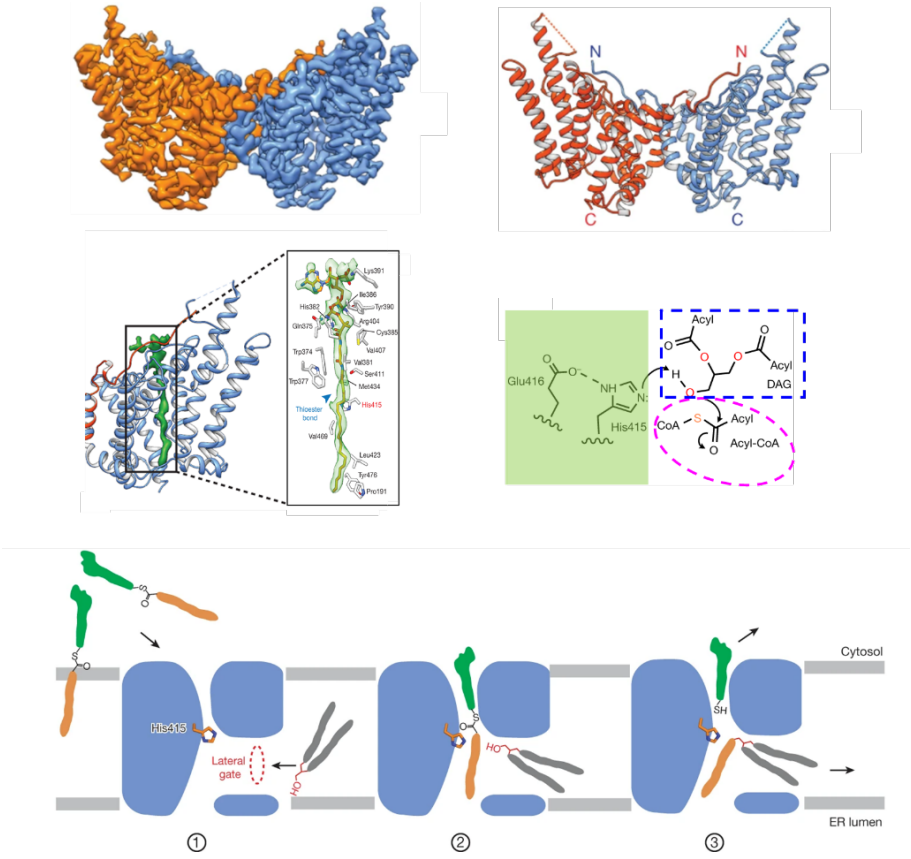

Figure 1-16 The human DGAT1 bound to an intact oleoyl-CoA molecule and hypothetical model for DGAT1-catalysed triacylglycerol formation [79, 80]

4.1.2. GDAT1 inhibitors

The initial DAGT1 inhibitors were mainly developed for the treatment of metabolic disorders, including obesity, insulin resistance syndrome, type II diabetes, dyslipidemia, hepatic steatosis, metabolic syndrome, and coronary heart disease[81-83]. Today most DGAT1 inhibitors are composed of three main parts: heterocyclic-phenyl cyclohexane-acetic acid (**Figure 1-17**). The earlier reported DGAT1 inhibitor T863 has been tested *in vitro* and *in vivo*. It delays fat absorption, reduces body weight, improves insulin sensitivity and corrects hepatic steatosis, among other effects[84]. Studies on T863 identified the carboxylic acid group as an essential pharmacodynamic group. In subsequent

studies, potency, safety, and selectivity were improved to generated derivatives for clinical evaluation. The structures of main DGAT1 inhibitor compounds that have entered clinical studies are presented below (**Figure 1-17**).

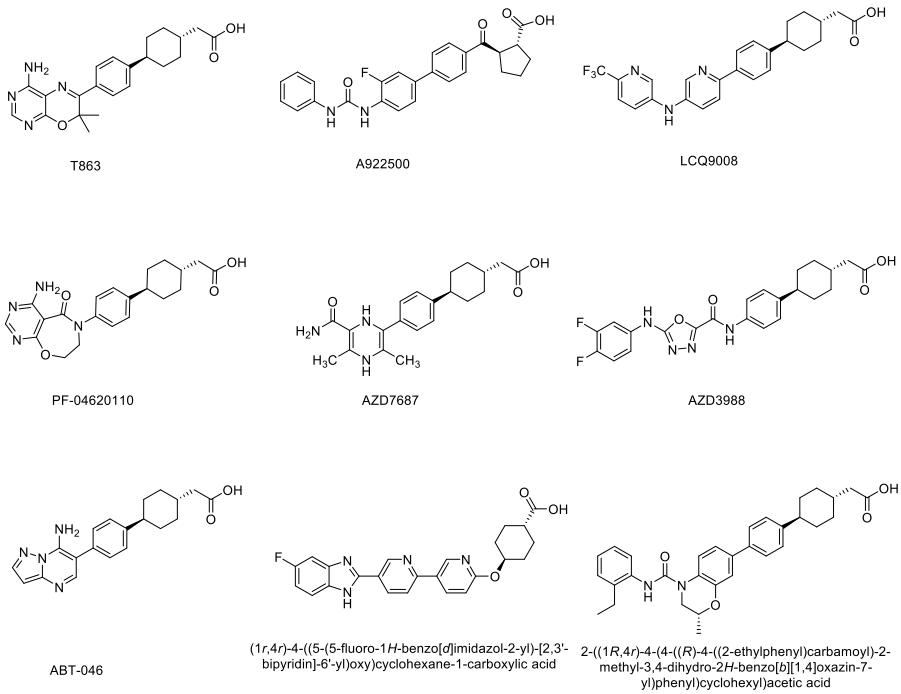

Figure 1-17 DGAT1 inhibitors

DGAT1 is also a potential anticancer target. Compound A922500 has for instance led to encouraging results to treat glioblastoma (GBM). A922500 was shown to disrupt lipid homeostasis through excessive FA shuttling into the mitochondria, resulting in severe oxidative stress and GBM cell killing[85]. As for OXPHOSi, to make DGAT1 inhibitor a real hope for cancer patients, more investigation is needed to optimize the therapeutic window. This thesis will describe the design and synthesis of a DGAT1 inhibitor delivery system that may potentially increase tumor selectivity (see Chapter II).

4.2. Fatty Acid Oxidation

Fatty acid oxidation (FAO) is an essential source of NADH, $FADH_2$, NADPH and ATP, and therefore represents a critical metabolic route for many cancer cells, in particular for those located in the hypoxic and acidic microenvironment of solid tumors[10].

FAO is a multi-step catabolic process. Fatty acids can be obtained through direct exogenous uptake from the surrounding microenvironment or intracellular lipid droplets. In the cytoplasm, long-chain fatty acids are converted to acetyl-CoA by the action of the fatty acyl CoA synthetase (ACSL1). Acyl-CoA is shuttled into the mitochondria *via* the CPT system, consisting of CPT1, CPT2, and carnitine acylcarnitine translocase (CACT) (see below for further details). The next step in the *β*-oxidation of fatty acids in the mitochondria is a repeated cleaving cycle catalyzed by a sequence of four enzymes, acyl-CoA dehydrogenase (ACADs), hydroxyacyl-CoA dehydrogenase (HADH), enoyl-CoA hydratase (ECHD) and 3-ketoacyl-CoA thiolase (3-KAT). Resulting acetyl-CoA enters the TCA cycle thereby supporting OXPHOS[86, 87, 76].

Numerous studies have shown that inhibition of FAO promotes apoptosis in leukaemia, myeloma, glioma and glioblastoma as well as prostate, breast and ovarian cancers[88-91]. The key rate-limiting enzyme of FAO is carnitine palmitoyltransferase 1 (CPT1), making this enzyme an attractive target to develop FAO inhibitors.

4.2.1. CPT1

The CPT system consists of CPT1, CPT2, and carnitine acylcarnitine translocase (CACT). In the outer mitochondrial membrane, acyl-CoA is converted to acyl-carnitine by the action of CPT1. Carnitine/acylcarnitine translocase (CACT) located at the inner mitochondrial membrane shuttles

acyl-carnitine into the mitochondrial matrix. Carnitine palmitoyltransferase 2 (CPT2) on the matrix side of the inner mitochondrial membrane reconverts acyl-carnitine to acyl-CoA, ready for β-oxidation and energy substrate generation[92] (**Figure 1-18**).

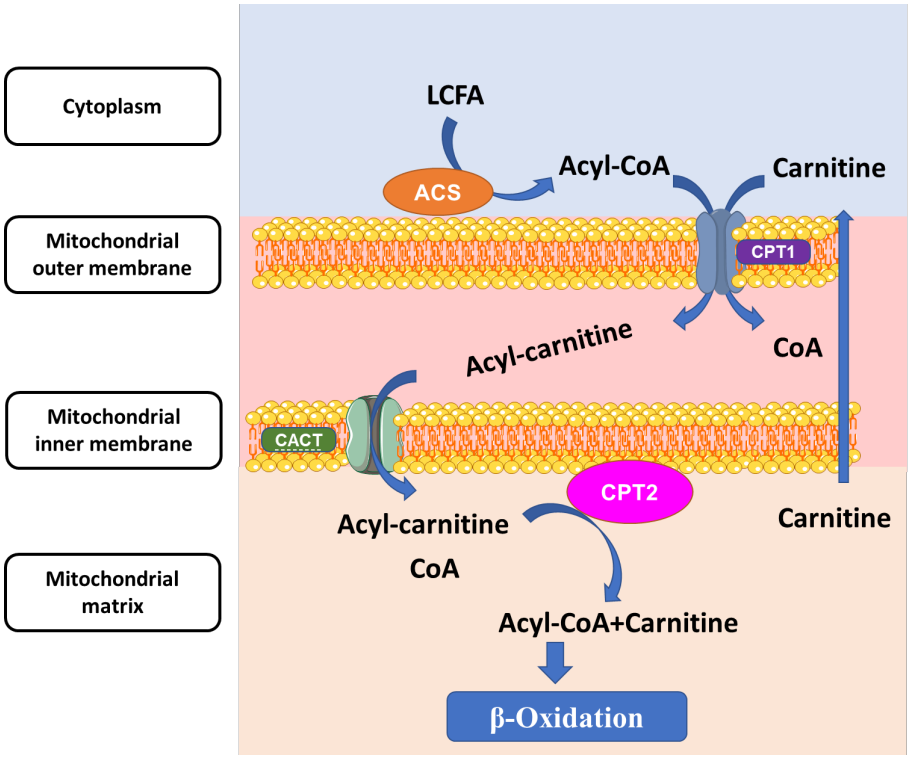

Figure 1-18 The mitochondria carnitine system[92]

CPT1 has been found to be upregulated in prostate, breast, ovarian, leukemia, glioblastoma, lymphoma, gastric, and colon cancers[93-95]. The abnormal expression of CPT1 is reflected by a high extent of FAO and more generally a global rewiring of tumor metabolism with consecutive alterations in aerobic glycolysis and fatty acid synthesis[90].

The crystal structure of human CPT1 protein has not been obtained so far. However, the crystal structure of rat CPT2 with homologous similarity has

revealed that three binding sites (CoA, acyl and carnitine) form a "Y" shaped binding pocket in the transport protein, in which the amino acid residue His372 is essential to catalyze the formation of acyl-carnitine[96, 97]. These data together with the homology between CPT1 and CPT2 have contributed to the development of CPT1 inhibitors (**Figure 1-19**).

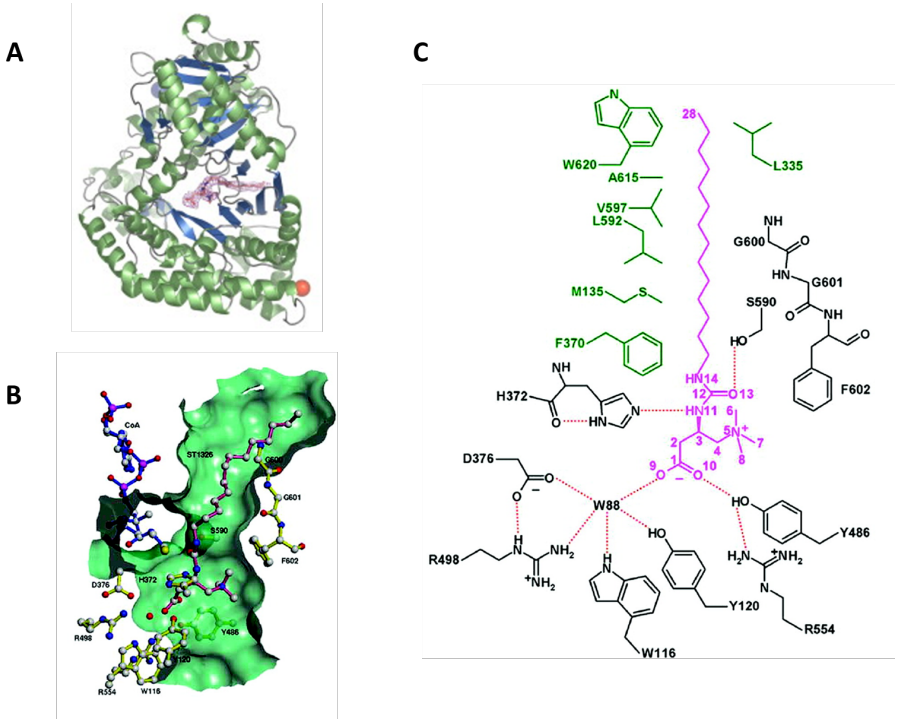

Figure 1-19 Structure of the rCPT2 complex with ST-1326 and interactions[96] A: Structure of rCPT-2 in complex with the CPT inhibitor ST-1326, B and C: ST-1326 interacts with protein residues

4.2.2. CPT1 inhibitors

One of the most reported and promising compounds are the oxirane carboxylic acids, which require conversion to the CoA form in the cell to exert their action under the form of an irreversible inhibition (**Figure 1-20**). Etomoxir was developed primarily to treat diabetes and heart failure. In a phase II clinical trial, Etomoxir exhibited severe hepatotoxicity leading to the abandon of this drug[98]. The oxirane carboxylic acids were then used as tool drugs for

pharmacological studies. In many studies, Etomoxir was shown to efficiently reduce tumor growth and inhibit cancer cell migration, suggesting that reducing FAO has a great potential to block tumor progression[87, 99, 100]. The derivatives include Etomoxir ethyl ester and Etomoxir-CoA.

These data suggest that preventing Etomoxir to act on healthy tissues while promoting its delivery in tumors could offer this efficient drug a second chance to be used to treat cancer patients. First steps to address this objective will be presented in the current thesis (see Chapter II).

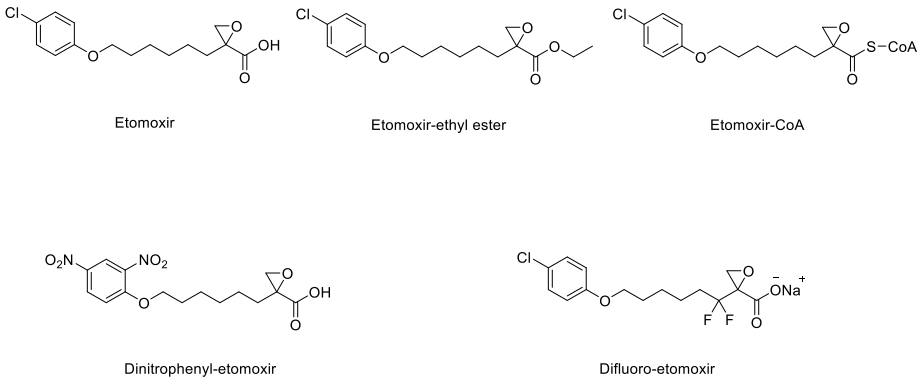

Figure 1-20 Oxirane carboxylic acid and derivatives with CPT1 inhibitory activity

Carnitine derivatives such as the acyl derivative of the unnatural isomer, (*S*)-Octanoylcarnitine and Aminocarnitine (ST1326) have been described as potential CPT1 inhibitors[101, 102]. The anticancer potential of other CPT1 inhibitors, such as Perhexiline and Oxfenicine, which are already approved as antianginal treatments in several countries, remains to be determined[103, 104] (**Figure 1-21**)

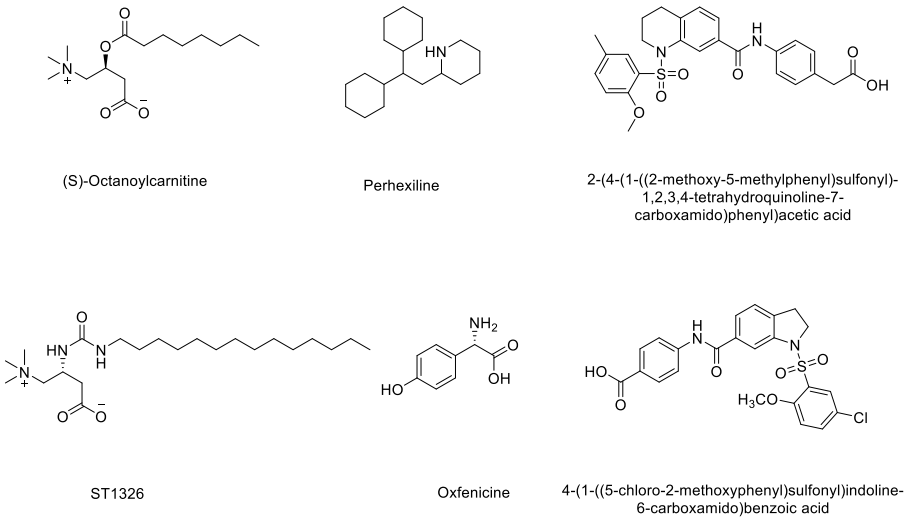

Figure 1-21 CPT1 inhibitors

5. Harnessing the TME to make metabolism-targeting drug tumor-selective

As emphasized above, although inhibiting metabolic routes such as OXPHOS or FAO may be particularly detrimental for cancer cells, a main issue is the selectivity of these approaches. The TME may however offers some rationale to design tumor-selective drugs targeting metabolism. Both hypoxia and acidosis have been exploited in this thesis to propose innovative approaches aiming to minimize adverse effects of such drugs while increasing their efficacy.

5.1. Tumor acidosis and pH-sensitive drug delivery systems (DDS)

Tumor acidosis is increasingly recognized as a significant hallmark of tumors. Indeed, while there is a slight difference between the intra- and extracellular pH (7.2 vs 7.4) in normal cells, the difference is more pronounced in cancer cells with actually a more alkaline intracellular pH (pH_i=7.4-7.6) and a more acidic extracellular pH (pH_e=6.5)[105] (**Figure 1-22**).

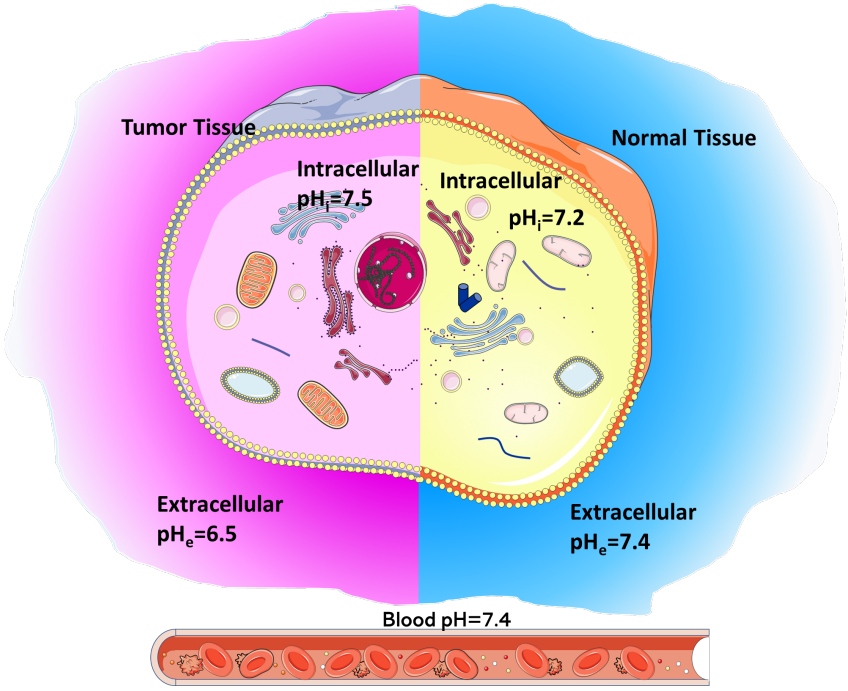

Figure 1-22 Intracellular and intercellular pH in normal and tumor cells[10, 106]

To maintain a stable intracellular pH, tumor cells transport acidic substances to the outside of the tumor cell or base substances from the outside to the inside of the tumor cell *via* a series of transport proteins. The lactate and H^+ accumulated in the cells are transferred to the extracellular space with the participation of transporters, such as MCT4 but also H^+-ATPases and Na^+/H^+ exchanger 1 (NHE1). CO_2 release leads to acidification upon hydration and further dissociation into H^+ and HCO_3^-, in part via the activity of carbonic anhydrase (CAIX). In addition, Na^+/HCO_3^- co-transporters (NBCs) transport HCO_3^- into the cells for neutralizing the acidic substances in cells [10, 106](**Figure 1-23**).

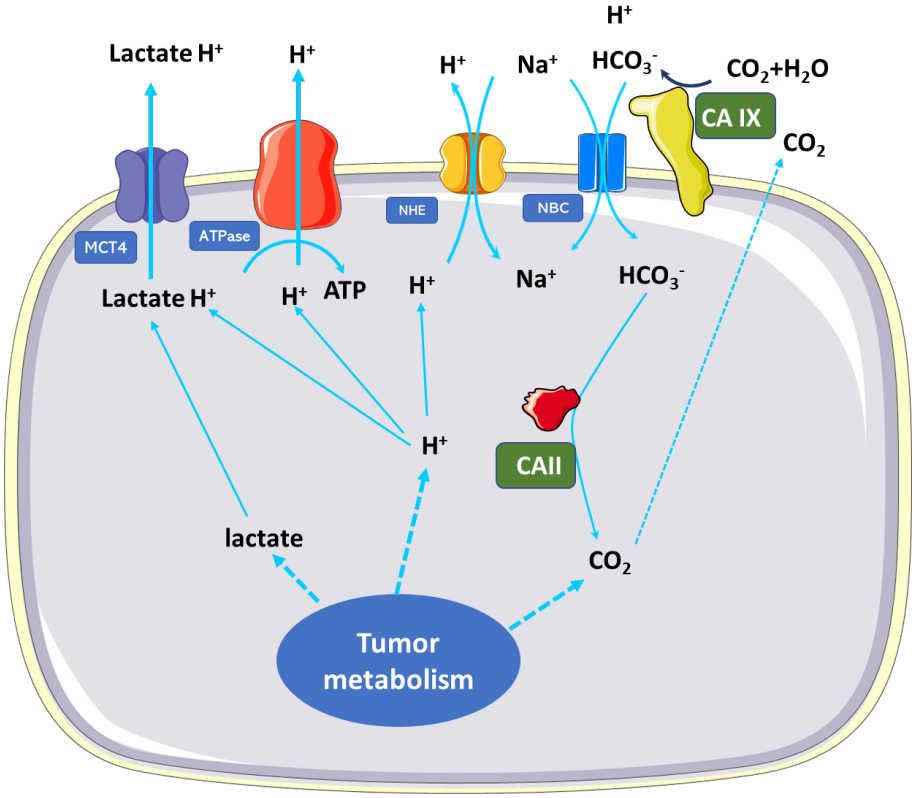

Figure 1-23 Tumor pH regulation by carbonic anhydrase and acid/base transporters[10, 106]

There are two main therapeutic modalities that takes advantage of tumor acidosis[10]: 1) direct action on tumor cell pH regulating systems, such as proton pump inhibitors or the inhibition of carbonic anhydrase activity; 2) pH-sensitive drug delivery systems (DDS)aiming to locally release therapeutics in tumors (while sparing healthy tissues at neutral pH). This second option was exploited in this thesis and will thus be briefly discussed here below.

DDSs are engineered technologies for the targeted delivery and/or controlled release of therapeutic agents. They can be divided into two main families: *in vivo* factor-mediated drug release and *in vitro* factor-mediated drug release. *In vivo* factors include for instance enzymes, redox status and pH while *in vitro* factors mainly include light, heat, magnetic field, or ultrasound. Formulations are often based on encapsulation in carriers such as liposomes, micelles or

nanoparticles. Other modalities are however increasingly reported where drugs are covalently bound to a target moiety [107, 108]. In this case, DDS can be divided into three main components: the pharmacologically active parent structure or derivative, the metabolically unstable chemical connector and the target for specific binding.

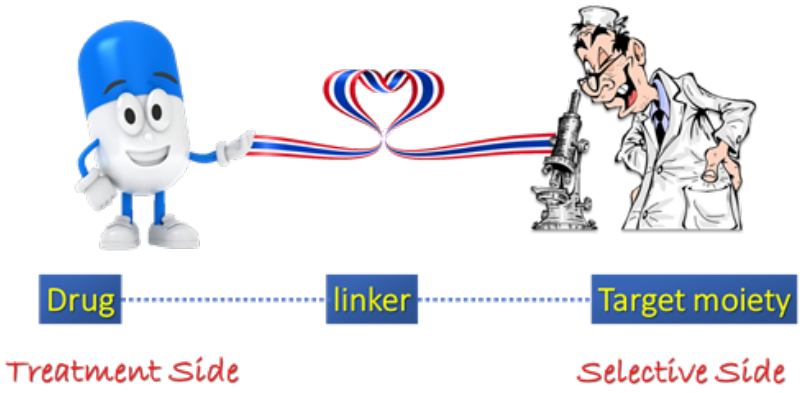

Figure1-24 General structure of Drug delivery systems

pH has been widely explored as an endogenous trigger generate DDS. Acidic pH is exploited to selectively promote the release of anticancer drugs in tumors, resulting in an effective inhibition of cancer cell growth while reducing systemic cytotoxicity. Three main forms of DDSs have been designed to respond to the acidic microenvironment in tumors. Firstly, polymers composed of nanomaterials with ionisable chemical groups that can accept or provide protons in response to changes in environmental pH. At physiological pH, they remain deprotonated or deionised, while at acidic pH, the polymers undergo protonation or charge inversion resulting in structural damage leading and drug specific release. Secondly, acid-unstable chemical bonds, hydrolysed when cells are in an acidic microenvironment or within the cellular lysosome to facilitate drug release. Acid-unstable bonds with linkage effects include ester, carbonate, carbamate, amide, urea, hydrazone, imine, orthoester (**Table 1-3**).

Table 1-3 The chemical bonds in prodrug conjugates and hydrolysis in the acidic environment

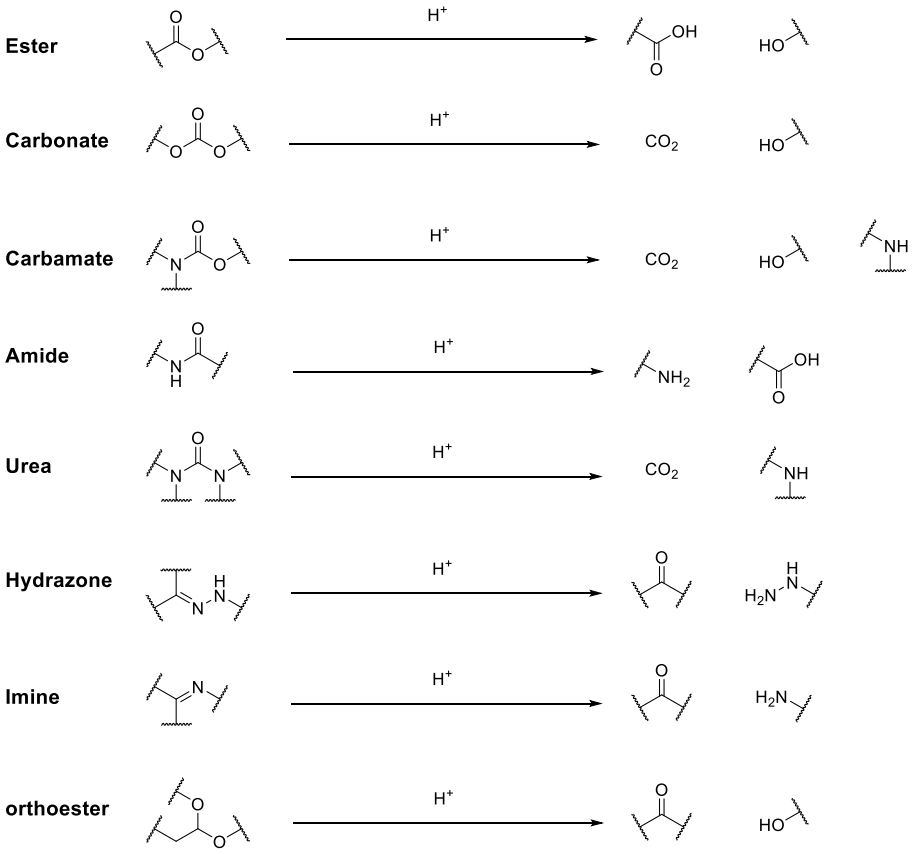

The third option that was exploited in this thesis is the use of pH-sensitive cell penetrating peptides (CPPs). Peptide-based delivery systems were discovered during research about the fusion of viruses with cells. Cell penetrating peptides (CPPs) are currently used as cargo carriers and currently represent a hotspot in medical research[109, 110]. A pH-Low Insertion Peptide (pHLIP) has been discovered recently. It is a pH-sensitive peptide that undergoes membrane insertion, resulting in the creation of a transmembrane helix, when exposed to acidity at a tumor cell surface. As a result, pHLIPs preferentially accumulate within tumors and can be used for tumor targeted imaging and

drug delivery[111]. Details about pHLIP are described in Chapter II.

5.2. Tumor Hypoxia and bioreductive drugs

As emphasized above, one of the hallmarks of solid tumors is the hypoxia resulting from inadequate blood supply. Due to the abnormal vascular network within solid tumors, some tumor cells located at distance from the blood vessels (> 150 μm) are considered as hypoxic (usually described as <1% O_2 in the oncology field). Importantly, oxygen consumption by some cancer cells (located at proximity of blood vessels) is also directly contribute to a lesser availability of O_2 in the deeper tumor cell layers. When the oxygen supply is insufficient, tumor cells stabilize the expression of HIF1α, which in turn promotes the expression of genes facilitating the adaptation to hypoxia, including through the upregulation of glucose transporter, glycolytic enzymes and MCT4.

As for acidosis, hypoxia has inspired scientists in the development of anticancer drugs. One approach is based on the use of small molecule inhibitors to counteract the pro-survival effects of HIF-1α (as well as UPR and mTOR). The second strategy is to develop bio-reductive prodrugs that will be exclusively activated in hypoxic tumor regions; these compounds are known as "hypoxia-activated prodrugs (HAPs)". The trigger that targets the hypoxic microenvironment accounts for the selective prodrug activation via electron transfer through the linker to *in fine* release the antitumor drug. Trigger activation relies primarily on oxidoreductases giving rise to reduction reactions with single or double electron transfer. In general terms, one-electron reduction generates a radical prodrug species that can be back-oxidized in the presence of oxygen to generate the parental prodrug and reactive oxygen species. In hypoxia, the radical prodrug species undergo further reduction, disproportionation, or fragmentation reactions to generate anticancer drug products. Two-electron reduction, in contrast, bypasses the

oxygen-sensitive prodrug radical intermediate. In this case, selectivity is determined mainly by elevated levels of the enzyme in tumor tissue (**Figure 1-25**).

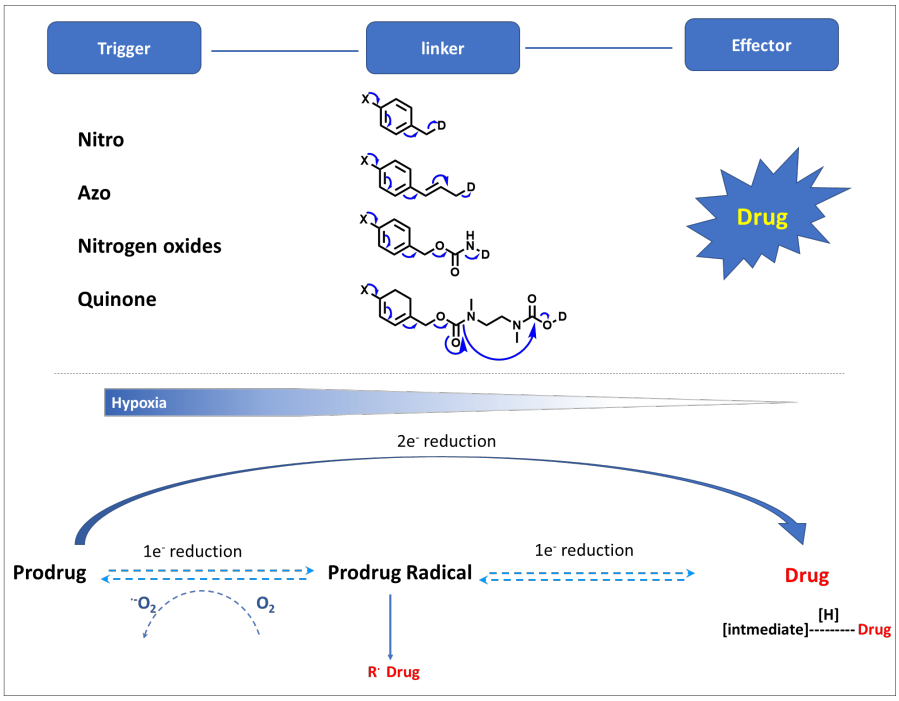

Figure 1-25 Hypoxia-activated prodrug system and the mechanism of activation of hypoxia-activated prodrugs[112, 113]

Here below are a few examples of HAPs recently described in the literature. Banoxantrone is an aliphatic *N*-oxide that is catalyzed by cytochrome P450 (CYP) isozymes and inducible nitric oxide synthase (iNOS) to produce AQ4 by two double electron transfer reductions, and the product AQ4 is a potent inhibitor of topoisomerase II (**Scheme 1-1**)[114]. Apaziquone is derived from an indolequinone derivative produced by mitomycin C. It causes DNA damage through the production of metabolites by single-electron reduction (cytochrome P450 reductase) or two-electron reduction (Quinone oxidoreductase 1) (**Scheme 1-1**)[115]. Evofosfamide is activated upon reduction by one-electron oxidoreductases or radiolytic reduction, leading to

fragmentation and release (at very low oxygen concentrations) of the potent DNA alkylating agent bromo-isophosphoramide mustard, a potent alkylating agent (**Scheme 1-1**)[116]. The pre-prodrug PR-104 is converted to PR-104A by phosphatases in the systemic circulation, and then undergoes either one- or two-electron reduction. One-electron reduction by enzymes such as cytochrome P450 reductase generates a nitro radical intermediate that can undergo rapid redox cycling back to the parent compound in the presence of oxygen. In the absence of oxygen, the nitro radical intermediate undergoes a series of reactions leading to the formation of the toxic PR-104H and PR-104M derivatives. Two-electron reduction by AKR1C3 bypasses the oxygen-sensitive intermediate and generates the active metabolites under aerobic and hypoxic conditions (**Scheme 1-1**)[117]. Details about HAPs are described in Chapter III

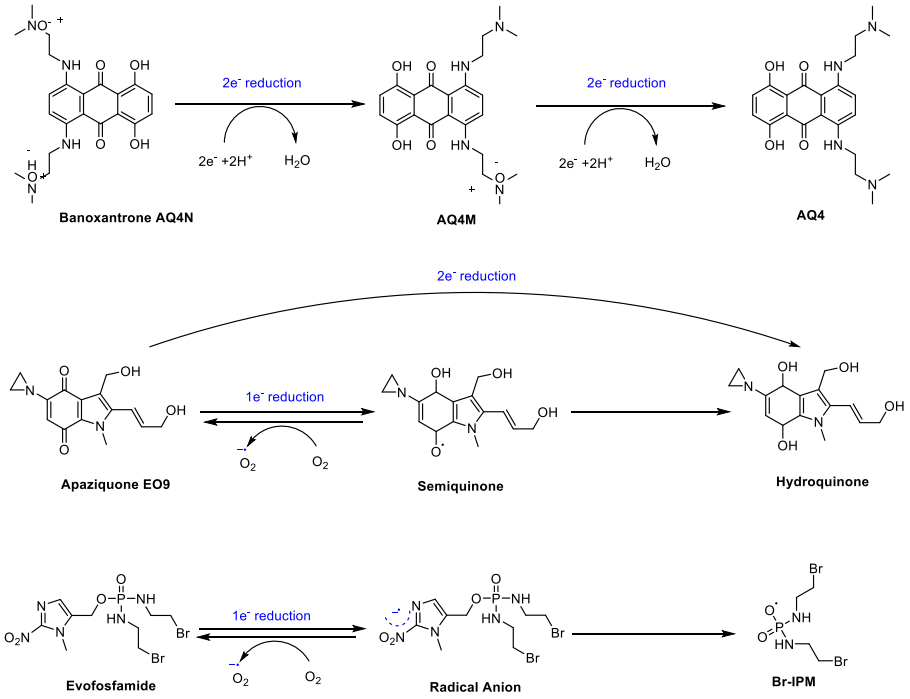

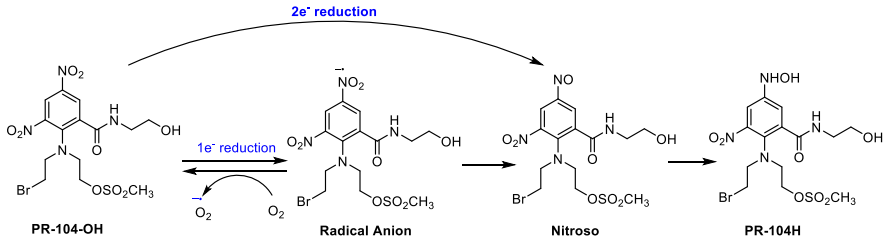

Scheme 1-1 Mechanisms of metabolic activation of bioreductive prodrug in hypoxia tumor microenvironmental [112, 117]

6. Reference

1. Zhu, J.; Thompson, C. B., Metabolic regulation of cell growth and proliferation. *Nat Rev Mol Cell Biol* **2019,** *20* (7), 436-450.
2. Martinez-Outschoorn, U. E.; Peiris-Pages, M.; Pestell, R. G.; Sotgia, F., et al., Cancer metabolism: a therapeutic perspective. *Nat Rev Clin Oncol* **2017,** *14* (2), 11-13.
3. DeBerardinis, R. J.; Chandel, N. S., Fundamentals of cancer metabolism. *Sci Adv* **2016,** *2* (5), e1600200.
4. Warburg, O., On respiratory impairment in cancer cells. *Science* **1956,** *124* (3215), 269-270.
5. Warburg, O., On the origin of cancer cells. *Science* **1956,** *123* (3191), 309-314.
6. Corbet, C.; Feron, O., Cancer cell metabolism and mitochondria: Nutrient plasticity for TCA cycle fueling. *Biochim Biophys Acta Rev Cancer* **2017,** *1868* (1), 7-15.
7. Halestrap, A. P.; Meredith, D., The SLC16 gene family-from monocarboxylate transporters (MCTs) to aromatic amino acid transporters and beyond. *Pflugers Arch* **2004,** *447* (5), 619-628.
8. Halestrap, A. P.; Wilson, M. C., The monocarboxylate transporter family--role and regulation. *IUBMB Life* **2012,** *64* (2), 109-119.
9. Wilson, M. C.; Meredith, D.; Fox, J. E.; Manoharan, C., et al., Basigin (CD147) is the target for organomercurial inhibition of monocarboxylate transporter isoforms 1 and 4: the ancillary protein for the insensitive MCT2 is EMBIGIN (gp70). *J Biol Chem* **2005,** *280* (29), 27213-27221.
10. Corbet, C.; Feron, O., Tumour acidosis: from the passenger to the driver's seat. *Nat Rev Cancer* **2017,** *17* (10), 577-593.
11. Payen, V. L.; Mina, E.; Van Hee, V. F.; Porporato, P. E., et al., Monocarboxylate transporters in cancer. *Mol Metab* **2020,** *33*, 48-66.
12. Becker, H. M.; Mohebbi, N.; Perna, A.; Ganapathy, V., et al., Localization of members of MCT monocarboxylate transporter family Slc16 in the kidney and regulation during metabolic acidosis. *Am J Physiol Renal Physiol* **2010,** *299* (1), 141-154.
13. Philp, N. J.; Yoon, H.; Lombardi, L., Mouse MCT3 gene is expressed preferentially in retinal pigment and choroid plexus epithelia. *Am J Physiol Cell Physiol* **2001,** *280* (5), 1319-1326.
14. Puri, S.; Juvale, K., Monocarboxylate transporter 1 and 4 inhibitors as potential therapeutics for treating solid tumours: A review with structure-activity relationship insights. *Eur J Med Chem* **2020,** *199*, 112393.
15. Guan, X.; Rodriguez-Cruz, V.; Morris, M. E., Cellular Uptake of MCT1 Inhibitors AR-C155858 and AZD3965 and Their Effects on MCT-Mediated Transport of L-Lactate in Murine 4T1 Breast Tumor Cancer Cells. *AAPS J* **2019,** *21* (2), 1-10.
16. Quanz, M.; Bender, E.; Kopitz, C.; Grunewald, S., et al., Preclinical Efficacy of the Novel Monocarboxylate Transporter 1 Inhibitor BAY-8002 and Associated Markers of Resistance. *Mol Cancer Ther* **2018,** *17* (11), 2285-2296.
17. Wang, N.; Jiang, X.; Zhang, S.; Zhu, A., et al., Structural basis of human monocarboxylate transporter 1 inhibition by anti-cancer drug candidates. *Cell* **2021,** *184* (2), 370-383.
18. Beloueche-Babari, M.; Casals Galobart, T.; Delgado-Goni, T.; Wantuch, S., et al., Monocarboxylate transporter 1 blockade with AZD3965 inhibits lipid biosynthesis and increases tumour immune cell infiltration. *Br J Cancer* **2020,** *122* (6), 895-903.
19. Draoui, N.; Schicke, O.; Seront, E.; Bouzin, C., et al., Antitumor activity of 7-aminocarboxycoumarin derivatives, a new class of potent inhibitors of lactate influx but not efflux. *Mol Cancer Ther* **2014,** *13* (6), 1410-1418.
20. Halestrap, A. P., The monocarboxylate transporter family--Structure and functional characterization. *IUBMB Life* **2012,** *64* (1), 1-9.
21. Vander Linden, C.; Corbet, C.; Bastien, E.; Martherus, R., et al., Therapy-induced DNA methylation inactivates MCT1 and renders tumor cells vulnerable to MCT4 inhibition.

Cell Rep **2021,** *35* (9), 109202.
22. Parnell, K. M.; McCall, J.; Romero, D. Heterocyclic inhibitors of MCT4. 2019.
23. Takenaga, K.; Koshikawa, N.; Akimoto, M.; Tatsumi, Y., et al., MCT4 is induced by metastasis-enhancing pathogenic mitochondrial NADH dehydrogenase gene mutations and can be a therapeutic target. *Sci Rep* **2021,** *11* (1), 1-19.
24. Manning Fox, J. E.; Meredith, D.; Halestrap, A. P., Characterisation of human monocarboxylate transporter 4 substantiates its role in lactic acid efflux from skeletal muscle. *J Physiol* **2000,** *529 2* (2), 285-293.
25. Sasaki, S.; Futagi, Y.; Ideno, M.; Kobayashi, M., et al., Effect of diclofenac on SLC16A3/MCT4 by the Caco-2 cell line. *Drug Metab Pharmacokinet* **2016,** *31* (3), 218-223.
26. Whitaker-Menezes, D.; Martinez-Outschoorn, U. E.; Lin, Z.; Ertel, A., et al., Evidence for a stromal-epithelial "lactate shuttle" in human tumors: MCT4 is a marker of oxidative stress in cancer-associated fibroblasts. *Cell Cycle* **2011,** *10* (11), 1772-1783.
27. Pisarsky, L.; Bill, R.; Fagiani, E.; Dimeloe, S., et al., Targeting Metabolic Symbiosis to Overcome Resistance to Anti-angiogenic Therapy. *Cell Rep* **2016,** *15* (6), 1161-1174.
28. Perez-Escuredo, J.; Van Hee, V. F.; Sboarina, M.; Falces, J., et al., Monocarboxylate transporters in the brain and in cancer. *Biochim Biophys Acta* **2016,** *1863* (10), 2481-2497.
29. Fischer, K.; Hoffmann, P.; Voelkl, S.; Meidenbauer, N., et al., Inhibitory effect of tumor cell-derived lactic acid on human T cells. *Blood* **2007,** *109* (9), 3812-3819.
30. Benjamin, D.; Robay, D.; Hindupur, S. K.; Pohlmann, J., et al., Dual Inhibition of the Lactate Transporters MCT1 and MCT4 Is Synthetic Lethal with Metformin due to NAD^+ Depletion in Cancer Cells. *Cell Rep* **2018,** *25* (11), 3047-3058.
31. Mereddy, V. R. Indole and indazole compounds and therapeutic uses thereof. **2019**.
32. Critchlow, S. E.; Hughes, G.; Staniszewska, A.; King, M., et al., Reversing lactate-driven immunosuppression using the novel, potent and selective MCT4 inhibitor AZD0095. *Cancer Res* **2019**.
33. Renner, K.; Bruss, C.; Schnell, A.; Koehl, G., et al., Restricting Glycolysis Preserves T Cell Effector Functions and Augments Checkpoint Therapy. *Cell Rep* **2019,** *29* (1), 135-150 e139.
34. Vyas, S.; Zaganjor, E.; Haigis, M. C., Mitochondria and Cancer. *Cell* **2016,** *166* (3), 555-566.
35. Hensley, C. T.; Faubert, B.; Yuan, Q.; Lev-Cohain, N., et al., Metabolic Heterogeneity in Human Lung Tumors. *Cell* **2016,** *164* (4), 681-694.
36. Buescher, J. M.; Antoniewicz, M. R.; Boros, L. G.; Burgess, S. C., et al., A roadmap for interpreting (13)C metabolite labeling patterns from cells. *Curr Opin Biotechnol* **2015,** *34*, 189-201.
37. Martinez-Reyes, I.; Chandel, N. S., Mitochondrial TCA cycle metabolites control physiology and disease. *Nat Commun* **2020,** *11* (1), 1-11.
38. Liu, Y. e.; Shi, Y., Mitochondria as a target in cancer treatment. *MedComm* **2020,** *1* (2), 129-139.
39. Ward, P. S.; Patel, J.; Wise, D. R.; Abdel-Wahab, O., et al., The common feature of leukemia-associated IDH1 and IDH2 mutations is a neomorphic enzyme activity converting alpha-ketoglutarate to 2-hydroxyglutarate. *Cancer Cell* **2010,** *17* (3), 225-234.
40. Chen, C.; Liu, Y.; Lu, C.; Cross, J. R., et al., Cancer-associated IDH2 mutants drive an acute myeloid leukemia that is susceptible to Brd4 inhibition. *Genes Dev* **2013,** *27* (18), 1974-1985.
41. Stephenson, Z. A.; Harvey, R. F.; Pryde, K. R.; Mistry, S., et al., Identification of a novel toxicophore in anti-cancer chemotherapeutics that targets mitochondrial respiratory complex I. *Elife* **2020,** *9*, e55845.
42. Ashton, T. M.; McKenna, W. G.; Kunz-Schughart, L. A.; Higgins, G. S., Oxidative Phosphorylation as an Emerging Target in Cancer Therapy. *Clin Cancer Res* **2018,** *24* (11), 2482-2490.
43. Ben Sahra, I.; Le Marchand-Brustel, Y.; Tanti, J. F.; Bost, F., Metformin in cancer therapy: a new perspective for an old antidiabetic drug? *Mol Cancer Ther* **2010,** *9* (5), 1092-1099.

44. Pollak, M. N., Investigating metformin for cancer prevention and treatment: the end of the beginning. *Cancer Discov* **2012,** *2* (9), 778-790.
45. Scotland, S.; Saland, E.; Skuli, N.; de Toni, F., et al., Mitochondrial energetic and AKT status mediate metabolic effects and apoptosis of metformin in human leukemic cells. *Leukemia* **2013,** *27* (11), 2129-2138.
46. Quinn, B. J.; Dallos, M.; Kitagawa, H.; Kunnumakkara, A. B., et al., Inhibition of lung tumorigenesis by metformin is associated with decreased plasma IGF-I and diminished receptor tyrosine kinase signaling. *Cancer Prev Res (Phila)* **2013,** *6* (8), 801-810.
47. McGuinness, M. E.; Talbert, R. L., Phenformin-induced lactic acidosis: a forgotten adverse drug reaction. *Ann Pharmacother* **1993,** *27* (10), 1183-1187.
48. Cheng, G.; Zielonka, J.; Ouari, O.; Lopez, M., et al., Mitochondria-Targeted Analogues of Metformin Exhibit Enhanced Antiproliferative and Radiosensitizing Effects in Pancreatic Cancer Cells. *Cancer Res* **2016,** *76* (13), 3904-3915.
49. Rha, S. Y.; Beom, S.-H.; Jung, M.; Shin, Y. G., et al., Phase 1 study of an oxidative phosphorylation inhibitor IM156 in patients with advanced solid tumors. *J Clin Oncol* **2018,** *36* (15), 2620.
50. Benej, M.; Hong, X.; Vibhute, S.; Scott, S., et al., Papaverine and its derivatives radiosensitize solid tumors by inhibiting mitochondrial metabolism. *Proc Natl Acad Sci U S A* **2018,** *115* (42), 10756-10761.
51. Lakhia, R.; Yheskel, M.; Flaten, A.; Quittner-Strom, E. B., et al., PPARalpha agonist fenofibrate enhances fatty acid beta-oxidation and attenuates polycystic kidney and liver disease in mice. *Am J Physiol Renal Physiol* **2018,** *314* (1), 122-131.
52. Naguib, A.; Mathew, G.; Reczek, C. R.; Watrud, K., et al., Mitochondrial Complex I Inhibitors Expose a Vulnerability for Selective Killing of Pten-Null Cells. *Cell Rep* **2018,** *23* (1), 58-67.
53. Gangjee, A.; Zaware, N.; Raghavan, S.; Ihnat, M., et al., Single agents with designed combination chemotherapy potential: synthesis and evaluation of substituted pyrimido[4,5-b]indoles as receptor tyrosine kinase and thymidylate synthase inhibitors and as antitumor agents. *J Med Chem* **2010,** *53* (4), 1563-1578.
54. Baccelli, I.; Gareau, Y.; Lehnertz, B.; Gingras, S., et al., Mubritinib Targets the Electron Transport Chain Complex I and Reveals the Landscape of OXPHOS Dependency in Acute Myeloid Leukemia. *Cancer Cell* **2019,** *36* (1), 84-99.
55. Lim, S. C.; Carey, K. T.; McKenzie, M., Anti-cancer analogues ME-143 and ME-344 exert toxicity by directly inhibiting mitochondrial NADH: ubiquinone oxidoreductase (Complex I). *Am J Cancer Res* **2015,** *5* (2), 689-701.
56. Schockel, L.; Glasauer, A.; Basit, F.; Bitschar, K., et al., Targeting mitochondrial complex I using BAY 87-2243 reduces melanoma tumor growth. *Cancer Metab* **2015,** *3* (1), 1-16.
57. Ju, R.; Guo, L.; Li, J.; Zhu, L., et al., Carboxyamidotriazole inhibits oxidative phosphorylation in cancer cells and exerts synergistic anti-cancer effect with glycolysis inhibition. *Cancer Lett* **2016,** *370* (2), 232-241.
58. Tsuji, A.; Akao, T.; Masuya, T.; Murai, M., et al., IACS-010759, a potent inhibitor of glycolysis-deficient hypoxic tumor cells, inhibits mitochondrial respiratory complex I through a unique mechanism. *J Biol Chem* **2020,** *295* (21), 7481-7491.
59. Yap, T. A.; Rodon Ahnert, J.; Piha-Paul, S. A.; Fu, S., et al., Phase I trial of IACS-010759 (IACS), a potent, selective inhibitor of complex I of the mitochondrial electron transport chain, in patients (pts) with advanced solid tumors. *J Clin Oncol* **2019,** *37* (15), 3014.
60. Angulo-Molina, A.; Reyes-Leyva, J.; Lopez-Malo, A.; Hernandez, J., The role of alpha tocopheryl succinate (alpha-TOS) as a potential anticancer agent. *Nutr Cancer* **2014,** *66* (2), 167-176.
61. Xiang, M.; Kim, H.; Ho, V. T.; Walker, S. R., et al., Gene expression-based discovery of atovaquone as a STAT3 inhibitor and anticancer agent. *Blood* **2016,** *128* (14), 1845-1853.
62. Kim, H.; Esser, L.; Hossain, M. B.; Xia, D., et al., Structure of Antimycin A1, a Specific Electron Transfer Inhibitor of Ubiquinol−Cytochrome c Oxidoreductase. *J Am Chem Soc* **1999,** *121* (20), 4902-4903.

63. Liu, L.; Zhu, H.; Wu, W.; Shen, Y., et al., Neoantimycin F, a Streptomyces-Derived Natural Product Induces Mitochondria-Related Apoptotic Death in Human Non-Small Cell Lung Cancer Cells. *Front Pharmacol* **2019,** *10*, 1-13.
64. Oliva, C. R.; Markert, T.; Ross, L. J.; White, E. L., et al., Identification of Small Molecule Inhibitors of Human Cytochrome c Oxidase That Target Chemoresistant Glioma Cells. *J Biol Chem* **2016,** *291* (46), 24188-24199.
65. Viale, A.; Pettazzoni, P.; Lyssiotis, C. A.; Ying, H., et al., Oncogene ablation-resistant pancreatic cancer cells depend on mitochondrial function. *Nature* **2014,** *514* (7524), 628-632.
66. Fiorillo, M.; Lamb, R.; Tanowitz, H. B.; Cappello, A. R., et al., Bedaquiline, an FDA-approved antibiotic, inhibits mitochondrial function and potently blocks the proliferative expansion of stem-like cancer cells (CSCs). *Aging (Albany NY)* **2016,** *8* (8), 1593-1607.
67. Daniel, P. T.; Koert, U.; Schuppan, J., Apoptolidin: induction of apoptosis by a natural product. *Angew Chem Int Ed* **2006,** *45* (6), 872-893.
68. Shi, Y.; Lim, S. K.; Liang, Q.; Iyer, S. V., et al., Gboxin is an oxidative phosphorylation inhibitor that targets glioblastoma. *Nature* **2019,** *567* (7748), 341-346.
69. Fryknas, M.; Zhang, X.; Bremberg, U.; Senkowski, W., et al., Iron chelators target both proliferating and quiescent cancer cells. *Sci Rep* **2016,** *6*, 38343.
70. Sazanov, L. A., A giant molecular proton pump: structure and mechanism of respiratory complex I. *Nat Rev Mol Cell Biol* **2015,** *16* (6), 375-388.
71. Zhu, J.; Vinothkumar, K. R.; Hirst, J., Structure of mammalian respiratory complex I. *Nature* **2016,** *536* (7616), 354-358.
72. Dröse, S.; Brandt, U., Molecular Mechanisms of Superoxide Production by the Mitochondrial Respiratory Chain. *Mitochondrial oxidative phosphorylation*, 2012; 748, 145-159.
73. Xu, Y.; Xue, D.; Bankhead, A., 3rd; Neamati, N., Why All the Fuss about Oxidative Phosphorylation (OXPHOS)? *J Med Chem* **2020,** *63* (23), 14276-14307.
74. Röhrig, F.; Schulze, A. J. N. R. C., The multifaceted roles of fatty acid synthesis in cancer. *Nat. Rev. Cancer*, **2016,** *16* (11), 732-749.
75. Koundouros, N.; Poulogiannis, G., Reprogramming of fatty acid metabolism in cancer. *Br J Cancer* **2020,** *122* (1), 4-22.
76. Corbet, C.; Feron, O., Emerging roles of lipid metabolism in cancer progression. *Curr Opin Clin Nutr Metab Care* **2017,** *20* (4), 254-260.
77. Cases, S.; Stone, S. J.; Zhou, P.; Yen, E., et al., Cloning of DGAT2, a second mammalian diacylglycerol acyltransferase, and related family members. *J Biol Chem* **2001,** *276* (42), 38870-38876.
78. Cheng, X.; Geng, F.; Guo, D., DGAT1 protects tumor from lipotoxicity, emerging as a promising metabolic target for cancer therapy. *Mol Cell Oncol* **2020,** *7* (6), 1805257.
79. Sui, X.; Wang, K.; Gluchowski, N. L.; Elliott, S. D., et al., Structure and catalytic mechanism of a human triacylglycerol-synthesis enzyme. *Nature* **2020,** *581* (7808), 323-328.
80. Wang, L.; Qian, H.; Nian, Y.; Han, Y., et al., Structure and mechanism of human diacylglycerol O-acyltransferase 1. *Nature* **2020,** *581* (7808), 329-332.
81. Kahn, C. R., Triglycerides and toggling the tummy. *Nat Genet* **2000,** *25* (1), 6-7.
82. Kahn, S. E.; Hull, R. L.; Utzschneider, K. M., Mechanisms linking obesity to insulin resistance and type 2 diabetes. *Nature* **2006,** *444* (7121), 840-846.
83. Unger, R. H., Lipotoxic diseases. *Annu Rev Med* **2002,** *53*, 319-336.
84. Cao, J.; Zhou, Y.; Peng, H.; Huang, X., et al., Targeting Acyl-CoA:diacylglycerol acyltransferase 1 (DGAT1) with small molecule inhibitors for the treatment of metabolic diseases. *J Biol Chem* **2011,** *286* (48), 41838-41851.
85. Cheng, X.; Geng, F.; Pan, M.; Wu, X., et al., Targeting DGAT1 Ameliorates Glioblastoma by Increasing Fat Catabolism and Oxidative Stress. *Cell Metab* **2020,** *32* (2), 229-242.
86. Ma, Y.; Temkin, S. M.; Hawkridge, A. M.; Guo, C., et al., Fatty acid oxidation: An emerging facet of metabolic transformation in cancer. *Cancer Lett* **2018,** *435*, 92-100.

87. Sawyer, B. T.; Qamar, L.; Yamamoto, T. M.; McMellen, A., et al., Targeting Fatty Acid Oxidation to Promote Anoikis and Inhibit Ovarian Cancer Progression. *Mol Cancer Res* **2020,** *18* (7), 1088-1098.
88. Melone, M. A. B.; Valentino, A.; Margarucci, S.; Galderisi, U., et al., The carnitine system and cancer metabolic plasticity. *Cell Death Dis* **2018,** *9* (2), 1-12.
89. Pike, L. S.; Smift, A. L.; Croteau, N. J.; Ferrick, D. A., et al., Inhibition of fatty acid oxidation by etomoxir impairs NADPH production and increases reactive oxygen species resulting in ATP depletion and cell death in human glioblastoma cells. *Biochim Biophys Acta* **2011,** *1807* (6), 726-734.
90. Qu, Q.; Zeng, F.; Liu, X.; Wang, Q. J., et al., Fatty acid oxidation and carnitine palmitoyltransferase I: emerging therapeutic targets in cancer. *Cell Death Dis* **2016,** *7* (5), e2226.
91. Camarda, R.; Zhou, A. Y.; Kohnz, R. A.; Balakrishnan, S., et al., Inhibition of fatty acid oxidation as a therapy for MYC-overexpressing triple-negative breast cancer. *Nat Med* **2016,** *22* (4), 427-432.
92. Lundsgaard, A. M.; Fritzen, A. M.; Kiens, B., Molecular Regulation of Fatty Acid Oxidation in Skeletal Muscle during Aerobic Exercise. *Trends Endocrinol Metab* **2018,** *29* (1), 18-30.
93. Joshi, M.; Stoykova, G. E.; Salzmann-Sullivan, M.; Dzieciatkowska, M., et al., CPT1A Supports Castration-Resistant Prostate Cancer in Androgen-Deprived Conditions. *Cells* **2019,** *8* (10), 1115.
94. Xiong, Y.; Liu, Z.; Zhao, X.; Ruan, S., et al., CPT1A regulates breast cancer-associated lymphangiogenesis via VEGF signaling. *Biomed Pharmacother* **2018,** *106*, 1-7.
95. Schlaepfer, I. R.; Joshi, M., CPT1A-mediated Fat Oxidation, Mechanisms, and Therapeutic Potential. *Endocrinology* **2020,** *161* (2).
96. Rufer, A. C.; Thoma, R.; Benz, J.; Stihle, M., et al., The crystal structure of carnitine palmitoyltransferase 2 and implications for diabetes treatment. *Structure* **2006,** *14* (4), 713-723.
97. Kashfi, K.; Cook, G. A., Topology of hepatic mitochondrial carnitine palmitoyltransferase I. *Adv Exp Med Biol* **1999,** *466*, 27-42.
98. Holubarsch, C. J.; Rohrbach, M.; Karrasch, M.; Boehm, E., et al., A double-blind randomized multicentre clinical trial to evaluate the efficacy and safety of two doses of etomoxir in comparison with placebo in patients with moderate congestive heart failure: the ERGO (etomoxir for the recovery of glucose oxidation) study. *Clin Sci (Lond)* **2007,** *113* (4), 205-212.
99. Schlaepfer, I. R.; Rider, L.; Rodrigues, L. U.; Gijon, M. A., et al., Lipid catabolism via CPT1 as a therapeutic target for prostate cancer. *Mol Cancer Ther* **2014,** *13* (10), 2361-2371.
100. Wang, Y. N.; Zeng, Z. L.; Lu, J.; Wang, Y., et al., CPT1A-mediated fatty acid oxidation promotes colorectal cancer cell metastasis by inhibiting anoikis. *Oncogene* **2018,** *37* (46), 6025-6040.
101. Baillet, L.; Mullur, R. S.; Esser, V.; McGarry, J. D., Elucidation of the mechanism by which (+)-acylcarnitines inhibit mitochondrial fatty acid transport. *J Biol Chem* **2000,** *275* (47), 36766-36768.
102. Giannessi, F.; Pessotto, P.; Tassoni, E.; Chiodi, P., et al., Discovery of a long-chain carbamoyl aminocarnitine derivative, a reversible carnitine palmitoyltransferase inhibitor with antiketotic and antidiabetic activity. *J Med Chem* **2003,** *46* (2), 303-309.
103. Gehmlich, K.; Dodd, M. S.; Allwood, J. W.; Kelly, M., et al., Changes in the cardiac metabolome caused by perhexiline treatment in a mouse model of hypertrophic cardiomyopathy. *Mol Biosyst* **2015,** *11* (2), 564-573.
104. Kim, T.; He, L.; Johnson, M. S.; Li, Y., et al., Carnitine Palmitoyltransferase 1b Deficiency Protects Mice from Diet-Induced Insulin Resistance. *J Diabetes Metab* **2014,** *5* (4), 361.
105. Hao, G.; Xu, Z. P.; Li, L., Manipulating extracellular tumour pH: an effective target for cancer therapy. *RSC Advances* **2018,** *8* (39), 22182-22192.
106. Webb, B. A.; Chimenti, M.; Jacobson, M. P.; Barber, D. L., Dysregulated pH: a perfect storm for cancer progression. *Nat Rev Cancer* **2011,** *11* (9), 671-677.
107. He, X.; Li, J.; An, S.; Jiang, C., pH-sensitive drug-delivery systems for tumor

targeting. *Ther Deliv* **2013,** *4* (12), 1499-1510.
108. Kanamala, M.; Wilson, W. R.; Yang, M.; Palmer, B. D., et al., Mechanisms and biomaterials in pH-responsive tumour targeted drug delivery: A review. *Biomaterials* **2016,** *85*, 152-167.
109. Subbarao, N. K.; Parente, R. A.; Szoka, F. C., Jr.; Nadasdi, L., et al., pH-dependent bilayer destabilization by an amphipathic peptide. *Biochemistry* **1987,** *26* (11), 2964-2972.
110. Miura, N.; Akita, H.; Tateshita, N.; Nakamura, T., et al., Modifying Antigen-Encapsulating Liposomes with KALA Facilitates MHC Class I Antigen Presentation and Enhances Anti-tumor Effects. *Mol Ther* **2017,** *25* (4), 1003-1013.
111. Reshetnyak, Y. K.; Andreev, O. A.; Segala, M.; Markin, V. S., et al., Energetics of peptide (pHLIP) binding to and folding across a lipid bilayer membrane. *Proc Natl Acad Sci U S A* **2008,** *105* (40), 15340-15345.
112. Wilson, W. R.; Hay, M. P., Targeting hypoxia in cancer therapy. *Nat Rev Cancer* **2011,** *11* (6), 393-410.
113. O'Connor, L. J.; Cazares-Korner, C.; Saha, J.; Evans, C. N., et al., Design, synthesis and evaluation of molecularly targeted hypoxia-activated prodrugs. *Nat Protoc* **2016,** *11* (4), 781-794.
114. Nishida, C. R.; Ortiz de Montellano, P. R., Reductive heme-dependent activation of the n-oxide prodrug AQ4N by nitric oxide synthase. *J Med Chem* **2008,** *51* (16), 5118-5120.
115. Workman, P., Enzyme-directed bioreductive drug development revisited: a commentary on recent progress and future prospects with emphasis on quinone anticancer agents and quinone metabolizing enzymes, particularly DT-diaphorase. *Oncol Res* **1994,** *6* (10-11), 461-475.
116. Meng, F.; Evans, J. W.; Bhupathi, D.; Banica, M., et al., Molecular and cellular pharmacology of the hypoxia-activated prodrug TH-302. *Mol Cancer Ther* **2012,** *11* (3), 740-751.
117. Phillips, R. M., Targeting the hypoxic fraction of tumours using hypoxia-activated prodrugs. *Cancer Chemother Pharmacol* **2016,** *77* (3), 441-457.

Objectives

Since the Warburg's hypothesis[1], tumor metabolism has gradually attracted the attention of researchers, and become a popular field in the past decade. The Riant's and Feron's research teams have an interest for drugs targeting tumor metabolic preferences associated with specificities of the tumor microenvironment. This thesis applies medicinal chemistry techniques to design and synthesize small molecule compounds or drug delivery systems aiming to target specific metabolic routes in tumors, and to validate their pharmacological activities in cultured cancer cells.

There are two main areas of interest in this thesis. Firstly, among the metabolic targets, we considered oxidative phosphorylation (OXPHOS) and in particular complex I within the electron transport chain (ETC), fatty acid metabolism (oxidation and storage as triglycerides) and the glycolytic pathway via the inhibition of the release of lactate, the glycolytic end-product. Second, physicochemical features of the tumor microenvironment, namely acidosis and hypoxia, were exploited (in conjunction with a controlled drug release system) to design acid-sensitive or redox-sensitive prodrugs in the hope of achieving precise drug release in vivo while reducing side effects and improving efficacy.

The main objectives of this thesis were therefore:

I) To design and synthesize OXPHOS inhibitors, and to carry out structure-activity relationship analysis (SARA) through in-depth pharmacological activity study (**Scheme 2-1**). *See Chapter I*

[1] Warburg O, Wind F, Negelein E. The metabolism of tumors in the body[J]. Journal of General Physiology, 1927, 8(6): 519-530.

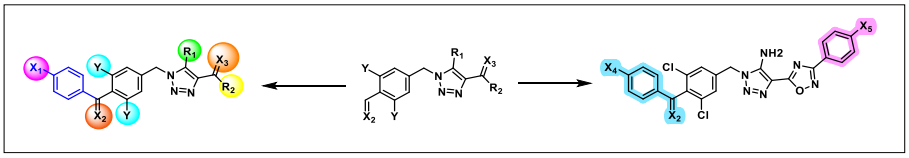

Scheme 2-1 OXPHOS inhibitor

II) To design and synthesize conjugates between inhibitors of fatty acid metabolism (i.e., blockers of CPT1/DGAT1) and a pH-sensitive peptide, to evaluate the capacity of drug release in an acidic environment and the consecutive inhibitory activity on the target site (**Scheme 2-2**). *See Chapter II*

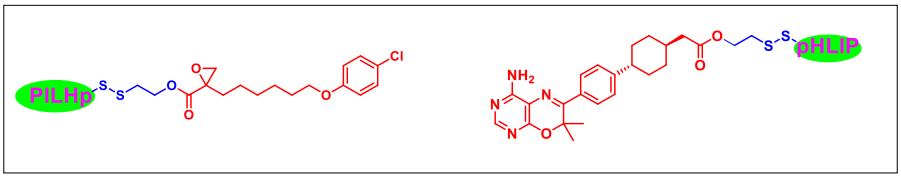

Scheme 2-2 pH sensitive conjugate system

III) To design and synthesize a diclofenac prodrug sensitive to hypoxic conditions and to evaluate its inhibitory activity on lactate transporter MCT4 in a bioreductive environment (**Scheme 2-3 A**). *See Chapter III*

IV) To design and synthesize hypoxia-activated systems based on a triazene probe, validate the release capacity of fluorescein under bio-reductive conditions, and synthesize prodrugs including the triazene moiety (**Scheme 2-3 B**). *See Chapter III*

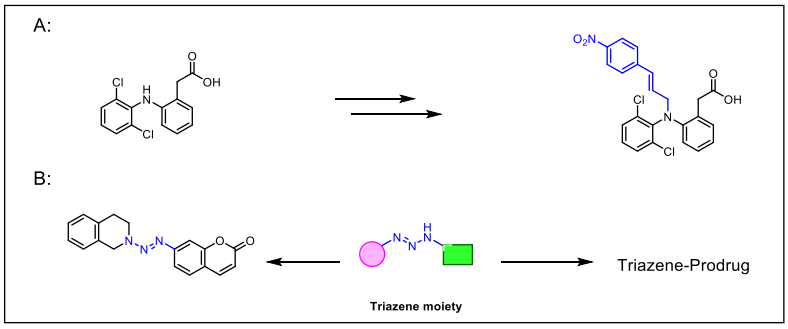

Scheme 2-3 Synthesis of hypoxia-activated prodrugs

The work plan of this thesis is depicted schematically in **Figure** 2-1.

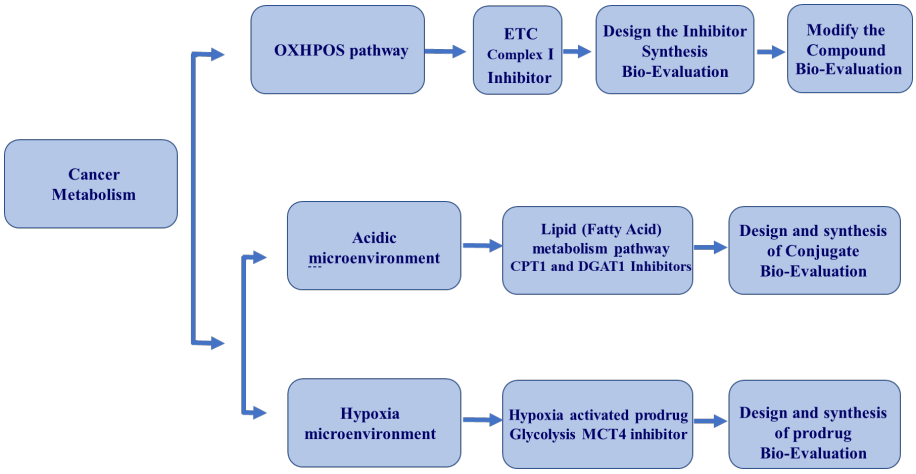

Figure 2-1 The thesis work plan process

Chapter I

Design, Synthesis and Biological Evaluation of Oxidative Phosphorylation (OXPHOS) Complex I Inhibitor

Biological experiments were provided by Dr. Octavia Cadassou from *Prof.* Oliver Feron team

1 Introduction

As described in the general introduction, metabolism of tumor cells switches between glycolytic and oxidative phosphorylation (OXPHOS), depending on the tumor microenvironment and activated oncogenes[1, 2]. While glycolysis is often related to proliferative status of cancer cells, there is mounting evidence that upregulation of OXPHOS is strongly associated with cancer cell invasion, migration, and drug resistance[3, 4].

While inhibition of mitochondrial respiration has long been thought to be non-druggable, recent findings have led to reconsider electron transport chain as a potential anticancer target. Indeed, while cytosolic glycolysis is a major pathway in cancer cells including in the presence of oxygen (the Warburg effect), mitochondria also fulfill the bioenergetic and biosynthetic needs of growing cancer cells [5-7]. While a large variety of substrates including pyruvate, lactate, amino acids and fatty acids can supply the TCA cycle at different stages, they all eventually end up generating NADH and $FADH_2$ that in turn support OXPHOS[8].

Complex I is a promising therapeutic target in the OXPHOS electron transport chain (ETC). Biguanides (*e.g.* metformin, phenylephrine), which have been evaluated for the treatment of diabetes and metabolic disorders, provide a rationale clinical benefit for safely targeting OXPHOS. However, drugs such as metformin targeting Complex I have pharmacological limitations, including insufficient potency, transport-mediated accumulation, and lack of appropriate drug concentrations, which limit their use as a therapeutic agent in oncology[9, 10]. As a traditional ETC toxic agent rotenone limits its use as an antitumor therapeutic agent due to its multiple mechanisms causing cytotoxicity[11]. In recent years, the compounds containing 1,2,3-triazole, 1,2,4-triazole, pyrazole, imidazole and other five-membered nitrogen-containing

heterocyclic moiety, were found to have a direct inhibitory effect on Complex I[5, 12-15], which provided some insight into the research of this project.

The antitumor drug carboxyamidotriazole (CAI), containing a chemical moiety 5-amino-1,2,3-triazole-4-carboxamide, has been used in clinical I-III studies[16, 17]. Initially, its antitumor pharmacological effects were shown to be mediated by the inhibition of non-voltage gated Ca^{2+} channels in non-excitable cells[18]. Other studies found that CAI cause acidification of the culture medium through *in vitro* experiments[19]. Further research revealed that the suppression of Complex I in mitochondrial respiration caused the overexpression of the glycolytic pathway in tumor cells, resulting in the acidification of the medium[12] (**Figure 3-01**).

Mubritinib, which contains 1,2,3-triazole, was initially assumed to be a HER2-targeting tyrosine kinase inhibitor. But it is direct inhibition on mitochondrial respiration Complex I rather than HER2.[20]. Further studies have shown that mubritinib inhibits tumor Complex 1 activity to the extent that it activates AMPK and thus inhibits HER2[21]. Phase I clinical trials of mubritinib against HER2 positive cancers were completed. The drug indicated efficacy against leukemia *in vivo*; nevertheless, the possibility of unpredicted toxicities from off-targeting led to the cessation of future clinical trials. The unpredictable harm caused by off-targeting of the drug should be avoided as much as possible, but it can be another way to discover new targets or new clinical uses. In this case, mubritinib offers insights into the development of Complex I inhibitors (**Figure 3-01**).

BAY 87-2243 is a class of aminoalkyl substituted compounds obtained by high-throughput screening of chemical small molecule libraries[13]. Initially, BAY 87-2243 was found to inhibit the accumulation of HIF-1α and HIF-2α proteins without affecting the expression levels of HIF target genes[13]. Further studies showed that BAY 87-2243 inhibited the activity of mitochondrial

Complex I *in vitro* and *in vivo*, which prevented the ROS mediated inhibition of HIF-1. Due to its excellent performance in preclinical development, however, unexpected adverse events that were not expected in the preclinical studies occurred in the clinical trial, which led to the termination of the clinical trial (*ClinicalTrials.gov:* NCT01297530)[22]. IACS-010759, a structurally similar compound based on BAY 87-2243, was developed as the latest generation of OXPHOS inhibitors with potent Complex I inhibition (OCR IC_{50} = 1.4 nM), minimal effect on normal human cell mitochondria, and acceptable accumulation of glycolytic metabolites due to mitochondrial inhibition[5]. IACS-010759 has entered clinical trials for AML and solid tumors with promising initial results (**Figure 3-01**) (*ClinicalTrials.gov*: NCT02882321 and NCT03291938)[23, 24].

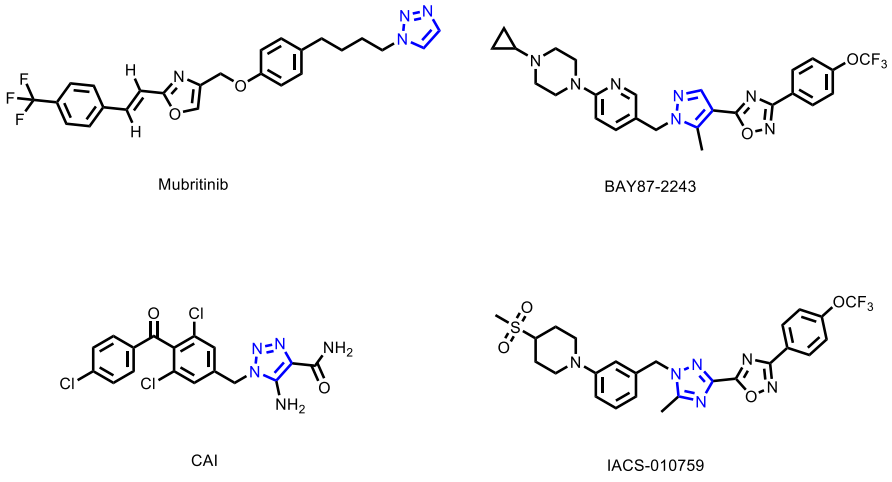

Figure 3-01 Complex I inhibitor

The development of drugs that can block the electron transport of Complex I in tumor cells is currently challenging. Given the intricacy of the size and structure of Complex I while acting as a receptor, it is challenging to acquire high-quality co-crystal structures for the complexes formed by Complex I and inhibitors in the presence of these inhibitors. The design of lead compounds based on Complex I target structures is difficult to realize in short time

available. Optimizing and designing drug molecules based on current preclinical and clinical trials as lead compounds may be a fair approach currently, depending on the situation.

Recent technological developments offered new perspectives to identify compounds able to block OXPHOS Complex I. First, there is the need to track cellular respiration which cannot be easily done with conventional high-throughput methodology. In the last decade, the development of respirometer adapted to handle 96 well plates, the so-called Seahorse technology, has however made available the possibility to measure oxygen consumption rate (OCR) on living cells. Secondly, reduction in OCR will not necessarily lead to cell death since treated cancer cells will shift towards the preferred used of glycolysis. Pyruvate is then reduced into lactate instead of being taken up by mitochondria to generate acetyl-CoA. Measurements of lactate production may thus represent a well-suited primary assay to identify hit compounds that could then be tested for a specific capacity to inhibit OXPHOS.

Another hurdle in the *in vitro* search for Complex I inhibitor is the need to integrate the hypoxic and more oxygenated cancer cell phenotypes that co-exist *in vivo* to have a better understanding of the resulting effects of the potential hits. While hypoxia workstation allows to handle cancer cells under hypoxia, potential metabolic reoxygenation will be rapidly suppressed though the forced low pO_2 imposed in the chamber. On the other hand, mouse tumors do not offer the necessary throughput for the screening of drug candidates. An attractive option consists of the use of 3D cultures of cancer cells such as tumor spheroids wherein hypoxia spontaneously develops at some distance from the periphery[25]. These 3D models actually recapitulate the interdependence between cancer cells with distinct metabolic preferences as we previously reported with symbiotic lactate exchange[26, 27]. The use of spheroids as a drug screening model is still in its infancy but offers other advantages than recapitulating *in vitro* the metabolic heterogeneity observed

in vivo. For the discovery and/or optimization of OXPHOSi, 3D tumor spheroids may indeed provide an additional filter to determine whether physicochemical structures of selected compounds are compatible with their need to go through plasma membranes but also mitochondrial membranes before reaching their target.

In this chapter, the molecular structures of four drugs described above were explored, and it was speculated that the inhibition of Complex I activity may be related to five-membered *N*-heterocyclic fragments such as 1,2,3-triazole, 1,2,4-triazole, and other derivatives of the triazole family. Therefore, we have developed three different types of compounds. The first type of the compounds are the CAI analogues containing 1,2,3-triazole (**Part A**). The second type of compounds are derived from CAI derivatives that have been further modified, primarily by changing the structure of the carboxamide moiety in 1,2,3-triazole-5-amine-4-carboxamide and synthesis of 4-(1,2,4-oxadiazol-5-yl)- 1,2,3-triazol-5-amine derivatives (**Part B**). The third type of compounds are based on the lead compounds IACS-010759 and BAY87-2243, which are designed to include 5-(5-methyl-1,2,4-triazol-3-yl)-1,2,4-oxadiazole moiety of the compounds (**Part C**).

2. Results and discussion

2.1. Part A: CAI analogues containing 5-amine-1,2,3-triazol-4-carboxamide group

2.1.1. Rational design

The compound 5-amino-1-(3,5-dichloro-4-(4-chlorobenzoyl)benzyl)-1H-1,2,3-triazole-4-carboxamide CAI has been reported in the literature to inhibit the mitochondrial Complex I activity of tumor cells, and its pharmacophore is presumed to be 5-amino-1,2,3-triazole-4-carboxamide moiety[12, 20]. However,

most of the literature reported that CAI analogs mainly inhibit tumor cell proliferation without evidence that they work through inhibition of mitochondrial complex I, except for three derivatives reported by Stephenson Z A *et.al.*[20]. Therefore, design, synthesis of CAI derivatives and evaluation of their effects on mitochondrial respiration are of major interest to unravel *bona fide* complex I inhibitors. Here, we developed and synthesized a series of CAI analogs to better understand the structure-activity relationship and took advantage of this approach to implement a procedure of *in vitro* screening to identify new complex I inhibitors.

For the purpose of reverse synthesis analysis, the chemical CAI was divided into three fragments: benzoyl (**I**), disubstituted benzyl (**II**), and triazole (**III**) (**Figure 3-02**). Firstly, we substituted benzoyl for *p*-chlorobenzoyl. Then we studied how linker "X_2" affects activity. Next, we replaced the benzoyl group with a morpholine group, and used methylene to link moiety **I** and moiety **II** (**Figure 3-02 3-001, 3-002**). The distinctions among 3,5-dichlorobenzyl azide, 3,5-difluorobenzyl azide, and 3,5-dimethylbenzyl azide were explored in the disubstituted benzyl moiety (**II**). To explore the effect of substitution on activity, the amino-substituted benzyl azide was also examined. The linker "methylene" or "amide group" was used to connect moiety **I** and moiety **II** (**Figure 3-02 3-001**, **3-003**). In triazole moiety **III**, two types of compounds were mainly prepared by dipolar cyclization reaction with benzyl azide group. The first type is 2-cyanoacetamide, and the second type is propynic acid compounds, such as propargyl amide, propynol and alkynyl acid esters (**Figure 3-02 3-005**).

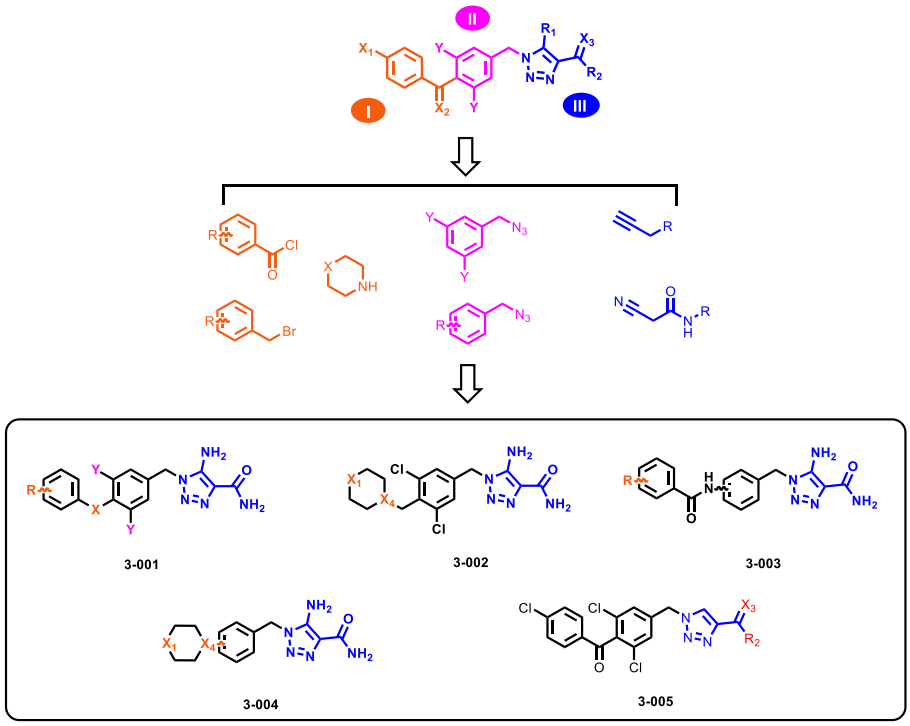

Figure 3-02 design CAI derivatives

2.1.2. Synthesis of CAI derivatives

2.1.2.1. Synthetic strategy of substituting benzyl azide $A_{1\text{-}6}$

CAI derivatives were synthesized mainly by substituting benzyl azide $\mathbf{A_{1\text{-}6}}$ and fragment $\mathbf{B_{1\text{-}2}}$ by regular cyclization methods. We designed six synthetic methods to synthesize substituted benzyl azide compounds $\mathbf{A_{1\text{-}6}}$ (**Scheme 3-01**).

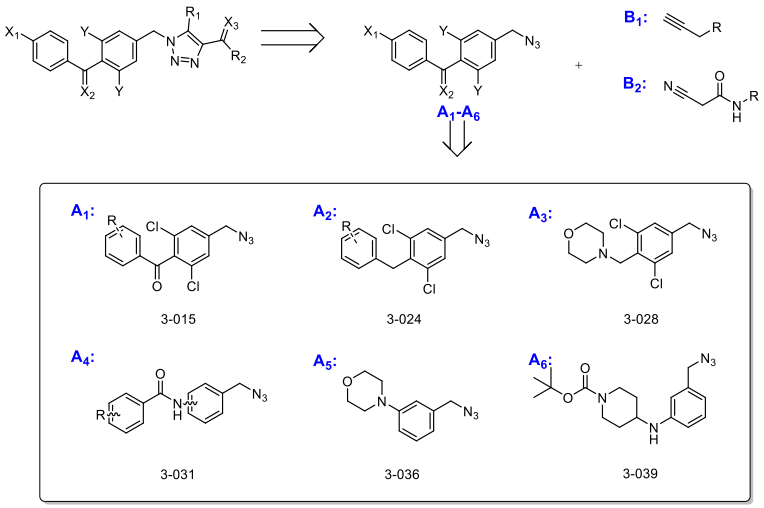

Scheme 3-01 Synthetic scheme for benzyl azide

2.1.2.2. Strategy A_1

The first synthetic strategy was to synthesize different substituted benzoylbenzyl azides compounds. We selected hydrophobic groups *p*- and *m*-methyl-substituted benzoyl, sterically hindered naphthoyl, strongly electron-withdrawing trifluoromethylbenzoyl, trifluoromethoxy benzoyl, methoxy benzoyl, as well as substitution of aromatic rings with cyclohexane and acetyl group.

Using (3,5-dichlorophenyl) methanol (**3-011**) as a starting material, TBSCl was used to protect the hydroxyl group. After regioselective lithiation by treatment with *n*-BuLi, the aryllithium intermediate was trapped by a substituted benzoyl chloride to form the substituted benzophenone. Using TABF or 36% HCl to remove the TBS group, it was found that shorter time and using TBAF to give higher yields (**Table: 3-01**). DPPA (Diphenyl phosphoryazide) was then used with DBU as a base to convert the benzylic alcohols into their corresponding substituted benzoylbenzyl azides [28](**3-015a-i**) in fair to excellent yields (**Scheme 3-02**).

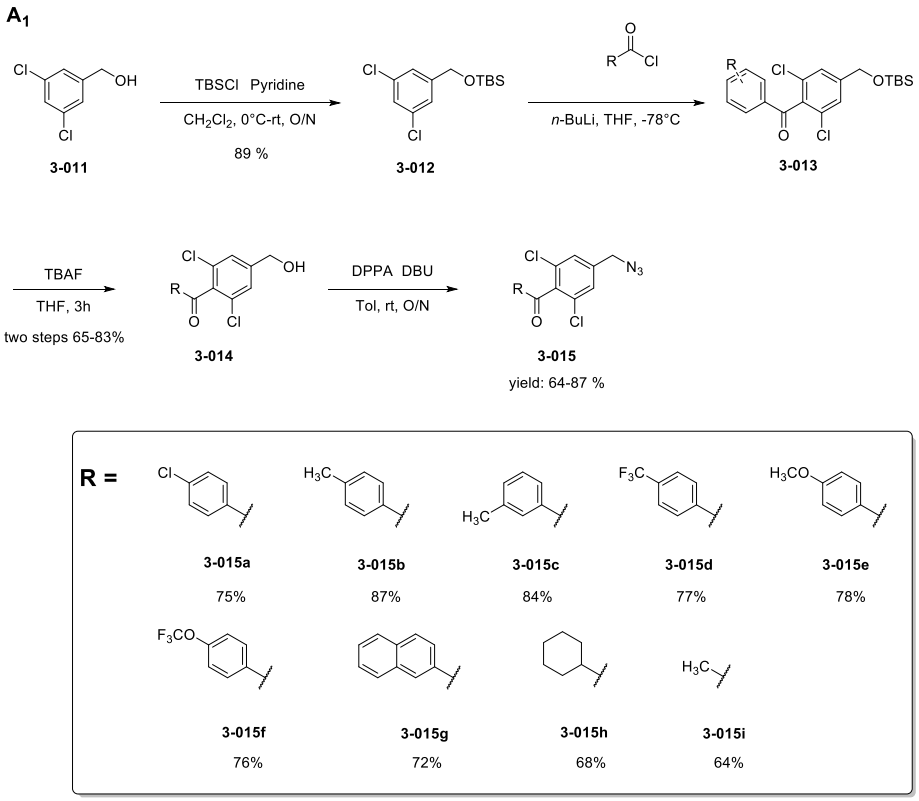

Scheme 3-02. Synthetic route A_1 of benzyl azide

Table 3-01. Optimization of deprotection conditions

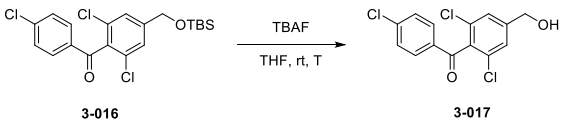

Condition	Time	Yield
TBAF 1eq	2 h	70 %
TBAF 1eq	3 h	81 %
HCl 36% 30eq	3 h	45 %
HCl 36% 30eq	Over night	76 %

2.1.2.3. Strategy A_2

We employed methylene instead of carbonyl to link the two aryl groups in the synthetic sequence for the preparation of the benzyl azide intermediates. Substituted benzyl bromides (**3-021**) were synthesized in three steps. The substituted benzoic acids were firstly esterified *via* a standard Fisher condensation and the resulting esters were reduced by DIBAL-H to produce the desired benzyl alcohols. Finally, bromination was carried out with PBr_3 to give the substituted benzyl bromides in good yields (**3-021**). The following steps of the synthesis were identical to the first synthetic route, giving the substituted 5-(azidomethyl)-2-benzyl-1,3-dichlorobenzene intermediate (**3-024a, b**), with a yield of 71-82 %. (**Scheme 3-03**).

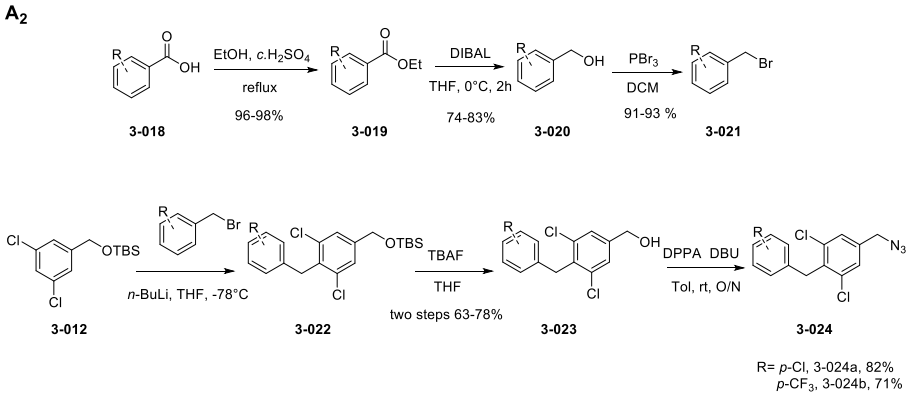

Scheme 3-03. Synthetic route A_2 of benzyl azide

2.1.2.4. Strategy A_3

The third synthetic approach aimed to replace benzoyl with morpholine. Morpholine is a versatile moiety, a privileged pharmacophore and an outstanding heterocyclic motif with wide ranges of pharmacological activities due to different mechanisms of action[29]. We wanted to study if substituting morpholine for benzoyl has an influence on inhibitory activity, and if morpholine increases the stability of drug metabolism[30] and improves the compound's water solubility[29].

The benzyl ether (**3-012**) was synthesized using the Bouveault aldehyde reaction (1- lithiation with *n*-BuLi, 2-quenching with DMF followed by hydrolysis) to form the 2,6-dichlorobenzaldehyde [31](**3-025**), the aldehyde and morpholine were treated with $NaBH(OAc)_3$ to undergo the Borch reductive amination reaction to form **3-026**, which was directly deprotected to give substituted benzyl alcohol[32] (**3-027**) in a 71% yield over the two steps. Finally, the azidation reaction of substituted benzyl alcohol (**3-027**) follows the procedures outlined above to make 4-(4-(azidomethyl)-2,6-dichlorobenzyl) morpholine (**3-028**) (**Scheme 3-04**).

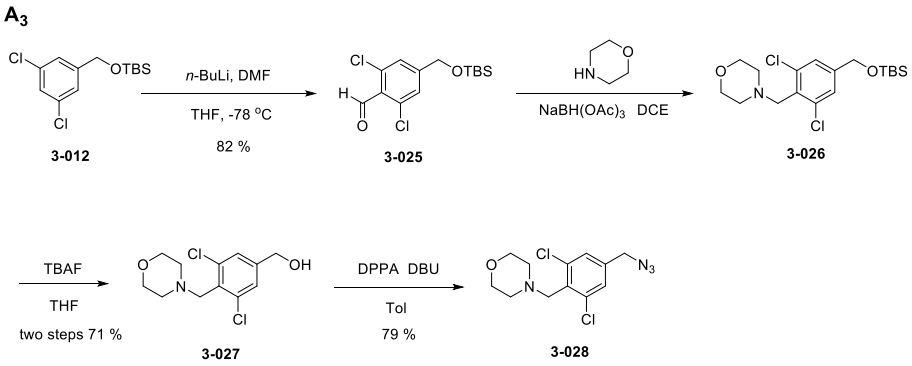

Scheme 3-04 synthetic route A_3 of benzyl azide

2.1.2.5. Strategy A_4

The fourth synthetic approach was devised to produce benzyl azides that had been substituted with *o*-, *m*-, and *p*-benzamides. The benzamides were prepared starting from the corresponding (*o*-, *p*-, *m*-) amino-substituted benzyl alcohols **3-029** and a chosen benzoyl chloride. Controlling the temperature of the reaction system, as well as the slow addition of the acylating agent were necessary to obtain amides in good yields (**3-030**). These were converted to the corresponding azides using DPPA and DBU as previously described to give the benzamides substitute benzyl azide compounds (**3-031**), with a yield of 64-86 %. (**Scheme 3-05**).

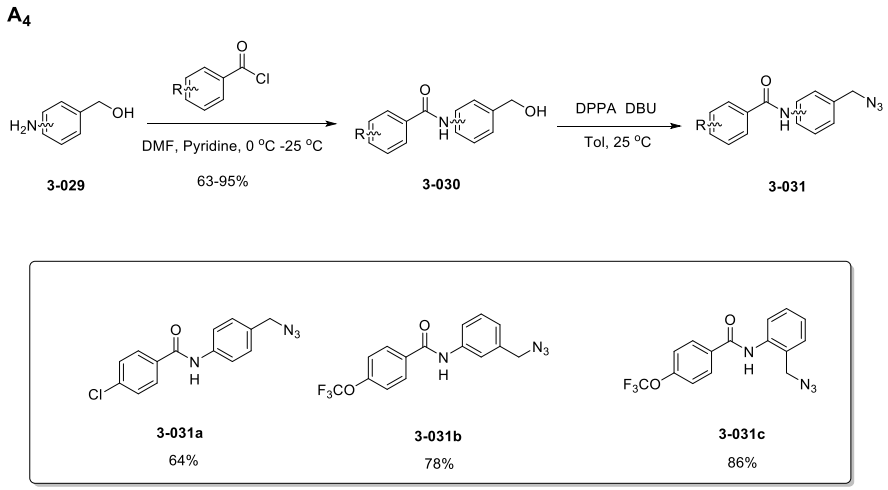

Scheme 3-05 synthetic route A_4 of benzyl azide

2.1.2.6. Strategy A_5

The fifth synthetic approach was to derivatize the third synthetic route even more through the direct coupling of the heterocyclic moiety **I** with the benzyl group **II**, without linker. First, the alcohol was protected by TBS, and the Buchwald-Hartwig reaction was used to couple the bromobenzyl moiety and morpholine to give 4-(3-(((tert-butyldimethylsilyl)oxy)methyl)phenyl) morpholine[33](**3-024**) in a 72 % yield. After removing the hydroxyl protecting group with TBAF, and treatment with the azide reagent DPPA, 4-(3-(azidomethyl)phenyl)morpholine (**3-036**) is produced in a yield of 78% (**Scheme 3-06**). The same procedure was used to synthesize 4-(2-(azidomethyl)phenyl)thiomorpholine (**3-036-1**), with a yield of 61%.

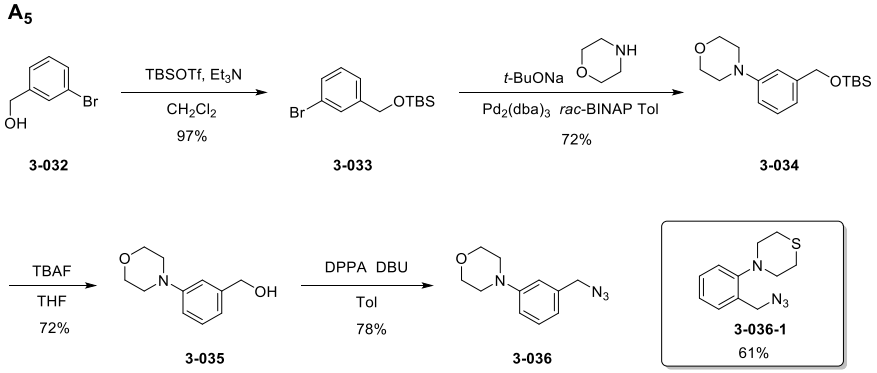

Scheme 3-06 synthetic route A_5 of benzyl azide

2.1.2.7. Strategy A_6

The sixth synthetic route uses "amino" instead of "carbonyl", similarly using the Borch reduction amination reaction to couple the amino and ketone, and replace the alcohol with the benzyl azide moiety to give **3-039** in a 67% yield (**Scheme 3-07**).

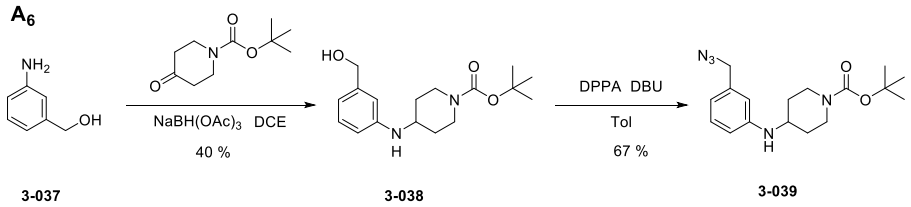

Scheme 3-07 synthetic route A_6 of benzyl azide

2.1.2.8. 1,3-dipolar cycloaddition reaction to give CAI derivatives

Next, the key fragments benzyl azide, *N*-substituted-2-cyanoacetamides and alkynes were prepared by conventional synthetic methods. The 5-amino-4-carboxyamido-1,2,3-triazole derivatives were assembled by a 1,3-dipolar cycloaddition between 2-cyanoacetamide or *N*-substituted 2-cyanoacetamides with the corresponding benzyl azides, using sodium ethoxide as a base, as

reported in the literature, usually with modest yields (**Scheme 3-08** left and **Table 3-02**)[28, 34].

Another series of *N*-substituted 1,2,3-triazoles, lacking the amino group on the 5-position of the heterocycle, were also prepared by Huisgen-Click cycloaddition reaction between a suitable benzyl azide and an alkyne, using the standard copper acetate/sodium ascorbate system as a catalyst[35] (**Scheme 3-08** right and **Table 3-02**). For yields, see the experimental section. Using both reactions, we were able to produce a small library of 29 compounds, including the reference CAI (**3-040**), which were characterized by ^{1}H ,^{13}C-NMR and HRMS, before biological testing.

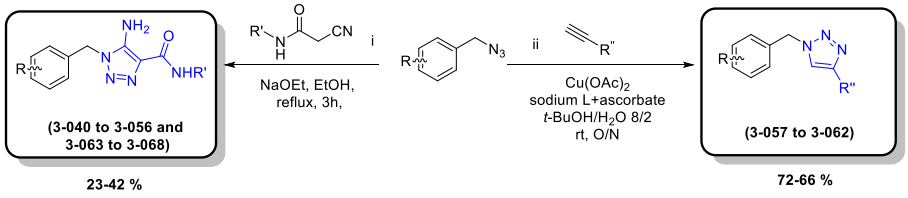

Scheme 3-08 synthetic route of CAI derivatives

Table 3-02 CAI derivatives

No.	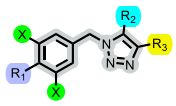				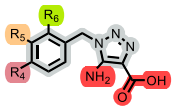		
	X	**R_1**	**R_2**	**R_3**	**R_4**	**R_5**	**R_6**
3-040	-Cl		$-NH_2$	$-CONH_2$	-	-	-
3-041	-Cl		$-NH_2$	$-CONH_2$	-	-	-
3-042	-Cl		$-NH_2$	$-CONH_2$	-	-	-
3-043	-Cl		$-NH_2$	$-CONH_2$	-	-	-

3-044	-Cl	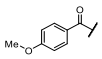	$-NH_2$	$-CONH_2$	-	-	-
3-045	-Cl	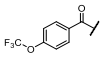	$-NH_2$	$-CONH_2$	-	-	-
3-046	-Cl		$-NH_2$	$-CONH_2$	-	-	-
3-047	-Cl		$-NH_2$	$-CONH_2$	-	-	-
3-048	-Cl		$-NH_2$	$-CONH_2$	-	-	-
3-049	-Cl		$-NH_2$	$-CONH_2$	-	-	-
3-050	-Cl		$-NH_2$	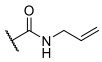	-	-	-
3-051	-Cl		$-NH_2$	$-CONH_2$	-	-	-
3-052	-Cl		$-NH_2$	$-CONH_2$	-	-	-
3-053	-F		$-NH_2$	$-CONH_2$	-	-	-
3-054	-Cl		$-NH_2$	$-CONH_2$	-	-	-
3-055	$-CH_3$	-H	$-NH_2$	$-CONH_2$	-	-	-
3-056	-Cl	-H	$-NH_2$	$-CONH_2$	-	-	-
3-057	-Cl		-H	-COOH	-	-	-
3-058	-Cl		-H	$-CONH_2$	-	-	-
3-059	-Cl		-H	$-CH_2NH_2$	-	-	-
3-060	-Cl		-H	$-COOCH_3$	-	-	-
3-061	-Cl		-H	$-CH_2OH$	-	-	-

3-062	-F		-H	-$CONH_2$	-	-	-
3-063	-	-	-	-		-H	-H
3-064	-	-	-	-	-H	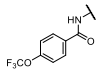	-H
3-065	-	-	-	-	-H	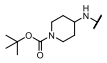	-H
3-066	-	-	-	-	-H		-H
3-067	-	-	-	-	-H	-H	
3-068	-	-	-	-	-H	-H	

2.1.3. *In vitro* biological evaluation

2.1.3.1. Three-step procedure to select for mitochondrial Complex I inhibitors as anticancer drugs

We used a 3-step screening procedure to identify CAI derivatives endowed with the highest capacity to act as Complex I inhibitors in conditions mimicking the *in vivo* tumor microenvironment (**Figure 3-03**). Stimulation of glycolysis upon mitochondrial OXPHOS inhibition is a well-known observation[25, 26], making increase in lactate release an attractive first screening step. Measuring real-time oxygen consumption rate (OCR) may then be used as a secondary assay to identify bona fide Complex I inhibitor (**Figure 3-03**). This requires exposing permeabilized cancer cells to a mixture of pyruvate and malate as an NADH-generating system (fueling Complex I) and then to evaluate the reversibility by adding succinate as a fuel of Complex II[36]. The third step of our screening procedure aimed to test hit compounds in 3D tumor spheroids to recapitulate the tumor organization with the co-existence of both

hypoxic and oxygenated cancer cells (**Figure 3-03**). This 3D cell culture setup is indeed more likely to reveal the impact of drugs with possible bystander effects.

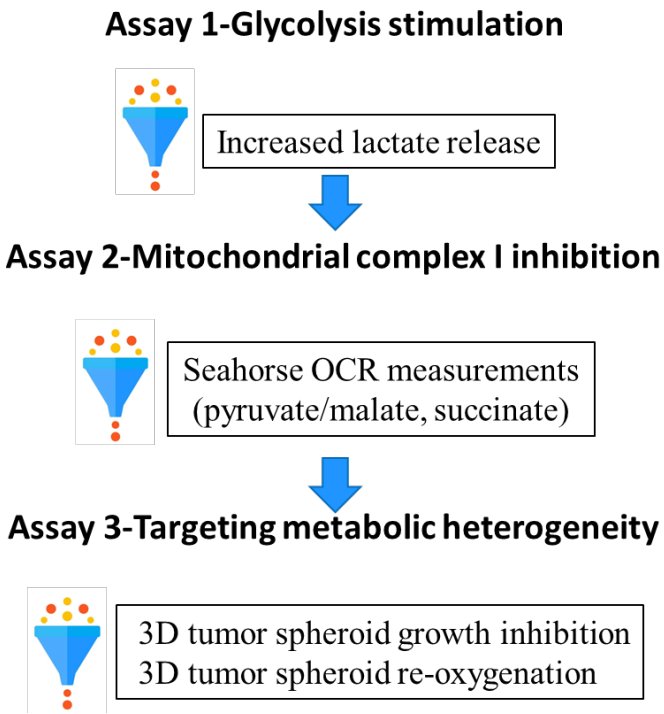

Figure 3-03 Screening process for mitochondrial Complex I inhibitors

2.1.3.2. Lactate release measurement as a primary assay to identify potential OXPHOS inhibitors

As mentioned above, upon pharmacological inhibition of mitochondrial respiration, pyruvate will preferentially be reduced into lactate that will in turn be released in the extracellular medium. Collection of culture medium after 24h exposure to CAI (**3-040**) derivatives and semi-automated measurements of lactate content led us to identify 15 compounds (including **3-040** reference compound) endowed with the capacity to significantly stimulate lactate release from colorectal CT26 cancer cells (**Figure 3-04 A**). Among them, 9

were as active as **3-040**, and 5 were even more potent inducers of lactate release (**3-046**, **3-049, 3-052, 3-053 and 3-060**) (see **Figure 3-04 A and Table 3-03**). Similar results were obtained in breast cancer 4T1 cancer cells when comparing the lactate-inducing effects of **3-040** compound with **3-060** compound identified as more potent and lactate non-inducer compound at (**Figure 3-04 B**). Of note, we used 4T1 and CT26 cancer cells because these cancer cells are of mouse origin and may therefore be used to induce tumors in immunocompetent (syngeneic) mice thereby offering the possibility to use them in *in vivo* models more appropriate to explore the systemic impact of drugs interfering with the metabolism. Indeed, to generate tumors in mice from human cancer cells requires the use of nude mice which do not have lymphocytes and may thus fail to reveal the beneficial or detrimental effects of systemically administered OXPHOS inhibitors. These two cell lines can also form 3D organoids (see below).

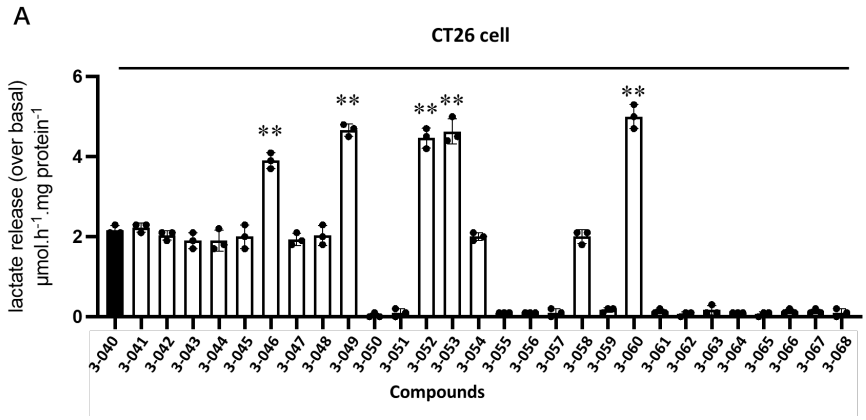

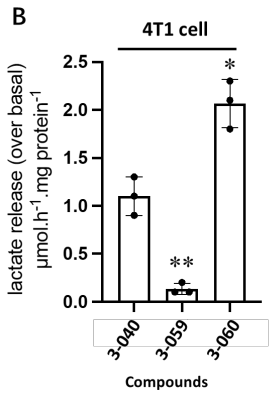

Figure 3-04. Compound-induced lactate release. Culture medium was collected after 24h exposure to the indicated compounds and lactate content was determined in a semi-automated manner. Bar graph depicts the extent of lactate secretion above the basal release as determined in the absence of any compound (**P<0.01 for increased lactate release *vs.* reference compound **3-040**).

2.1.3.3. Validation of Complex I inhibitors using Seahorse-based OCR measurements

To establish a direct link between induction of lactate release and the capacity of CAI derivatives to inhibit Complex I, we then used the Seahorse technology that measures real-time oxygen consumption rate (OCR) from label-free cancer cells in a 96-well plate format.

Figure 3-05A depicts how the mitochondrial tricarboxylic acid (TCA) cycle provides NADH and $FADH_2$ to the electron transport chain. NADH transfers electrons to Complex I while $FADH_2$ transfers electrons to Complex II of the electron transport chain where in fine O_2 acts as the final acceptor (complex IV) and the proton pump (complex V) catalyzes the production of ATP. Therefore, OCR as monitored by the Seahorse XF analyzer, may be used to determine the effects of different substrates and specific inhibitors. A shosn in **Figure 3-05B**, pyruvate and malate can for instance be used to provide NADH to the complex I while succinate can support the production of FADH2 to fuel the complex II. Therefore, any drug exhibiting a reduction in OCR in the

presence of malate and pyruvate but the effects of which are reversed by succinate represents a *bona fide* complex I inhibitor.

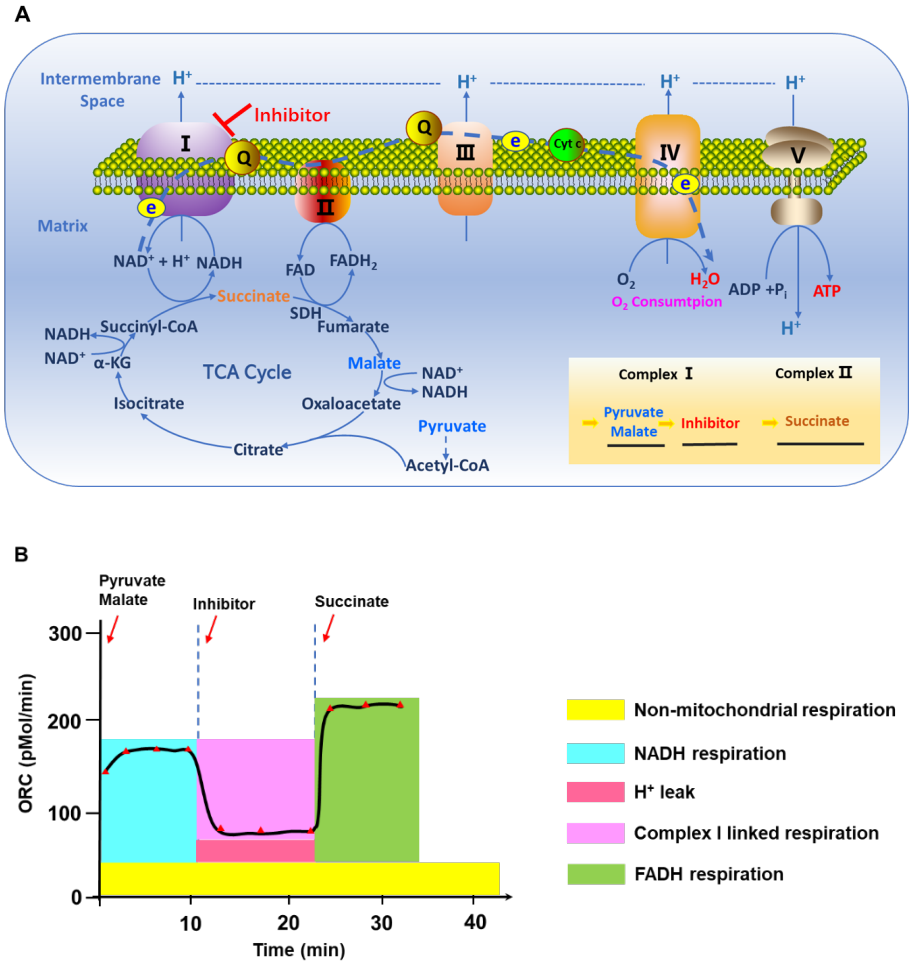

Figure 3-05 A. Scheme depicting how NADH and FADH2 generated by the TCA cycle fuel the mitochondrial electron transport chain. **B.** Profile of OCR measurements upon succesive addition of malata/pyruvate, inhibitory compound and succinate to identify complex I inhibitors using the Seahorse technology

Using the protocol described above (*i.e.*, sequential addition of pyruvate and malate, compounds and succinate), we first compared the behavior of compound **3-040** at 10, 100 and 1000 nM with the well described mitochondrial Complex I inhibitor IACS-010759 currently under clinical

investigation[5]. We found that OCR reduction in permeabilized colorectal CT26 cancer cells was detectable at 1 μM and was maximal at 10 μM (*i.e.*, the same extent of maximal inhibition as obtained with IACS-010759) (**Figures 3-06**).

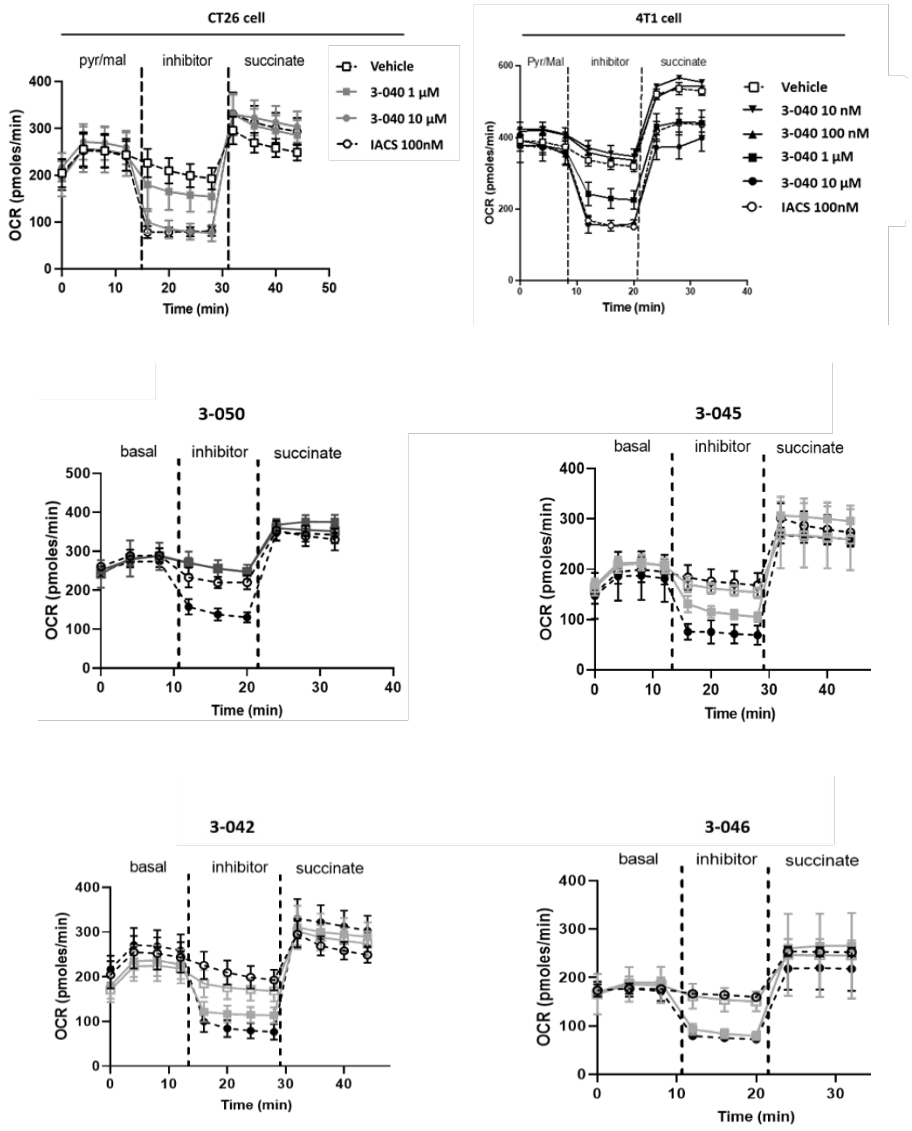

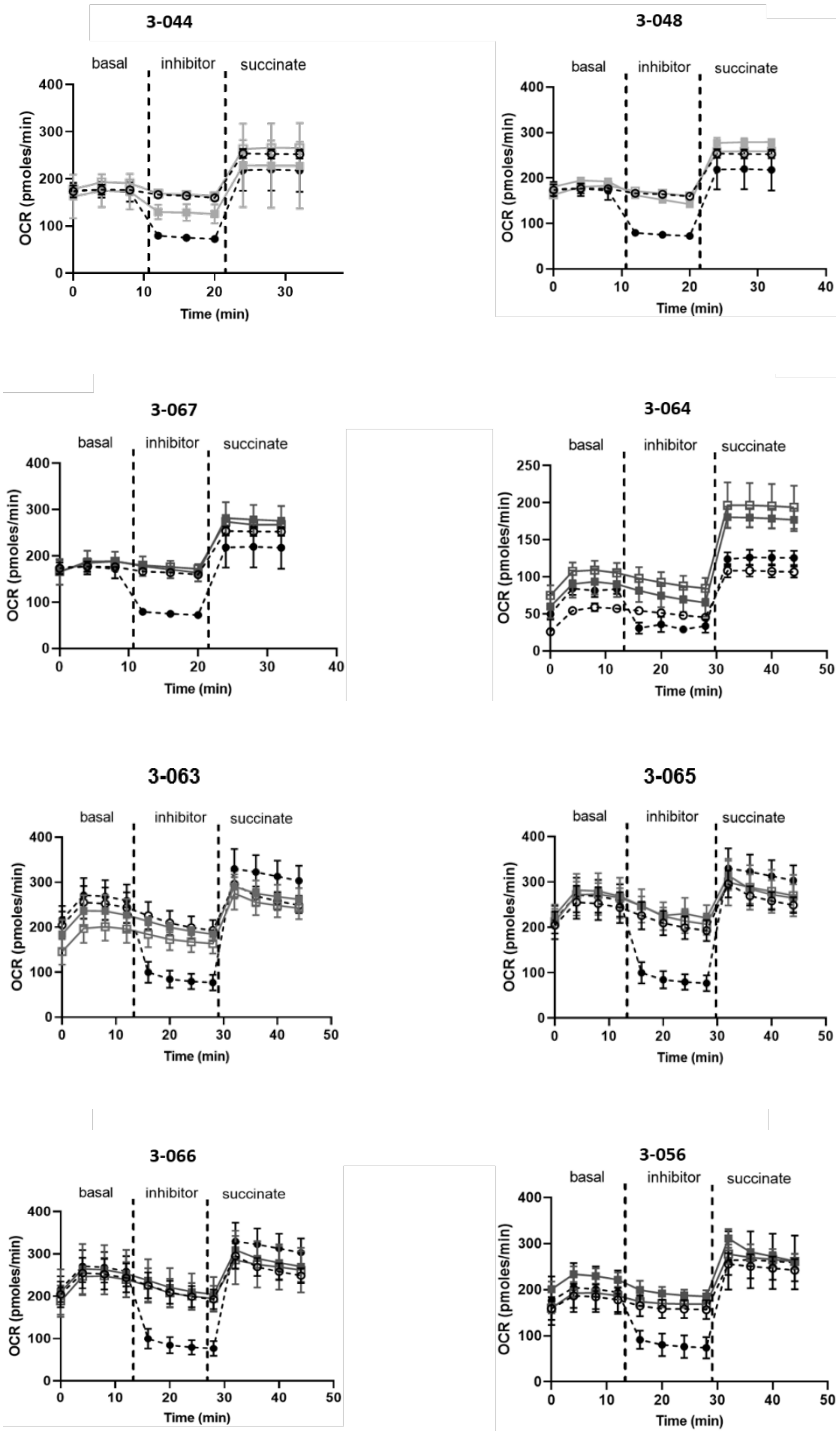
3-044
basal
inhibitor
succinate
OCR (pmoles/min)
Time (min)
3-048
basal
inhibitor
succinate
OCR (pmoles/min)
Time (min)
3-067
basal
inhibitor
succinate
OCR (pmoles/min)
Time (min)
3-064
basal
inhibitor
succinate
OCR (pmoles/min)
Time (min)
3-063
basal
inhibitor
succinate
OCR (pmoles/min)
Time (min)
3-065
basal
inhibitor
succinate
OCR (pmoles/min)
Time (min)
3-066
basal
inhibitor
succinate
OCR (pmoles/min)
Time (min)
3-056
basal
inhibitor
succinate
OCR (pmoles/min)
Time (min)

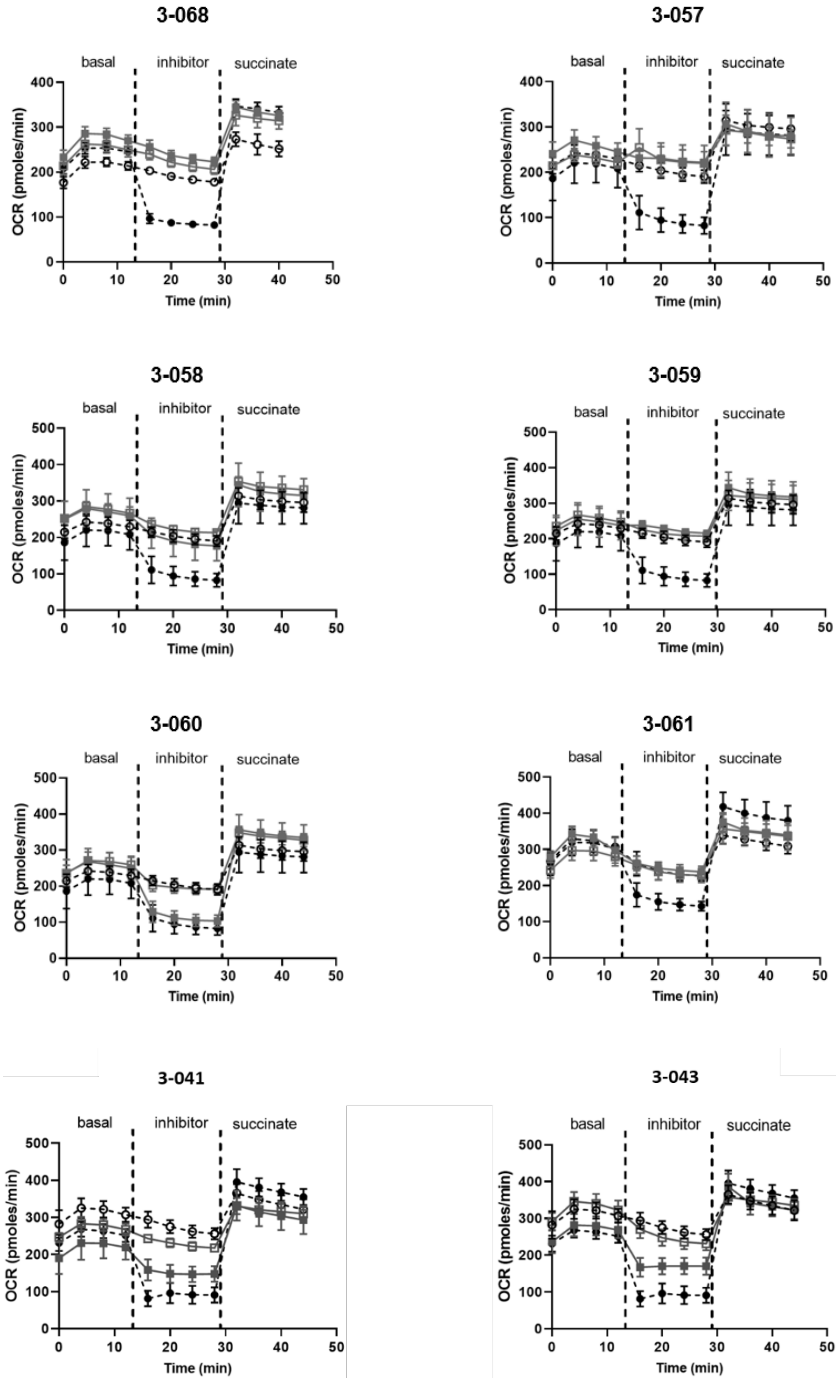
3-068
basal
inhibitor
succinate
OCR (pmoles/min)
Time (min)
3-057
basal
inhibitor
succinate
OCR (pmoles/min)
Time (min)
3-058
basal
inhibitor
succinate
OCR (pmoles/min)
Time (min)
3-059
basal
inhibitor
succinate
OCR (pmoles/min)
Time (min)
3-060
basal
inhibitor
succinate
OCR (pmoles/min)
Time (min)
3-061
basal
inhibitor
succinate
OCR (pmoles/min)
Time (min)
3-041
basal
inhibitor
succinate
OCR (pmoles/min)
Time (min)
3-043
basal
inhibitor
succinate
OCR (pmoles/min)
Time (min)

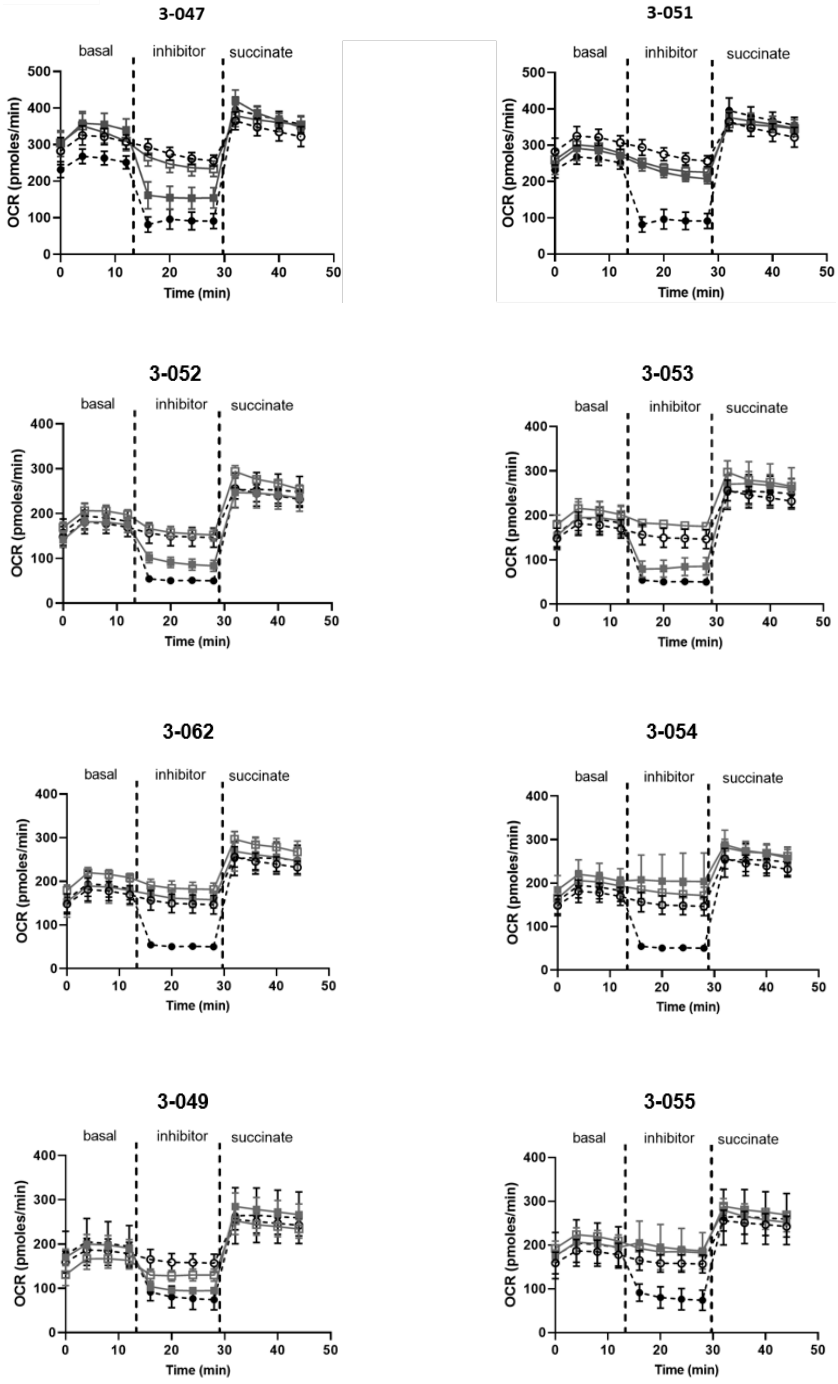

Figure 3-06 Mitochondrial Complex I activity inhibition for Seahorse technology OCR analysis. Graphs depict changes in O_2 consumption rate (OCR) measured with the Seahorse

technology on permeabilized CT26 cancer cells upon successive addition of pyruvate/malate, the indicated inhibitor and succinate. OXPHOS complex I inhibitor IACS was used as a control in the experiments testing reference compound **3-040**, and compound **3-040** (10μM) was used as reference for testing the other derivatives (1 and 10 μM).

In our hands, the Seahorse technology requires to work with 6 replicates per condition. To use it as a screening procedure with a reasonable throughput, we restricted the testing of CAI derivatives at two concentrations (1 and 10 μM). Although the goal of the primary assay was to reduce the list of compounds of interest to those inducing an increase in lactate secretion, we have here tested all the compounds to identify possible false negative hits. Out of the evaluated 28 CAI derivatives, different patterns of activity were observed (see representative patterns of equiactive (**3-060**), hypoactive (**3-047**) and inactive compounds (**3-059**) (**Figures 3-06**). Three hits were identified to be equiactive with **3-040** with an IC_{50} below 10 μM, namely **3-046**, **3-049** and **3-060** (see also **Table 3-03**). Eight other compounds (**3-041, 3-042, 3-043, 3-044, 3-045, 3-047, 3-052** and **3-053**) inhibited Complex I activity to a smaller extent than **3-040** with an IC_{50} around 10 μM (*i.e.*, the highest concentration tested) (**Table 3-03**). All the other compounds did not significantly inhibited Complex I activity (**Table 3-03**). This secondary assay did not identify false negative compounds and actually confirmed 12 compounds out of the 15 hits identified thanks to the primary assay; only compounds **3-048**, **3-054** and **3-058** were able to promote lactate release but did not show significant inhibition of Complex I even at 10 μM (**Table 3-03**). Similar results were obtained in permeabilized breast cancer 4T1 cancer cells (**Figures 3-06**).

2.1.3.4. Validation of the cytotoxic and radiosensitizing potentials of CAI derivatives

The third and last step of our screening procedure aimed to further gain in knowledge of the most appropriate compound to be used in future *in vivo* evaluation. For this purpose, we evaluated in tumor-mimicking 3D spheroids made of the same cells as used above (*i.e.* 4T1 and CT26) the cytotoxicity of

the above 3 hit compounds (**3-046**, **3-049** and **3-060)** and the 2 hypoactive compounds with however a higher capacity to induce lactate release (**3-052** and **3-053**). The profile of spheroid growth reveals that compounds **3-049** and **3-052** were more active than reference compound **3-040** (**Figure 3-07 A**); compounds **3-046** and **3-053** inhibited spheroid growth to the same extent as compound **3-040**, and compound **3-060** exhibited significantly lesser growth inhibitory effects than compound **3-040** (**Figure 5A**). We also took advantage of 3D tumor spheroids to evaluate whether they could radiosensitize tumors. O_2 is indeed known to stabilize the damages to DNA induced by ionizing radiations and thereby to induce irreversible lesions. In the presence of hypoxia (*i.e.* below 10 mm Hg O_2), radiotherapy is thus less efficient so that OXPHOS inhibitors by blocking O_2 consumption can spare O_2 and restore a response to radiotherapy. When a 6 Gy irradiation was administered, a further reduction in spheroid growth was obtained for each tested compound (**Figure 3-07 B**). Interestingly, compounds **3-049** and **3-052** showed a net reduction in the spheroid size indicating a significant contribution of cell death to the reduced growth (**Figure 3-07 B**).

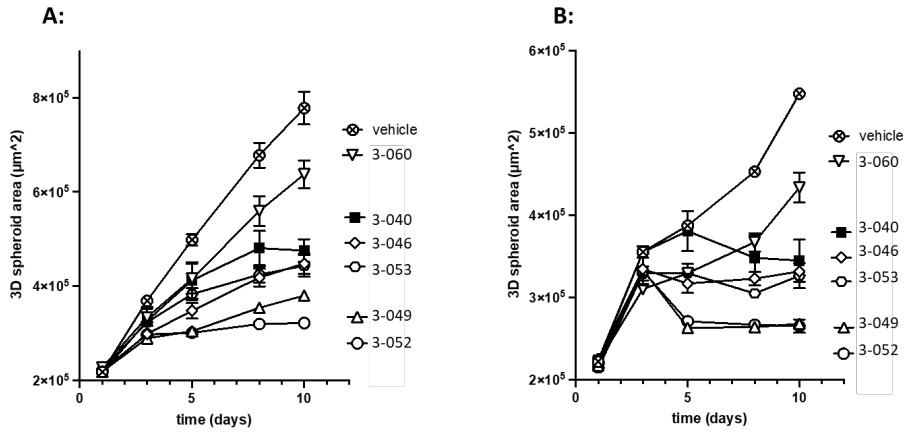

Figure 3-07 Inhibition of 3D tumor spheroid growth (Assay #3). Graphs depict (**A.**) the direct growth inhibitory effects of the indicated compouns and (**B.**) their capacity to exert radiosensitizing effects as determined using 3D tumor spheroids.

To further prove the radiosensitizing effects, spheroids treated with compounds **3-040, 3-049** and **3-052** were dissociated and collected cells were plated to grow for 14 days. This assay revealed that cancer cell exposed to both irradiation and compounds **3-049** and **3-052** exhibited a much lesser ability to grow, suggesting that the extent of catastrophic mitosis was significantly higher than with reference compound **3-040** (**Figure 3-08 A**). Finally, to document the expected re-oxygenation, spheroids treated with compounds **3-040, 3-049** and **3-052** were exposed to the hypoxia probe pimonidazole. While pimonidazole labelled the core of untreated spheroids, immunofluorescence staining confirmed that **3-049** and **3-052** compounds reduced hypoxia to a larger extent than compound **3-040** (**Figure 3-08 B**).

A:

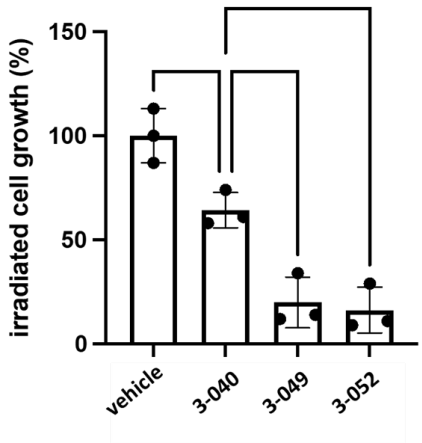

B:

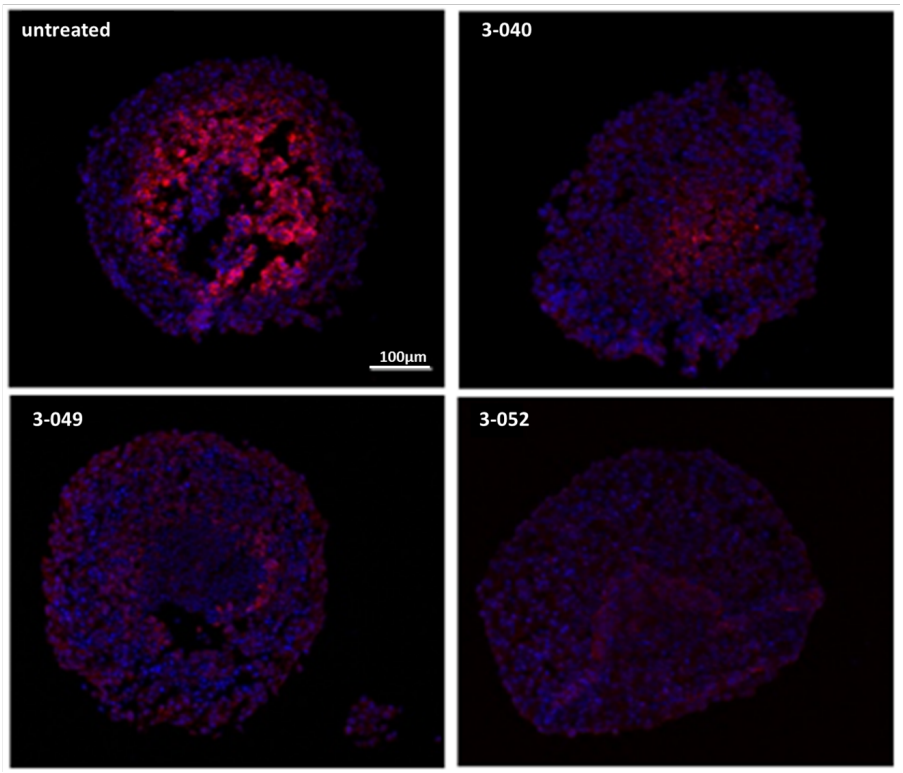

Figure 3-08 radiosensitizing effects of selected Complex I inhibitors. A. Extent of surviving cancer cells post-exposure to radiotherapy and the indicated compounds. **B.** Reduction in the hypoxic fraction of 3D spheroids (as determined upon pimonidazole staining) exposed for 24 hours to the indicated compounds.

2.1.3.5. Evaluation of CAI derivative activity

The inhibitory activity of mitochondrial oxidative phosphorylation complex I was evaluated using a three-step screening methodology based on the above 28 CAI derivatives and the positive control CAI (**3-040**). We display all the results in the form of **table 3-03**. Assays include stimulation of lactate release (assay #1), mitochondrial Complex I inhibition (assay #2) and 3D tumor spheroids growth inhibitory effects (assay #3).

Table 3-03 Evaluation of CAI derivative activity

Compounds	**Assay #1**	**Assay #2**	**Assay #3**
	LAC stim.	OCR inhib.	3D growth inhib.
3-040	**(+)**	**(+++)**	**(+)**
3-041	**(+)**	**(+)**	n.d.
3-042	**(+)**	**(+)**	n.d.
3-043	**(+)**	**(+)**	n.d.
3-044	**(+)**	**(+)**	n.d.
3-045	**(+)**	**(+)**	n.d.
3-046	**(+++)**	**(+++)**	**(+)**
3-047	**(+)**	**(+)**	n.d.
3-048	**(+)**	0	n.d.
3-049	**(+++)**	**(+++)**	**(++)**
3-050	0	0	n.d.
3-051	0	0	n.d.
3-052	**(+++)**	**(+)**	**(++)**
3-053	**(+++)**	**(+)**	**(+)**

3-054	**(+)**	0	n.d.
3-055	0	0	n.d.
3-056	0	0	n.d.
3-057	0	0	n.d.
3-058	**(+)**	0	n.d.
3-059	0	0	n.d.
3-060	**(+++)**	**(+++)**	0
3-061	0	0	n.d.
3-062	0	0	n.d.
3-063	0	0	n.d.
3-064	0	0	n.d.
3-065	0	0	n.d.
3-066	0	0	n.d.
3-067	0	0	n.d.
3-068	0	0	n.d.

The extent of activity is depicted as follows: (+++)- strong of activity, (+)-moderate of activity and (0)-lack of activity and (n.d.) = non determined.

2.1.4. Discussion

In this study, we synthesized derivatives of a drug already reported to exert OXPHOS inhibitory effects (*i.e.* CAI **3-040**) and used our assays to optimize hit development. In pharmacological activity testing，we have documented the feasibility to screen in 96-well plate format for compounds endowed with the capacity to inhibit mitochondrial Complex I and to be further selected to efficiently reach their targets in 3D organized cancer cells. Classical cytotoxic assays cannot be used to identify OXPHOSi including Complex I inhibitors, from a classical *in vitro* screening campaign since the metabolic plasticity of cancer cells offers them the possibility to rapidly adapt to inhibition of cell respiration. The method described here aims to be used for mid- to high-throughput screening of banks of compounds. Remarkably, a primary assay exploring the induction of lactate release as a direct response to respiration inhibition led us to identify 13 out of 28 derivatives deprived of this capacity. Importantly, these 13 compounds also failed to show Complex I inhibitory activity proving the validity of the procedure while 12 out of the remaining 15 inducers of lactate release were further validated as Complex I inhibitors in our secondary assay. These results indicate the value of the pre-screening primary assay since measurements of lactate can be carried out in volume as low as 10µl. We used here a semi-automated approach but a robotic plate handler could easily convert this simplistic assay in a fully automated strategy. It should also be emphasized that the same equipment may measure glucose content in the extracellular medium. Glucose concentration evolves in mirror to lactate concentration upon stimulation of glycolysis so that measurements of the two parameters could offer a yet more robust primary assay. Simultaneous measurement of glucose consumption could also discriminate OXPHOSi from cytotoxic drugs which may increase extracellular lactate concentration without consumption of glucose (because of the release of internal lactate pool upon alterations in plasma membrane integrity).

While induction of lactate release can be used to restrict a list of hits endowed with OXPHOS inhibitory activity, the nature of the drug-dependent mitochondrial dysfunction may vary. We recently reported that the blockade of the mitochondrial transport of pyruvate led to a progressive shift toward glycolysis and the associated increase in lactate release[25]. Inhibiting the activity of TCA cycle enzymes could also reduce mitochondrial activity without directly impacting OXPHOS. The reversibility of the inhibition by the addition of the metabolite acting downstream of the inhibition is therefore critical. Here, we measured O_2 consumption upon consecutive addition of a NADH-generating system (i.e. a mixture of pyruvate and malate) to fuel Complex I and succinate to fuel Complex II and thus reverse the potential inhibitory effects of compounds on Complex I.

Our ternary assay evaluating the efficacy of compounds identified as Complex I inhibitors on 3D tumor spheroids proved the interest of 3D structures to further select hits for future developments. First, this assay led to uncover a limited growth inhibitory effects for compounds **3-046** and **3-060** despite their identification in the top 3 compounds based on the induction of lactate release and the inhibition of Complex I. By contrast, compound **3-052** identified as a Complex I inhibitor with an intermediary potency showed a strong inhibitory activity on spheroid growth. The compound **3-049** was actually the only compound exhibiting the highest activity in the three assays of our protocol and could be considered as a lead compound for further development. The above conclusions actually fit our findings related to the radio-sensitizing potential of compounds **3-046** and **3-060** which showed the more profound inhibition of cancer cell regrowth post-irradiation. This finding was further supported by a larger reduction in hypoxic fractions than that obtained with reference compound **3-040**.

2.1.4.1. Preliminary structure-activity relationship analysis (SARA)

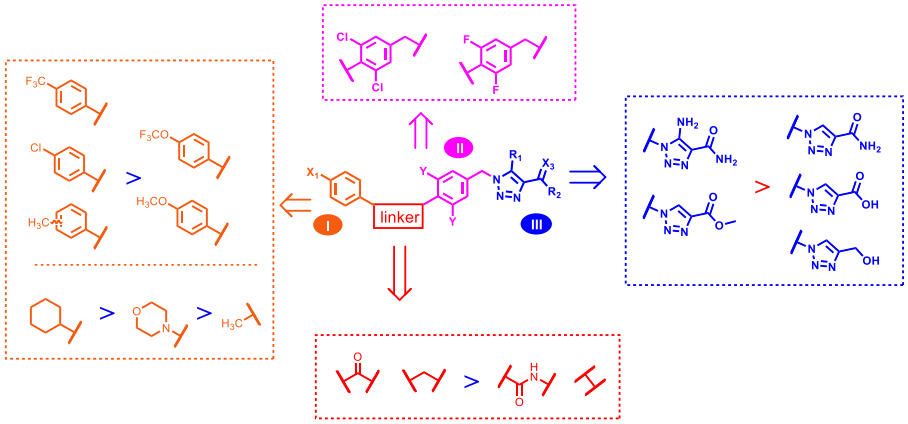

Figure 3-09 Preliminary summary of SAR studies on the target compounds

Based on the results for the inhibitory activity of the compounds against mitochondrial complex I, a brief structure- activity relationship analysis of the 28 derivatives was carried out (**Figure 3-09**).

In moiety **I**, the aromatic group is important to maintain the inhibitory activity; aromatic rings containing hydrophobic substituents are more active (**3-040**, **3-042**, **3-043**, **3-046**, **3-052** > **3-044**. **3-045**). The large sterically hindered naphthyl group did not significantly alter the activity (**3-047**). In the non-aromatic ring system, the cyclohexane substitution is more active than the morpholine group supporting the need of a hydrophobic structure for the maintenance of activity (**3-049** > **3-048**). As for the linker part, the "carbonyl" and "methylene" between moiety I and moiety II show superiority. In moiety **II**, the substitution of "-F" and "-Cl" in benzene ring maintains inhibitory activity (**3-040** to **3-049** and **3-053**). In the moiety **III** of the pharmacophore, the 5-amino-1,2,3-triazole-4-carboxamide fragment is particularly important for maintaining the pharmacological activity (**3-041** to **3-049**, **3-052** and **3-053**). The activity is reduced by removing the "5-amino" (**3-040** > **3-058**). Finally, when we examined the effects of "carboxyl, hydroxyl and amino"

groups instead of the “carboxamide” group, we observed a loss of the activity (**3-057**, **3-059**, **3-061**). However, upon change of the “carboxamide” by a methyl ester (**3-060**), the activity was larger than control **3-040** (**Figure 3-09**).

2.2. Part B : CAI derivatives containing 1,2,3-triazol-5-amine group

2.2.1. Rational design

The second type of compounds are derivatives of the first type of compounds. They are based on the complex I inhibitors CAI, BAY87-2243 and IACS-010759 as lead compounds. The goal was to change the carboxamide group in the CAI derivative 1,2,3-triazole-4-carboxamide group (**Figure 3-10 3-006**, **3-007**, **3-008, 3-009**). We directly grafted the 3-phenyl-1,2,4-oxadiazole group from BAY87-2243 and IACS-010759 to the carboxamide group of CAI.

The second type of compound mainly contains four fragments, substituted benzoyl or nitrogen-containing heterocycle (**I**), substituted benzyl (**II**), 4-(1,2,4-oxadiazol-5-yl)-1,2,3-triazol-5-amine or 5-amino-1,2,3-triazole-4-carboxamide (**III**), substituted phenyl (**IV**). The moiety **I** and **II** are generally similar to the first type of compounds, including piperidine and pyrrolidine moieties. 3-(4-(trifluoromethoxy) phenyl) -1,2,4-oxadiazole group, which is included in both compounds BAY87-2243 and IACS-010759, is attempted to integrate into moiety **III** and **IV** (**Figure 3-10 3-006**, **3-008, 3-009**). Another type of chemical is the carboxamide group of 5-amino-1,2,3-triazole-4-carboxamide moiety **III** to further derive the **3-007** type compounds (**Figure 3-10**). Then use seahorse technology to evaluate the compounds inhibitory efficacy on tumor cell oxidative phosphorylation complex I.

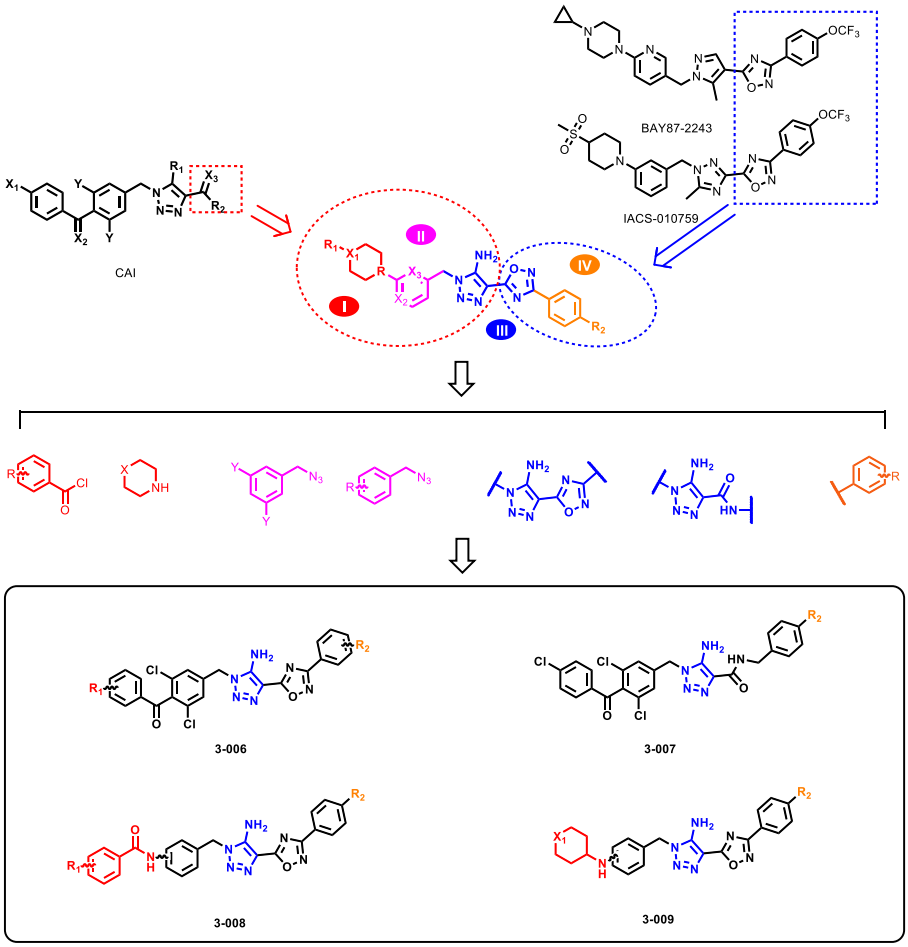

Figure 3-10 Part B Complex I inhibitor design

2.2.2. Synthesis of 1,2,3-triazol-5-amine derivatives

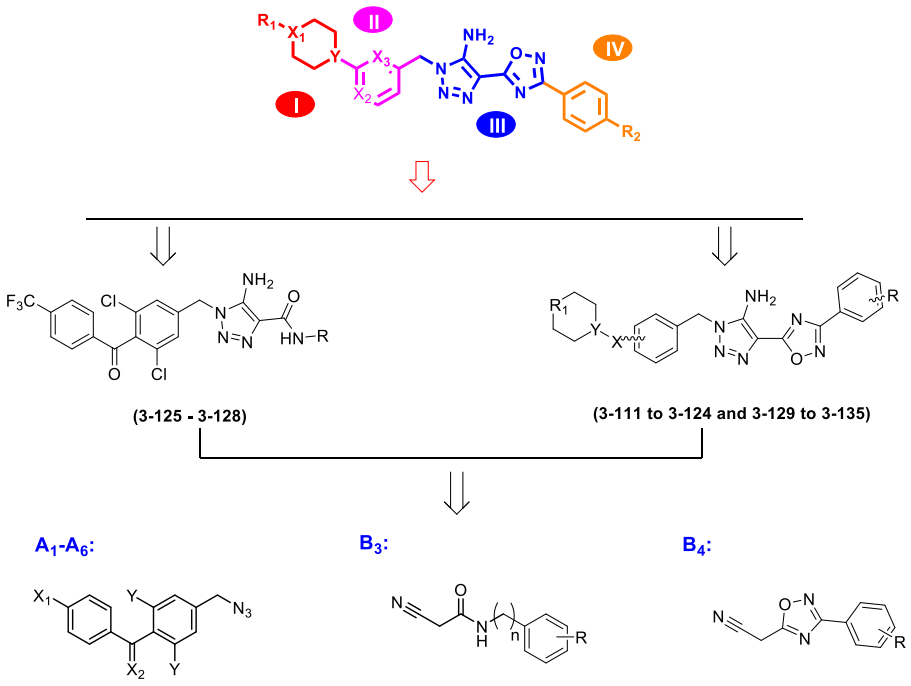

Scheme 3-09 synthetic scheme of 1,2,3-triazol-5-amine derivatives

To achieve the desired counterpart of the Complex I inhibitor, we synthesized the appropriate fragment, followed by coupling or cycling the fragment to obtain the desired compounds. The synthesis of fragments **I** and **II** are carried out in the same way as the synthesis of the benzyl azide intermediate of the CAI analogue described earlier. And the synthesis of moiety **III**, **IV** are given obtained by the following two methods (**Scheme 3-09 $B_{3\text{-}4}$**).

2.2.2.1. Synthetic strategy of benzyl-2-cyanoacetamide or 2-(3-phenyl-1,2,4-oxadiazol-5-yl) acetonitrile $B_{3\text{-}4}$

The moiety *N*-substituted-2-cyanoacetamides was synthesized in two steps, starting with the acid catalyzed cyclization of 2-cyanoacetylhydrazine and acetylacetonate to form **3-070**, followed by the nucleophilic substitution of benzylamine and **3-070** to obtain *N*-substituted-2-cyanoacetamides (**3-071**), in a good yield (**Scheme 3-10 B_3**). The intermediate 2-(3-phenyl-1,2,4-

oxadiazol-5-yl) acetonitrile was synthesized from aromatic aldehydes (**3-072**) and hydroxylamine hydrochloride under base conditions to form oximes (**3-072**). Under reflux conditions [$RuCl_2$ (*p*-cymene)]$_2$ catalyzes the dehydration of oxime to form nitrile[37] (**3-074**), in a yield for 74-82 %, which is further treated with hydroxylamine hydrochloride under $NaHCO_3$ to give amine oxime (**3-075**). Next amine oxime condensed with 3-(3,5-dimethyl-1*H*-pyrazol-1-yl)-3-oxopropanenitrile to synthesize compound 2-(3-phenyl-1,2,4-oxadiazol-5-yl) acetonitrile [34](**3-076**), in a good yield (**Scheme 3-10 B$_4$**).

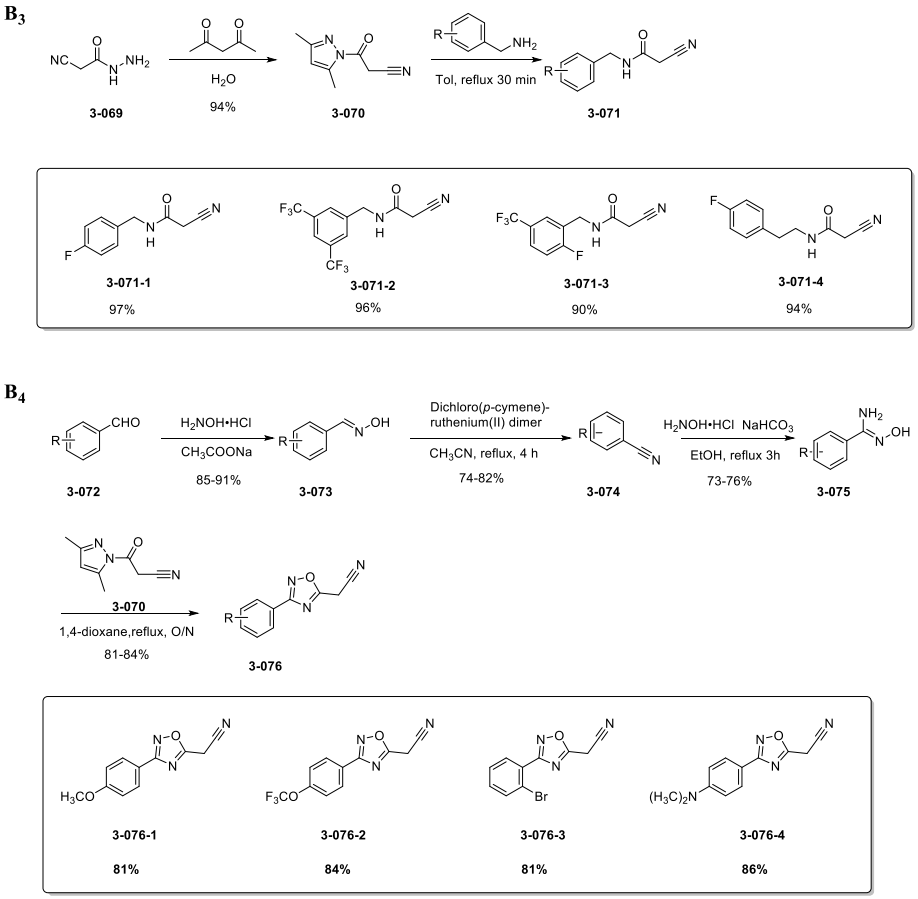

Scheme 3-10 synthetic route of moiety B (B$_3$-B$_4$)

2.2.2.2. 1,3-dipolar cycloaddition reaction to give 1,2,3-triazol-5-amine derivatives

The final products are produced by 1,3-dipolar cycloaddition of α-cyanoamide or α-cyanooxadiazole with benzyl azide in the strong base to give the target compound [34](**3-111** to **3-135**) in fair to excellent yields (**Scheme 3-11** and **Table 3-04**). For yields, see the experimental section.

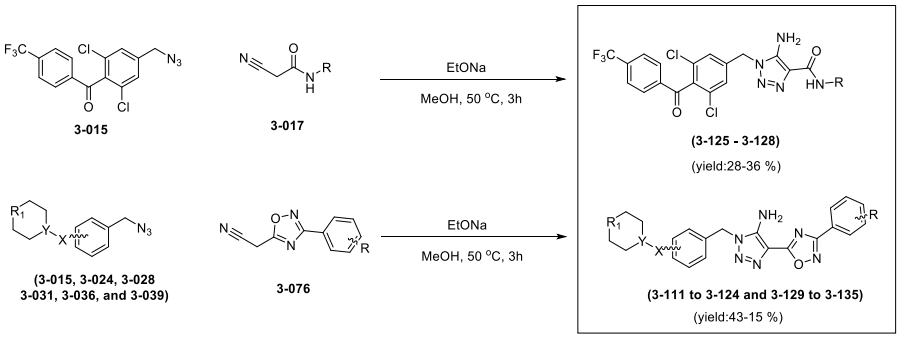

Scheme 3-11 synthetic route of 1,2,3-triazol-5-amine derivatives

Table 3-04 the structure of 1,2,3-triazol-5-amine derivatives

NO.	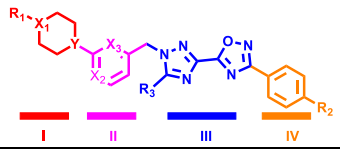			
	I	II	III	IV
3-111	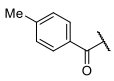		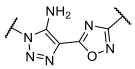	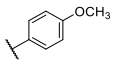
3-112	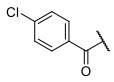		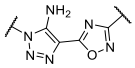	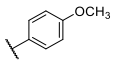
3-113	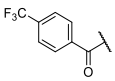		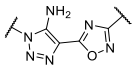	
3-114	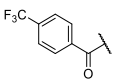		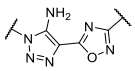	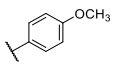

3-115	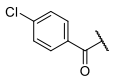		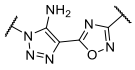	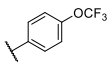
3-116	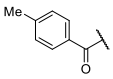		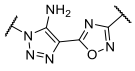	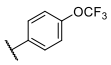
3-117	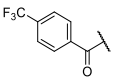		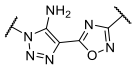	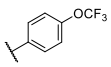
3-118	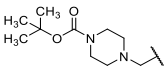		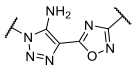	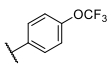
3-119	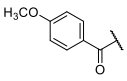		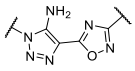	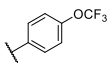
3-120			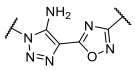	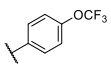
3-121			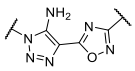	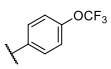
3-122			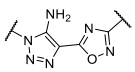	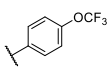
3-123			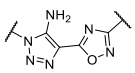	
3-124			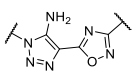	
3-125				
3-126				

3-127	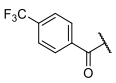			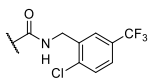
3-128	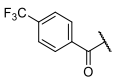			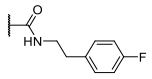
3-129			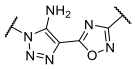	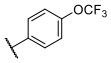
3-130			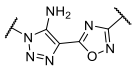	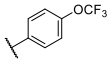
3-131	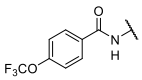		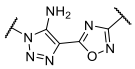	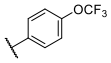
3-132	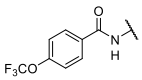		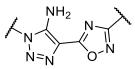	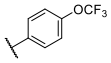
3-133	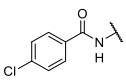		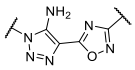	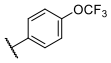
3-134	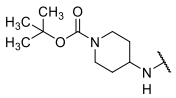		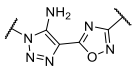	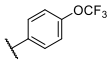
3-135	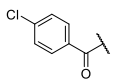		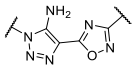	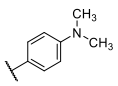

2.2.3. Biological evaluation

Similarly, 25 CAI derivatives containing 1,2,3-triazol-5-amine group and the positive control IACS-010759 and **4-040** using Seahorse technology were analyzed. At 10, 100, 1000 nM and 10, 100 μM inhibitor doses, the oxygen consumption rate (OCR) was analyzed as detailed in **part A** (assay #2).

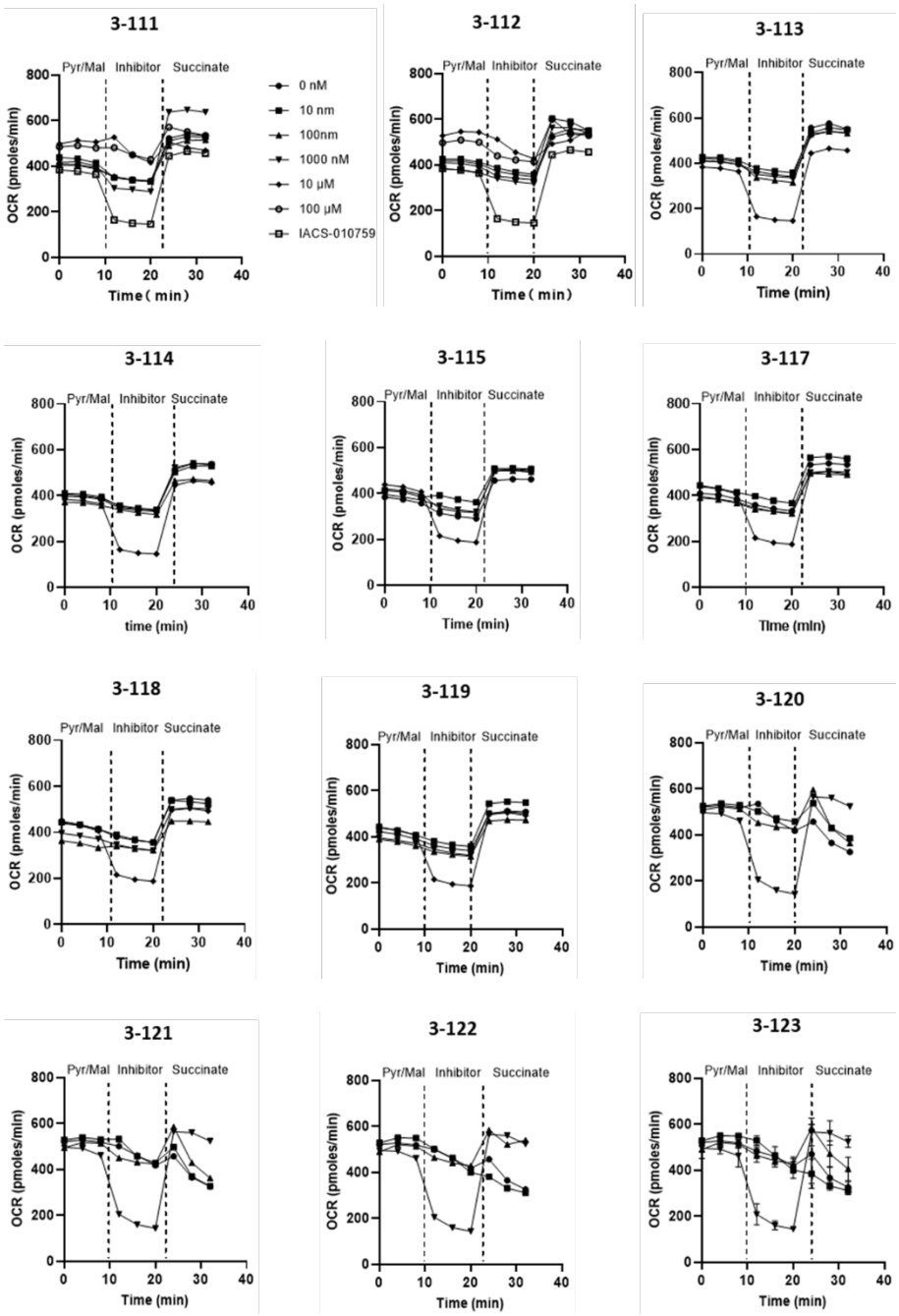
3-111
Pyr/Mal Inhibitor Succinate
OCR (pmoles/min)
Time (min)
0 nM
10 nm
100nm
1000 nM
10 µM
100 µM
IACS-010759
3-112
Pyr/Mal Inhibitor Succinate
OCR (pmoles/min)
Time (min)
3-113
Pyr/Mal Inhibitor Succinate
OCR (pmoles/min)
Time (min)
3-114
Pyr/Mal Inhibitor Succinate
OCR (pmoles/min)
time (min)
3-115
Pyr/Mal Inhibitor Succinate
OCR (pmoles/min)
Time (min)
3-117
Pyr/Mal Inhibitor Succinate
OCR (pmoles/min)
Time (min)
3-118
Pyr/Mal Inhibitor Succinate
OCR (pmoles/min)
Time (min)
3-119
Pyr/Mal Inhibitor Succinate
OCR (pmoles/min)
Time (min)
3-120
Pyr/Mal Inhibitor Succinate
OCR (pmoles/min)
Time (min)
3-121
Pyr/Mal Inhibitor Succinate
OCR (pmoles/min)
Time (min)
3-122
Pyr/Mal Inhibitor Succinate
OCR (pmoles/min)
Time (min)
3-123
Pyr/Mal Inhibitor Succinate
OCR (pmoles/min)
Time (min)

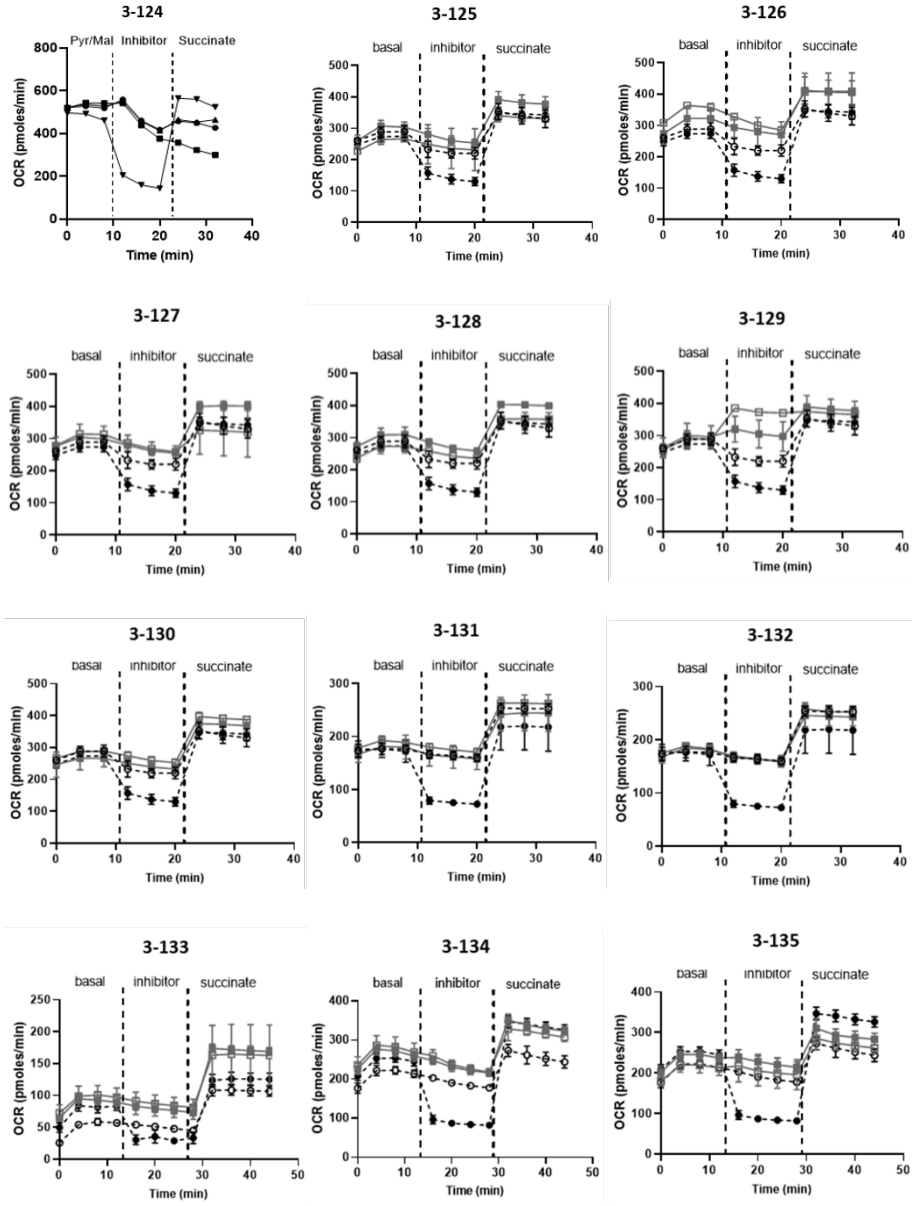

Figure 3-11 Mitochondrial Complex I activity inhibition for Seahorse technology OCR analysis.

Unfortunately, we did not hit any compounds (**Figure 3-11**). As there were no hits on the mitochondrial complex I, we did not perform further *in vitro* cellular experiments.

2.2.4. Discussion

The Seahorse-based measurements of OCR revealed that compounds corresponding to the second design scheme did not exhibit inhibitory activity on mitochondria complex I. This strongly suggest that the carboxamide group in the structure of 1,2,3-triazol-5-amine-carboxamide is necessary to support mitochondrial complex I inhibitory activity. The limited literature dealing with the design and synthesis of inhibitors of mitochondrial complex I in tumor cells led us to speculate about a rationale to explain these results. Accordingly, direct grafting of two fragments from CAI and IACS-010759 is likely to alter the respective conformation of active groups. Indeed, the moiety I of compound CAI is a hydrophobic junction which is beneficial for activity, and the moiety I of compound IACS-010759 is a hydrophilic junction which is also beneficial for activity. Thus, one may postulate that direct grafting of the two parts may lead to a loss of activity. It could potentially be related to the amino group substitution position in the 1,2,3-triazol-5-amine structure or the triazole heterocycle, according to structural study of the compounds BAY87-2243 and IACS-010759.

Next, we design and synthesize **Part C** in order to better understand why the **Part B** is no inhibitory activity on mitochondria complex I (**Part C** see below).

2.3. Part C: Aminoalkyl substituted compounds containing 5-(5-methyl-1,2,4-triazol-3-yl)-1,2,4-oxadiazole group

2.3.1. Rational design

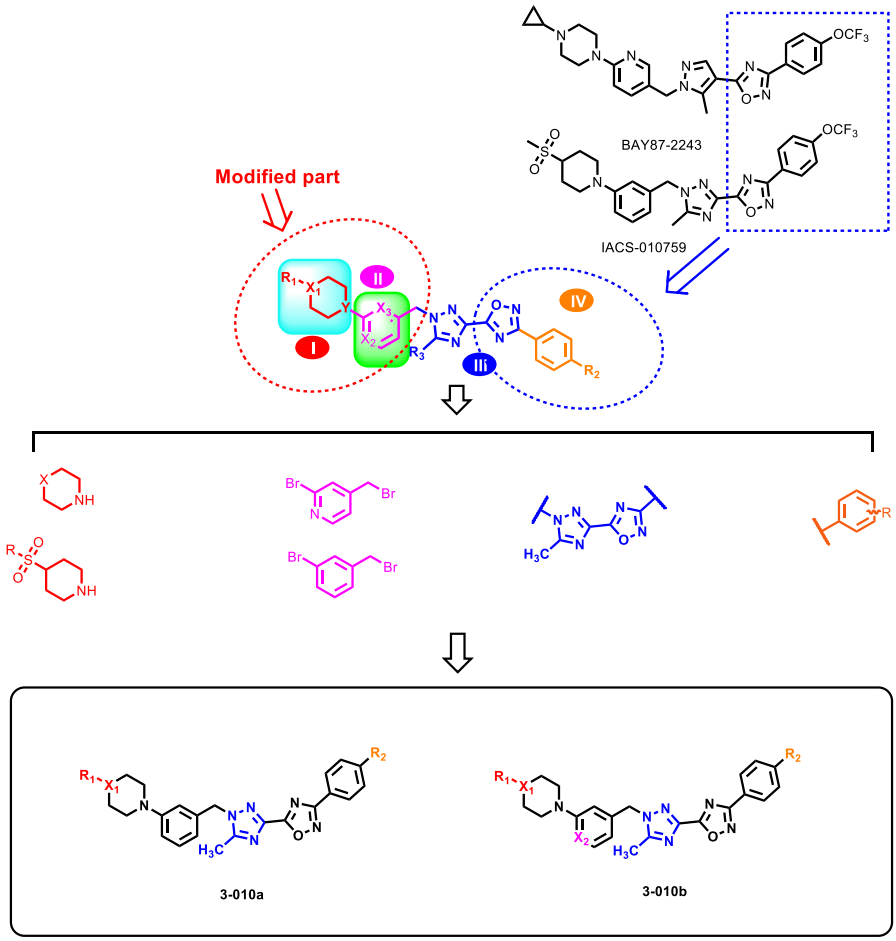

Figure 3-12 design Complex I inhibitor

Since we did not find any inhibitory activity against Complex I for the second type of compounds (**part B**), we next though that the methyl group in 5-methyl-1,2,4-triazole moiety could have lost its activity due to amino group substitution. In **part C**, we therefore synthesized derivatives with the core structure of 5-(5-methyl-1,2,4-triazol-3-yl)-1,2,4-oxadiazole to avoid

changing the overall conformation of the molecule, and we studied the substitution and modification of moiety **I** and moiety **II**.

Based on the chemical structures of compounds BAY87-2243 and IACS-010759, we designed the third type of compounds. Similarly, the third type of compounds can be divided into four main parts. Moiety **I** is a heterocyclic containing nitrogen and sulfur. Moiety **II**, which uses *m*-bromine substituted benzyl and attempted to replace the benzene with a pyridine. Moiety **III**, 5-(5-methyl-1,2,4-triazol-3-yl)-1,2,4-oxadiazole. Moiety **IV**, 4-(trifluoro-methoxy) phenyl. (**Figure 3-12 3-010ab**)

2.3.2. Synthesis of 5-(5-methyl-1,2,4-triazol-3-yl)-1,2,4-oxadiazole derivatives

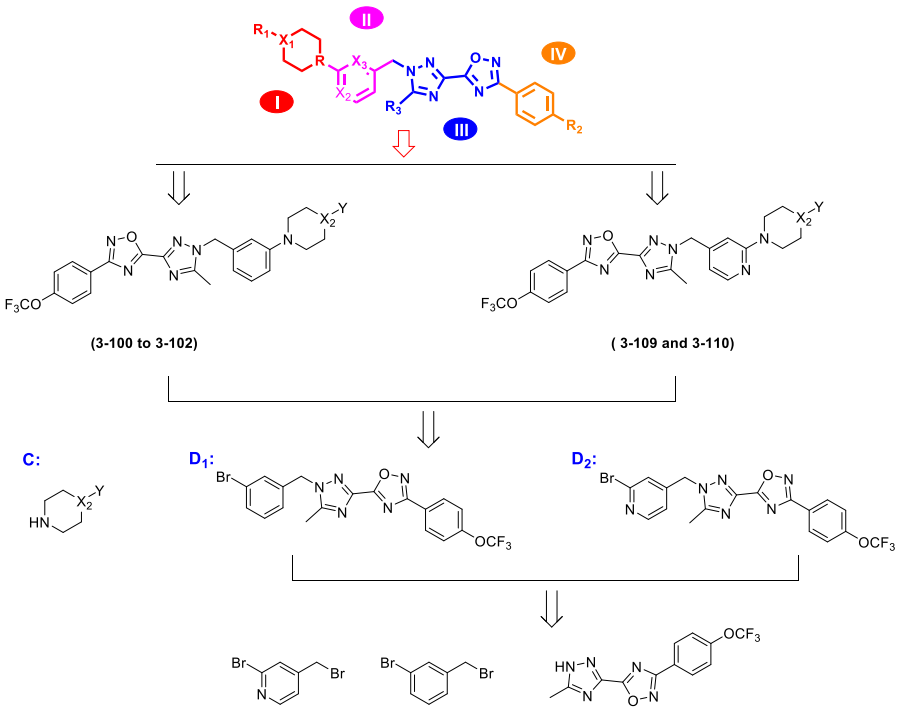

Scheme 3-12 Synthetic route of 5-(5-methyl-1,2,4-triazol-3-yl)-1,2,4-oxadiazole derivatives

In moiety **I**, we used analogues to replace 4-(methylsulfonyl)piperidine. and in particular we examined the effects of 4-(ethylsulfonyl)piperidine, 1-(methylsulfonyl)piperazine, thiomorpholine 1,1-dioxide, thiomorpholine substitution on the inhibitory activity of complex I. In the substituent part, methylsulfonyl being a hydrophilic group, we kept a hydrophilic sulfide group in the design.

To prepare the sulphur moiety **I**, we designed three synthetic schemes. The nucleophile reagent sodium ethylthiolate attacked *tert*-butyl 4-bromopiperidine-1-carboxylate (**3-079**) to form a thioether[38](**3-080**), which was oxidized by *m*-CPBA and treated with HCl to give 4-(ethylsulphonyl) piperidine (**3-082**) in a good yield (**Scheme 3-13**, **C1**). Then mono-*N*-protected piperazine was reacted with mesyl chloride and finally treated with TFA to removal the -Boc group, giving 1-(methylsulfonyl)piperazine (**3-086**) in a 85% yield (**Scheme 3-13**, **C2**). Finally, the *N*-protected thiomorpholine was oxidized with *m*-CPBA and then deprotected with TFA to give thiomorpholine-1,1-dioxide (**3-090**) in an 82% yield (**Scheme 3-13**, **C3**).

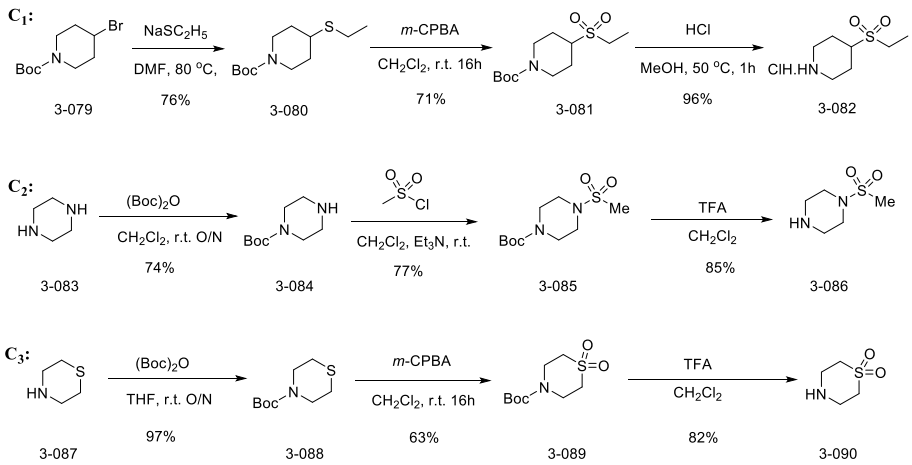

Scheme 3-13 synthetic route of sulfur moiety $C_{1\text{-}3}$

To synthesize aminoalkyl substituted compounds (**3-100**, **3-101**, **3-102**, **3-109** and **3-110**) are show and follow reported procedures[5, 14, 39] (**Scheme 3-14 and Scheme 3-15**). The amine oxime (**3-092)** was synthesized as described above using *p*-trifluoromethoxybenzaldehyde as a starting material. The reaction of amine oxime with ethyl oxalyl chloride gives oxadiazole (**3-093)** in an 82% yield. The exchange of hydrazine with the ester gives **3-094**, the reaction of hydrazide with acetamidine gives **3-095**, and the cyclization of **3-095** at high temperature to form triazole **3-096** in a 42 % yield for the three steps. Under base K_2CO_3, **3-096** reacts with 3-bromobenzyl bromide (**3-097**) to form the two compounds **3-098** and **3-099**, the yields were 29% and 47%, and the main product **3-099** was used in the next step. In the next step, palladium-catalyzed Buchwald-Hartwig cross-coupling of **3-099** with moiety **I** (**3-082 or3-090**) generates the final products **3-100**, **3-101** and **3-102**, in the yields of 8-11% (**Scheme 3-14**).

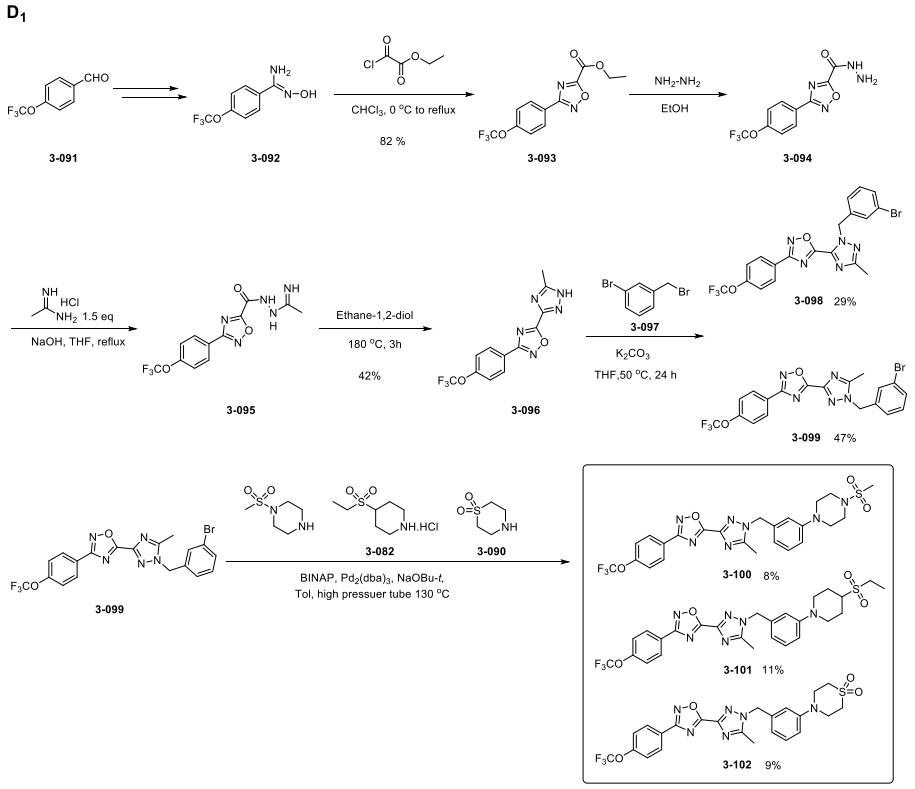

Scheme 3-14 synthetic route of 5-(5-methyl-1,2,4-triazol-3-yl)-1,2,4-oxadiazole derivatives D1

Moreover, we have optimized the conditions for the Buchwald-Hartwig amination reaction. The ligand RuPhos was employed in the literatures[5, 14], but BINAP was used in our experiments instead, showing a direct impact on the reaction yield. When the reaction time was appropriately extended under sealed tube and high temperature conditions, the yield was discovered to be slightly improved (**Table 3-05**). It's also possible that some of the products were lost owing to the interaction with the silica gel during the purifying process.

Table 3-05 optimization of reaction conditions

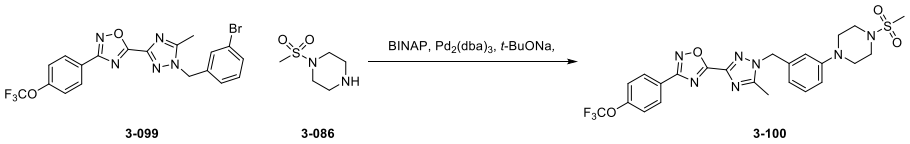

3-099 3-086 3-100

Entry	Condition	Solvent	Temperature	Time	Yield
1	General	THF	reflux	18h	<5%
2	Sealed tube	THF	90 °C	18h	<5%
3	Sealed tube	THF	90 °C	36h	6%
4	General	Tol	reflux	18h	<5%
5	Sealed tube	Tol	130 °C	36h	8%

The benzene ring is the most prevalent ring system in drugs and can act as a pharmacophore or possibly a scaffolding part of the drug. In moiety **II**, the benzene ring may primarily serve as a scaffold for drugs linked to moiety **I** and moiety **III**. Here we use the bioisosteric pyridine heterocycle substitution of the benzene ring, hoping to optimize its physicochemical parameters such as increasing the polarity of the compound, that is, increasing its solubility[40].

The starting material, 2-chloroisonicotinic acid (**3-103**) was treated by esterification, reduction and bromination to give 4-(bromomethyl)-2-chloropyridine (**3-106**) in a good yield. Intermediates **3-107** was synthesized in the same way as described above. Direct coupling of **3-107** and moiety **C** at high temperature under base condition to give final products **3-109** and **3-110**[39] (**Scheme 3-15**), with yields of 36% and 14%.

D2

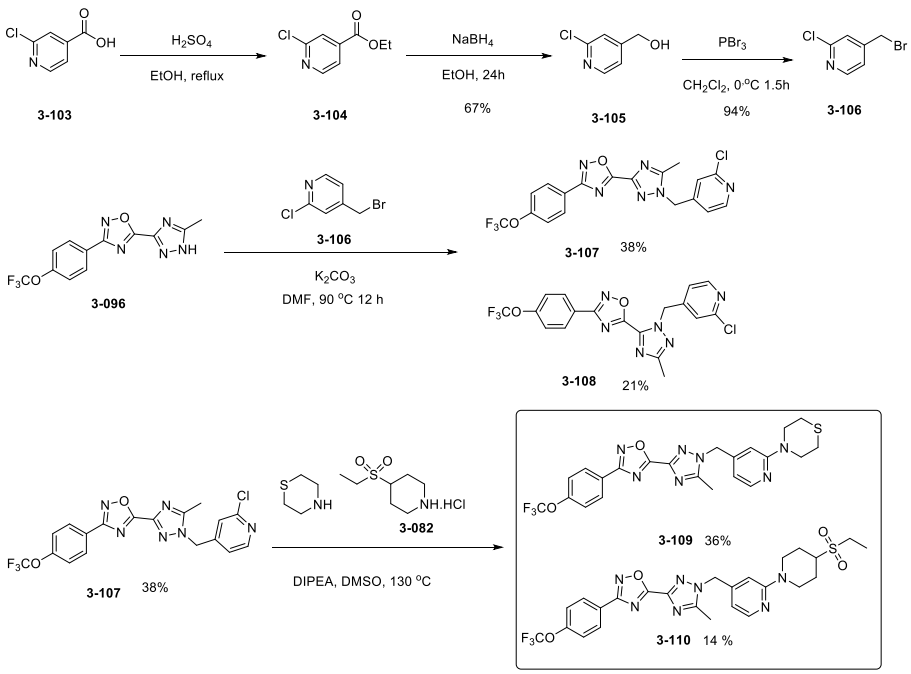

Scheme 3-15 synthetic route of 5-(5-methyl-1,2,4-triazol-3-yl)-1,2,4-oxadiazole derivatives D2

Table 3-06 Potential Complex I inhibitor of 5-(5-methyl-1,2,4-triazol-3-yl)-1,2,4-oxadiazole derivatives

NO.	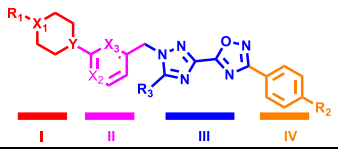			
	I	II	III	IV
3-100	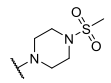		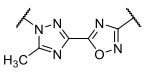	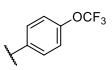
3-101	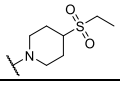		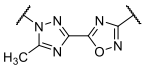	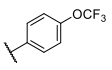

3-102			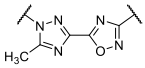	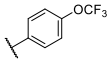
3-109			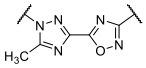	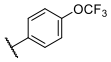
3-110	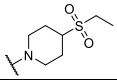		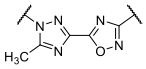	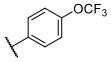

2.3.3. Biological evaluation

Five aminoalkyl substituted compounds and the positive control IACS-010759 using Seahorse technology were analyzed. At 100 nM doses, the oxygen consumption rate (OCR) was analyzed as detailed in **part A** (assay #2).

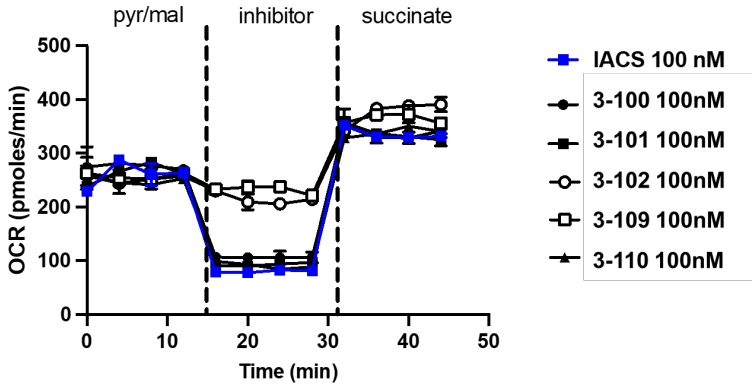

Figure 3-13 Mitochondrial Complex I activity inhibition for Seahorse technology OCR analysis.

The results showed that compounds **3-100**, **3-101**, and **3-110** had mitochondria Complex I inhibitory activity, but compounds **3-102** and **3-109** was not detected. Due to time restrictions, we only employed a 100nM inhibitor concentration and did not set a concentration gradient in the OCR analysis of this data, making it difficult to determine the degree of inhibition

of Complex I compared to the positive control IACS-010759 (**Figure 3-13**), but this didn't affect the results of the study.

2.3.4. Discussion

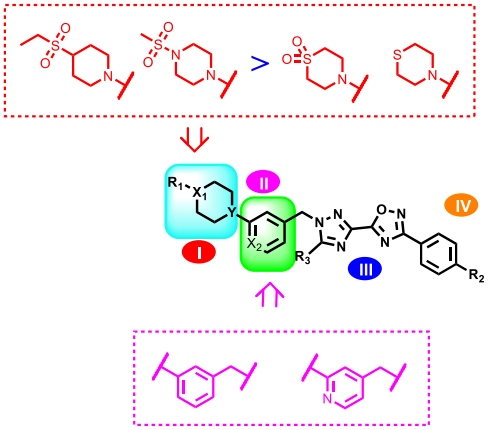

Figure 3-14 Preliminary summary of moiety I and moiety II on the target compounds

In part **C**, we used some analogues of heterocyclic fragments to replace moiety **I** and moiety **II** of the compounds, and a total of five analogues were synthesized. According to the Seahorse-based OCR measurements, three of the five compounds showed inhibitory activity against complex I. In moiety **I**, the compounds containing the 4-(ethylsulfonyl)piperidine (**3-101**, **3-110**), 1-(methylsulfonyl)piperazine (**3-100**) fragment were more efficient that the compounds containing the thiomorpholine (**3-109**), thiomorpholine 1,1-dioxide (**3-102**) fragment. One possible reason for that is the heterocyclic fragment requires a hydrophilic group and the hydrophilic group is in the extended part of the heterocycle (**Figure 3-14**). In moiety **II**, we used the bioisosteric pyridine heterocycle substitution of the benzene ring, and the results showed that compounds **3-101** (benzene ring) and **3-110** (pyridine ring) have the same inhibitory activity at 100 nM (**Figure 3-14**). The CAI analogs

at ± 10 μM produced the same degree of inhibition (OCR) of mitochondrial Complex I as the IACS-010759 analogs at ± 100 nM.

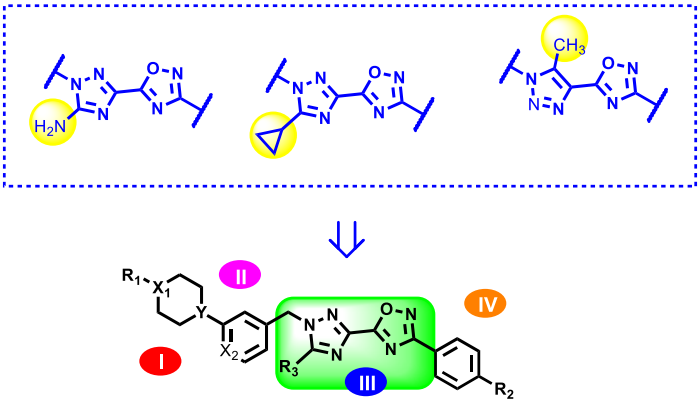

Figure 3-15 Design moiety III on the IACS-010759 analogs

Due to time constraints, we did not make structural changes to moiety **III**. Fragments such as 1,2,4-triazol-5-amine, 5-cyclopropyl-1,2,4-triazole, 5-methyl-1,2,3-triazole, *etc* (**Figure 3-15**) could help us to analyze the effect of moiety III substituent and triazole on the inhibitory activity of complex I.

3. Conclusion

Part A

Based on the design and synthesis of 28 CAI analogues, and how 96-well plates may be used today to screen for compounds with a suspected OXPHOS inhibitory activity *via* detection of lactate release and consecutively for their specific ability to block Complex I and to profoundly alter the growth of cancer cells within tumor-mimicking 3D structures. The latter model can be used to identify reoxygenation resulting from OXPHOS blockade and further prove radiosensitizing effects. Also, the results derived from our 28 CAI derivatives provide new insights on the structure-activity relationship of drugs

aiming to inhibit mitochondrial complex I, and will assist us in the design of further Complex I inhibitors.

Part B

The carboxyamine of the compound CAI structure was further derivatized in order to generate 25 new derivatives. According to the ROC data, none of the 25 derivatives had an effect on mitochondrial Complex I. Because of this, we conducted an analysis of the hypotheses that could lead to the lack of inhibitory activity and provided the groundwork for the subsequent design of Complex I inhibitors.

Part C

In this part, we synthesized five compounds containing 5-(5-methyl-1,2,4-triazol-3-yl)-1,2,4-oxadiazole group based on the experimental results of **part B** and the chemical structures of BAY87-2243 and IACS-010759. OCR studies revealed that three compounds have inhibitory activity on the mitochondrial Complex I. These results suggest that the moiety **I** heterocyclic ring contains a hydrophilic sulfonyl group and skeleton have a 5-(5-methyl-1,2,4-triazol-3-yl)-1,2,4-oxadiazole to maintain Complex I inhibitory activity have a positive effect.

4. Reference

1. Jose, C.; Bellance, N.; Rossignol, R., Choosing between glycolysis and oxidative phosphorylation: a tumor's dilemma? *Biochim Biophys Acta* **2011,** *1807* (6), 552-561.
2. Lee, M.; Hirpara, J. L.; Eu, J. Q.; Sethi, G., et al., Targeting STAT3 and oxidative phosphorylation in oncogene-addicted tumors. *Redox Biol* **2019,** *25*, 101073.
3. Ashton, T. M.; McKenna, W. G.; Kunz-Schughart, L. A.; Higgins, G. S., Oxidative Phosphorylation as an Emerging Target in Cancer Therapy. *Clin Cancer Res* **2018,** *24* (11), 2482-2490.
4. Nayak, A. P.; Kapur, A.; Barroilhet, L.; Patankar, M. S., Oxidative Phosphorylation: A Target for Novel Therapeutic Strategies Against Ovarian Cancer. *Cancers* **2018,** *10* (9), 337.
5. Molina, J. R.; Sun, Y.; Protopopova, M.; Gera, S., et al., An inhibitor of oxidative phosphorylation exploits cancer vulnerability. *Nat Med* **2018,** *24* (7), 1036-1046.
6. Lissanu Deribe, Y.; Sun, Y.; Terranova, C.; Khan, F., et al., Mutations in the SWI/SNF complex induce a targetable dependence on oxidative phosphorylation in lung cancer. *Nat Med* **2018,** *24* (7), 1047-1057.
7. Stuani, L.; Sabatier, M.; Saland, E.; Cognet, G., et al., Mitochondrial metabolism supports resistance to IDH mutant inhibitors in acute myeloid leukemia. *J Exp Med* **2021,** *218* (5), e20200924.
8. Corbet, C.; Feron, O., Cancer cell metabolism and mitochondria: Nutrient plasticity for TCA cycle fueling. *Biochim Biophys Acta Rev Cancer* **2017,** *1868* (1), 7-15.
9. Bridges, H. R.; Jones, A. J.; Pollak, M. N.; Hirst, J., Effects of metformin and other biguanides on oxidative phosphorylation in mitochondria. *Biochem J* **2014,** *462* (3), 475-487.
10. Wang, D. S.; Jonker, J. W.; Kato, Y.; Kusuhara, H., et al., Involvement of organic cation transporter 1 in hepatic and intestinal distribution of metformin. *J Pharmacol Exp Ther* **2002,** *302* (2), 510-515.
11. Sanchez, M.; Gastaldi, L.; Remedi, M.; Caceres, A., et al., Rotenone-induced toxicity is mediated by Rho-GTPases in hippocampal neurons. *Toxicol Sci* **2008,** *104* (2), 352-361.
12. Ju, R.; Guo, L.; Li, J.; Zhu, L., et al., Carboxyamidotriazole inhibits oxidative phosphorylation in cancer cells and exerts synergistic anti-cancer effect with glycolysis inhibition. *Cancer Lett* **2016,** *370* (2), 232-241.
13. Ellinghaus, P.; Heisler, I.; Unterschemmann, K.; Haerter, M., et al., BAY 87-2243, a highly potent and selective inhibitor of hypoxia-induced gene activation has antitumor activities by inhibition of mitochondrial complex I. *Cancer Med* **2013,** *2* (5), 611-624.
14. Tsuji, A.; Akao, T.; Masuya, T.; Murai, M., et al., IACS-010759, a potent inhibitor of glycolysis-deficient hypoxic tumor cells, inhibits mitochondrial respiratory complex I through a unique mechanism. *J Biol Chem* **2020,** *295* (21), 7481-7491.
15. Baccelli, I.; Gareau, Y.; Lehnertz, B.; Gingras, S., et al., Mubritinib Targets the Electron Transport Chain Complex I and Reveals the Landscape of OXPHOS Dependency in Acute Myeloid Leukemia. *Cancer Cell* **2019,** *36* (1), 84-99.
16. Azad, N.; Perroy, A.; Gardner, E.; Imamura, C. K., et al., A phase I study of paclitaxel and continuous daily CAI in patients with refractory solid tumors. *Cancer Biol Ther* **2009,** *8* (19), 1800-1805.
17. Johnson, E. A.; Marks, R. S.; Mandrekar, S. J.; Hillman, S. L., et al., Phase III randomized, double-blind study of maintenance CAI or placebo in patients with advanced non-small cell lung cancer (NSCLC) after completion of initial therapy (NCCTG 97-24-51). *Lung Cancer* **2008,** *60* (2), 200-207.
18. Hupe, D. J.; Behrens, N. D.; Boltz, R., Anti-proliferative activity of L-651,582 correlates with calcium-mediated regulation of nucleotide metabolism at phosphoribosyl pyrophosphate synthetase. *J Cell Physiol* **1990,** *144* (3), 457-466.
19. Oliver, V. K.; Patton, A. M.; Desai, S.; Lorang, D., et al., Regulation of the pro-angiogenic microenvironment by carboxyamido-triazole. *J Cell Physiol* **2003,** *197* (1), 139-148.

20. Stephenson, Z. A.; Harvey, R. F.; Pryde, K. R.; Mistry, S., et al., Identification of a novel toxicophore in anti-cancer chemotherapeutics that targets mitochondrial respiratory complex I. *Elife* **2020,** *9*, e55845.
21. Jhaveri, T. Z.; Woo, J.; Shang, X.; Park, B. H., et al., AMP-activated kinase (AMPK) regulates activity of HER2 and EGFR in breast cancer. *Oncotarget* **2015,** *6* (17), 14754-14765.
22. Clinical Study to Evaluate the Maximum Tolerated Dose of BAY87-2243 in Patients With Advanced Malignancies. https://clinicaltrials.gov/ct2/show/NCT01297530.
23. Oxidative Phosphorylation Inhibitor IACS-010759 in Treating Patients With Relapsed or Refractory Acute Myeloid Leukemia.
24. IACS-010759 in Advanced Cancers.
25. Corbet, C.; Bastien, E.; Draoui, N.; Doix, B., et al., Interruption of lactate uptake by inhibiting mitochondrial pyruvate transport unravels direct antitumor and radiosensitizing effects. *Nat Commun* **2018,** *9* (1), 1208.
26. Feron, O., Pyruvate into lactate and back: from the Warburg effect to symbiotic energy fuel exchange in cancer cells. *Radiother Oncol* **2009,** *92* (3), 329-333.
27. Sonveaux, P.; Vegran, F.; Schroeder, T.; Wergin, M. C., et al., Targeting lactate-fueled respiration selectively kills hypoxic tumor cells in mice. *J Clin Invest* **2008,** *118* (12), 3930-3942.
28. Bochis, R. J.; Chabala, J. C.; Harris, E.; Peterson, L. H., et al., Benzylated 1,2,3-triazoles as anticoccidiostats. *J Med Chem* **1991,** *34* (9), 2843-2852.
29. Kumari, A.; Singh, R. K., Morpholine as ubiquitous pharmacophore in medicinal chemistry: Deep insight into the structure-activity relationship (SAR). *Bioorg Chem* **2020,** *96*, 103578.
30. Kourounakis, A. P.; Xanthopoulos, D.; Tzara, A., Morpholine as a privileged structure: A review on the medicinal chemistry and pharmacological activity of morpholine containing bioactive molecules. *Med Res Rev* **2020,** *40* (2), 709-752.
31. Wang, L.; Wang, Y.; Guo, F.; Zheng, Y., et al., Regioselective formylation of 1,3-disubstituted benzenes through in situ lithiation. *Tetrahedron Lett.* **2013,** *54* (45), 6053-6056.
32. Dai, J. L.; Shao, N. Q.; Zhang, J.; Jia, R. P., et al., Cu(II)-Catalyzed ortho-Selective Aminomethylation of Phenols. *J Am Chem Soc* **2017,** *139* (36), 12390-12393.
33. Yang, M. H.; Hunt, J. R.; Sharifi, N.; Altman, R. A., Palladium Catalysis Enables Benzylation of alpha,alpha-Difluoroketone Enolates. *Angew Chem Int Ed* **2016,** *55* (31), 9080-9083.
34. Brand, S.; Ko, E. J.; Viayna, E.; Thompson, S., et al., Discovery and Optimization of 5-Amino-1,2,3-triazole-4-carboxamide Series against Trypanosoma cruzi. *J Med Chem* **2017,** *60* (17), 7284-7299.
35. Thomson, C. G.; Le Grand, D.; Dowling, M.; Brocklehurst, C. E., et al., Development of autotaxin inhibitors: A series of zinc binding triazoles. *Bioorg Med Chem Lett* **2018,** *28* (13), 2279-2284.
36. Corbet, C.; Pinto, A.; Martherus, R.; Santiago de Jesus, J. P., et al., Acidosis Drives the Reprogramming of Fatty Acid Metabolism in Cancer Cells through Changes in Mitochondrial and Histone Acetylation. *Cell Metab* **2016,** *24* (2), 311-323.
37. Liu, J.; Li, H.; Chen, K. X.; Zuo, J. P., et al., Design and Synthesis of Marine Phidianidine Derivatives as Potential Immunosuppressive Agents. *J Med Chem* **2018,** *61* (24), 11298-11308.
38. Menet, C. J. M.; Hodges, A. J.; Vater, H. D. Novel compound useful for the treatment of degenerative and inflammatory diseases. 2012 patent.
39. Jones, P.; Di Francesco, M. E.; McAfoos, T. Salts of heterocyclic modulators of HIF activity for treatment of disease. 2017 patent.
40. Subbaiah, M. A. M.; Meanwell, N. A., Bioisosteres of the Phenyl Ring: Recent Strategic Applications in Lead Optimization and Drug Design. *J Med Chem* **2021,** *64* (19), 14046-14128.

Chapter II

Design and Synthesis of pH-sensitive Anticancer Drug Conjugates

pHLIP parts and conjugate physicochemical property data provided by Marine Deskeuvre from *Prof.* Raphaël Frédérick's team

Pharmacological evaluation data for conjugate provided by Emeline Dierge form *Prof.* Olivier Feron's team

1. Introduction

Drug delivery systems can prioritize drug action on target tissues and avoid unnecessary side effects. The acidic microenvironment represents a major discrepancy between tumor and normal tissues. There are two main reasons for this: the accumulation of H^+ from highly glycolytic cancer cells and the release of CO_2 diffusion from oxidative cancer cells[1]. In order to target acidic tumor areas, pH-sensitive peptides have been developed to facilitate the intracellular delivery of a conjugated therapeutic payload[2, 3].

This chapter is dedicated to the design and synthesis of pH-sensitive drug delivery systems that primarily targets fatty acid metabolism in tumor cells. The drug delivery system consists of three components: a pH-sensitive insertion peptide, a linker and the drug compound.

1.1. pH low insertion peptide (pHLIP)

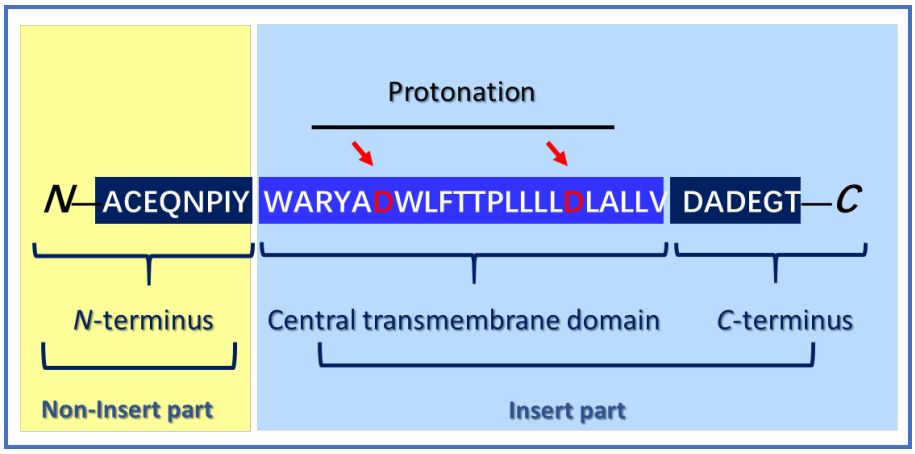

Figure 4-01 The Main Features of Sequences of the pHLIP[2]. Members of the peptide of pHLIP family follow a similar pattern in terms of peptide sequence: an *N*-terminal flanking region (deep blue left) comprising mainly polar residues; a central transmembrane domain (blue) comprising mainly hydrophobic residues, but also including protonatable residues, which prevent insertion at physiological pH; and a C-terminal flanking region (deep blue right), which may not be present in all peptides (Var3[4]), containing a few additional protonatable residues. Cargo can be conjugated either to the C or N terminus via single cysteine or lysine residues.

pH low insertion peptide (pHLIP) is a water-soluble peptide of 36 amino acids derived from the transmembrane helix C of the protein bacteriorhodopsin[5]. pHLIP is able to sense changes in the pH of the microenvironment. When exposed to the acidic environment, protonation of aspartic acid residues in pHLIP leads to a conformational change in folding and an insertion into the transmembrane already forming a stable transmembrane α-helix[6, 7].

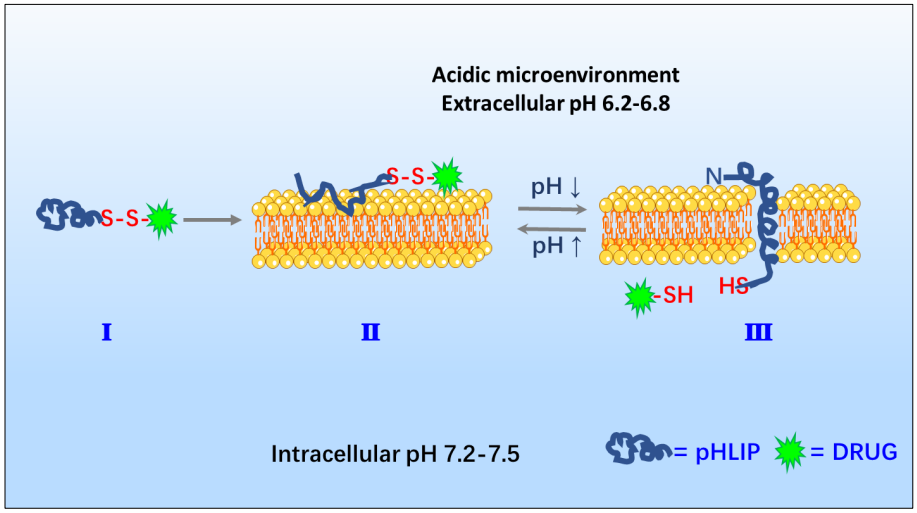

Figure 4-02 Schematic diagram of the delivery of drugs into a cell[2, 8] The peptides of the pHLIP family exist in equilibrium between a solvated and membrane-adsorbed conformation at the normal extracellular pH found in healthy tissue, whereas they insert across the cellular membrane at the low extracellular pH found in acidic, diseased tissues including tumors, transport cargo inside cells.

Protonatable amino acid residues in pHLIP have negative surface charges and are largely unstructured and disordered as soluble monomers or low-order multimers (**Figure 4-02 I**). In the presence of a lipid membrane, pHLIP adsorbs to the surface in a disordered state (**Figure 4-02 II**). Under acidic conditions, the negatively charged amino acid residues in pHLIP are protonated due to increased H^+ concentration. This protonation increases the hydrophobicity of the central transmembrane structural domain in such a way that the pHLIP monomer folds to form an α-helix, which in turn helixes across

the cell membrane, inserting the ***C***-terminus into the cytoplasmic lysis (**Figure 4-01** and **Figure 4-02 III**)[9, 10].

The group D. M. Engelman reported the pH-selective insertion and folding of a membrane peptide, pHLIP useable to target acidic tumor tissues *in vivo*[11]. In a mouse breast adenocarcinoma model, fluorescently labeled pHLIP allows to detect early stage solid (acidic) tumors with high precision.[11] The fluorescent signal was stable for > 4 days and was approximately five times higher in the tumor than in the healthy counterpart tissue[11](**Figure 4-03**).

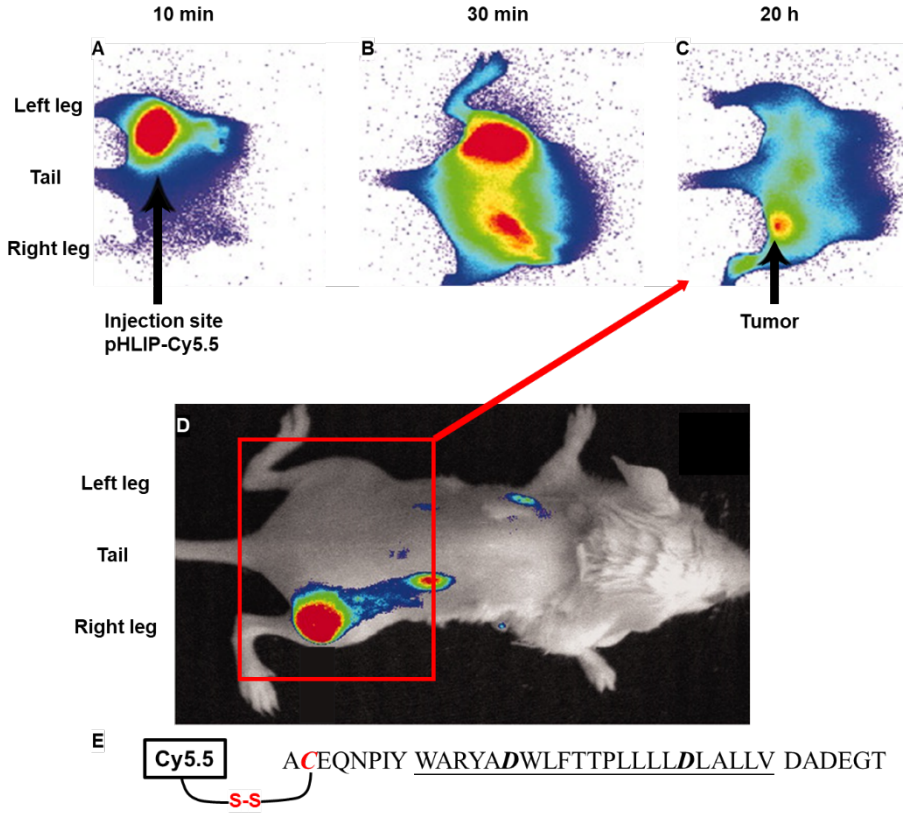

Figure 4-03 Whole-body near-infrared (NIR) fluorescence and light images of mouse bearing tumor is shown[11]. (**A-C**) Using a mouse model with breast cancer on the right side, pHLIP-Cy5.5 given as a single *i.p.* injection into the left side of mice initially diffused into the left flank, but 20 h later it accumulated in a tumor on the right flank. The NIR fluorescent image of the back part of each mouse is presented. Blue color represents the background fluorescent signal, and the red color represents a high intensity of the fluorescence signal. (**D**) Overlay of

pHLIP-Cy5.5 fluorescence and light images of mice bearing a tumor in the right flank (*i.p.* injection of pHLIP-Cy5.5 before imaging). (**E**) Conjugate formed by disulfide bonding fluorescent probe Cy5.5 to pHLIP *N*-terminus Cys residue.

pHLIP was identified to be particularly suited to target cancer cells located in acidic tumor areas[12]. Diagnostic reagents or drugs can be linked to the non-insertion end (***N***-terminal) or the insertion end (***C***-terminal) of the pHLIP to deliver these reagents to the tumor cell surface or intracellularly, repectively. For polar or macromolecular drug molecules, pHLIP crosses the cell membrane to deliver cargo directly to the cytoplasm[13-16]. This drug delivery system, which does not rely on cell surface receptors, cell fusion, and other effects, show therefore unique advantages[17-19].

1.2. Targeting tumor lipid metabolism

In acidic cancer cells, instead of glucose, fatty acids are used as energy supply [20-22]. The transport of fatty acyl-CoA into the mitochondria through CPT1 is a rate-limiting step in fatty acid oxidation [23]. Inhibition of CPT1 can thus block the main pathway providing energy under acidosis (**Figure 4-04)**. In this chapter, we have selected Etomoxir, one of the most representative oxirane carboxylic acid compound[24] acting as a bona fide CPT1 inhibitor. It is largely used as a pharmacological tool in research laboratories but not in the clinic since liver toxicity actually stopped its development. Here we thus aimed to preparing an etomoxir-pHLIP conjugate to overcome adverse effects[25].

Another target of interest is DGAT1, the enzyme that catalyzes the last reaction in the formation of triglycerides (TG) [22, 26]. Whatever the extracellular origin or the de novo synthesis of fatty acids, acidic cancer cells have a propensity to store FA into lipid droplets (upon incorporation into TG)[27] (**Figure 4-04)**. Lipid droplets represents energy stores that cancer cells may mobilize in case of needs (e.g., during metastatic spreading) but also a strategy to protect cancer cells from lipotoxicity, in particular from peroxidation of

polyunsaturated fatty acids. Blocking TG formation may thus lead to cytotoxic effects either through energy deprivation or oxidative stress[28]. As a DGAT1 inhibitor to be combined with pHLIP peptide, we have chosen compound T863[29].

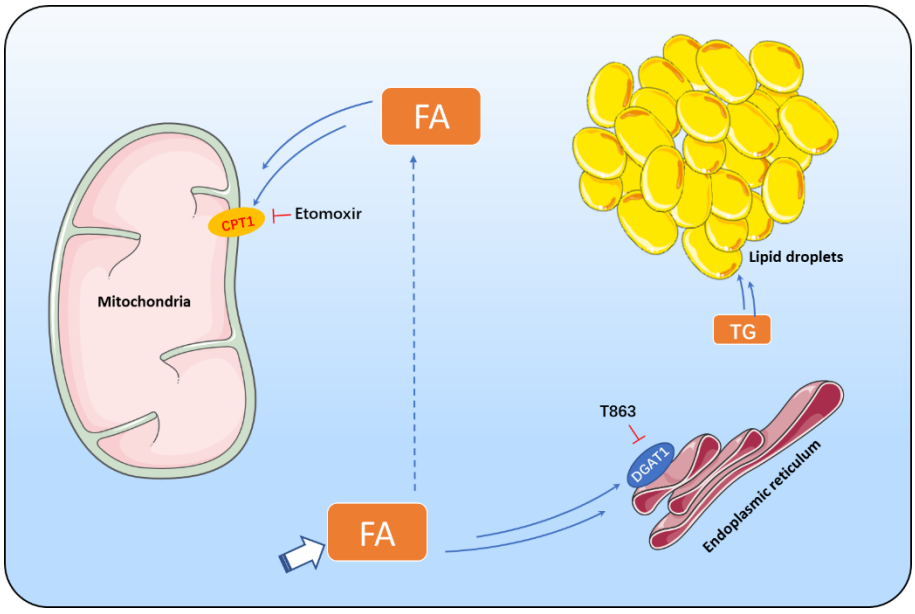

Figure 4-04 The important targets of lipid anabolism and fatty acid catabolism: DGAT1, CPT1

2. Results and discussion

2.1. Rational design

Here we designed a conjugate containing the modified ***C***-terminus sequence of pHLIP containing cysteine (C) residues, the linker arm disulfide bond and the drug molecules Etomoxir and T863 (**Figure 4-05)**. The strategy is thus the following: when the ***C***-terminus of pHLIP conjugates enters the tumor cell, glutathione (GSH *reduced form*), a major cell redox regulator, reduces the disulphide bond and releases the prodrug compound[30]. The prodrug is further hydrolyzed to release the drug (under the form of R-COOH) that may diffuse to its effector site.

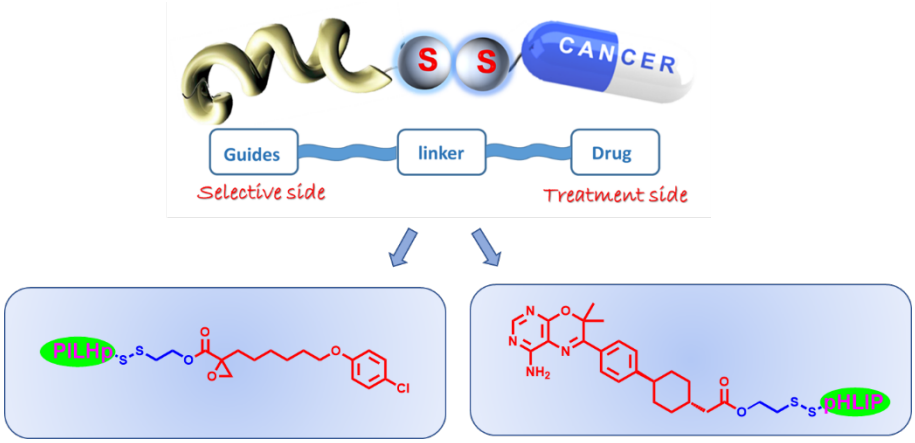

Figure 4-05 pH sensitive conjugates

The project consists of three main parts: the design and synthesis of the drug fragments and linker arms, the design of pHLIP amino acid sequences, and the evaluation of the physicochemical properties of peptides and conjugates in different pH, the pharmacological evaluation of pH-sensitive conjugates (**Figure 4-06)**. The design and synthesis of drug fragments and linker arms are the focus of my effort on this project.

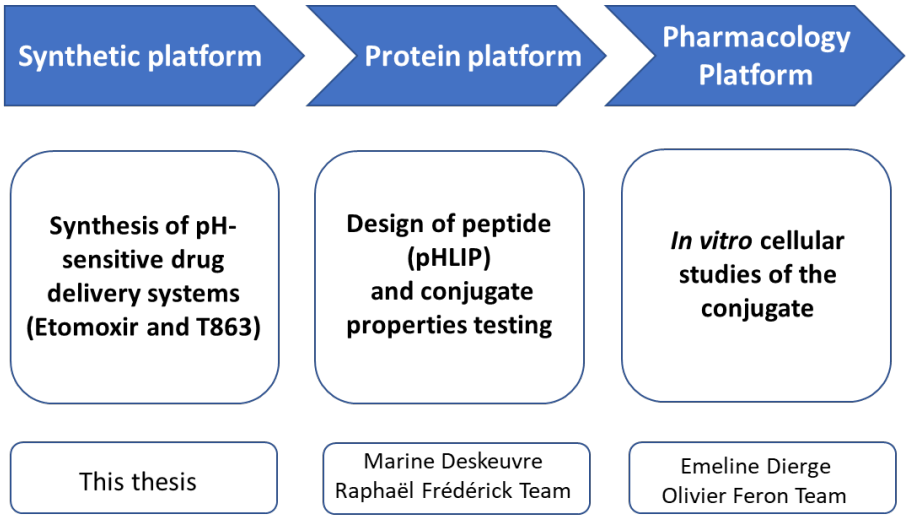

Figure 4-06 Project flow chart

2.2. Synthesis of a pH-sensitive CPT1 inhibitor conjugate

The synthesis of Etomoxir **4-010** is shown **Scheme 4-02** and follows reported procedures[31, 32]. **4-006** was synthesized in three steps: the commercially available diol **4-001** was monosubstituted with hydrogen bromide solution to form **4-002** in a 90% yield. Mitsunobu reaction of the alcohol group with phenol **4-003** was followed by nucleophilic substitution with the sodium salt of diethyl malonate **4-005** to give the diester **4-006**. Finally, full saponification of both esters functions give the diacid **4-011**, which was in turn treated with paraformaldehyde and diethylamine to give the unsaturated carboxylic acid **4-012**. Finally, the unsaturated double bond was treated with various oxidizing agent to provide the ethyl oxirane carboxylic acid Etomoxir **4-010**. Unfortunately, we tried several different oxidation reagents to treat the double bond in the last step of the synthesis, but failed.

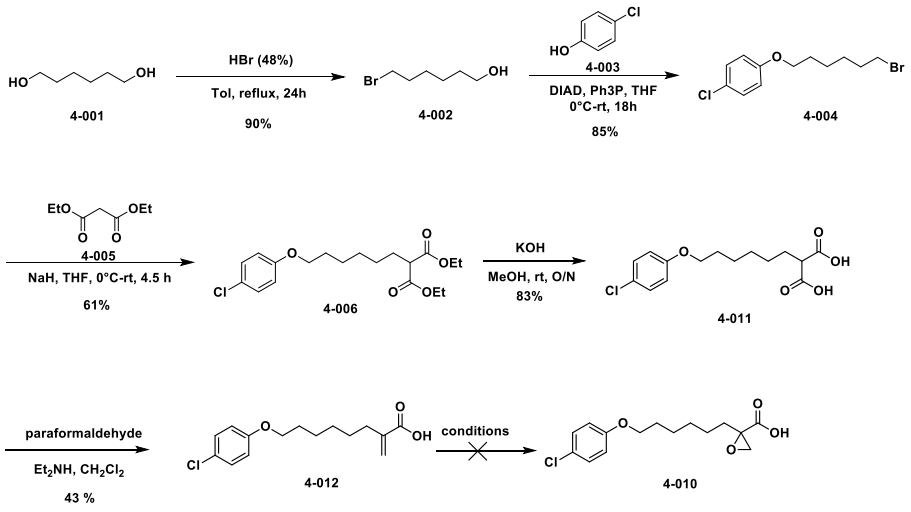

Scheme 4-01 the synthetic route 1 for Etomoxir

Firstly, we tried the oxidation of the double bond by an excess (3 eq) of 3-chloroperoxybenzoic acid (*m*-CPBA), but did not observe any formation of the desired epoxide. Then after treatment with a larger amount of *m*-CPBA

(10eq), ^{1}H-NMR analysis of the crude reaction mixture showed that the product was formed, but the conversion was very low. We tried to purify the compound by column chromatography was unsuccessful because the product was close to the Rf of *m*-chlorobenzoic acid. After that, we tried H_2O_2, $Ni(OAc)_2/NaOH$[33] and OXONE, albeit without any success (**Table 4-01)**.

Table 4-01 Screening of oxidation reagents

Entry	Condition	Solvent	Time	Yield
1	*m*-CPBA (3eq)	CH_2Cl_2	O/N	no
2	*m*-CPBA (10eq)	CH_2Cl_2	O/N	<10% (NMR)
3	H_2O_2, K_2CO_3	$MeOH/H_2O$	>24h	no
4	$Ni(AcO)_2/NaOH$	CH_2Cl_2/H_2O	12h	no
5	OXONE	CH_3CN/H_2O	4h	no

OXONE= Potassium peroxymonosulfate

Hypothesizing that the failure of the aforesaid reaction to properly oxidize the double bond was due to the presence of the nearby -COOH group, and so we followed the synthetic approach described in the literature to synthesize **4-009,** bearing an ester group instead of a carboxylic acid. Controlled saponification of diester **4-006** could be achieved to obtain monoester **4-007**, which on treatment with paraformaldehyde and diethylamine yielded the unsaturated ester **4-008**. The ethyl oxirane carboxylates **4-009** was then obtained by oxidation of **4-008** with *m*-CPBA (**Scheme 4-02**). To get the desired product Etomoxir **4-010**, a mild hydrolysis condition was optimized to hydrolyze the ester without destroying the nucleophile-sensitive epoxide group in the final step.

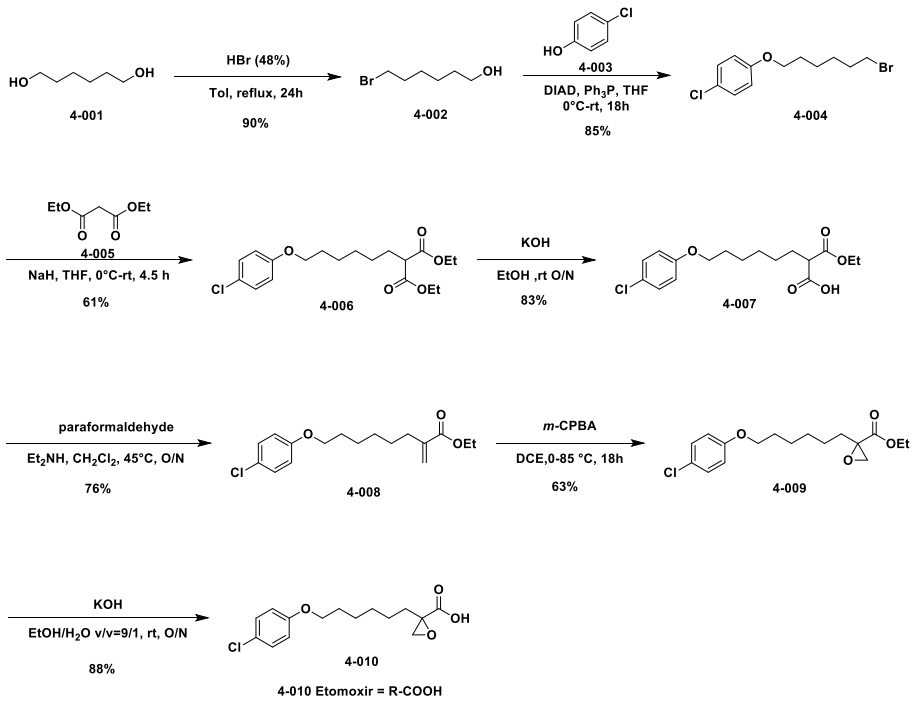

Scheme 4-02 the synthetic route 2 for Etomoxir

Targeting on hydrolyzing the ethyl oxirane carboxylate **4-009**, a KOH/MeOH system was initially explored, which revealed that the exchange of ester groups, resulted in formation of the methyl ester compound **4-013**. Therefore, we increased the amount of KOH and found that the oxirane was indeed decomposed *via* ring opening during the saponification and led mainly to diol-acid **4-014**. Further study into the solvent system revealed that the solvent (KOH/MeOH 90/10) effectively hydrolyzed the ester group in 81% yield. However, this yield was reduced as the amount of water in the solvent system increased. Therefore, we decided to keep the previous conditions for the production of our target compounds (**Table 4-02**).

Table 4-02 Optimization of hydrolysis conditions

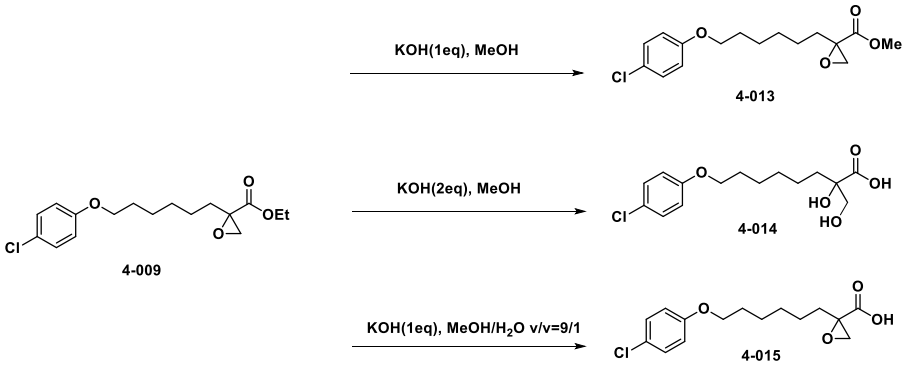

Entry	KOH	MeOH/H_2O	Temp.	Results
1	1.0	100:0	rt	Ester change
2	1.0	90:10	rt	81%
3	1.0	80:20	rt	< 60%
4	2.0	100:0	rt	< 20%

The **Scheme 4-03** describes the synthesis of pHLIP conjugates **4-020*d*** and **4-020*r*** from Etomoxir. In the preparation of intermediate **4-018**, 2-mercaptoethanol **4-017** reacted dropwise with an excess of 2'-aldrithiol **4-016** (two or three equivalents), but the yields lower than reported in the literature[34]. It was possible that caused by the fast dropwise addition of **4-017**. After dilution of **4-017** in methanol in a slow titration into the reaction showed an increase in yield but also lower than reported in the literature. The production of $(HOCH_2CH_2S)_2$ causes such low yield[8]. Therefore, the glacial acetic acid was added to inhibit the production of side-products. The results reveal yields of 65 %, or 81%, respectively, when two or three equivalents of **4-016** are added (**Table 4-03**). The Etomoxir ester **4-020** was then obtained from **4-018** and **4-010** *via* esterification using EDCI as a coupling agent. Finally, the

Etomoxir conjugates (**4-020*d*** and **4-020*r***) were obtained after another disulfide exchange reaction[2].

Table 4-03 Optimization of reaction conditions

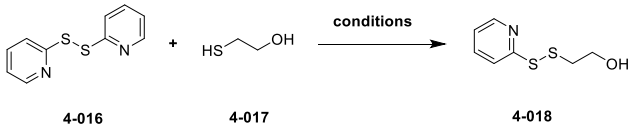

Entry	4-016	4-017	H^+	Solvent	Temp.	Yield
1	2 eq	1 eq	-	MeOH	rt	30%
2	3 eq	1 eq	-	MeOH	rt	35%
3▲	2 eq	1 eq	-	MeOH	rt	47%
4▲	2 eq	1 eq	AcOH	MeOH	rt	65%
5▲	3 eq	1 eq	AcOH	MeOH	rt	81%

▲Dilute 2-Mercaptoethanol (**4-017**) with methanol and add slowly dropwise into the reaction

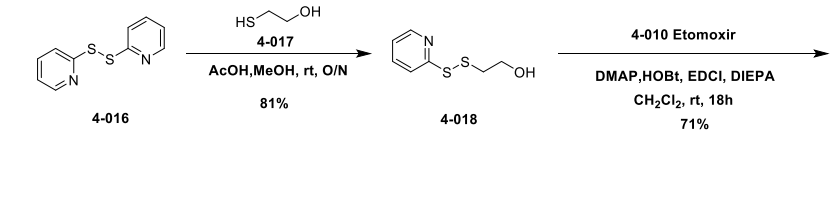

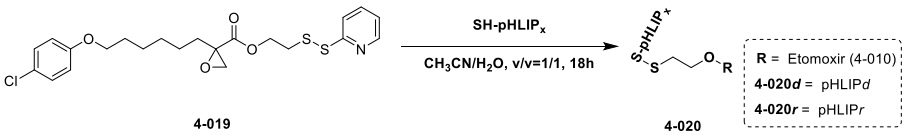

[2] The last step of coupling the peptide was finished by our collaborator *Prof.* Raphaël Frédérick's team Marine Deskeuvre.

	N-	*C*-
WT-pHLIP	A***C***EQNPIY WARYA***D***WLFTTPLLLL***D***LALLV DADEGT	
Var3	A***C***DDQNP WRAYL***D***LLFPT***D***TLLL***D***LLW	
pHLIP*r*	AAEQNPIY WARYA***D***WLFTTPLLLL***D***LALLV DADEGT***C***G	
pHLIP*d*	AADDQNP WRAYL***D***LLFPT***D***TLLL***D***LLV VDADEGT***C***G	

Scheme 4-03 Synthesis of the pHLIP conjugate 4-020 Amino acid sequence of pHLIP: WT-pHLIP is the wild-type sequence, Var3 is the sequence designed by Reshetnyak's team to screen for superiority over WT in tumor cells. pHLIP*r* retains the transmembrane domain amino acid sequence of WT-pHLIP, and modifies the *N* and *C* termini accordingly because of the need for drug delivery through amino acid **C** residues and insertion into the cell. pHLIP*d* was designed and developed based on the Var3 transmembrane domain amino acid sequence (underlining indicates the transmembrane domain of the peptide)

2.3. The properties of conjugates 4-020*d* and 4-020*r*

pHLIP*d* and pHLIP*r* were synthesized and purified by Genecust company. The Etomoxir conjugates (**4-020*d*** and **4-020*r***) were determined by analytical HPLC-MS and conjugates were purified through semi-preparative liquid chromatography. After sample lyophilization, the purity was measured by HPLC-MS. The pKa refers to the pH value at which 50% of the peptides (pHLIP*d* and pHLIP*r*) are inserted into the bilayer of the POPC liposome. The results are shown in **Table 4-04**.

Table 4-04 The properties of conjugates

Peptide	**pHLIP*r***	**pHLIP*d***
pKa	6.25	4.95
Conjugate	**4-020*r***	**4-020*d***
Molecular weight	4596.7	4208.1
Predicted MS	4595.2	4206.9

m/z		
MS m/z $[M+3H^+]^{3+}/3$	1532.8	1402.8
Purity	>95%	>95%
Yield	35%	49%

2.4. Verification of conjugates properties

To study the interaction of pHLIP conjugate with cell membranes, liposomes was prepared from phosphatidylcholine (POPC) to mimic cell membranes. The Intrinsic Tryptophan Fluorescence (ITF) can be used to monitor the interaction of Etomoxir conjugates (**4-020*d*** and **4-020*r***) with POPC liposomes. The insertion process is accompanied with the transfer of the tryptophan fluorophore from aqueous solution to the hydrophobic environment of the lipid bilayer. The change in polarity results in an enhanced emission fluorescence and a shift of the spectrum to shorter wavelengths[35, 36]. There are three tryptophan residues in conjugates **4-020*d*** and **4-020*r***, which are useful for sample analysis. Next, the peptide formation process of the α-helix is monitored using circular dichroism (CD) spectroscopy, which reflects the secondary structure of the peptide[37, 38].

Using the two techniques above, we tested the effect of conjugates (**4-020*d*** and **4-020*r***) with liposome bilayers at different pH. Three states were studied in this work, in state **I** (the black line), conjugates were dissolved in pH 8.0 buffer solution without the addition of POPC liposomes; In state **II** (the blue line), conjugates were dissolved in pH 8.0 buffer solution with the addition of POPC liposomes; In state **III** (the red line), conjugates dissolved in pH 5.0 buffer solution with the addition of POPC liposomes (**Figure 4-07**).

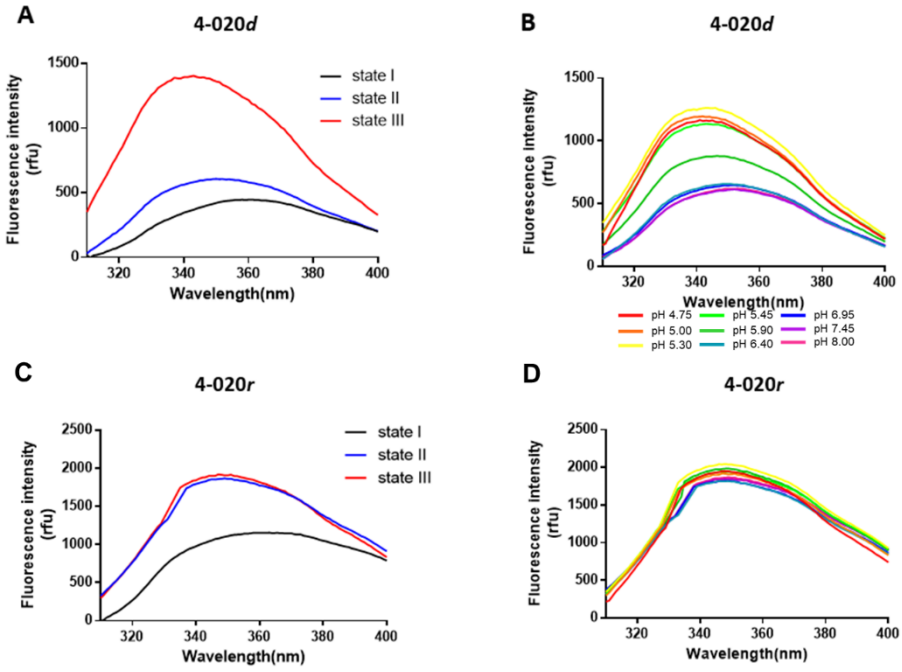

Figure 4-07. Interactions of conjugates (4-020*d* and 4-020*r*) with lipid bilayer. Intrinsic tryptophan fluorescence measurements (**A**, **B**, **C**, **D**) of peptides in state **I** (pH 8), state **II** (pH 8 and POPC vesicles) and state **III** (pH 5 and POPC vesicles).

We monitored the insertion of tryptophan fluorescence into the lipid bilayer in the transition among three states. The states of conjugates (**4-020*d*** and **4-020*r***) are described in **Figure 4-07 A** and **C**. As shown in **Figure 4-07 A**, the intrinsic tryptophan fluorescence emission maximum of **4-020*d*** in a pH 8.0 buffer solution is at 360 nm and its highest fluorescence intensity is below 500. When conjugate **4-020*d*** is at pH 8.0 together with liposomes, the intrinsic tryptophan fluorescence emission maximum undergoes a blue shift at 350 nm and the fluorescence intensity is around 500. In the acidic condition (pH=5), the intrinsic tryptophan fluorescence intensity increases up to 1500 and the maximum emission wavelength decreases to 340 nm, in agreement with the insertion of conjugate **4-020*d*** into liposome vesicles at pH=5. **Figure 4-07 B** clearly shows the interaction of **4-020*d*** and liposome with pH change. When the pH decreases, the intrinsic tryptophan fluorescence emission maximum

gradually exhibit a blue shift while the fluorescence intensity gradually increases. This supports the concept that the conjugate is gradually deionized in the acidic environment thereby increasing the polarity to facilitate peptide insertion into the liposomes. As for **4-020*r*** (**Figure 4-07 C**), when changing the pH, the intrinsic tryptophan fluorescence of State II and State III did not reveal any change, indicating that **4-020*r*** does not interact with the liposome. In order to observe clearly the state of conjugates presented in liposomes, we next set up a larger pH gradient. The intrinsic tryptophan fluorescence of **4-020*r*** did not change with the pH decrease in **Figure 4-06 D,** confirming that **4-020*r*** was not inserted into the liposome.

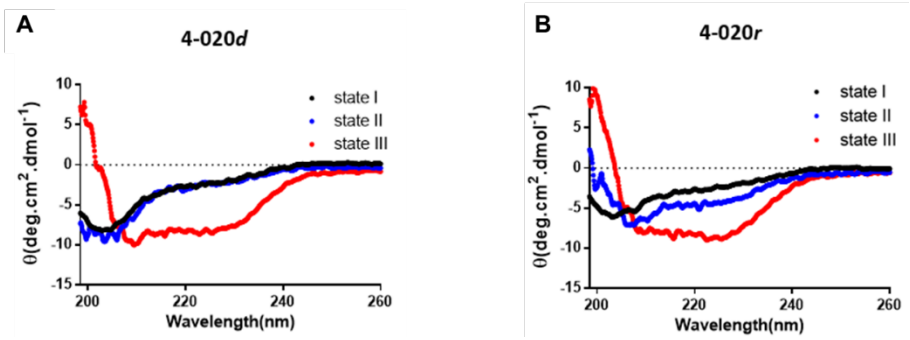

Figure 4-08. Interactions of conjugates (4-020*d* and 4-020*r*) with lipid bilayer. CD spectroscopy (**A** and **B**) of peptides in state **I** (pH 8), state **II** (pH 8 and POPC vesicles) and state **III** (pH 5 and POPC vesicles).

The secondary structure of the peptide is shown in the CD spectrum. Three state transitions reveal that the CD value of **4-020*d*** has a negative band at 202 nm at pH 8.0, which means that pHLIP*d* is in an unstructured conformational state (**Figure 4-08 A**). In state III, there are two negative bands at 210 nm and 225 nm, indicating that the conformation of pHLIP is changed and exhibits α-helix insertion into the liposome in the acidic environment (**Figure 4-08 A**). According to the literature, peptides that occur in the α-helix have two negative bands at 208 nm and 220 nm[38, 39]. No obvious negative band (205-

210 nm) could be observed in **Figure 4-08 B**, providing further evidence of a lack of α-helix formation for **4-020*r*** under acidic conditions.

The results of the intrinsic tryptophan fluorescence assay and CD spectrum analysis indicate that the **4-020*d*** present transmembrane domain more prone to respond to acidic conditions than the wild type **4-020*r***.

2.5. *In vitro* cellular studies of the conjugate

To evaluate the ability of the conjugates targeting the acidic compartment of spheroids and induce equivalent toxicity as etomoxir alone, 3D tumor FaDu (Epithelial squamous cell carcinoma) spheroids were treated with 10 μM of etomoxir or conjugates. We also used the addition of polyunsaturated fatty acids (PUFAs) such as DHA to exacerbate lipotoxicity in the presence of etomoxir. The lab of O. Feron indeed reported that blocking the oxidation of PUFAs led to an increase in their cytosolic concentration and consecutive induction of ferroptosis, a mode of cell death resulting from lipid peroxidation[40].

In the **Figure 4-09A**, Without the addition of DHA, **4-020*d*** and **4-020*r*** did not lead to any toxicity and even induced an increase in the spheroid size. Upon treatment with **4-020*r***, DHA-exposed spheroid growth curve followed the same profile as in the presence of etomoxir **4-010**, suggesting that the conjugate is nearly as toxic as etomoxir alone (**Figure 4-09A** below). On the opposite, **4-020*d*** complemented with DHA had no deleterious impact on FaDu spheroids compared to DHA only (**Figure 4-09A** below). When we tested the behavior of pHLIP conjugates in 2D cell cultures, both **4-020*d*** and **4-020*r*** induced a decrease in cell density of pH 6.5/FaDu cancer cells exposed to 100 μM DHA to the same extent as etomoxir alone (**Figure 4-09B**). Importantly, pH 7.4/FaDu cancer cells did not reveal signs of toxicity when exposed to either conjugate (or etomoxir **4-010**) in the presence of DHA (**Figure 4-09B**).

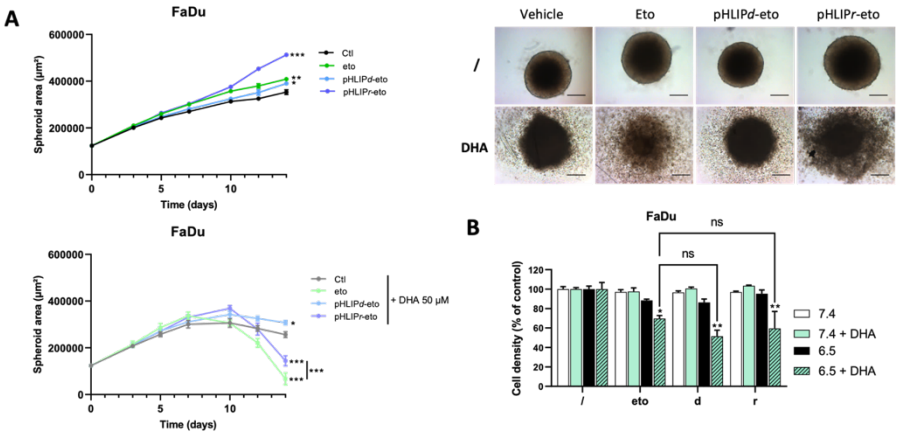

Remark: Eto=4-010, pHLIP*d*-eto = 4-020*d*, pHLIP*r*-eto = 4-020*r*

Figure 4-09 4-020*d* and 4-020*r* increases DHA toxicity in 2D and 3D culture A-B. Effects of 10 µM **4-010** (etomoxir, eto), **4-020*d*** (pHLIP*d*-etomoxir, pHLIP*d*-eto) and **4-020*r*** (pHLIP*r*-etomoxir pHLIP*r*-eto) on 3D FaDu spheroids (**A**) and 2D FaDu cancer cells (**B**) exposed to 50 µM or 100 µM of docosahexaenoic acid (DHA), respectively. Representative pictures of spheroids at day 14 are shown. Scale bar: 500 µm. Data are represented as mean ± SEM of 6 different spheroids (**A**) or 6 different wells (**B**). Significance for the effects of etomoxir was determined by one-way ANOVA with Tukey's multiple comparison test at endpoint (**A**) or determined by two-way ANOVA with Sidak's multiple comparison (**B**) *p < 0.05; **p < 0.01; ***p <0.001.

In conclusion, intrinsic tryptophan fluorescence assay and CD experiments revealed a pH-dependent folding of **4-020*d*** as anticipated for a pHLIP conjugate (i.e. a structuration followed by insertion inside POPC liposomes). On the contrary, **4-020*r*** did not exhibit a preference for any of the pH-gradient tested. Whereas the pKa=4.95 for pHLIP*d*, pKa=6.25 for pHLIP*r* was significantly higher, as shown in **Table 4-04**. Theoretically, the insertion of **4-020*r*** into POPC liposomes should be superior to that of **4-020*d*** when the pH is at 5.0-6.0. Our experimental data however gave opposite results and since we did not observe that **4-020*r*** showed an acidic pH-dependent insertion into liposomes. we may hypothesize that pHLIP*r* sequence is too hydrophobic to be conjugated with a lipophilic drug to give rise to the expected acidic pH-preference for membrane insertion. As for the biological experiments, one may therefore postulate that contrary to the imposed pH value of 6.5 in 2D cancer cell culture, spontaneous acidity that naturally developed in growing

spheroids may not have reached a sufficiently low pH value to induce the insertion of **4-020*d*** (and the consecutive release of etomoxir). These data also suggest that the pHLIP sequence needs to be carefully selected to promote ideal insertion into the acidic compartment. The next step is to test etomoxir conjugates in mice fed a DHA-rich diet to confirm the anticancer effects while sparing healthy tissues such as the liver from the detrimental effects of etomoxir **4-010**[25] (as reported with the free form of the drug).

2.6. Synthesis of a pH-sensitive DGAT1 inhibitor conjugate

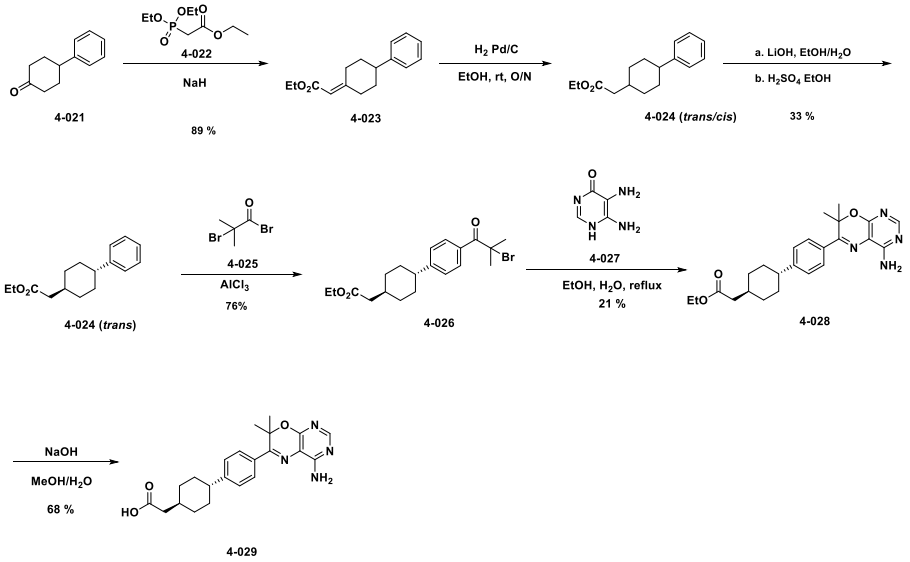

Scheme 4-04. Synthesis route of 4-029

The synthesis of T-863 (**4-029**) is shown in **Schemes 4-04**, **Schemes 4-05** and follow reported procedures[29, 41], using 4-phenylcyclohexanone **4-021** as a starting material. Frist the Horner-Wadsworth-Emmons (HWE) reaction with phosphoroacetate **4-022** give **4-023** in an 89 % yield (**Scheme 4-04**).

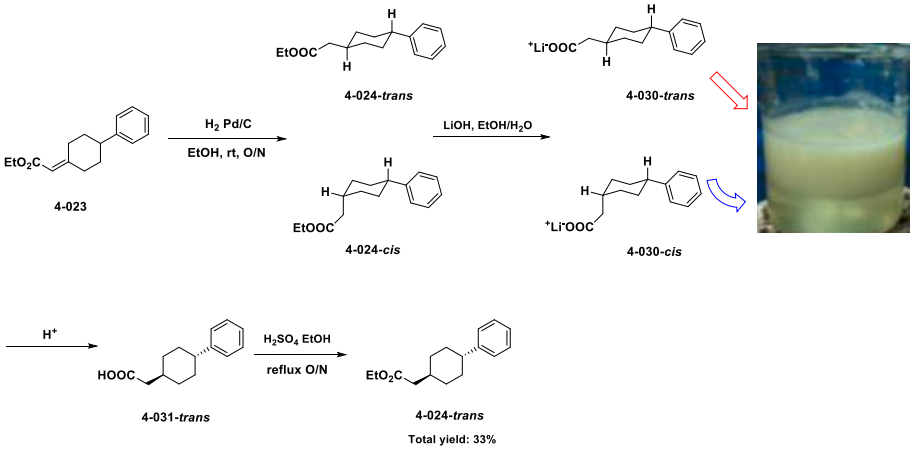

Scheme 4-05 the synthetic route for *trans*-isomer 4-024

Compound **4-023** hydrogenated in the presence of Pd/C to give a mixture of *cis* and *trans* alkanes isomers **4-024**, (in a *trans*/*cis* ratio of 2.8/1 measured by ^{1}H-NMR) (**Figure 4-10 A**). Because the pharmaceutically active structure is the *trans*-isomer, the lithium salt of the *trans*-isomer was precipitated after saponification of the mixture of esters by LiOH [29, 41]. Then the *trans*-isomer of **4-024** was obtained after acidification and Fisher esterification of the **4-031*trans***, giving a *trans*/*cis* ratio of 100/7 by ^{1}H-NMR (**Figure 4-10 B**) (**Scheme 4-05**). Friedel-Crafts acylation with 2-bromo-2-methylpropionyl bromide give bromide **4-026**. Finally, condensation of **4-026** with amino hydroxypyrimidine **4-027** give pyrimidooxazine **4-028** (**Scheme 4-04**).

A: ^{1}H-NMR spectra for the mixture of *cis* and *trans* isomers 4-024 (*trans/cis*)

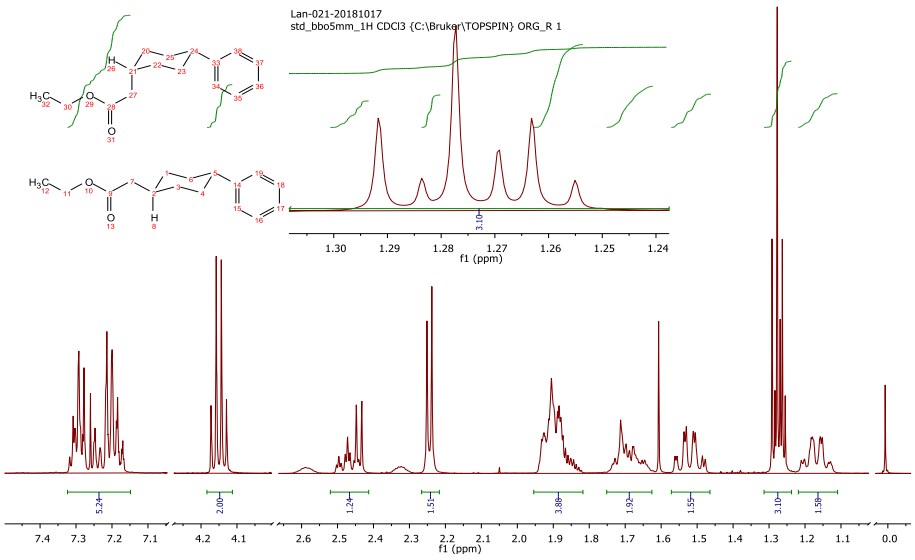

B: ^{1}H-NMR spectra for *trans* isomers 4-024(*trans*)

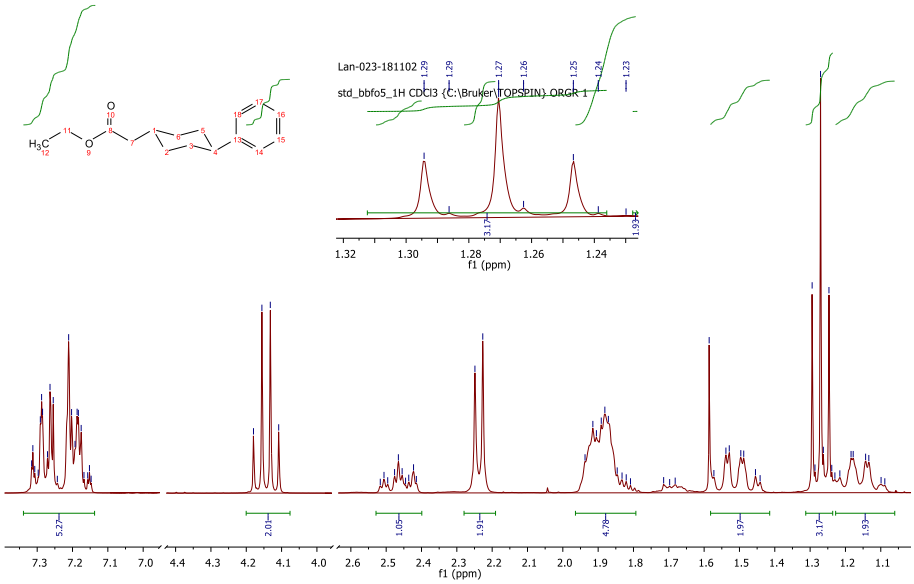

C: ^{1}H-NMR ratio for *trans* and *cis* isomers

NMR Yield	
Before *trans/cis*	**After *trans/cis***
2.8/1	100/7

Figure 4-10 ^{1}H-NMR ratio of *trans*/*cis* isomers 4-024

The initial route we designed was to couple the linker to the pyrimidine amino group *via* a carbamate, and then hydrolyzed the ester by saponification to obtain the target compound **4-030a**. However, when we tried to react **4-028** with triphosgene, to generate the carbamoyl chloride, or carbonate **4-031**, we did not observe any reaction (**Scheme 4-06**). Owing to either the low activity of the pyrimidine amino group, or the unstable pyrimidine carbamate.

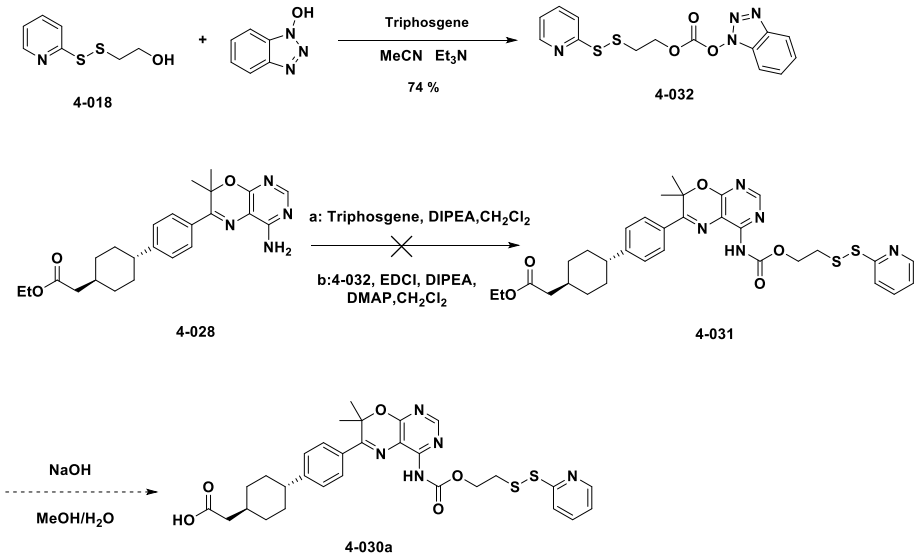

Scheme 4-06 Synthesis of intermediate 4-030a

Moving back to the conjugate design. We tried to hydrolyze **4-028** and couple the linker to the carboxyl group. For T863 **4-029**, carboxyl group (-COOH) is an important pharmacodynamic group. If T863 **4-029** the carboxyl group is not protected, normal tissues of the body might be inhibited in the later *in vivo* experiments. Therefore, **4-029** was obtained by hydrolysis of **4-028**, then **4-029** was coupled to **4-018** *via* EDCI catalysis to give **4-030b**. Finally, **4-030b** was exchanged with pHLIPx *via* disulfide to obtain conjugate **4-031**[3] (**Scheme 4-04** and **Scheme 4-07**)**.**

[3] The last step of coupling the peptide was finished by our collaborator *Prof.* Raphaël Frédérick's team Marine Deskeuvre.

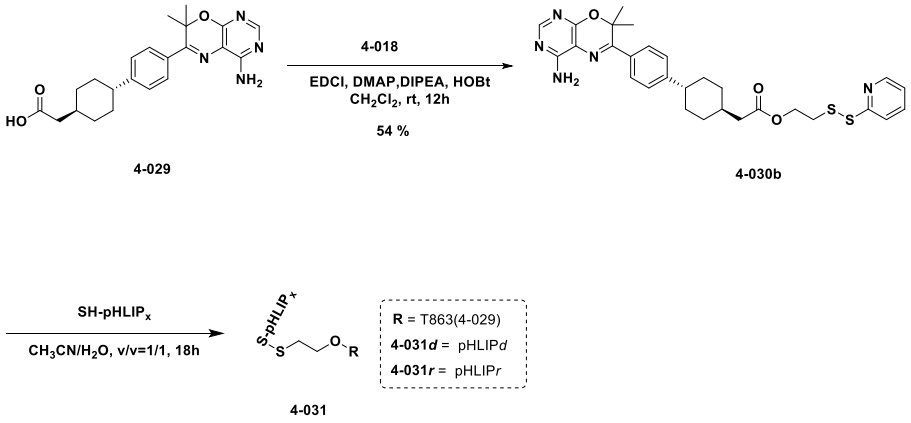

	N-	*C*-
WT-pHLIP	A***C***EQNPIY WARYA***D***WLFTTPLLLL***D***LALLV DADEGT	
Var3	A***C***DDQNP WRAYL***D***LLFPT***D***TLLL***D***LLW	
pHLIP*r*	AAEQNPIY WARYA***D***WLFTTPLLLL***D***LALLV DADEGT***C***G	
pHLIP*d*	AADDQNP WRAYL***D***LLFPT***D***TLLL***D***LLV VDADEGT***C***G	

Scheme 4-07 synthesis of the pHLIP conjugate 4-031 Amino acid sequence of pHLIP: WT-pHLIP is the wild-type sequence, Var3 is the sequence designed by Reshetnyak's team to screen for superiority over WT in tumor cells. pHLIP*r* retains the transmembrane domain amino acid sequence of WT-pHLIP, and modifies the *N* and *C* termini accordingly because of the need for drug delivery through amino acid **C** residues and insertion into the cell. pHLIP*d* was designed and developed based on the Var3 transmembrane domain amino acid sequence (underlining indicates the transmembrane domain of the peptide)

2.7. The properties of conjugates 4-031*d* and 4-031*r*

The Etomoxir conjugates (**4-031*d*** and **4-031*r***) were determined by the analytical HPLC-MS and these conjugates were purified by semi-preparative liquid chromatography. After sample lyophilization, the purity was checked by analytical HPLC-MS. The pKa refers to the pH value at which 50% of the peptides (pHLIP*d* and pHLIP*r*) are inserted into the bilayer of the POPC liposome. The results are shown in **Table 4-05**.

Table 4-05 The properties of conjugates

Peptide	pHLIP*r*	pHLIP*d*
pKa	6.25	4.95
Conjugate	**4-031*r***	**4-031*d***
Molecular weight	4692.4	4303.8
Predicted MS m/z	4691.3	4303.0
MS m/z $[M+3H^+]^{3+}/3$	1564.8	1435.7
Purity	>95%	>95%
Yield	44%	43%

2.8. Verification of the conjugate properties

Using the intrinsic tryptophan fluorescence assay and CD spectrum analysis, we tested the effect of conjugates (**4-031*d*** and **4-031*r***) with liposome bilayers at different pH. In state I (the black line), conjugates were dissolved in pH 8.0 buffer solution without the addition of POPC liposomes. In state II (the blue line), conjugates were dissolved in pH 8.0 buffer solution with the addition of POPC liposomes. In state III (the red line), conjugates were dissolved in pH 5.0 buffer solution with the addition of POPC liposomes (**Figure 4-11** and **Figure 4-12**).

In the pH 8.0 buffer solution (state I), the maximum intrinsic tryptophan fluorescence emission of **4-031*d*** was at 360 nm, and its highest fluorescence intensity was below 100 (**Figure 4-11 A**). The highest intrinsic tryptophan fluorescence emission was blue-shifted and the fluorescence intensity was below 200 when conjugate **4-031*d*** was in the buffer solution (pH 8.0) containing liposome (**Figure 4-11 A**). When exposed to a pH=5.0 acidic environment, intrinsic tryptophan fluorescence intensity increases while the

maximum emission wavelength decreases to 340 nm (**Figure 4-11 A** state III). The fluorescence intensity was thus significantly weaker compared with that of **4-020*d***. **Figure 4-11 B** shows the interaction of **4-031*d*** with liposomes under different pH gradient conditions. The results show that the **4-031*d*** intrinsic tryptophan fluorescence emission maximum shifts towards blue with increasing acidity, but exhibits a very weak fluorescence intensity. According to the intrinsic tryptophan fluorescence assay (**Figure 4-11 C** and **D**), conjugate **4-031*r*** does not have a blue shift and fluorescence intensity increases as pH decreases.

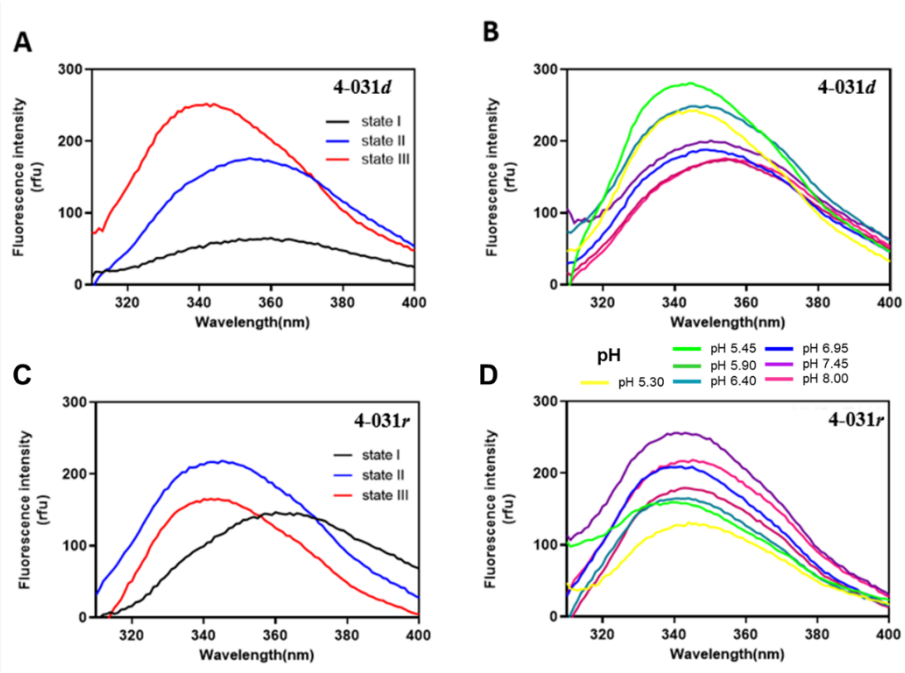

Figure 4-11 Interactions of conjugates (4-031*d* and 4-031*r*) with lipid bilayer Tryptophan fluorescence measurements (A, B, C, D) of peptides in state I (pH 8), state II (pH 8 and POPC vesicles) and state III (pH 5 and POPC vesicles).

The CD spectra showed three states in the negative band at 202 nm. In state III no other negative band was observed at 220-225 nm, so it cannot be proposed that pHLIP occurred in the α-helix under acidic conditions (**Figure**

4-12 A). In the results of **4-031*r***, **Figure 4-12 B** can on indicate that conjugate not occurred α-helix in state III.

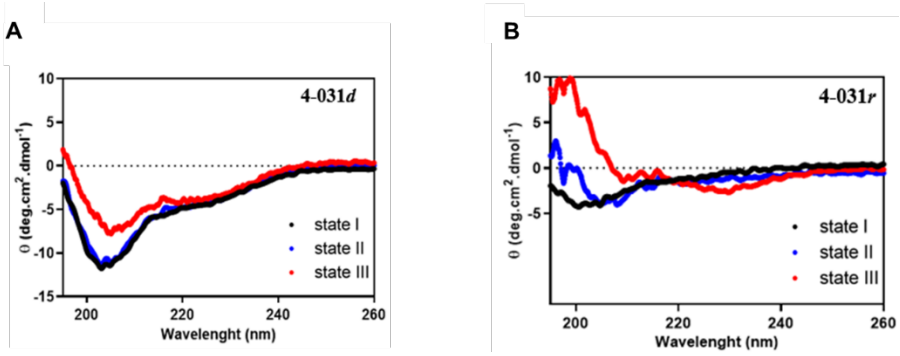

Figure 4-12 Interactions of conjugates (4-031*d* and 4-031*r*) with lipid bilayer. CD spectroscopy (A and B) of peptides in state I (pH 8), state II (pH 8 and POPC vesicles) and state III (pH 5 and POPC vesicles).

By the analysis of **Figures 4-11 A**, **B** and **Figures 4-12 A**, **4-031*d*** may interact with POPC liposomes although the polarity is reduced with decreasing pH. CD value however indicates that under acidic conditions pHLIP*d* does not undergo membrane insertion. There is thus a need of optimization of the α-helix amino acid sequence to overcome the inability of pHLIP*d* needs to deliver drug **4-029** in an acid-dependent manner. **4-031*r*** did not show secondary structure changes between normal and low pH in the presence of liposomes.

In an acidic microenvironment, conjugates **4-031*d*** and **4-031*r*** are unable to transport drug **4-029** into liposomes vesicles. We presume that *in vitro* cell study, the conjugates **4-031*d*** and **4-031*r*** were unable to permeate the cell membrane and deliver drug fragments to the cytoplasm, thus we had chosen not to continue with the next *in vitro* cell study. The pHLIP amino acid sequence will be re-optimized, and new conjugates will be prepared for studies.

3. Conclusion

In this chapter, we successfully synthesized the CPT1 inhibitor Etomoxir (**4-010**) and the DGAT1 inhibitor T863 (**4-029**). By designing and synthesizing the link arm containing the disulfide bond, the drug fragment and pHLIP were successfully combined to give conjugates (**4-020*d***, **4-020*r***, **4-031*d*** and **4-031*r***) (**Scheme 4-08**). Standard analysis and testing methods were used to prove the synthetic intermediates and final conjugates.

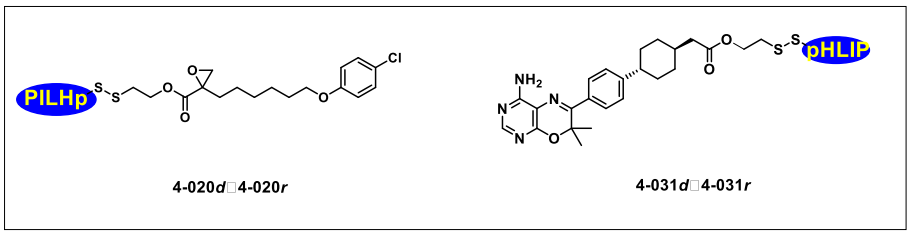

Scheme 4-08 pH sensitive conjugates

Results from the interaction between conjugates and phospholipid choline (POPC) liposome vesicles illustrate (i) that the ability of conjugate **4-020*d*** to insert into liposome in an acidic environment has a greater potential than the that of conjugate **4-020*r***, and (ii) that the optimized pHLIP*d* has more advantages than pHLIP*r*. However, under the same condition, neither conjugate **4-031*d*** or **4-031*r*** can be inserted into liposomes when pHLIP*d* or pHLIP*r* are used to couple DGAT1 inhibitor T863 (**4-029**). In *in vitro* cell studies, the pH-sensitive etomoxir conjugates **4-020*d*** and **4-020*r*** decrease the growth of acidic cancer cells (pre-challenged with DHA) in 2D assay. Optimizing the amino acid sequence of pHLIP to deliver non-polar medicines, such as increasing the percentage of polar amino acids without impacting peptide folding (α-helix), may thus represent an attractive strategy to transport hydrophobic pharmaceuticals.

In conclusion, our results demonstrate that pHLIP technology can be successfully applied to polar anticancer cargoes. Our work suggests that peptide insertion is dependent on the lipid composition but also the peptide sequence and cargo polarity.

4. Reference

1. Corbet, C.; Feron, O., Tumour acidosis: from the passenger to the driver's seat. *Nat Rev Cancer* **2017,** *17* (10), 577-593.
2. Wyatt, L. C.; Lewis, J. S.; Andreev, O. A.; Reshetnyak, Y. K., et al., Applications of pHLIP Technology for Cancer Imaging and Therapy. *Trends Biotechnol* **2017,** *35* (7), 653-664.
3. Svoronos, A. A.; Bahal, R.; Pereira, M. C.; Barrera, F. N., et al., Tumor-Targeted, Cytoplasmic Delivery of Large, Polar Molecules Using a pH-Low Insertion Peptide. *Mol Pharm* **2020,** *17* (2), 461-471.
4. Weerakkody, D.; Moshnikova, A.; Thakur, M. S.; Moshnikova, V., et al., Family of pH (low) insertion peptides for tumor targeting. *Proc Natl Acad Sci U S A* **2013,** *110* (15), 5834-5839.
5. Hunt, J. F.; Rath, P.; Rothschild, K. J.; Engelman, D. M., Spontaneous, pH-dependent membrane insertion of a transbilayer alpha-helix. *Biochemistry* **1997,** *36* (49), 15177-15192.
6. Hanz, S. Z.; Shu, N. S.; Qian, J.; Christman, N., et al., Protonation-Driven Membrane Insertion of a pH-Low Insertion Peptide. *Angew Chem Int Ed* **2016,** *128* (40), 12564-12569.
7. Otieno, S. A.; Hanz, S. Z.; Chakravorty, B.; Zhang, A., et al., pH-dependent thermodynamic intermediates of pHLIP membrane insertion determined by solid-state NMR spectroscopy. *Proc Natl Acad Sci U S A* **2018,** *115* (48), 12194-12199.
8. Song, Q.; Chuan, X.; Chen, B.; He, B., et al., A smart tumor targeting peptide-drug conjugate, pHLIP-SS-DOX: synthesis and cellular uptake on MCF-7 and MCF-7/Adr cells. *Drug Deliv* **2016,** *23* (5), 1734-1746.
9. Andreev, O. A.; Engelman, D. M.; Reshetnyak, Y. K., Targeting acidic diseased tissue: New technology based on use of the pH (Low) Insertion Peptide (pHLIP). *Chimica oggi* **2009,** *27* (2), 34.
10. Andreev, O. A.; Engelman, D. M.; Reshetnyak, Y. K., pH-sensitive membrane peptides (pHLIPs) as a novel class of delivery agents. *Mol Membr Biol* **2010,** *27* (7), 341-352.
11. Andreev, O. A.; Dupuy, A. D.; Segala, M.; Sandugu, S., et al., Mechanism and uses of a membrane peptide that targets tumors and other acidic tissues in vivo. *Proc Natl Acad Sci U S A* **2007,** *104* (19), 7893-7898.
12. Fendos, J.; Engelman, D., pHLIP and acidity as a universal biomarker for cancer. *Yale j. bio. med.* **2012,** *85* (1), 29.
13. Thevenin, D.; An, M.; Engelman, D. M., pHLIP-mediated translocation of membrane-impermeable molecules into cells. *Chem Biol* **2009,** *16* (7), 754-762.
14. An, M.; Wijesinghe, D.; Andreev, O. A.; Reshetnyak, Y. K., et al., pH-(low)-insertion-peptide (pHLIP) translocation of membrane impermeable phalloidin toxin inhibits cancer cell proliferation. *Proc Natl Acad Sci U S A* **2010,** *107* (47), 20246-20250.
15. Burns, K. E.; Robinson, M. K.; Thevenin, D., Inhibition of cancer cell proliferation and breast tumor targeting of pHLIP-monomethyl auristatin E conjugates. *Mol Pharm* **2015,** *12* (4), 1250-1258.
16. Burns, K. E.; Thevenin, D., Down-regulation of PAR1 activity with a pHLIP-based allosteric antagonist induces cancer cell death. *Biochem J* **2015,** *472* (3), 287-295.
17. Reshetnyak, Y. K.; Andreev, O. A.; Lehnert, U.; Engelman, D. M., Translocation of molecules into cells by pH-dependent insertion of a transmembrane helix. *Proc Natl Acad Sci U S A* **2006,** *103* (17), 6460-6465.
18. Zoonens, M.; Reshetnyak, Y. K.; Engelman, D. M., Bilayer interactions of pHLIP, a peptide that can deliver drugs and target tumors. *Biophys J* **2008,** *95* (1), 225-235.
19. Reshetnyak, Y. K.; Moshnikova, A.; Andreev, O. A.; Engelman, D. M., Targeting Acidic Diseased Tissues by pH-Triggered Membrane-Associated Peptide Folding. *Front Bioeng Biotechnol* **2020,** *8*, 335.
20. Corbet, C.; Feron, O., Emerging roles of lipid metabolism in cancer progression. *Curr Opin Clin Nutr Metab Care* **2017,** *20* (4), 254-260.

21. Carracedo, A.; Cantley, L. C.; Pandolfi, P. P., Cancer metabolism: fatty acid oxidation in the limelight. *Nat Rev Cancer* **2013,** *13* (4), 227-232.
22. Currie, E.; Schulze, A.; Zechner, R.; Walther, T. C., et al., Cellular fatty acid metabolism and cancer. *Cell Metab* **2013,** *18* (2), 153-161.
23. Linher-Melville, K.; Zantinge, S.; Sanli, T.; Gerstein, H., et al., Establishing a relationship between prolactin and altered fatty acid beta-oxidation via carnitine palmitoyl transferase 1 in breast cancer cells. *BMC Cancer* **2011,** *11*, 56.
24. Ceccarelli, S. M.; Chomienne, O.; Gubler, M.; Arduini, A., Carnitine palmitoyltransferase (CPT) modulators: a medicinal chemistry perspective on 35 years of research. *J Med Chem* **2011,** *54* (9), 3109-3152.
25. Holubarsch, C. J.; Rohrbach, M.; Karrasch, M.; Boehm, E., et al., A double-blind randomized multicentre clinical trial to evaluate the efficacy and safety of two doses of etomoxir in comparison with placebo in patients with moderate congestive heart failure: the ERGO (etomoxir for the recovery of glucose oxidation) study. *Clin Sci (Lond)* **2007,** *113* (4), 205-212.
26. Hernandez-Corbacho, M. J.; Obeid, L. M., A novel role for DGATs in cancer. *Adv Biol Regul* **2019,** *72*, 89-101.
27. Petan, T., Lipid Droplets in Cancer. In *Rev Physiol Biochem Pharmacol*, 2020 1-34.
28. Bacci, M.; Lorito, N.; Smiriglia, A.; Morandi, A., Fat and Furious: Lipid Metabolism in Antitumoral Therapy Response and Resistance. *Trends Cancer* **2021,** *7* (3), 198-213.
29. Fox, B. M.; Sugimoto, K.; Iio, K.; Yoshida, A., et al., Discovery of 6-phenylpyrimido [4, 5-b][1, 4] oxazines as potent and selective acyl CoA: diacylglycerol acyltransferase 1 (DGAT1) inhibitors with in vivo efficacy in rodents. *J Med Chem* **2014,** *57* (8), 3464-3483.
30. Sau, A.; Pellizzari Tregno, F.; Valentino, F.; Federici, G., et al., Glutathione transferases and development of new principles to overcome drug resistance. *Arch Biochem Biophys* **2010,** *500* (2), 116-122.
31. Eistetter, K.; Wolf, H. P., Synthesis and hypoglycemic activity of phenylalkyloxiranecarboxylic acid derivatives. *J Med Chem* **1982,** *25* (2), 109-113.
32. Scott, R.; Golding, B. T., Improved synthesis of enantiomerically pure Etomoxir and its 2, 4-dinitrophenyl analogue. *Arkivoc* **2004**.
33. Piatnitski Chekler, E. L.; Unwalla, R.; Khan, T. A.; Tangirala, R. S., et al., 1-(2-Hydroxy-2-methyl-3-phenoxypropanoyl)indoline-4-carbonitrile derivatives as potent and tissue selective androgen receptor modulators. *J Med Chem* **2014,** *57* (6), 2462-2471.
34. Latorre, A.; Couleaud, P.; Aires, A.; Cortajarena, A. L., et al., Multifunctionalization of magnetic nanoparticles for controlled drug release: a general approach. *Eur J Med Chem* **2014,** *82*, 355-362.
35. Anderson, J. S.; Bowitch, G. S.; Brewster, R. L., Influence of conformation on the fluorescence of tryptophan-containing peptides. *Biopolymers* **1983,** *22* (11), 2459-2476.
36. Alston, R. W.; Lasagna, M.; Grimsley, G. R.; Scholtz, J. M., et al., Peptide sequence and conformation strongly influence tryptophan fluorescence. *Biophys J* **2008,** *94* (6), 2280-2287.
37. Greenfield, N. J., Applications of circular dichroism in protein and peptide analysis. *TrAC Trend Anal Chem* **1999,** *18* (4), 236-244.
38. Greenfield, N. J., Using circular dichroism spectra to estimate protein secondary structure. *Nat Protoc* **2006,** *1* (6), 2876-2890.
39. Holzwarth, G.; Doty, P., The Ultraviolet Circular Dichroism of Polypeptides. *J Am Chem Soc* **1965,** *87*, 218-228.
40. Dierge, E.; Debock, E.; Guilbaud, C.; Corbet, C., et al., Peroxidation of n-3 and n-6 polyunsaturated fatty acids in the acidic tumor environment leads to ferroptosis-mediated anticancer effects. *Cell Metab* **2021,** *33* (8), 1701-1715.
41. Yeh, V. S.; Beno, D. W.; Brodjian, S.; Brune, M. E., et al., Identification and preliminary characterization of a potent, safe, and orally efficacious inhibitor of acyl-CoA:diacylglycerol acyltransferase 1. *J Med Chem* **2012,** *55* (4), 1751-1757.

Chapter III

Targeting Hypoxia Microenvironment of Tumors for the Design and Synthesis of Bio-reductive Prodrug

Pharmacological evaluation data for prodrug provided by Laurenne Petit from *Prof.* Olivier Feron's team

Part A

Design, synthesis and pharmacological evaluations of hypoxia-activated prodrugs containing aromatic Nitro- and Azo- moieties

1. Introduction

Hypoxia is a well-known feature of the microenvironment in solid tumors, which is usually attributed to the rapid growth of the tumor and an inefficient tumor vasculature, resulting in inadequate oxygen supply within the solid tumor. Oxygen (O_2) levels in normal tissues are 2%-9% v/v (approximately 40 mmHg pO_2 as a mean value) [1]. In contrast, O_2 levels in the hypoxic tumor microenvironment are 0.02 %-2.0 % v/v (usually considered to be below 10 mmHg pO_2) [2, 3]. Hypoxia plays a key role in cancer resistance and recurrence because hypoxia's effects on cellular controls that regulate the cell cycle and the escape from apoptosis. In addition, hypoxia increases cell invasion and metastasis, contributes to immune-evasion, and considerably alters metabolism of cancer cells[4]. Still, hypoxia offers therapeutic opportunities through the development the prodrugs able to reveal their activity at low pO_2. These agents are called hypoxia-activated prodrugs (HAPs). These bioreductive prodrugs are inactive compounds (under normoxia conditions) that can be selectively reduced under hypoxic conditions by endogenously expressed oxidoreductases to produce active antitumor effectors. These prodrugs are usually generated by chemically bonding a bioreductive protective group to the active parent compound's pharmacophore site[5].

HAPs can be classified according to chemical structures as nitro compounds, azo compounds, *N*-oxide compounds, quinones and transition metal complexes[6]. Depending on the threshold of hypoxia required for the activation of the prodrug compound, HAPs can be divided into two main groups, including those with relatively mild hypoxic activation, which include benzotriazine, *N*-oxide compounds, *etc*., and those with severe dependent deep hypoxic activation, which contain mainly nitro unit[7]. In a deeply hypoxic microenvironment, the radical prodrug intermediates formed by the 1-electron reductase initiation are more stable (i.e., low concentration of oxygen prevents

the oxidation of the radical to the starting prodrug) and can be further and more easily reduced to active drug molecules[8] (**Figure 5A-01**). Often, active drug molecules are compounds inducing DNA damages or inhibitors of enzymes (such as those involved in hypoxia-induced metabolic pathways in cancer cells).

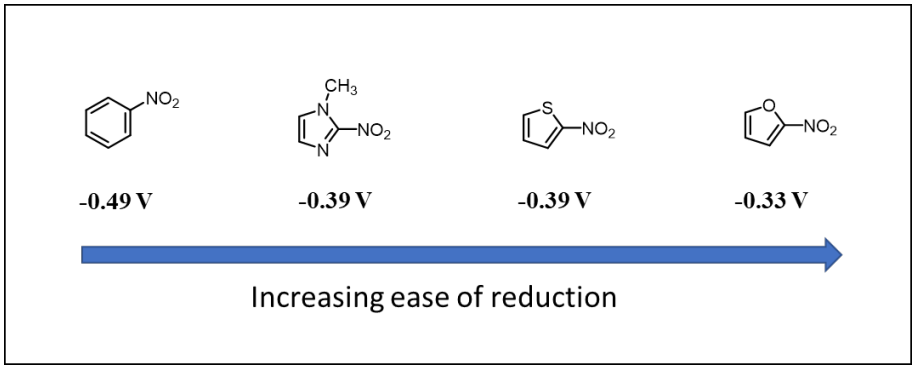

Figure 5A-01 Estimated values of reduction potentials $E(ArNO_2/ArNO_2^-)$ versus NHE in water at pH 7 for commonly used nitroaryl bioreductive systems [5, 9]

Nitro-based HAPs were the first group of compounds to show the oxygen-sensitive redox cycling which is a characteristic of bioreductive prodrugs[7]. Common bioreductive prodrugs of nitro-aromatic compounds include mainly 4-nitrobenzyl and 1-methyl-2-nitroimidazole groups, and nitro groups also include nitrofuranyl and nitrothiophene based groups as the basis of bioreductive compounds. Wardman has estimated the reduction potential $E(ArNO_2/ArNO_2^-)$ versus the normal hydrogen electrode (NHE) by an electrochemical reduction of the commonly used nitroaromatic bioreduction group in water at pH 7[5, 9] (**Figure 5A-02**). Although oxygen-dependent bioreduction in humans occurs mainly through a single-electron mechanism in contrast to the electrochemical reduction method described above, its pH is acidic in an oxygen-deficient microenvironment. The reduction potentials above demonstrate the ease of reduction of various nitro groups. The reduction potential shows that the nitrofuranyl group is easiest to reduce, and the most difficult and with the highest negative potential is the nitrobenzyl group.

Among them, the 1-methyl-2-nitroimidazolyl group has the same reduction potential as the nitrothiophenyl group, but its potential difference with the nitrofuranyl group is not particularly large. These 4-nitrobenzyl groups and 1-methyl-2-nitroimidazolyl are widely used in research.

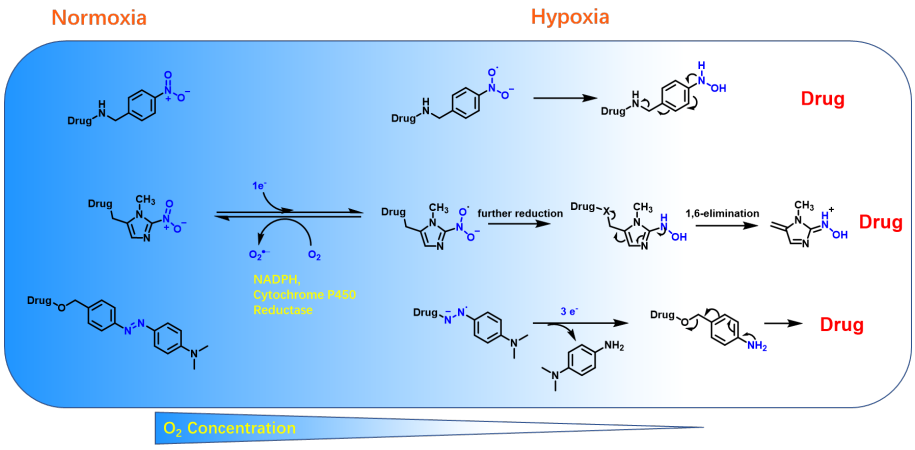

Figure 5A-02 Mechanism of hypoxia-activated prodrug release

Compounds containing azo groups are used commercially as brightly coloured dyes, in the textile, leather and food industries. The electron deficient nature of the azo group (-N=N-) increases the chemical reaction between the azo compound and the reducing agent[10]. In normoxia tissues, the reduction of azo bonds is inhibited. Still, in the internal microenvironment of solid tumors hypoxia leads to the accumulation of various reducing substances such as $FADH_2$ and NADH, which stimulates increased expression of reducing enzymes such as Azo reductases (AzoR)[11, 12]. Under low oxygen conditions, AzoR first reduces azo group (-N=N-) to hydrazine, and then further electron transfer cleaves the azo bond to the aniline metabolite[11](**Figure 5A-02**). Thus, compounds containing azo groups are prepared to be used hypoxia-sensitive probes and as prodrugs for tumor-targeted therapies.

In this thesis, we selected diclofenac (i.e., a repurposed MCT4 inhibitor) and tetrandrine (i.e., a more conventional anticancer cytotoxic compound) as two

drugs of interest that would gain to be converted into hypoxia-activated prodrugs.

Monocarboxylate transporter 4 (MCT4) is an H^+ coupled cotransport protein that is highly expressed in metastatic tumors and at sites of hypoxia or Warburg effect[13]. At these sites, extracellular lactate and/or acidosis contributes to malignancy and immune response evasion. Diclofenac **5A-001**, a member of the arylacetic acid family of NSAIDs, non-competitively inhibits lactate transport by MCT4[14]. The O. Feron's team reported that cancer cells become addicted to MCT4 to handle excess lactate production when the other lactate transporter isoform MCT1 is inhibited. This shift renders cancer cells particularly adapted to hypoxic conditions, and resistant to OXPHOS inhibitors and anti-proliferative chemotherapy[15]. When diclofenac is used to inhibit the activity of MCT4 or when knocking out the MCT4 gene tumor growth is inhibited[15]. Although encouraging, to treat cancers by applying high concentrations of diclofenac, various side effects caused by the inhibition of cyclooxygenase (COX) need to be overcome, such as gastrointestinal bleeding and peptic ulcers[16]. To avoid this issue, we aimed here to prepare diclofenac as a HAP that selectively targets glycolytic tumor cells in the hypoxic region.

The natural product tetrandrine **5A-002**, isolated from the plant *Stephania tandra*, belongs to the group of bisbenzylisoquinoline alkaloids[17]. Tetrandrine has a wide range of pharmacological activities, including anticancer[18-20], antiviral[21, 22], Ca^{2+} channel blocking[23], reversal of multidrug resistance (MDR)[24], *etc*. These pharmacological activities have received a lot of attention from pharmacologists as potential drug candidates. Unfortunately, these bisbenzylisoquinoline alkaloids exhibited toxic reactions to the liver and lungs, which hinder their application[25-27]. Therefore, we aim to develop tetrandrine as a HAP able to exert anticancer effects while sparing detrimental systemic effects.

In this chapter, we selected three hypoxia-activated probes, including 4-nitrobenzyl unit, 1-methyl-2-nitroimidazolyl unit and azo groups. As the antitumor drug, tetrandrine which has broad-spectrum antitumor effects, and diclofenac which inhibits the efflux of lactic acid, a glycolytic product of tumor cells. The chemical bonds linking hypoxia-activated probes to antitumor drugs are mainly coupled by alkyl ethers (-O-), nitrogen (-NH-), ester groups (-OCO-) or carbamates (-OCON-)[28, 29] (**Figure 5A-03**).

Regarding the coupling site of the drug, we need to make sure that the pharmacological activity of the prodrug is inactivated during the period of non-reduction, or that the pharmacological activity of the prodrug in an inactive state is very weak. This means that the bioreducing group needs to be attached to the active group part of the drug, and the resulting prodrug molecule is lacking activity. In the case of diclofenac prodrugs, we have envisaged two approaches: coupling bioreductive groups to the *N*-diclofenac by carbamate or amination, and strategy where the coupling is directly at the carboxyl part by ester bonding (**Figure 5A-03 I**) (see below **2.1.1.**). In the tetrandrine section, an amino group is introduced at the position 14 of tetrandrine, which is coupled to the hypoxia-activating unit *via* the corresponding carbamate (**Figure 5A-03 II**) (see below **2.2.1.**).

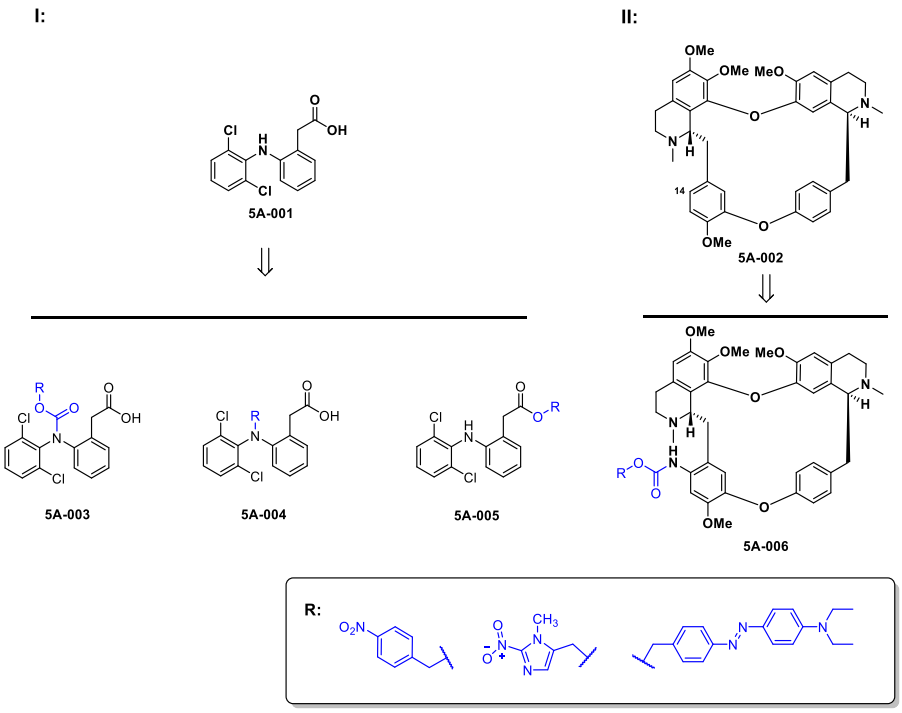

Figure 5A-03 Overall scheme for Part A

2. Results and discussion

2.1.1. Rational design hypoxia-sensitive prodrugs diclofenac

To synthesize hypoxia-sensitive diclofenac derivatives, four main synthetic schemes were designed to prepare the prodrugs containing nitro units (**Scheme 5A-01**). **Schemes 5A-01 A1** and **A2** refers to the grafting of hypoxia-sensitive nitro groups on diclofenac. **Schemes A3** and **A4** describe the generation of hypoxia-sensitive diclofenac prodrugs using organic synthesis strategies from inexpensive reagents as starting materials.

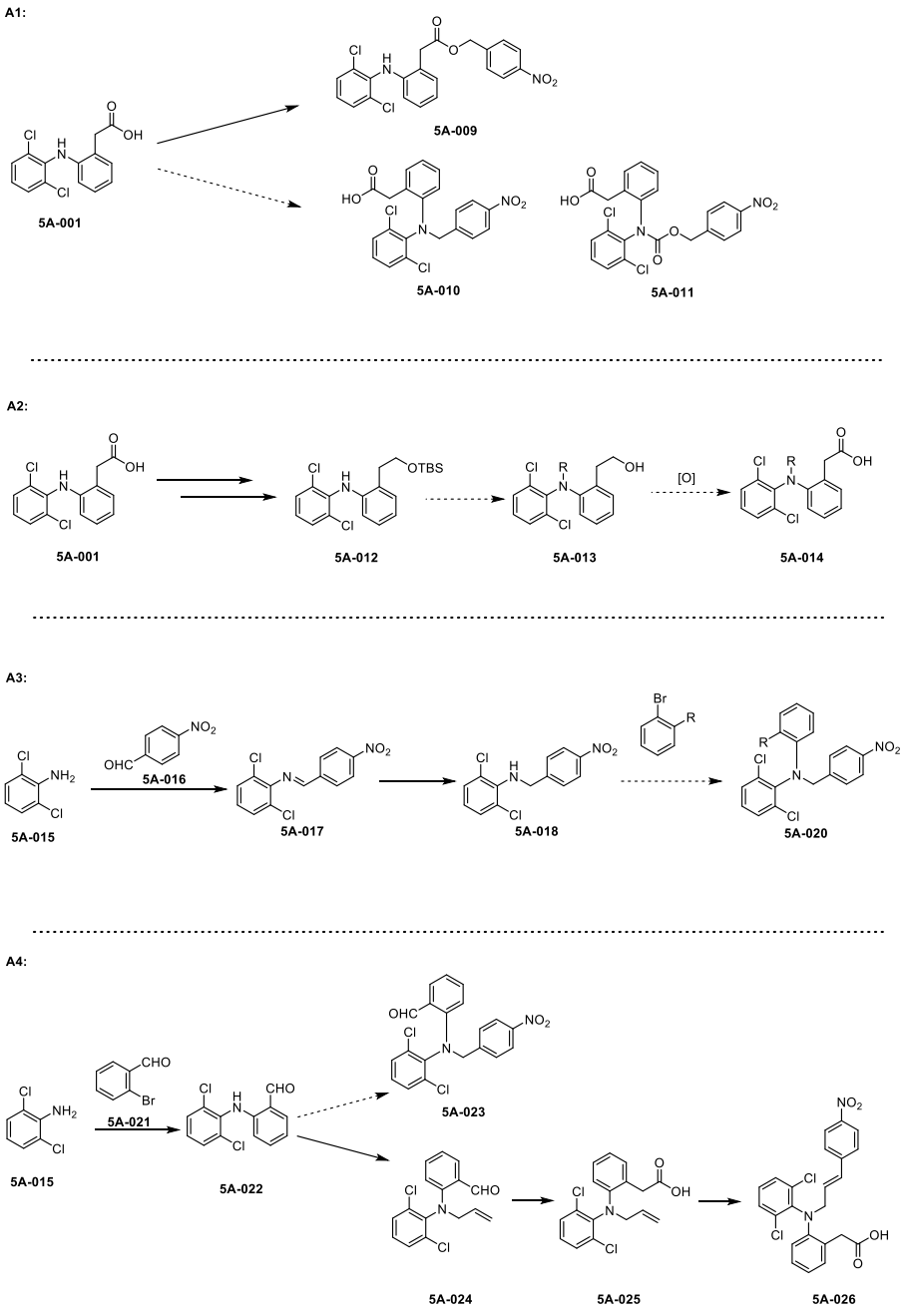

Scheme 5A-01 Synthesis strategies for hypoxia-activated diclofenac prodrugs

2.1.2. Synthesis of hypoxia-sensitive diclofenac prodrugs

2.1.2.1. Synthesis strategy A1

The initial synthetic strategy tried to directly modify the structure of diclofenac. Firstly, diclofenac was reacted with 4-nitrobenzyl bromide under weak base conditions to give the carboxyesterified **5A-009**[30] (**Scheme 5A-02 I**), with a good yield. Next, the nitro unit was introduced in the *N*-diclofenac to obtain the prodrug of the tertiary amine. The carboxyl group was first protected by esterification to give **5A-029**, but some of the diclofenac was found to undergo intermolecular spontaneous amidation catalyzed by concentrated sulfuric acid to give the side product **5A-030** in an 11% yield. Next, we attempted to couple **5A-029** and **5A-028,** by using first triphosgene in the presence of DIPEA, to generate the corresponding carbamoyl chloride, which would be reacted with **5A-028**[31]. However, we did not isolate the desired carbamate **5A-031**. The reaction of **5A-029** with **5A-027,** following treatment of the ester with the strong base NaH was then tested. In the presence of NaH, **5A-029** underwent cyclization to give the thermodynamically stable lactam **5A-030**. The weaker DIPEA base was also tried, but did not give the target product **5A-032** (**Scheme 5A-02 II**).

The possible reason is that the lone pair of electrons on the N-diclofenac forms a conjugation between two benzene rings, making it difficult to activate the N-H bond. Another possibility is that the spatial restriction created by the Cl atom adjacent to the benzene ring around the N atom makes it harder for the reaction to proceed.

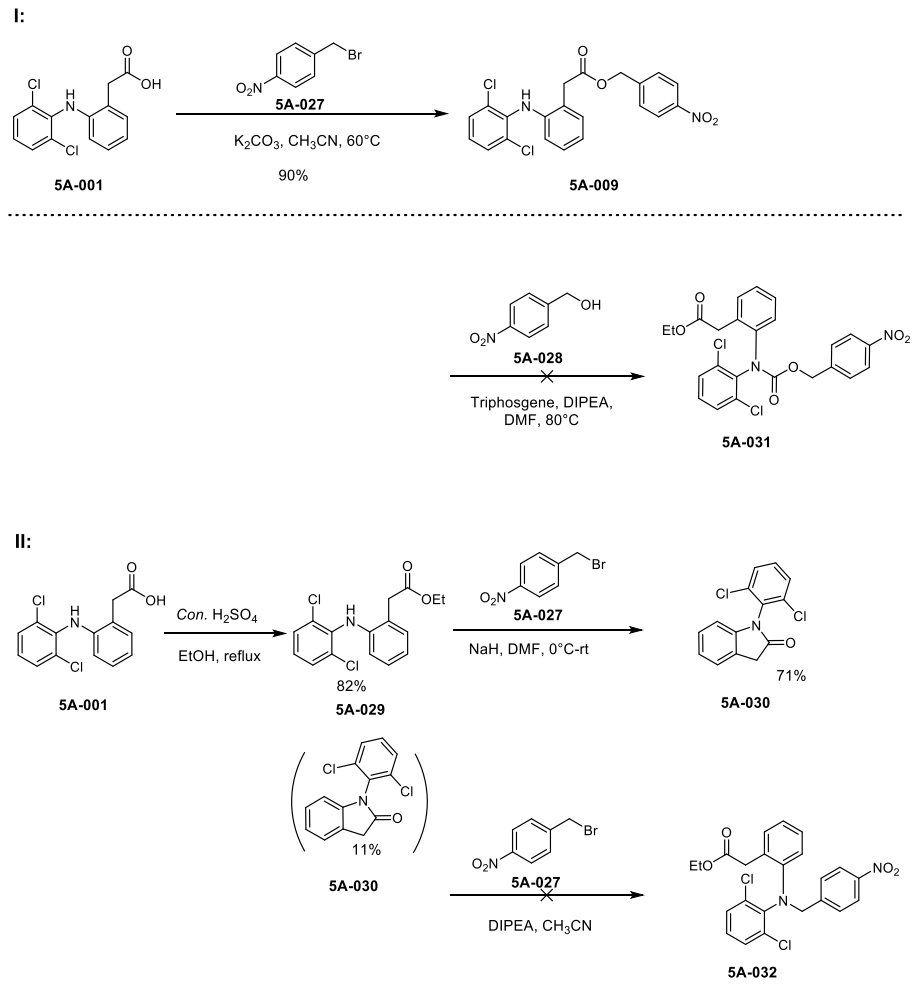

Scheme 5A-02 Synthetic route A1 for hypoxia-activated diclofenac prodrugs

2.1.2.2. Synthesis strategy A2

In order to avoid the carboxyl groups on the amidation and the strong capacity to cyclize the stable lactam. We decided to work on a non-reactive precursor group of this acid. In this part, DIBAL-H was used to reduce the ester **5A-029** to the corresponding primary alcohol **5A-033**[32]. The hydroxyl group was then protected by a TBS group to obtain **5A-012**. This time, NaH activated the (-NH-) bond before adding the bromide reagent **5A-027** to the reaction mixture.

However, we could not isolate the expected alkylation product. As a result, we were forced to abandon this synthetic route (**Scheme 5A-03**).

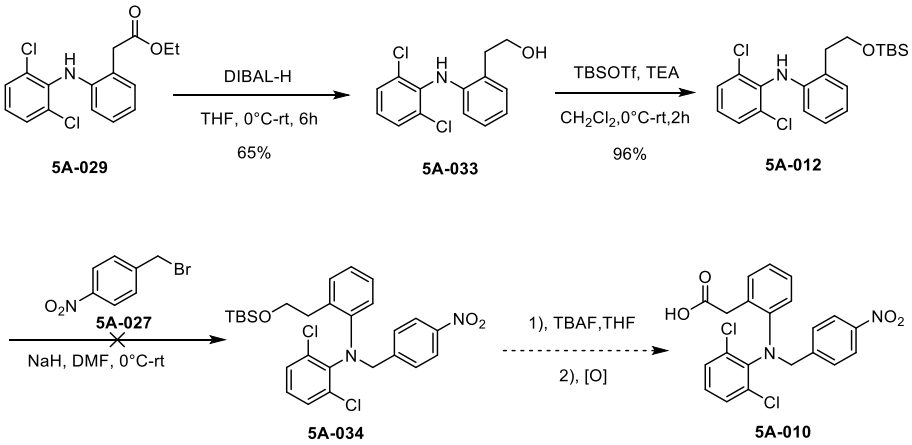

Scheme 5A-03 Synthetic route A2 for hypoxia-activated diclofenac prodrugs

2.1.2.3. Synthesis strategy A3

Because it was not possible to produce the *N*-substituted prodrugs directly from the alkylation of the nitrogen atom diclofenac, as presented in **Schemes 5A-02** and **5A-03**. We decided to build the molecule from commercially available precursors, and introduce the nitrobenzyl units at the early stage of the synthesis. Thus, in the third synthetic route, we tried a reformulation approach: first reacting *o,o'*-dichloro-aniline **5A-015** with *p*-nitro-benzaldehyde to obtain the corresponding Schiff base **5A-017**, next to reducing the Schiff base to the secondary amine **5A-018**, and finally using transition metal-catalyzed coupling reaction to introduce the last aromatic group, as described in **Scheme 5A-04**.

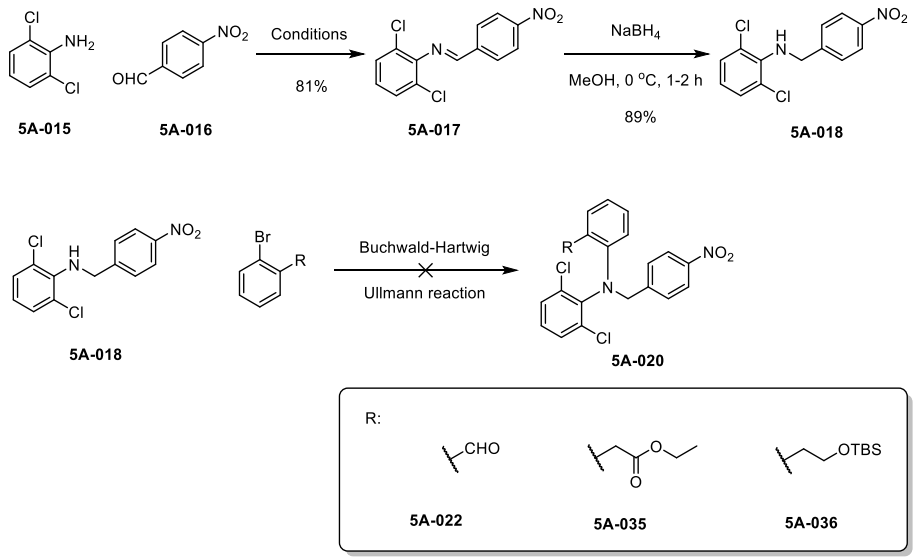

Scheme 5A-04 Synthetic route A3 for hypoxia-activated diclofenac prodrugs

For synthesize the Schiff base **5A-017**, we first tried the most widely used approach, where a PTSA (*p*-toluenesulfonic acid)-catalyzed Schiff base condensation between the aniline and aldehyde in refluxing toluene, using a Dean-Stark apparatus to separate the water generated during the reaction[33]. However, the reaction was unable to proceed as planned (**Table 5A-01 1**) and the starting materials were recovered. The $ZnCl_2$/AcOH-catalyzed reaction was also tried, albeit without any success[34] (**Table 5A-01 2**). Then the Borch reductive amination reaction with $NaBH(OAc)_3$ was also attempted[35]. However, the results were unsatisfactory (**Table 5A-01 3**).

All those failed attempts could be attributed to the low reactivity of the *o,o'*-disubstituted aniline, so we decided to check the literature for more efficient methods describing condensation reactions using sterically hindered aromatic amines such as **5A-015**. It has been reported that the activation of dichloroaniline **5A-015** with $AlMe_3$ as a Lewis acid result in the formation of Schiff base through condensation with aldehydes[36]. Therefore, we used $AlMe_3$ to activate dichloroaniline **5A-015** under heating reflux conditions to obtain

the metal complex intermediate and then added nitrobenzaldehyde **5A-016** to the reaction under reflux conditions for 6h to obtain Schiff base **5A-017** (**Table 5A-01 3**) in an 81% yield. The Schiff base **5A-017** was then treated with $NaBH_4$ to give the secondary amine **5A-018** (**Scheme 5A-04**) in an 89% yield.

Table 5A-01 Optimization of reaction conditions

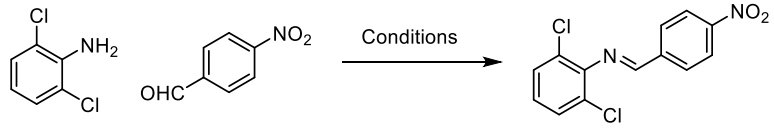

5A-015 **5A-016** **5A-017**

Entry	Reagents and Conditions	Result	Yield
1	PTSA, Tol, reflux, 36h	N.D.	-
2	$ZnCl_2$, AcOH, EtOH, reflux, 24h	N.D.	-
3	$NaBH(OAc)_3$, AcOH, DCE, r.t.,48h	N.D.	-
4	1) $AlMe_3$, Tol, reflux, 6h 2) *p*-NO_2-benzaldehyde, reflux, 6h	Working	81%

Following that, we introduced the second aromatic group on the nitrogen atom by using a palladium-catalyzed Buchwald-Hartwig reaction of **5A-018** with ortho substituted bromo-benzene derivatives (**5A-022**, **5A-035**, or **5A-036**), where the *ortho*-substituent is a precursor of the "-CH_2-COOH" fragment. Many experiments were carried out by the variations of the reaction parameters in sealed tubes and representative examples are presented in (**Table 5A-02**) [37, 38]. We were not able to isolate any expected arylation product. So, we turned to the catalyzed Ullmman reaction under high-temperature sealing conditions[39], but no reaction occurred (**Table 5A-02**).

The lack of reactivity of these metal-catalyzed coupling reactions was attributed to the strong steric hindrance of the *ortho*-substituted bromo derivatives and the poor reactivity of the secondary aromatic amine. Therefore, we decided to abandon this route and change again our strategy.

Table 5A-02 Screening reaction conditions

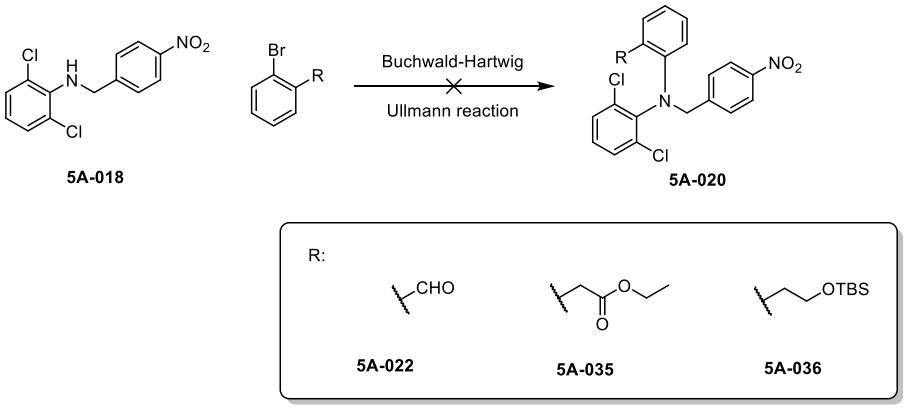

Entry	Reagents and Conditions	Result
1	$Pd_2(dba)_3$, *r*-BINAP, *t*-BuONa, Tol, 130 °C, 12-24h sealed tube	N.D.
2	$Pd_2(dba)_3$, *r*-BINAP, *t*-BuONa, Mesitylene, 165 °C, 12-24h sealed tube	N.D.
3	CuI, KI, K_2CO_3, DMF, 165 °C sealed tube	N.D.

2.1.2.4. Synthesis strategy A4-1

As none of the three synthetic strategies described above yielded the target products, we conducted a more extensive literature survey. A patent reported that treatment of 2-((2,6-dichlorophenyl) amino) benzaldehyde **5A-022** with NaH, followed by addition of allyl bromide, gave the *N*-allylated product **5A-040**[40]. Inspired by this result, we designed a new strategy described here in **Scheme 5A-05**. Using a copper-catalyzed Ullmman reaction, 2-((2,6-dichlorophenyl) amino) benzaldehyde **5A-022** was synthesized from commercially available inexpensive dichloroaniline and *o*-bromo

benzaldehyde[39]. We planned to adapt the reported synthesis by alkylation or acylation of **5A-022** to prepare the *N*-substituted aldehydes **5A-040**. It should be noted that the *N*-allyl diclofenac synthesis was previously optimized in our group by Marine Lefevre and was the base of our synthesis. These aldehydes could be transformed into the target acids **5A-044**, using a three-step synthesis described in the literature[40].

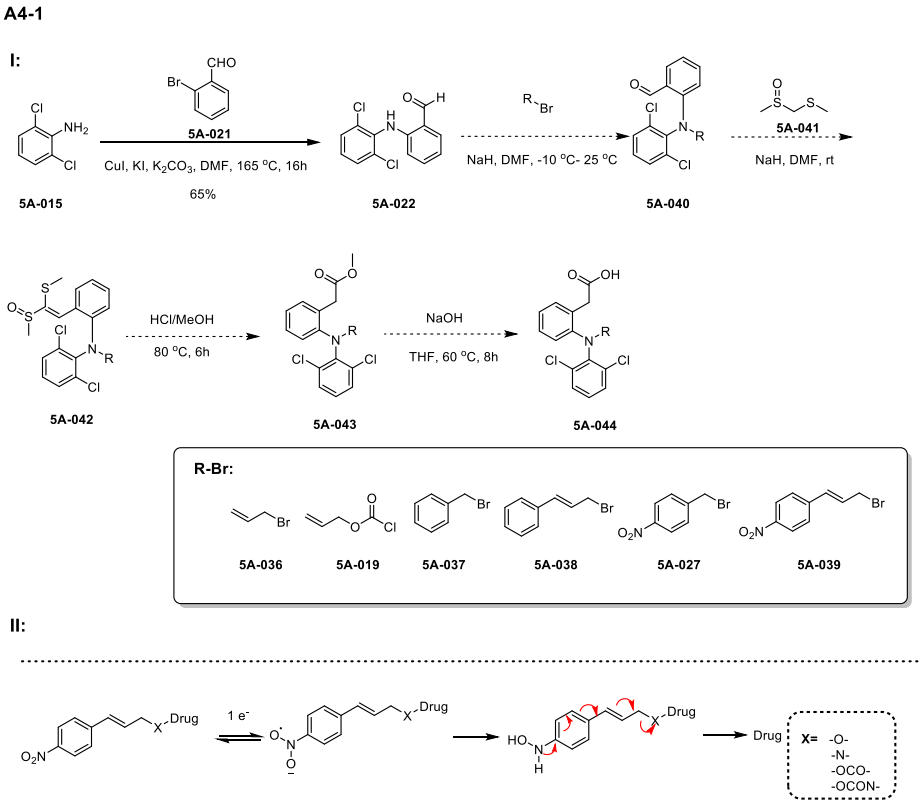

Scheme 5A-05 Synthetic route A4-1 for hypoxia-activated diclofenac prodrugs

To demonstrate the feasibility of this synthetic strategy, the copper-catalyzed Ullmman reaction was used to prepare **5A-022** in a 65% yield. This aldehyde first reacted with NaH in DMF to generate the amide anion, followed by an electrophile. We first reproduced the work of Marine Lefevre with allyl bromide and obtained the *N*-allylated product **5A-024** in an 82% yield.

However, when an acyl derivative like allyl chloroformate **5A-019** was used, we did not observe the formation of the *N*-acylated product. So, we turned to benzylic bromides **5A-037** and cinnamyl bromides **5A-038**. The coupling was successful when using simple benzyl bromide, allowing the formation of the *N*-benzylated product **5A-045** in an 84% yield. Cinnamyl bromide was equally active in this reaction and we finally turned to the nitro-derivatives of those two electrophiles. Unfortunately, when *p*-nitro-benzyl bromide **5A-027** and *p*-nitro-cinnamyl bromide **5A-039** were used, we were not able to isolate the expected *N*-alkylation adducts.

We tried to understand why the use nitro-substituted alkylating agents did not give the expected substitution reactions. These electrophiles are indeed much more reactive than their non-substituted counterparts, but they can also react with soft nucleophiles though radical anion mechanisms[41, 42]. In our case, single electron transfer reactions between these electrophiles and the amide anion, could give a rise to the decomposition and formation of various side products.

Table 5A-03 Screening reaction conditions

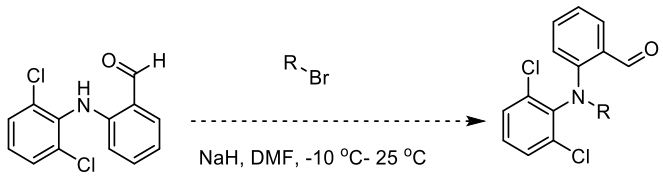

5A-022 **5A-040**

Entry	5A-040	Result	Yield
1	5A-024 R= 	working	82%
2	5A-019 R= 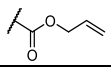	N.D.	-

3	5A-045 R= 	working	84%
4	5A-046 R= 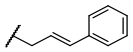	working	64%
5	5A-047 R= 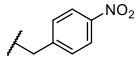	N.D.	-
6	5A-048 R= 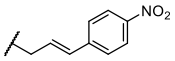	N.D.	-

2.1.2.5. Synthesis strategy A4-2

From these observations and experiments, we could conclude that it was not possible to directly introduce the nitro-group on the aromatic of the alkylating agent, so we devised some alternate strategies to introduce this group at a later stage of the synthesis. By using a bromine atom on the benzyl group and following the same synthetic group described in **Scheme 5A-06**. We replaced the bromine atom by a nitro-group in a two-steps sequence: a) a palladium catalyzed borylation with tetrahydroxydiboron (BBA) to form boronic acid **5A-054**[43, 44]. b) A photocatalyzed transformation of the boronic acid group into a nitro group of **5A-054** to form the target product **5A-057** or through the metal-free protocol nitration reaction, **5A-057** is prepared by electrophilic nitration reaction between *N*-nitroso saccharin **5A-056** and the substrate **5A-054** in the solvent HFIP[45, 46] (**Scheme 5A-06**).

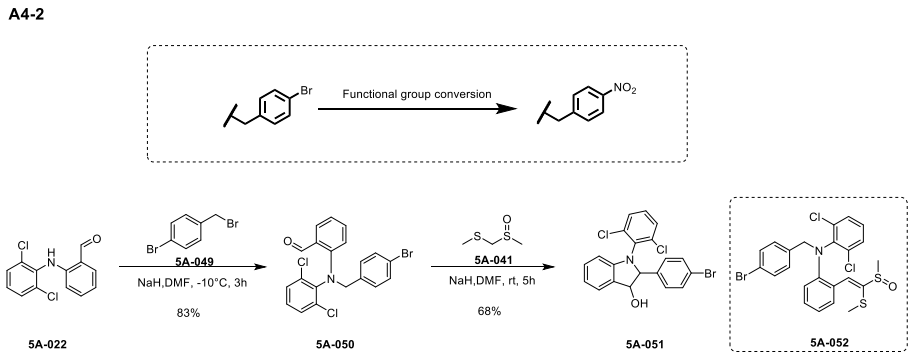

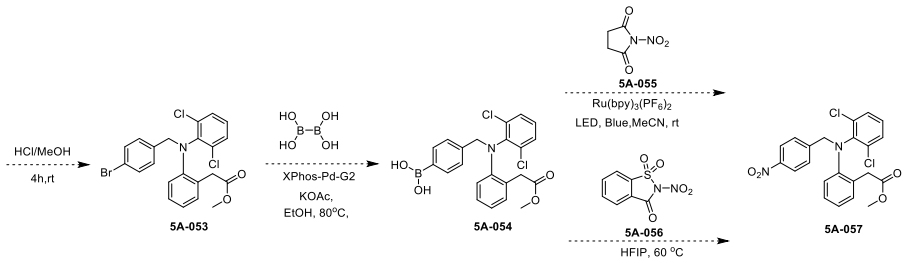

Scheme 5A-06 Synthetic route A4-2 for hypoxia-activated diclofenac prodrugs

The addition of 1-bromo-4-(bromomethyl)-benzene **5A-049,** after NaH treatment of **5A-022**, gave the tertiary amine compound **5A-050** in an 83% yield. The major compound obtained by stirring the sulfoxide **5A-041** and aldehyde **5A-050** in the presence of NaH was purified by silica gel chromatography and analyzed. However, structural analysis showed that we did not obtain the product **5A-052** we had predicted, the compound for which we attributed the structure **5A-051** (**Scheme 5A-06**). This compound could be formed through an intramolecular cyclisation of the starting aldehyde and we could not find any example of intramolecular cyclisation in various databases about this structure. This structure should be probably confirmed by the 1D and 2D NMR and single crystal X-ray analysis. Although we could not get crystals for this compound, the structure has been analyzed using 1D and 2D NMR and HRMS.

Table 5A-04 Screening reaction conditions

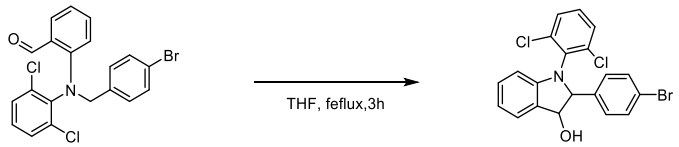

5A-050 5A-051

Entry	 5A-041	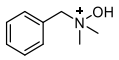 5A-058	Result
1	+	+	**5A-051**

Considering the fact that we used a strong base in our reaction, we also tried a milder base such as benzyltrimethylammonium hydroxide, and obtained a similar result. And as expected, we could also carry out the transformation without using the sulfoxide[47, 48]. (**Table 5A-04**).

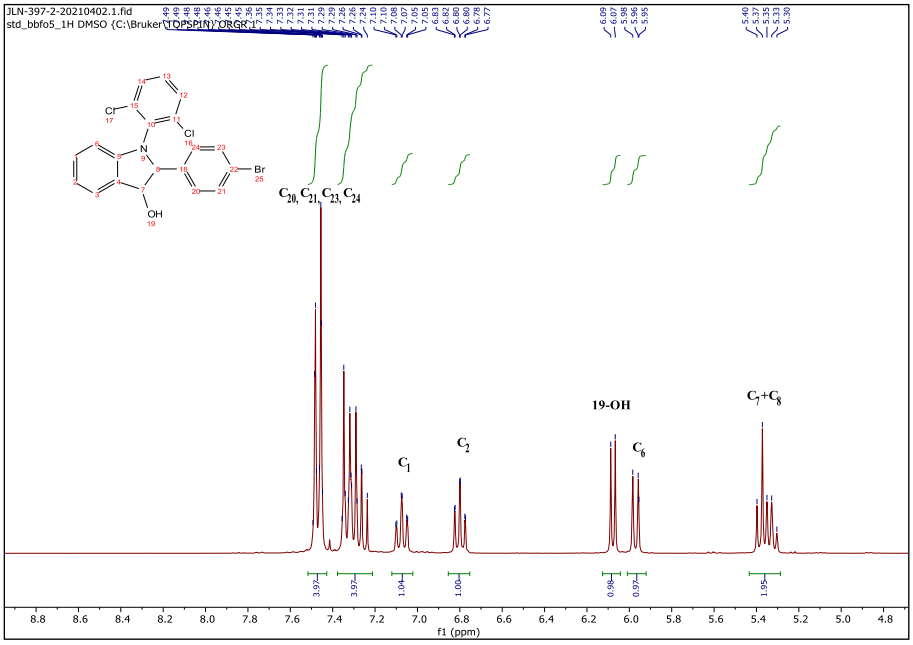

Figure 5A-04a ^{1}H-NMR spectrum of 5A-051 in DMSO-*d6*

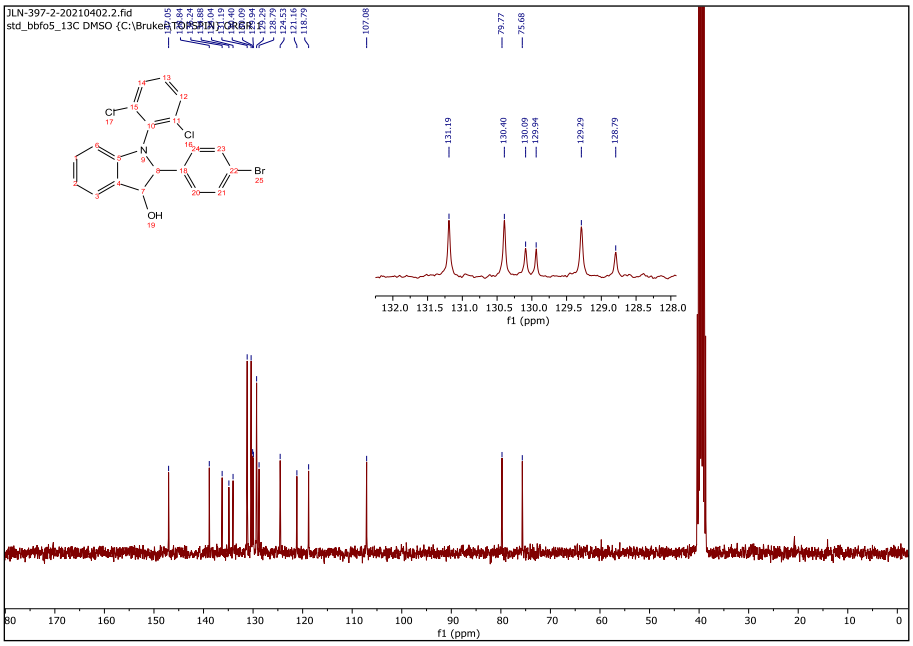

Figure 5A-04b ^{13}C-NMR spectrum of 5A-051 in DMSO-*d6*

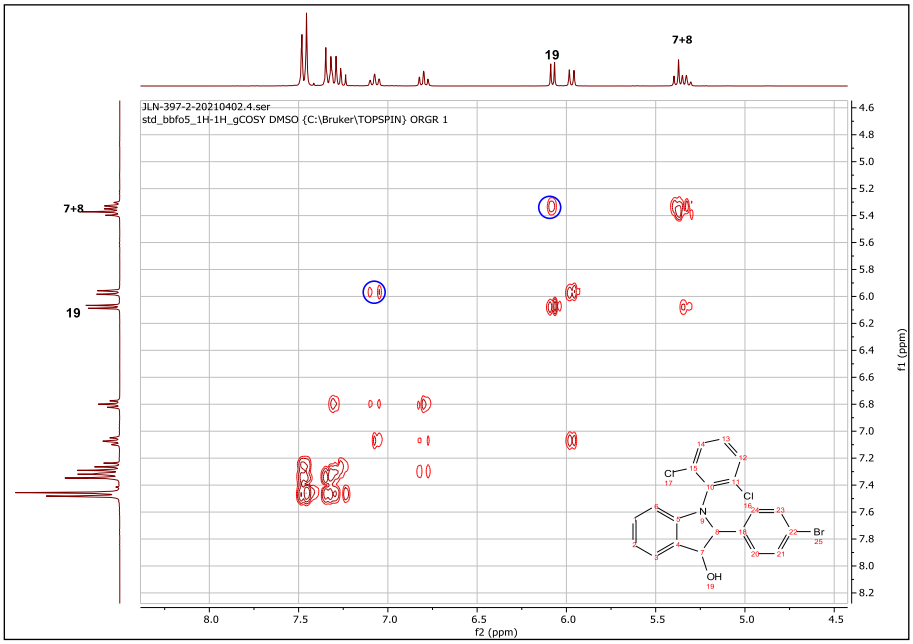

Figure 5A-04c ^{1}H-^{1}H COSY spectrum of 5A-051 in DMSO-*d6*

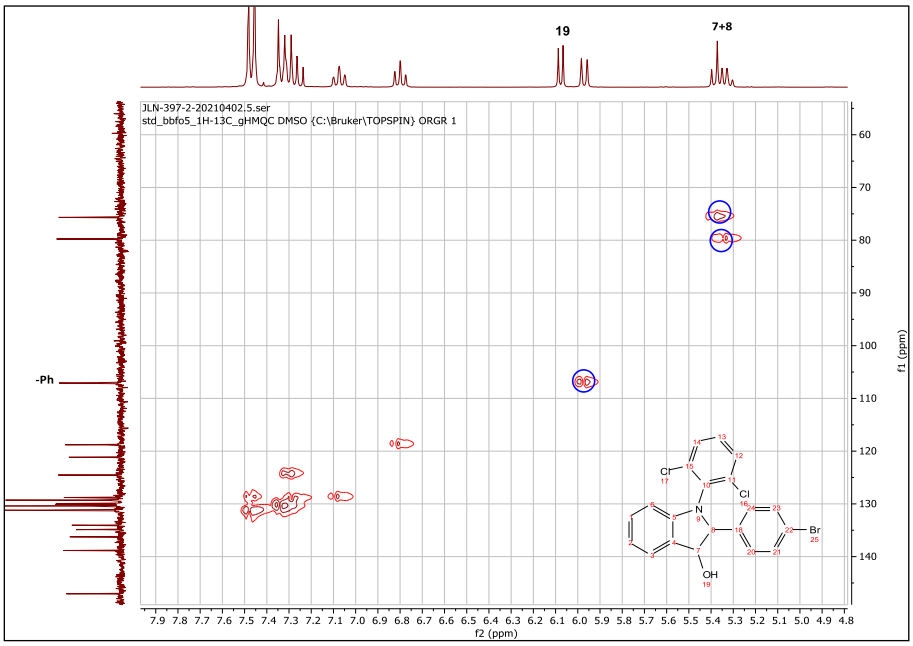

Figure 5A-04d ^{1}H-^{13}C HMQC spectrum of 5A-051 in DMSO-*d6*

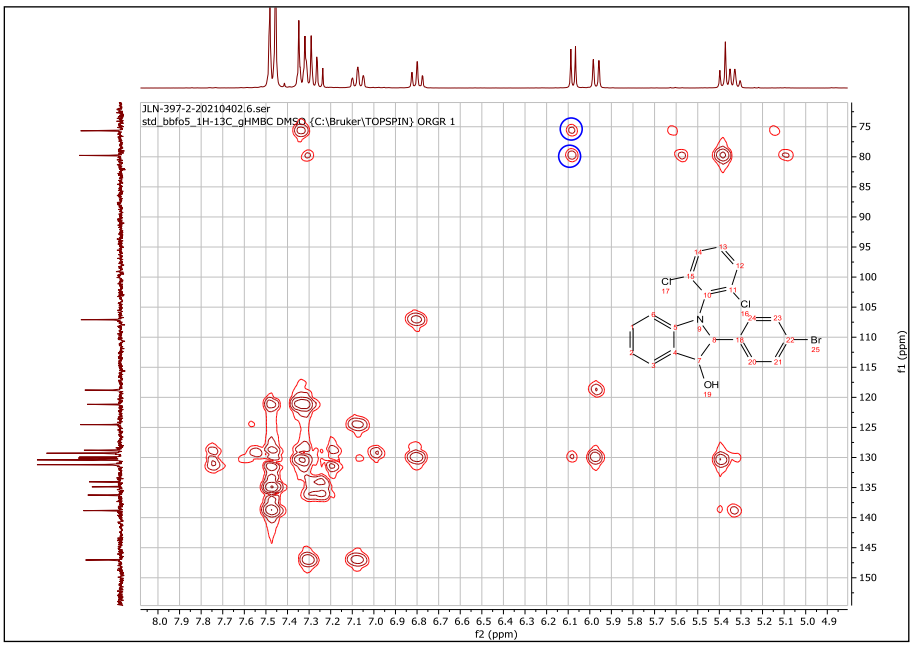

Figure 5A-04e ^{1}H-^{13}C HMBC spectrum of 5A-051 in DMSO-*d6*

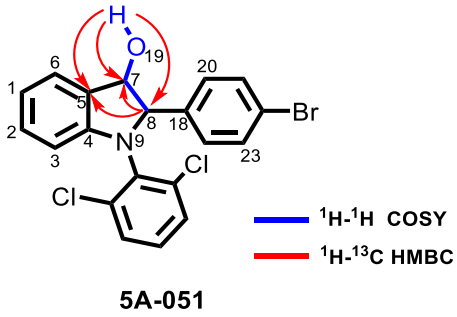

Figure 5A-04f. ^{1}H-^{1}H COSY and ^{1}H-^{13}C-HMBC correlation of compound 5A-051

Table 5A-05 HRMS result of 5A-051

HRMS Result			
Source Type	Formula	Exact mass	$[M+Na]^+$
ESI^+	$C_{20}H_{14}BrCl_2NO$	432.9636	*C* 455.9534 *T* 455.9528

C: calculate T: test

2-(4-bromophenyl)-1-(2,6-dichlorophenyl) indolin-3-ol (**5A-051**). The molecular formula was established as $C_{20}H_{14}BrCl_2NO$ from its HRMS (m/z 471.9287, $[M + K]^+$ calculate 471.9287), indicating 13 degrees of unsaturation. The ^{1}H-NMR and ^{1}H-^{13}C HMQC spectrum (**Figure 5A-04a** and **Figure 5A-04d**) revealed the presence of one hydroxyl group (δ_H 6.08, d, J = 6.00 Hz, -OH), the H-7 and H-8 methyne group (δ_H 5.40-5.30, m, -CH-). The remaining H is associated with the benzene ring. The DEPT shows no methylene group. The ^{13}C-NMR spectrum (**Figure 5A-04b**) revealed the presence of two methyne group of C-7 and C-8 (δ_C 79.77, 75.68). ^{1}H-^{1}H COSY spectrum show the H-19 and H-7, H-8 and H-7 are correlations. The HMBC (**Figure 5A-04e**)

correlations of H-19 to C-5, C-7 and C-8, and HMBC correlations of H-8 to C-5 and C-7. According to the above information, the structure of compound **5A-051** is deduced as 2-(4-bromophenyl)-1-(2,6-dichlorophenyl) indolin-3-ol. Although we could not attribute with accuracy the relative stereochemistry of the two substituents, NMR data's of closely related compound described in 2009 by the group of A. Studer suggests a trans-relationship between those two substituents[49].

2.1.2.6. Synthesis strategy A4-3

The experimental results in **Scheme 5A-02 II** showed that the acetic acid group in diclofenac easily affects the reactivity of the N atom of diclofenac with *p*-substituted bromide, resulting in intramolecular amination and the formation of lactam **5A-030**. The reaction of the N atom of diclofenac with the *p*-substituted benzyl bromide can proceed smoothly if the *p*-position of the benzyl bromide does not contain a strong electron withdrawing group, as shown in **Scheme 5A-05**.

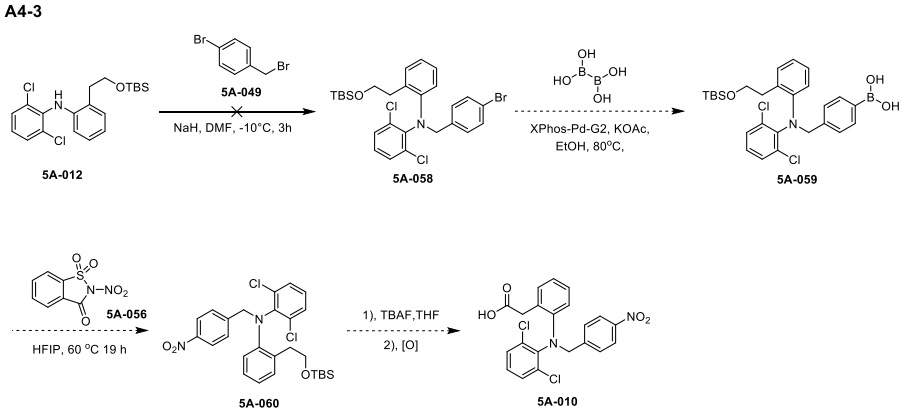

Scheme 5A-07 Synthetic route A4-3 for hypoxia-activated diclofenac prodrugs

We tried the reaction of compound **5A-012** with 4-bromo-bromobenzyl **5A-049** (**Scheme 5A-07**). After treating compound **5A-012** with sodium hydride, adding 4-bromo-bromobenzyl **5A-049**, and standard purification, analysis

processes failed to provide the desired result, and the starting materials were recovered. The same reaction was reported by the Moral team in May 2021, who used 10 equivalents of NaH in this step and succeeded in obtaining **5A-058**. In my case, only 1-1.2 equivalents of NaH was used in this reaction[50].

2.1.2.7. Synthesis strategy A4-4

The failure of the aforementioned synthetic strategy informed us that connecting a nitro probe to *N*-diclofenac can be difficult. Because of the effect of spatial site resistance, and the presence of a nitroaromatic group, which makes S_N2 reactions difficult. Because it is impossible to directly introduce the alkylating agent bearing a nitro group, we revised our strategy for the introduction of a *p*-nitro-cinnamyl group, by introducing first an allyl group *via* our methodology, and then adding the *p*-nitrophenyl on the double bond *via* the Heck reaction (**Scheme 5A-08 I**).

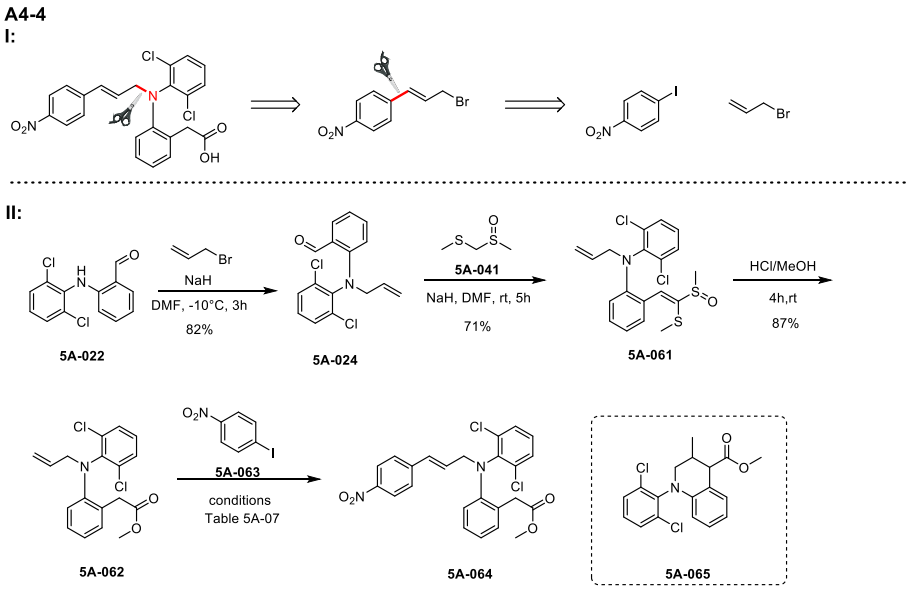

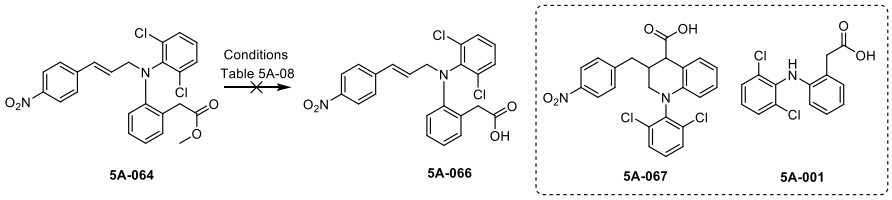

Scheme 5A-08 Synthetic route A4-4 for hypoxia-activated diclofenac prodrugs

As described earlier, **5A-022** was treated with NaH and then successfully reacted with allyl bromide **5A-036** to give the tertiary amine compound **5A-024**, which was then reacted with the sulfide **5A-041** under basic conditions to give **5A-061** in a 71 % yield. Treatment of compound **5A-061** with a fresh methanolic solution of HCl provided the ester **5A-062** in an excellent yield[40]. Finally, the Heck reaction was attempted under standard conditions from the literature[51] (**Table 5A-07**). When the product was purified and the structure analyzed by standard methods, the results showed that the reaction did not produce the target product **5A-064**. Instead, we found a new structure in which a cyclisation reaction occurred. The structure has been analyzed using 1D, 2D NMR and HRMS, which led us to attribute the structure to compound **5A-065** (**Scheme 5A-08 II**).

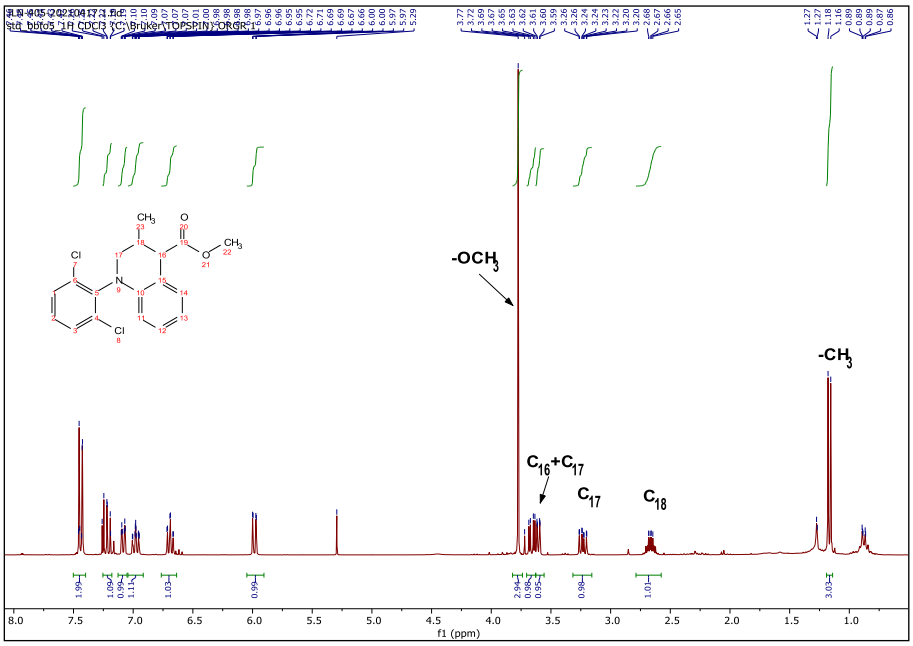

Figure 5A-05a ^{1}H-NMR spectrum of 5A-065 in $CDCl_3$-*d*

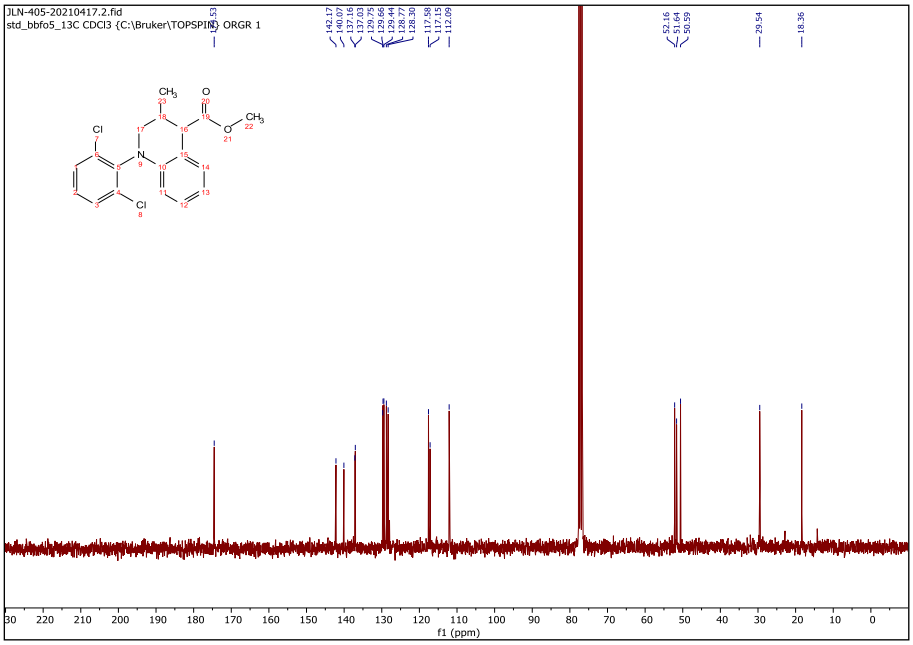

Figure 5A-05b ^{13}C-NMR spectrum of 5A-065 in $CDCl_3$-*d*

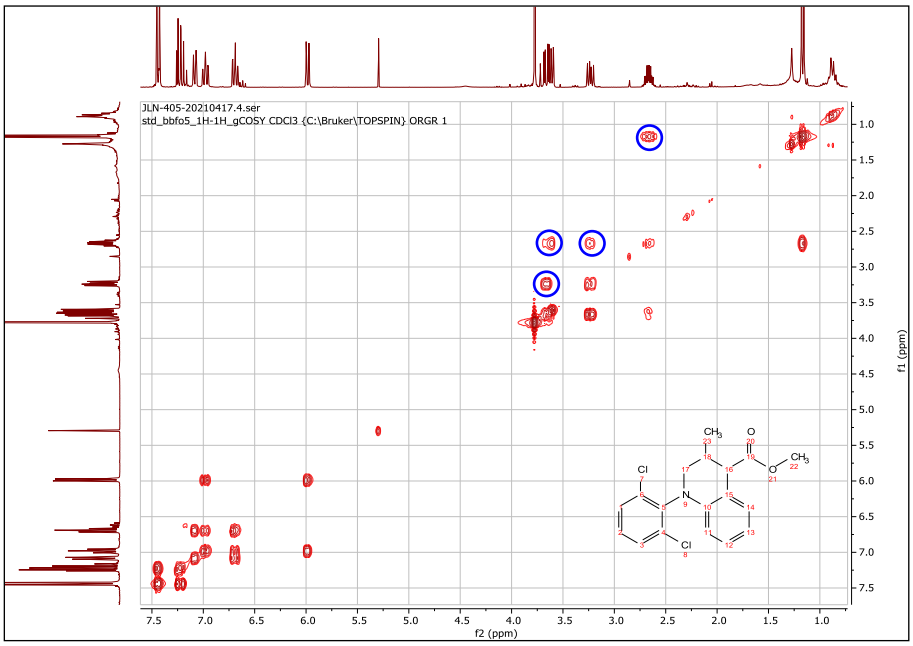

Figure 5A-05c ^{1}H-^{1}H COSY spectrum of 5A-065 in $CDCl_3$-*d*

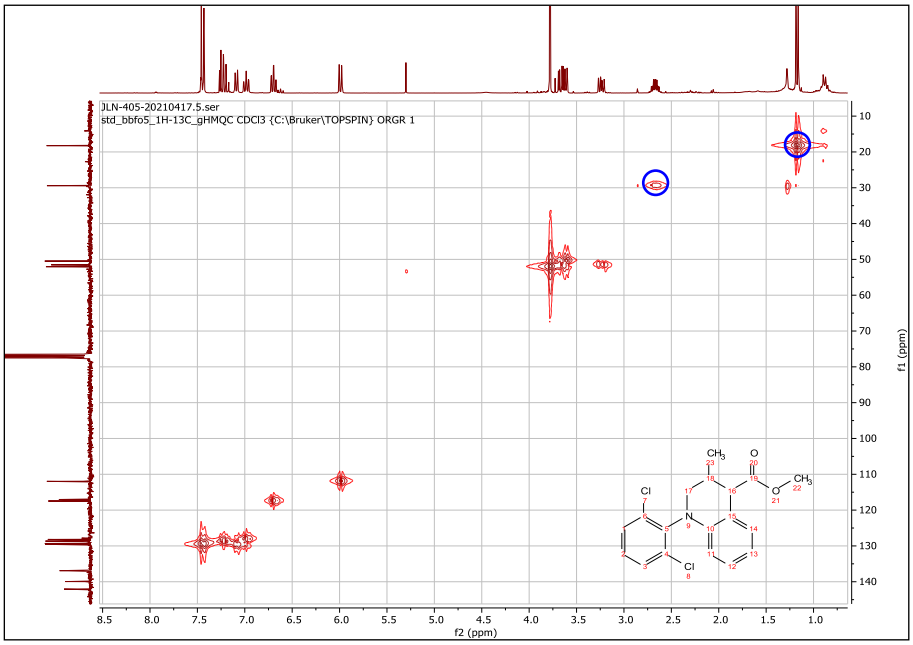

Figure 5A-05d ^{1}H-^{13}C-HMQC spectrum of 5A-065 in $CDCl_3$-*d*

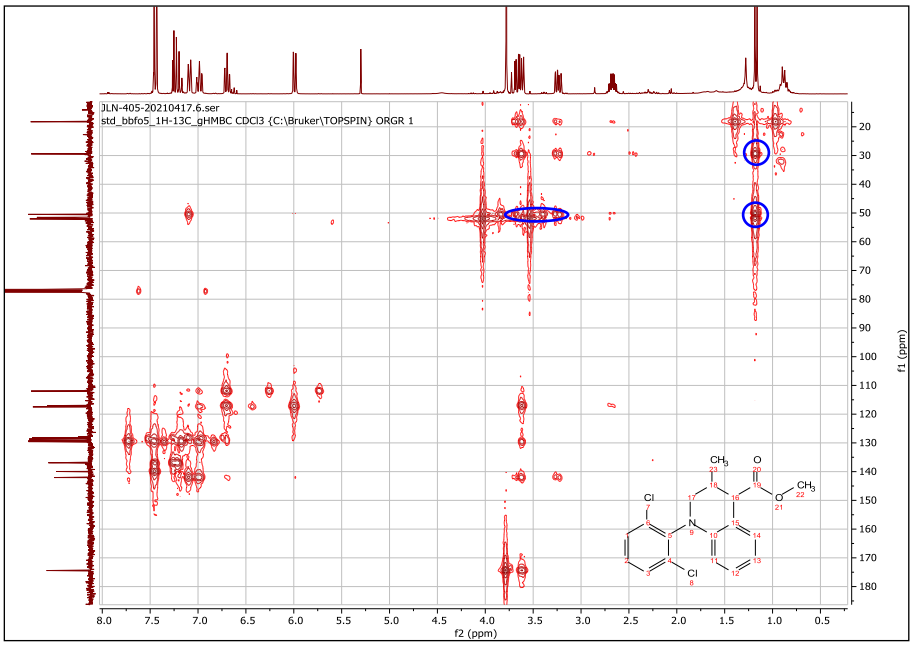

Figure 5A-05e ^{1}H-^{13}C-HMBC spectrum of 5A-065 in $CDCl_3$-*d*

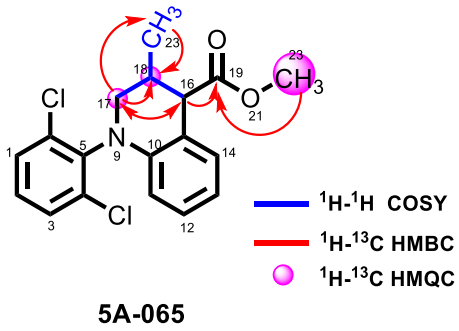

Figure 5A-05f ^{1}H-^{1}H COSY, ^{1}H-^{13}C-HMQC and ^{1}H-^{13}C-HMBC correlation of compound 5A-065

Table 5A-06 HRMS result of 5A-065

HRMS Result				
Source Type	Formula	Exact mass	$[M+H]^+$	$[M+Na]^+$

ESI^+	$C_{18}H_{17}Cl_2NO_2$	349.0636	*C:* 350.0715 *T:* 350.0709	*C:* 372.0534 *T:* 372.0529

C: calculate T: test

Methyl 1-(2,6-dichlorophenyl) -3-methyl- 1,2,3,4- tetrahydroquinoline -4-carboxylate (**5A-065**). The molecular formula was established as $C_{18}H_{17}Cl_2NO_2$ from its HRMS (m/z 350.0697, $[M+H]^+$ calculate 350.0715, m/z 372.0518, $[M+Na]^+$ calculate 372.0534) (**Table 5A-06**), indicating 10 degrees of unsaturation. The ^{1}H-NMR and ^{1}H-^{13}C HMQC spectrum (**Figure 5A-05a** and **Figure 5A-05d**) revealed the presence of one methoxy group (δ_H 3.77, s, -OCH_3), one methyl group (δ_H 1.17, d, J = 6.00 Hz, -CH_3), the H-16 and H-17a (δ_H 5.40-5.30, m, 2H), the H-17b (δ_H 3.26-3.20, m, 1H), the H-18 (δ_H 2.68-2.65, m, 2H). The remaining H is associated with the benzene ring. The DEPT shows one methylene group (δ_C 51.64 C-17). The ^{13}C-NMR and ^{1}H-^{13}C HMQC spectrum (**Figure 5A-05b**) revealed the presence of one methyl group (δ_C 18.36, C-23), one methoxy group (δ_C 52.16, C-22), and two methyne group of C-16 and C-18 (δ_C 50.59, 29.54). ^{1}H-^{1}H COSY spectrum show the H-18 and H-23, H-17a and H-17b, H-16 and H-17 are correlated. The HMBC (**Figure 5A-05e**) correlations of H-23 to C-18, H-23 to C-19, H-16 to C-19 and C-17, and H-17 to C-16, C-18 and C-23. According to the above information, the structure of compound **5A-065** is deduced as methyl 1-(2,6-dichlorophenyl)-3-methyl-1,2,3,4-tetrahydroquinoline-4-carboxylate.

Regarding the potential mechanism of this transformation, we proposed that a Pd (II) catalysts with a soft Lewis acidity can activate the double bond and allow the intramolecular attack of the carbanion generated by deprotonation of the acidic benzylic protons. The generated alkyl-palladium would be expected to undergo a fast β-hydride elimination, but we observed here the

reduction, which could occur from the *in-situ* formation of palladium hydride species (**Scheme 5A-09**).

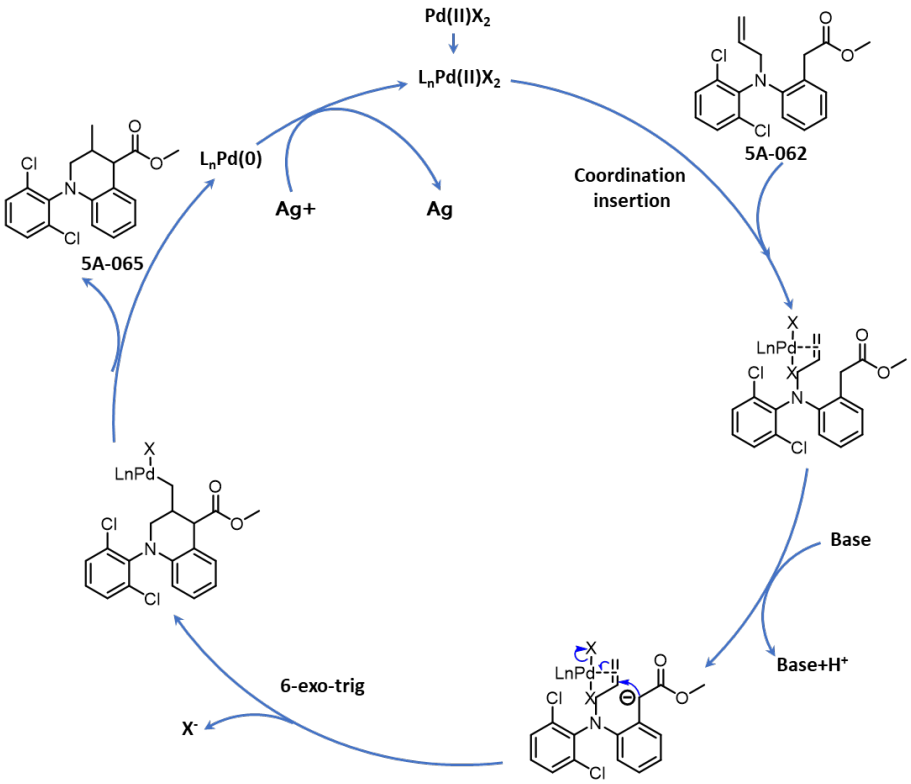

Scheme 5A-09 Potential mechanism of palladium-catalyzed intramolecular cyclization of allyl-N-diclofenac

Table 5A-07 Optimization of reaction conditions

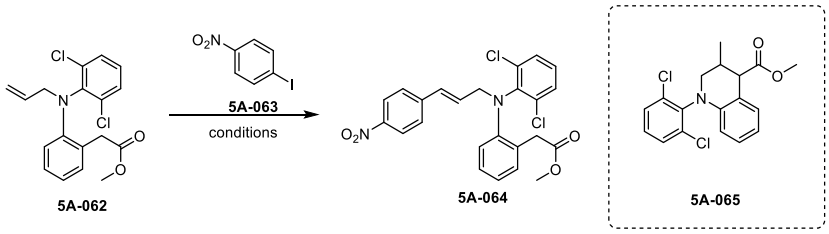

Entry	Conditions	Result	Yield
1	$Pd(OAc)_2$, *rac*-BINAP, Ag_2CO_3, K_2CO_3, NMP, 80°C,14h	**5A-065**	67%

2	$Pd(OAc)_2$, Ag_2CO_3, 1,4-Dioxane, 90 ºC	**5A-064**	64%

In order to avoid the formation of the stabilized carbanion and the subsequent cyclisation, we also tried alternative conditions for the Heck reaction in which no extra base was added. When these conditions were used, without the BINAP ligand, we could carry out the Heck reaction, obtaining the expected compound **5A-064** isolated in a 64% yield[52](**Table 5A-07**).

Table 5A-08 Screening reaction conditions

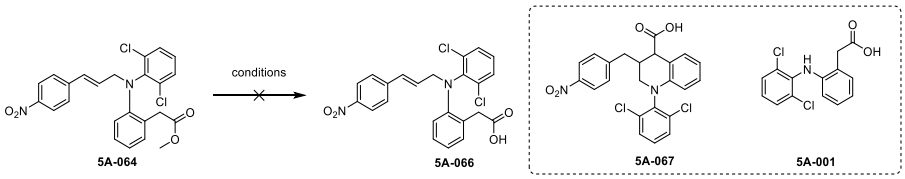

Entry	Reagents and Conditions	Result	Yield
1	NaOH (1eq), rt-60 ºC, $MeOH/H_2O$	N.D.	-
2	NaOH (3eq), 60 ºC, $MeOH/H_2O$	**5A-067**	42%
3	LiOH (1eq), 60 ºC, $MeOH/H_2O$	N.D.	-
4	LiOH (2eq), 60 ºC, $MeOH/H_2O$	**5A-067**	36%
5	BBr_3, CH_2Cl_2, -78-0ºC	**5A-001**	40%
6	TFA, 80ºC, CH_2Cl_2, sealed tube	N.D.	-
7	HCl in Dioxane, 110 ºC sealed tube	N.D.	-

Next, we tried to hydrolyze the methyl ester to obtain the final product **5A-066**. First, we tried hydrolysis in standard base conditions (**Table 5A-08 1-4**). Using one equivalent amount of base (NaOH or LiOH), we did not detect the product. However, when the equivalents of base were increased, the cyclization of the starting material was realized, obtaining **5A-067**. We tried

using a Lewis acid such as BBr_3, (**Table 5A-08 5**), but both methyl ester and benzyl group were removed to give diclofenac **5A-001**. Hydrolysis in acidic conditions were also tried, but neither TFA nor HCl in dioxane was able to hydrolyze the methyl ester[53, 54] (**Table 5A-08 6-7**).

The structure has been analyzed using 1D and 2D NMR and HRMS, which led us to attribute the structure to compound **5A-067**.

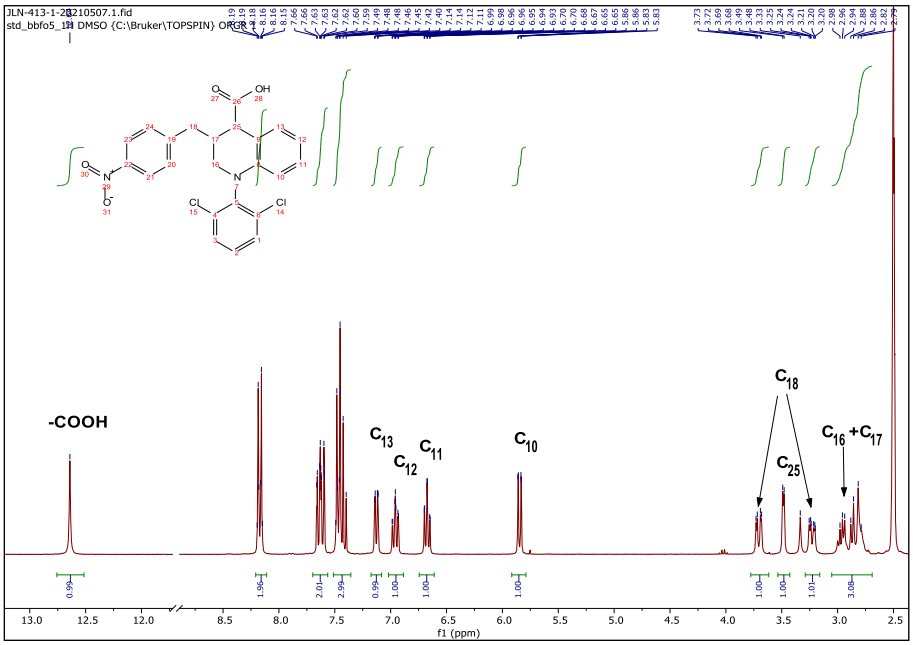

Figure 5A-06a ^{1}H-NMR spectrum of 5A-067 in DMSO-*d6*

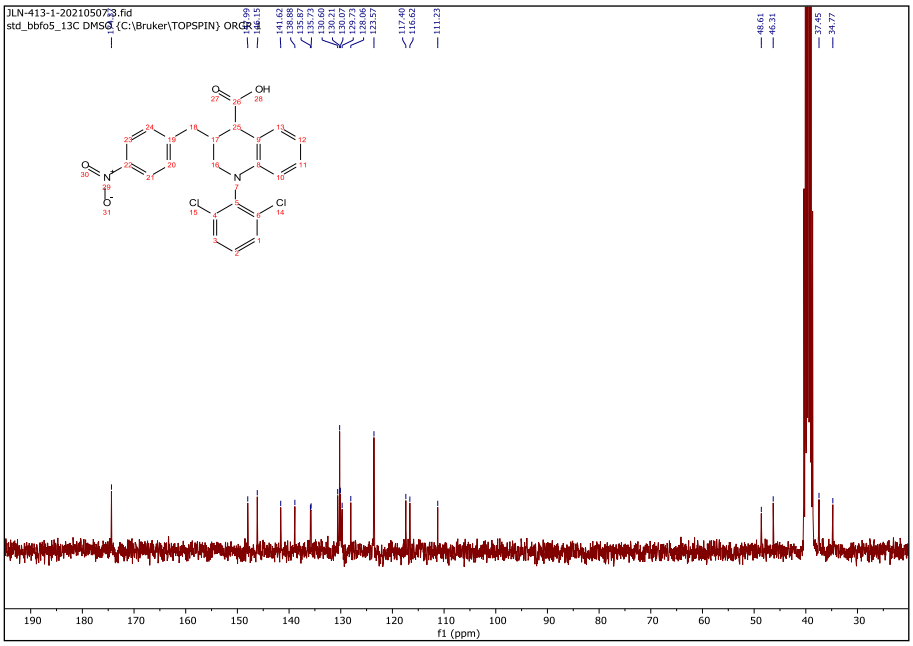

Figure 5A-06b ^{13}C-NMR spectrum of 5A-067 in DMSO-*d6*

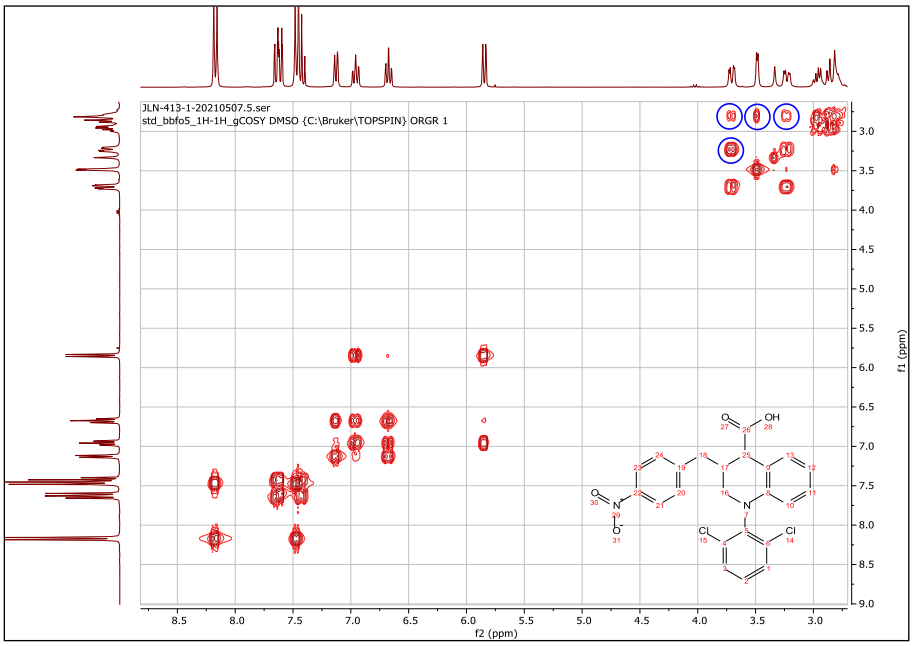

Figure 5A-06c ^{1}H-^{1}H COSY spectrum of 5A-067 in DMSO-*d6*

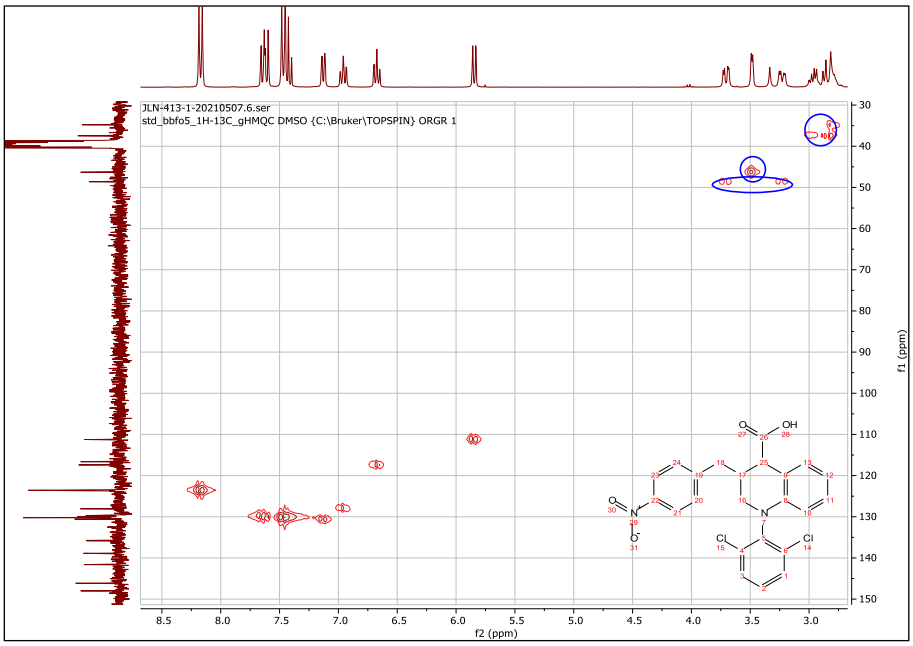

Figure 5A-06d ^{1}H-^{13}C HMQC spectrum of 5A-067 in DMSO-*d6*

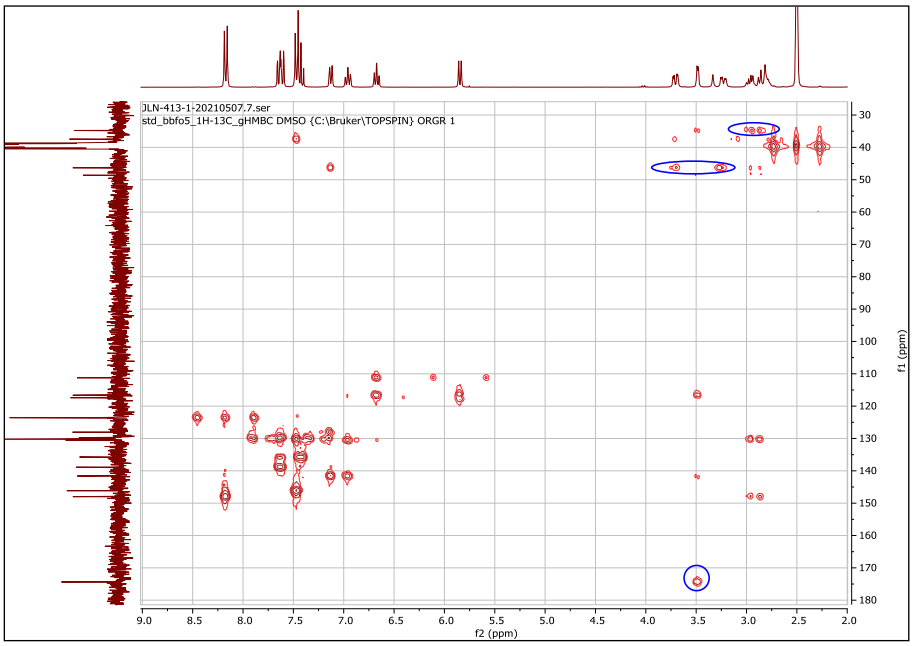

Figure 5A-06e ^{1}H-^{13}C HMBC spectrum of 5A-067 in DMSO-*d6*

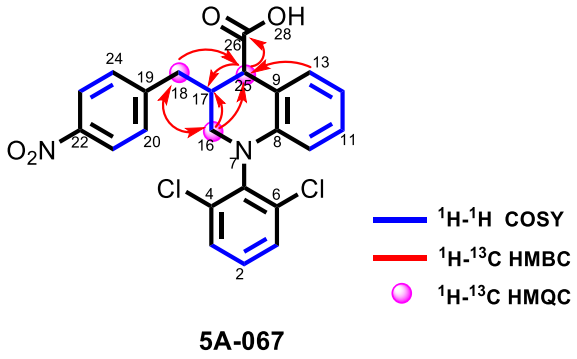

5A-067

Figure 5A-06f. ^{1}H-^{1}H COSY, ^{1}H-^{13}C-HMQC and ^{1}H-^{13}C-HMBC correlation of compound 5A-067

Table 5A-09 HRMS result of 5A-067

HRMS Result			
Source Type	Formula	Exact mass	[M-H]$^-$
ESI$^-$	$C_{23}H_{18}Cl_2N_2O_4$	456.0644	*C*: 455.0571 *T*: 455.0571

C: calculate T: test

1-(2,6-dichlorophenyl) -3- (4-nitrobenzyl) -1,2,3,4- tetrahydroquinoline-4-carboxylic acid (**5A-067**). The molecular formula was established as $C_{23}H_{18}Cl_2N_2O_4$ from its HRMS (m/z 455.0554, [M-H]$^-$ calculate 455.0571), indicating 15 degrees of unsaturation. The ^{1}H-NMR and ^{1}H-^{13}C HMQC spectrum (**Figure 5A-06a** and **Figure 5A-06d**) revealed the presence of one carboxylic acid group (δ_H 12.64, s, -COOH), one methyne group (δ_H 3.49, d, J = 3.00 Hz, -CH-), one methylene group (δ_{Ha} 3.70, dd, J = 3.00, 12.00 Hz, -CH(a+b)-), δ_{Hb} 3.22, dd, J = 3.00, 12.00 Hz, -CH(a+b)-), the H-16 and H-17 (δ_H 2.98-2.79, m, 2H). The remaining H is associated with the benzene ring. The DEPT shows two methylene group (δ_C 48.61, C-18, and δ_C 37.45, C-16). The ^{13}C-NMR and ^{1}H-^{13}C HMQC spectrum (**Figure 5A-06b**) revealed the

presence of two methyne group (δ_C 34.77, C-17, and δ_C 46.31, C-25), two methlyene group (δ_C 48.61, C-18, and δ_C 37.45, C-16). ^{1}H-^{1}H COSY spectrum shows that the H-16 and H-17, H-17 and H-18, H-17 and H-25 are correlations. The HMBC (**Figure 5A-06e**) correlations of H-25 to C-17 and C-26, H-18 to C-25 and C-16, H-16 to C-17, C-18 and C-25, and H-13 to C-25. According to the above information, the structure of compound **5A-067** is deduced as 1-(2,6-dichlorophenyl)-3-(4-nitrobenzyl)-1,2,3,4-tetrahydroquinoline-4-carboxylic acid.

As the target product could not be successfully obtained using the various chemical methods described above, we examined the use of enzyme-catalyzed esterification/hydrolysis reactions[55, 56, 57]. Unfortunately, the use of different lipases and reactions conditions did not lead to any conversion of the ester to the desired acid (**Table 5A-10**).

Table 5A-10 Screening reaction conditions

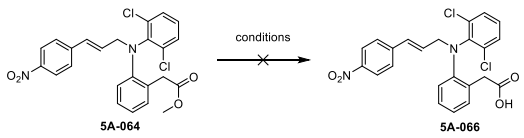

Entry	Enzyme	Conditions	Result
1	Lipase from *Candida rugosa*	THF/H_2O 5/1 37 - 40 °C	N.D.
2	Lipase from *Candida rugosa*	PBS (pH 7.4)/ MeOH (9/1) 37 °C	N.D.
3	Amano Lipase PS	THF/H_2O 5/1 37 - 40 °C	N.D.
4	Amano Lipase PS	PBS (pH 7.4)/ MeOH (9/1) 37 °C	N.D.
5	Lipase acrylic resin	CH_3CN/H_2O (98/2) 40 °C	N.D.
6	Lipase acrylic resin	PBS (pH 7.4)/ MeOH (95/5) 37 °C	N.D.

7	Esterase from porcine liver	PBS (pH 7.4)/ MeOH (95/5) 37 °C	N.D.
8	Lipase from *Candida Antarctic-B*	CH_3CN/H_2O (98/2) 40 °C	N.D.

2.1.2.8. Synthesis strategy A4-5

The compound **5A-064** is susceptible to intramolecular cyclization under alkaline circumstances, none of the other hydrolysis strategies tried so far have yielded satisfactory results. Hence, we tried hydrolyze **5A-062** under alkaline conditions before coupling it to a nitro unit *via* palladium catalysis (**Scheme 5A-10 I**). Compound **5A-062** was saponified to give **5A-068**, and **5A-068** was treated according to the conditions of the Heck reaction described above[52]. Unfortunately, we did not detect the product **5A-066**, contributing to the possible influence of carboxyl group "-COOH" on the reaction.

Considering that **5A-064** is a methyl ester compound that is difficult to hydrolyze under acidic conditions, we wondered if it was possible to convert it into the *t*-butyl ester **5A-067** or the benzyl ester **5A-069.** So, we tried to hydrolyze the *t*-butyl ester or the benzyl ester under acidic conditions after coupling with iodo-nitrobenzene. Initially, we tried the reactions described in **Scheme 5A-09 II**, in which the corresponding esters **5A-067** and **5A-069** were easily prepared and coupled with *p*-iodo-nitro benzene in our standard conditions[52]. However, when **5A-068** and **5A-070** were subjected to deprotection reactions with TFA/CH_2Cl_2 or HCl in dioxane[53, 54], we failed to carry out the deprotection and obtained **5A-066**.

Finally, considering the carboxylic acid group had a negative effect on the Heck reaction in **Scheme 5A-09 I**, we thought that the conversion of this carboxylic acid group of **5A-068** into a salt form, might allow us to carry out the Heck reaction. **5A-068** was first reacted with NaOH, and then the mixture was dried.. Following that, the target product **5A-066** was successfully

obtained utilizing the given conditions for the Heck reaction[52] (**Scheme 5A-10 III**).

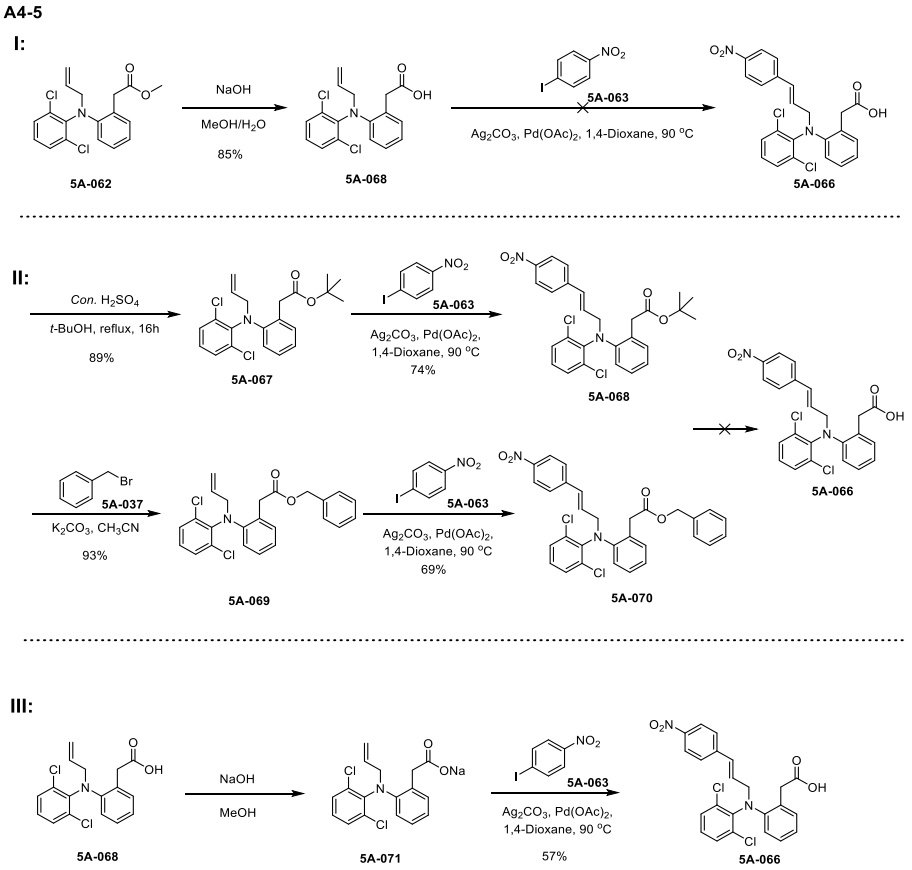

Scheme 5A-10 Synthetic route A4-5 for hypoxia-activated diclofenac prodrugs

2.1.2.9. Synthesis strategy A4-6

It was considering that the pharmacodynamic group of the NSAIDs diclofenac with inhibitory activity against cyclooxygenase (COX) is the acetic acid group. However, diclofenac inhibits the MCT4 activity of tumor cells and its pharmacodynamic group may be related to the acetic acid moiety[58, 59]. Although we synthesized compound **5A-066** successfully, its acetic acid moiety was exposed. Following the principle that a hypoxia-activated prodrug should have the properties of being inactive or less active before the activation

of the prodrug. We have devised a safer solution with a double nitro prodrug **5A-072**. These two nitro probes will be reduced in the hypoxic microenvironment to release diclofenac **5A-001** (**Scheme 5A-11**).

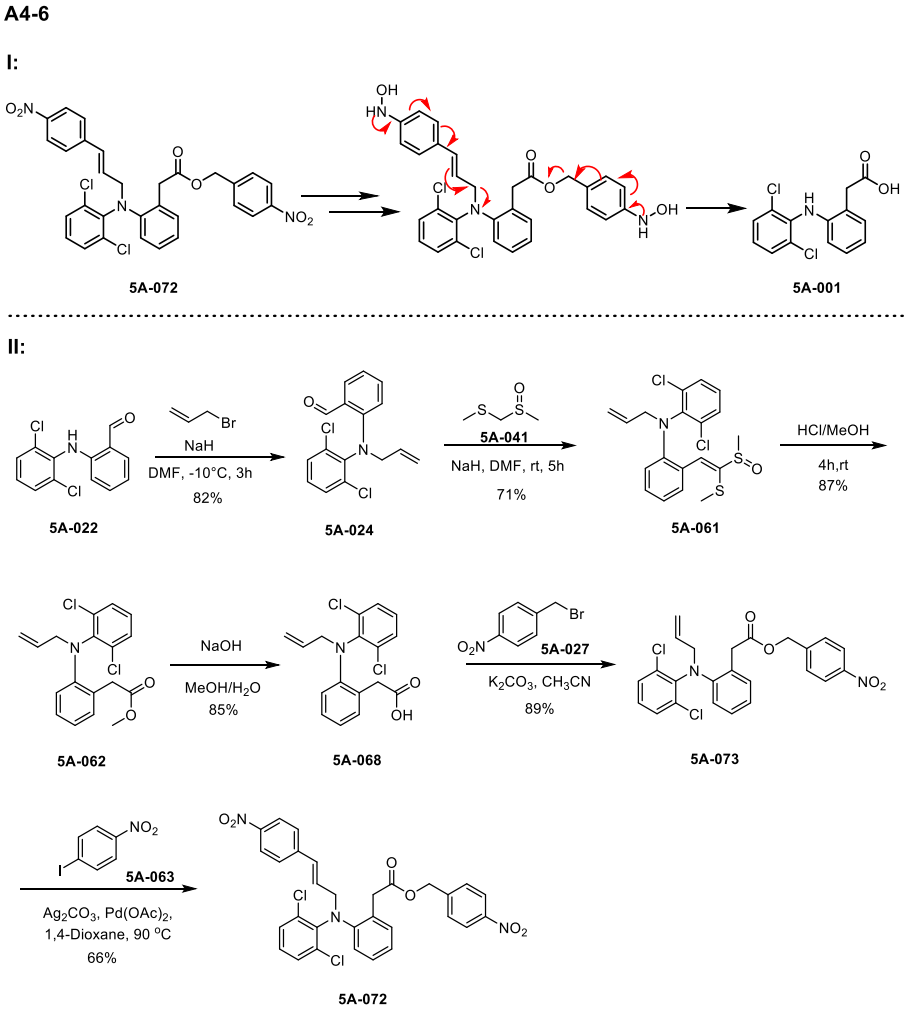

Scheme 5A-11 Synthetic route for hypoxia-activated diclofenac prodrugs

5A-068 was prepared like the same method above. **5A-068** and **5A-027** reacted in the presence of potassium carbonate to form **5A-073**. **5A-073** reacted with **5A-063** in the presence of palladium acetate to form the bis-nitro compound **5A-072**, in a 66 % yield (**Scheme 5A-10**).

2.2.1. Rational Design hypoxia-sensitive prodrugs tetrandrine

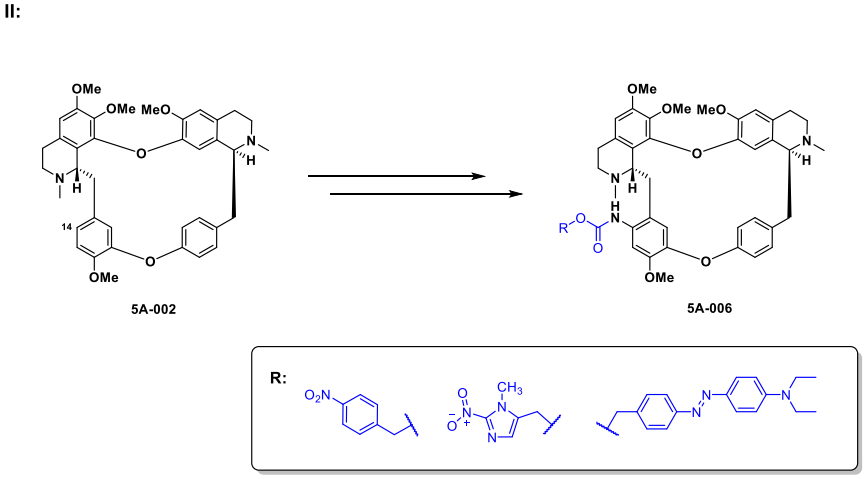

Figure 5A-07 Overall scheme for synthesis HAPs tetrandrine

Having successfully prepared the three diclofenac prodrugs, we could then turn to the next part of the project and start the synthesis of the tetrandrine prodrugs. We decided to focus on three bioreductive fragments which have been well studied in the literature and we now focus on their preparation and grafting on a tetrandrine derivatives (**Figure 5A-07**).

2.2.2. Synthesis of hypoxia-sensitive prodrugs for nature compound

2.2.2.1. Synthesis of hypoxia sensitive moiety

The 1-methyl-2-nitroimidazole fragment **5A-081** is less readily available through commercial sources, while the azo compound **5A-085** only needs to be prepared in one pot by a common chemical reagent. Therefore, we prepared the 1-methyl-2-nitroimidazole moiety **5A-081** and the azo compound **5A-085** based on the reported methods[5, 60, 61].

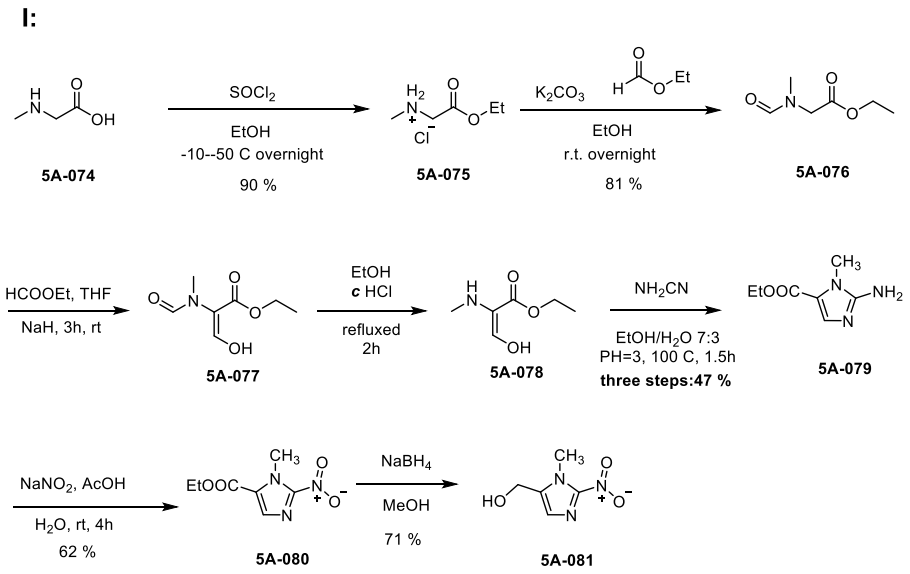

Scheme 5A-12 I Synthetic route for hypoxia sensitive moiety

The 1-methyl-2-nitroimidazole moiety **5A-081** was prepared from a commercially available inexpensive sarcosine as a starting material through an eight steps reactions sequence according to the reported procedures[5, 60]. The procedure started by from the preparation of the hydrochloride salt of the methyl ester of sarcosine **5A-074** though treatment of the amino acid with thionyl chloride in ethanol. This salt begins was then *N*-formylated by simple stirring in ethyl formate in the presence of potassium carbonate to give **5A-076** in excellent yield. Claisen condensation of was then carried out with ethyl formate in the presence of sodium hydride to give, after hydrolysis and acidic work up, the enol **5A-077,** which was not purified, by directly subjected to removal of the formyl group to give **5A-078**. The amino-imidazole aromatic was then assembled from **5A-078** by reaction with cyanamide at pH 3 to give **5A-079** in a 47% for the three steps. Then, the amino group was converted to a nitro group by diazotation with an excess of sodium nitrite to give the nitro imidazole **5A-080** in 62 % yield. Finally, the ester group was reduced with

sodium borohydride in ethanol to obtain the desired alcohol **5A-081** (**Scheme 5A-12 I**) in a fair 71% yield.

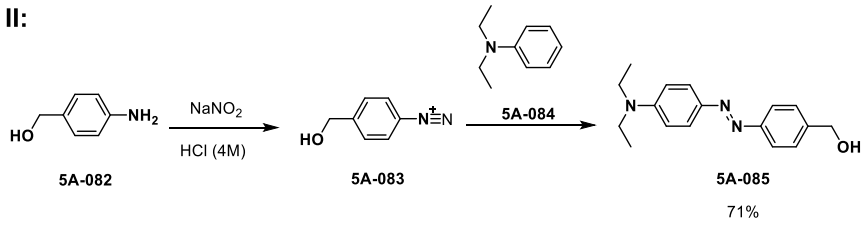

Scheme 5A-12 II Synthetic route for hypoxia sensitive moiety

The azo compound **5A-085** was prepared by dissolving 4-aminobenzyl alcohol in 4M HCl and controlling the temperature at 0°C by dropping in the $NaNO_2$ solution to produce the diazo salt intermediate **5A-083**. After dropping diethylaniline **5A-084** into the reaction, the reaction solution turned red immediately and the desired azo compound was isolated by column chromatography to give **5A-085**[61], in an 71% yield (**Scheme 5A-12 II**).

2.2.2.2. Synthesis of hypoxia-sensitive prodrugs for tetrandrine

The preparation of 14-NH_2-tetrandrine was based on previous reports[19, 20], tetrandrine was dissolved in CH_2Cl_2 with controlled reaction temperature and a freshly prepared solution of acetyl nitrate (from nitric/acetic anhydride) was dropped into the reaction mixture to produce nitro-tetrandrine **5A-086** in an 87% yield. The nitro group was reduced efficiently to give amino-tetrandrine **5A-087** by hydrazine hydrate Pd/C. The amino-tetrandrine was coupled with the three nitro-alcohols, by reaction of the amine with triphosgene to generate the corresponding carbamoyl chloride, and adding the selected alcohol and DIPEA to form the stable carbamates **5A-088**, **5A-089** or **5A-090** in fair to good overall yields 43%-68% (**Scheme 5A-13**)[62].

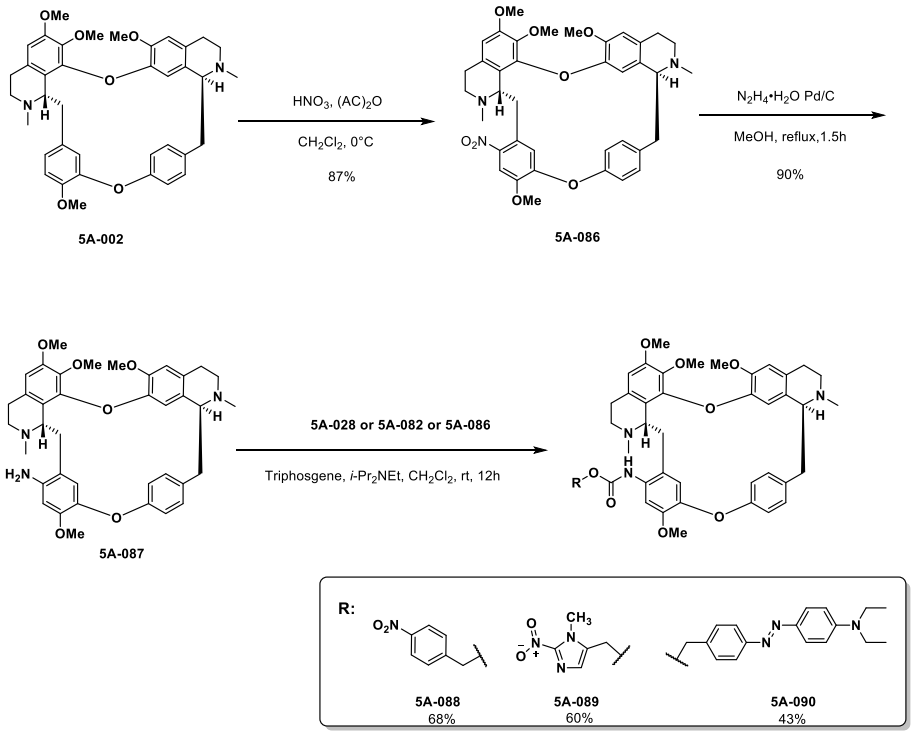

Scheme 5A-13 Synthetic route for hypoxia-activated prodrugs tetrandrine

3. Conclusion

Due to time limitations, the synthesis of diclofenac prodrugs described above occupied too much time that the late pharmacological period was significantly shorter than planned, and the pharmacological studies were still ongoing when I wrote the thesis. While the biological activity of the HAPs is not demonstrated in this section, we were able to obtain the target molecules through rational design and a variety of synthesis strategies, laying the groundwork for subsequent studies.

In **part A** of this chapter, based on the above reasonable design and synthesis route, we successfully synthesized three hypoxia-activated diclofenac prodrugs and three hypoxia-activated tetrandrine prodrugs (**Figure 5A-07**).

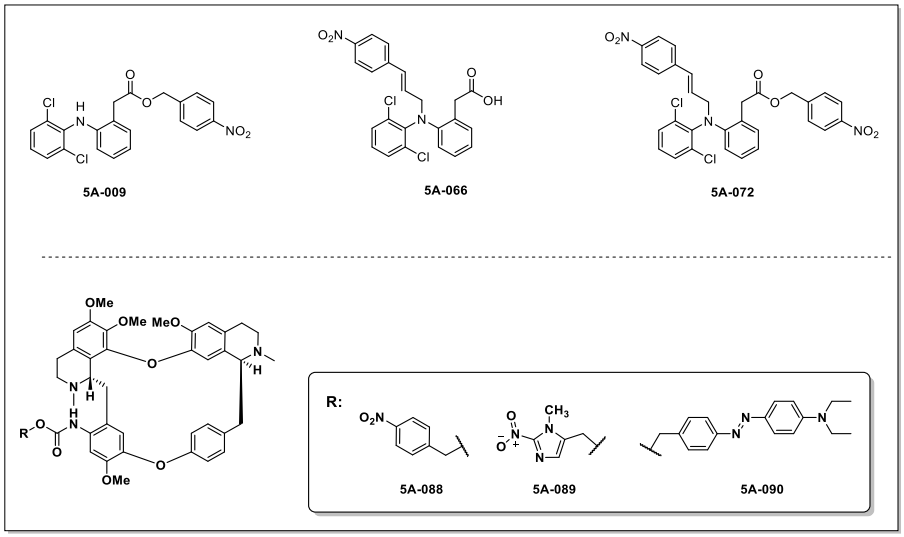

Figure 5A-07 hypoxia-activated prodrugs

We discovered three cyclic compounds while exploring the synthesis method for HAPs diclofenac, and their molecular structures were determined using standard 1D-NMR, 2D-NMR, and HRMS methods (**Figure 5A-08**). Unfortunately, no crystals of the compound have been obtained, and the absolute configuration of the compound cannot be identified.

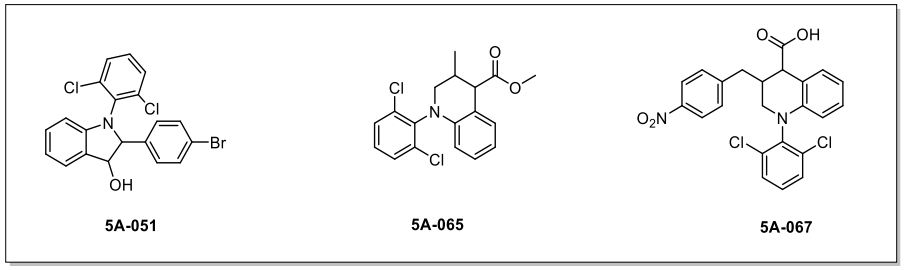

Figure 5A-08 three new compounds

Part B

Triazene, a novel bio-reductive moiety for potential hypoxia-activated prodrugs

1. Introduction

Anti-tumor drugs working on low oxygen environment are mainly based on targeted drug development and design of prodrugs that can be released in a low oxygen environment. Among them, prodrugs with nitro or azo moiety are mostly studied. We explored a new structure of triazene, and studied its release of drugs in a low-oxygen environment.

Temozolomide and Dacarbazine are widely used alkylating antineoplastic drugs, both of which need to be metabolized *in vivo* to triazenes MTIC in order to be effective. Temozolomide is metabolized in the body by decarboxylation and ring-opening of the hexameric ring, which is converted to MTIC with antitumor activity. Enzymes further metabolize MTIC to produce 5-amino-1*H*-imidazole-4-carboxamide and methyl diazonium ion, which alkylates DNA and releases nitrogen gas[63, 64]. Dacarbazine is firstly metabolized in the liver by cytochrome P450 to form the active molecule MTIC, which also forms methyl diazonium ions to damage tumor DNA[65, 66](**Figure 5B-01**).

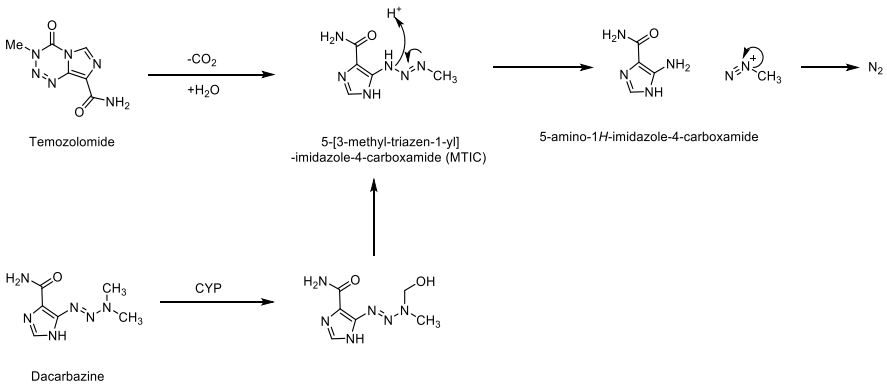

Figure 5B-01 Pathway of temozolomide and dacarbazine metabolism

Maria B. Kadiiska's team used the ESR spin-trapping techniques to identify drug radical metabolites generated by liver P450 enzymes and diphenyl triazene[67]. Protonation and single electron transfer, followed by homolytic

cleavage of the N-N bond (the proposed mechanism is presented as detailed in the publication, without the elementary steps), leads to the formation of aniline and a phenyldiazene radical. This radical undergoes fragmentation to the phenyl radical, which can easily react with DNA in the cell to induce toxicity by alkylation (**Figure 5B-02**).

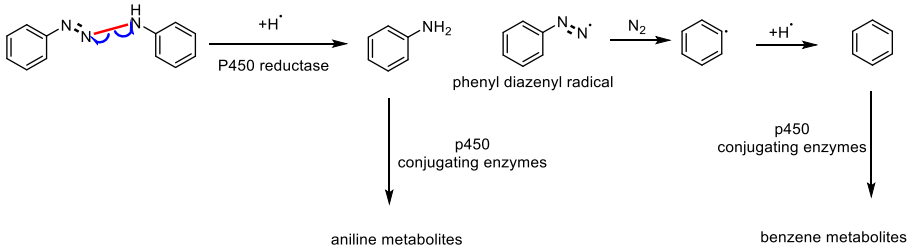

Figure 5B-02 Proposed pathway for the metabolism of diaryl-triazene

The observation that both products of this cascade are an aniline and an aromatic, and the known use of closely related azo groups as bioreductive fragments, inspired us to envisage the possibility to use the poorly studied triazene fragment as a base to design hypoxia-sensitive diclofenac prodrugs (see below).

2. Results and discussion

2.1.1. Rational design

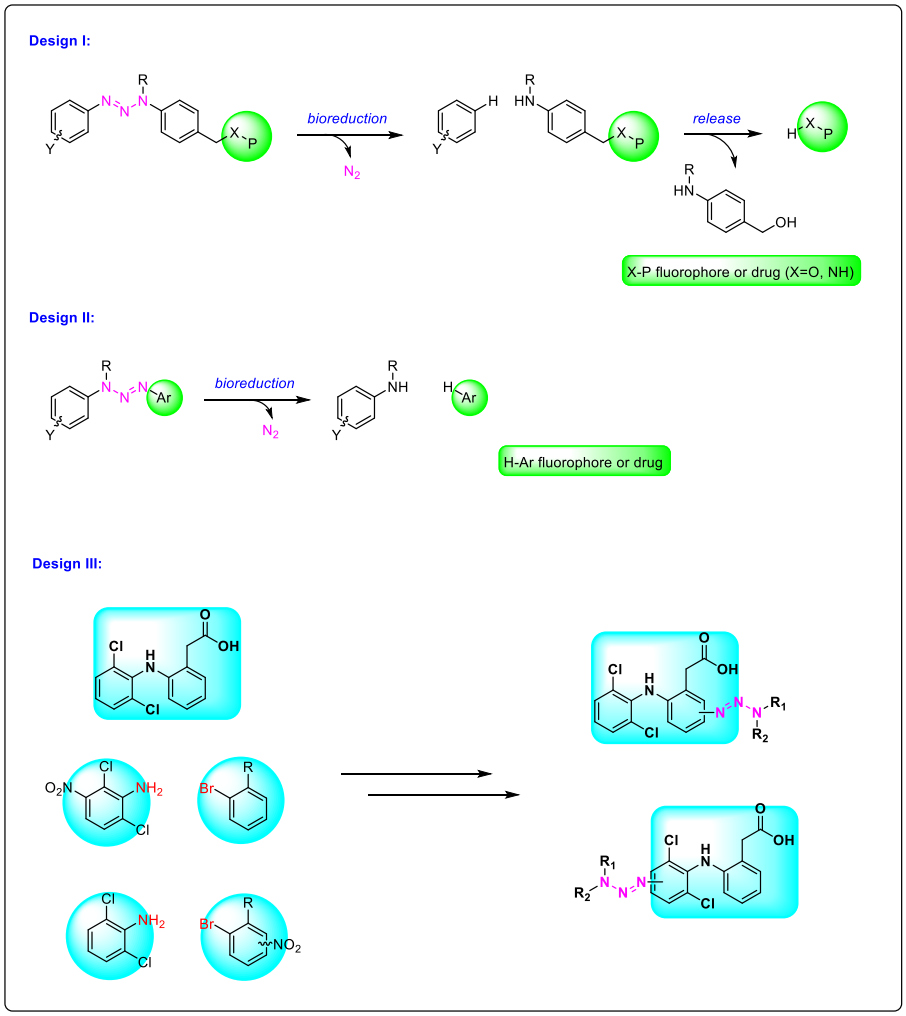

Scheme 5B-01 Overall plan for synthesis triazene HAPs

In this chapter part B, we used the triazene group as a bioreductive prodrug in two different and complementary designs. First, by analogy with the concept of azo groups as bioreductive fragments, the triazene fragment is incorporated as a self-immolative linker (**Scheme 5B-01 Design I**). Bioreduction leads to

the generation of a simple aromatic and an aniline-conjugated to the probe (fluorescence probe or cytotoxic drug). When the aniline is generated, elimination spontaneously occurs to release the probe. In such case, we hypothesized that the lone pair of the nitrogen atom of the triazene would be conjugated to the second aromatic (with possible introduction of electron-withdrawing group as $-NO_2$, $-CF_3$) and would not promote the elimination of the linker. In the second design (**Scheme 5B-01 Design II**), the probe is directly grafted on the -N=N- fragment of the triazene, and the bioreduction then directly releases the aromatic fluorophore or the drug. The release mechanism can be studied by using a chemical reductive environment and further examined using *in vitro* 3D tumor cell assay to validate the release of the fluorescent unit in a hypoxic microenvironment (**Figure 5B-03**).

In the third design (**Scheme 5B-01 Design III**), The amine-substituted diclofenac is reacted with a diazonium salt to produce a diclofenac prodrug containing a triazene fragment. This section will be introduced at the end of this chapter (**Figure 5B-03**).

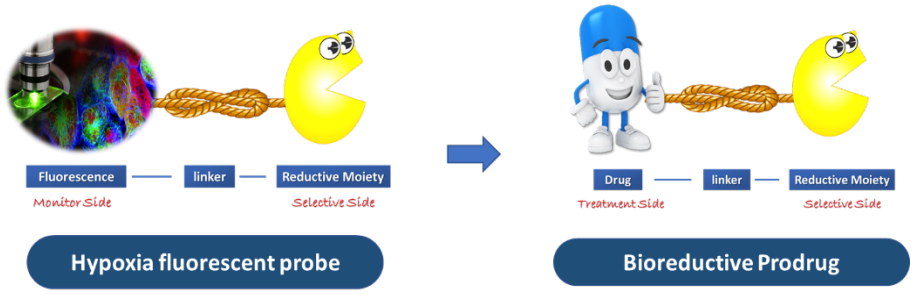

Figure 5B-03 Overall plan for Part B

2.1.2. Synthesis of triazene probe

In the triazene probe, the 4-aminobenzyl alcohol **5B-003** has a good electronic conjugation and the hydroxyl group can be easily transformed for grafting fluorescent units or drug molecules. Therefore, we first tried to design and

synthesize the **5B-004** intermediate, bearing substituents with electron-donating or withdrawing capacities (-NO_2, -CF_3, -OCH_3, -CH_3). The anilines were dissolved in 4M HCl solution with careful control of the temperature at the freezing point (ice and salt mixture), then a $NaNO_2$ solution was added dropwise to obtain the diazo salt intermediates **5B-002**. The pH of the solution was adjusted to neutral, and the 4-aminobenzyl alcohol **5B-003**, was added portionwise. The corresponding triazenes **5B-004 (5B-004a to 5B-004d)** usually precipitated from the solution and were obtained in good yields with this procedure. (**Scheme 5B-02**).

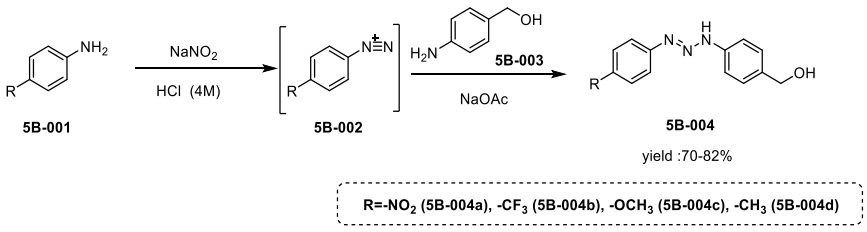

Scheme 5B-02 Synthetic route of triazene probe

Next, we linked the **5B-004** moiety to the fluorescent unit by ether bonds or carbamates to obtain the fluorescent probes. Firstly, triphosgene was used to couple the triazene and amino-coumarin **5B-005** or hydroxy-coumarin **5B-006.** Various conditions were tried, such as screening the solvent and temperature and increasing the amount of triphosgene, but we did not observe any coupling between the two fragments (**Scheme 5B-03 I**). We also tried to couple the hydroxyl-coumarin **5B-006** with a Mitsunobu reaction[68], albeit without any success (**Scheme 5B-03 II**). So, we turned to the prior activation of the alcohol group into a bromide by reaction with various brominating agents[69]. However, careful examination showed that the benzylic bromides could be formed, but were very unstable and prone to hydrolysis. Furthermore, when they were generated and directly reacted with the hydroxyl-coumarin **5B-006**, the starting materials were recovered. (**Scheme 5B-03 III**).

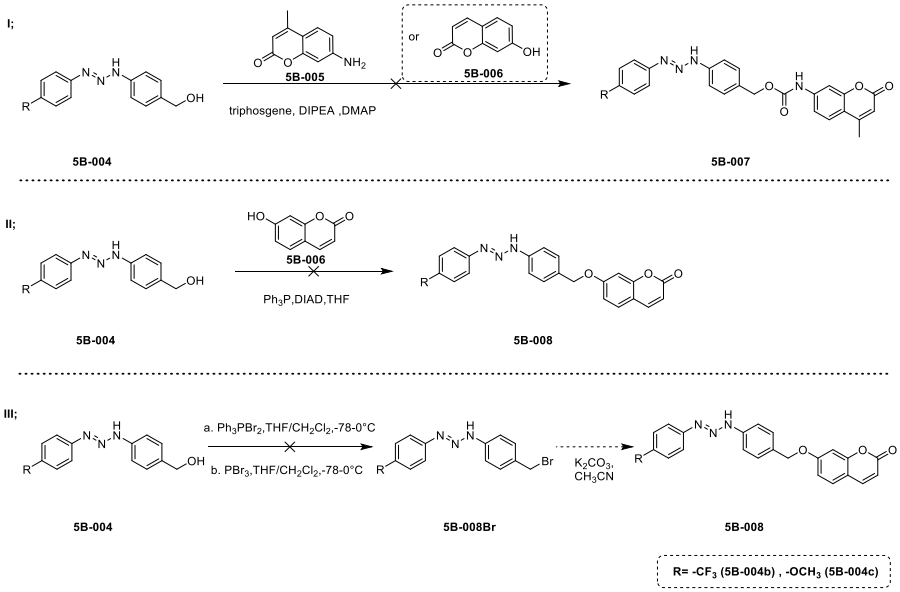

Scheme 5B-03 Synthetic route of the triazene fluorescent probes

The unsuccessful coupling of the two moieties in the above reactions could be attributed to the high capacity of the lone pair of the triazene to undergo elimination *via* the benzene ring. In order to decrease this capacity, we introduced electron-withdrawing groups on both aromatic rings and prepared two new triazene **5B-009a** and **5B-009b**. However, all attempts to carry out the coupling with the amino-coumarin **5B-005** failed again (**Scheme 5B-04**).

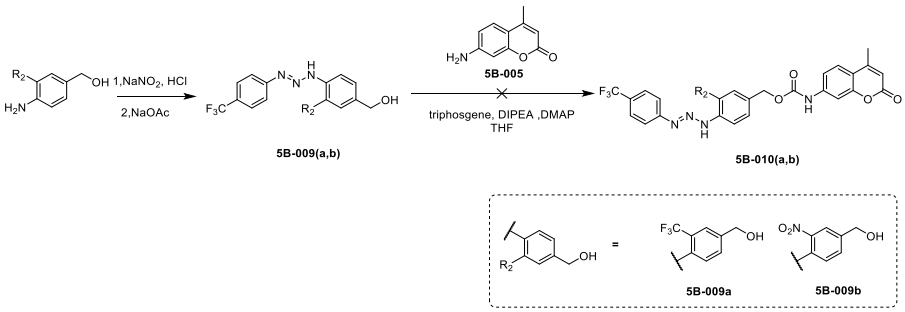

Scheme 5B-04 Synthetic route of the triazene

As the methods above use the linker 4-aminobenzyl alcohol, it was impossible to successfully couple the triazene to the fluorescent unit. Here we tried to

couple the triazene directly to the fluorescence unit. Considering the low solubility of 7-Amino-4-methylcoumarin in water, we replaced the solvent with acetonitrile. We used nitrosyl tetrafluoroborate as the diazotization reagent to synthesize a fluorescent probe containing a triazene according to the same method to give[70] **5B-013** (**Scheme 5B-05**).

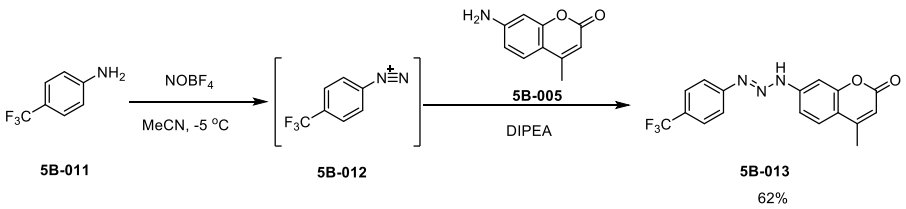

Scheme 5B-05 Synthetic route of the triazene

As the ^{1}H-NMR of compound **5B-013** showed that the hydrogen in the triazene (-N=N-N**H**-) was very mobile, suggesting the possible existence of tautomer or compound **5B-013** is not stable. (**Figure 5B-04**)

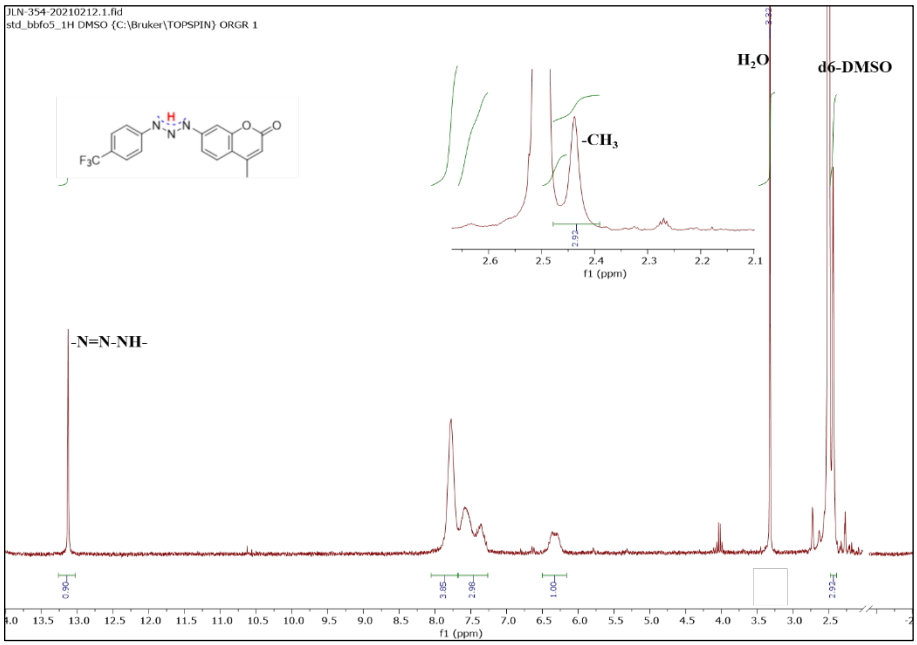

Figure 5B-04 ^{1}H-NMR of compound 5B-013

In order to improve the stability of the compounds, we used secondary amines instead of aniline. Morpholine was first employed as the secondary amine, and compound **5B-016** was prepared using the same method[70]. Because of the small molecular weight of morpholine and the absence of UV absorption, morpholine was not suitable for the next analysis, given the need to study its release under reductive conditions. Therefore, we selected tetrahydroisoquinoline and *N*-methylaniline containing π-p conjugate as secondary amines and synthesized **5B-017** and **5B-018** (**Scheme 5B-06**). As the ^{1}H-NMR of compound **5B-016** show in **Figure 5B-05.**

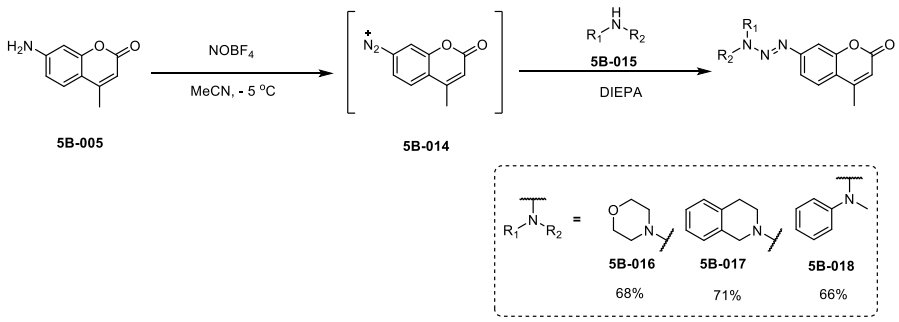

Scheme 5B-06 Synthetic route of the triazene

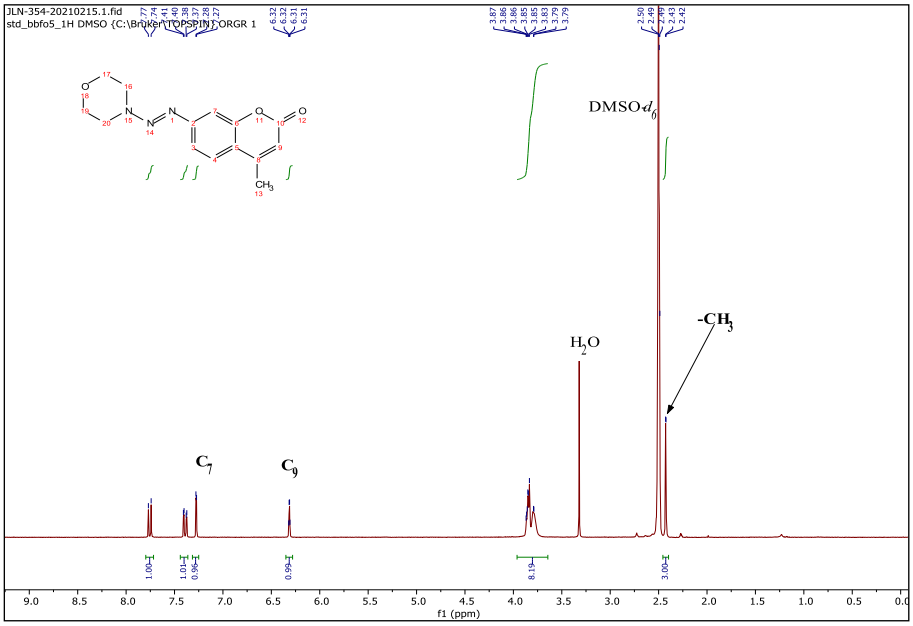

Figure 5B-05 ^{1}H-NMR of compound 5B-016

2.1.3. Mechanistic study of triazene based probes under chemical reduction conditions

2.1.3.1. Triazene probe B5-017 fluorescence study

In order to explore whether our new triazene based probes can release fluorescence under hypoxic reducing conditions, we first chose to study the probe release mechanism by chemically modeling its release in a weakly acidic reducing environment[71]. The acidic reducing conditions used here are: 50 mM Tris-HCl, 10 mM EDTA, pH=6.5, the Zn dust approximately 4 mg/ml. Initially, we tried to treat the triazene compound **B5-017** in those reducing conditions for 12 hours at room temperature, followed by analysis by thin-layer chromatography and detection of fluorescence at 365 nm. The results indicate that the triazene compound **B5-017** releases some fluorescent spots under chemical reductive conditions (**Figure 5B-06 a**). For further analysis, we tested the approximate rate and time of the reduction of the triazene compound **B5-017** by fluorescence spectroscopy, irradiating the sample with 324 nm excitation light and measuring the emission wavelength of the sample every 5 minutes. The emission of fluorescence in the weakly acidic reducing environment reaches a plateau in about 40 min, with a gradual slowdown in the rate of release, as can be seen from **Figure 5B-06 d**.

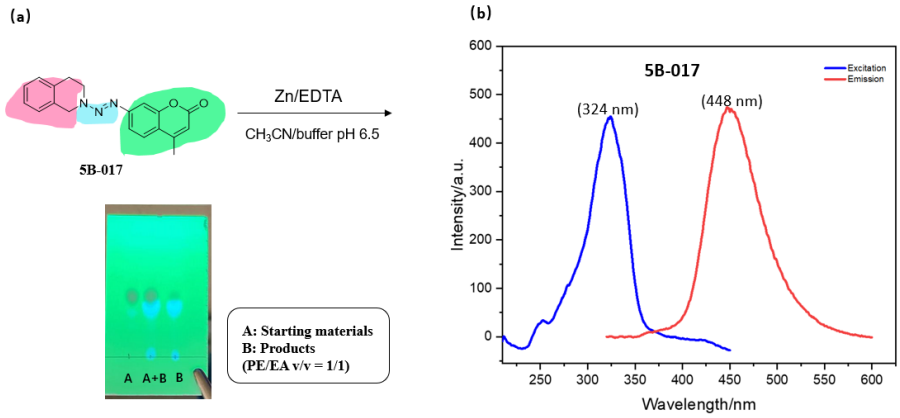

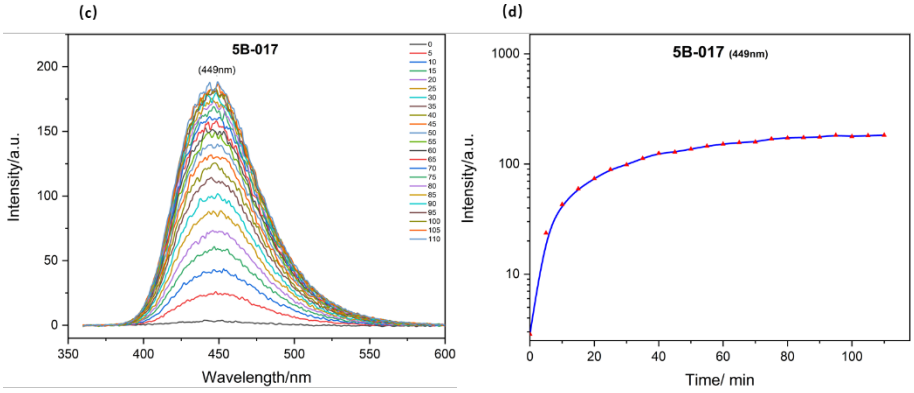

Figure 5B-06 Fluorescence spectrum of compound B5-017. (a) TLC **5B-017** at 1 mmol/L in Tris-HCl buffer pH=6.5, 10 mmol/L EDTA, 4 mg/mL Zn 10% acetonitrile t=2h. (**b**) Absorption (blue) and emission (red) spectra of **5B-017** at 1 mmol/L in Tris-HCl buffer pH=6.5 containing 10 % acetonitrile as a cosolvent. Excitation wavelength for fluorescence spectra was 324 nm. (**c**) Emission spectra of **5B-017** (1 mmol/L), upon treatment with Zn (4 mg/mL) in Tris-HCl buffer pH=6.5, 10 mmol/L EDTA 10% acetonitrile at 25 °C for 0-110 min. (**d**) Relative fluorescence intensity at 449 nm at 0-110 min.

2.1.3.2. Triazene probe B5-017 HPLC study

The fluorescence spectroscopy did not allow to analyze which products were formed under the reductive conditions. We therefore used HPLC to study the retention times (Rt) of various released compounds. As the HPLC analysis required standards compound as controls, we speculated on several compounds that might result from the release of compound **5B-017**. We obtained **5B-019** and **5B-005** commercially, while synthesis procedure of **5B-020** was reported in the literature[72, 73].

HPLC analyses are applied to investigate the chemical reductive release behavior of **5B-017**. As shown in **Figure 5B-07**, after the **5B-017** is incubated with Zn dust, the peak of Rt=8.09 and Rt=9.06 are observed in HPLC chromatogram. The retention time of the substance at Rt=8.09 is almost identical to that of compounds **5B-019** and **5B-005**, and it is difficult to determine which of the two was the product.

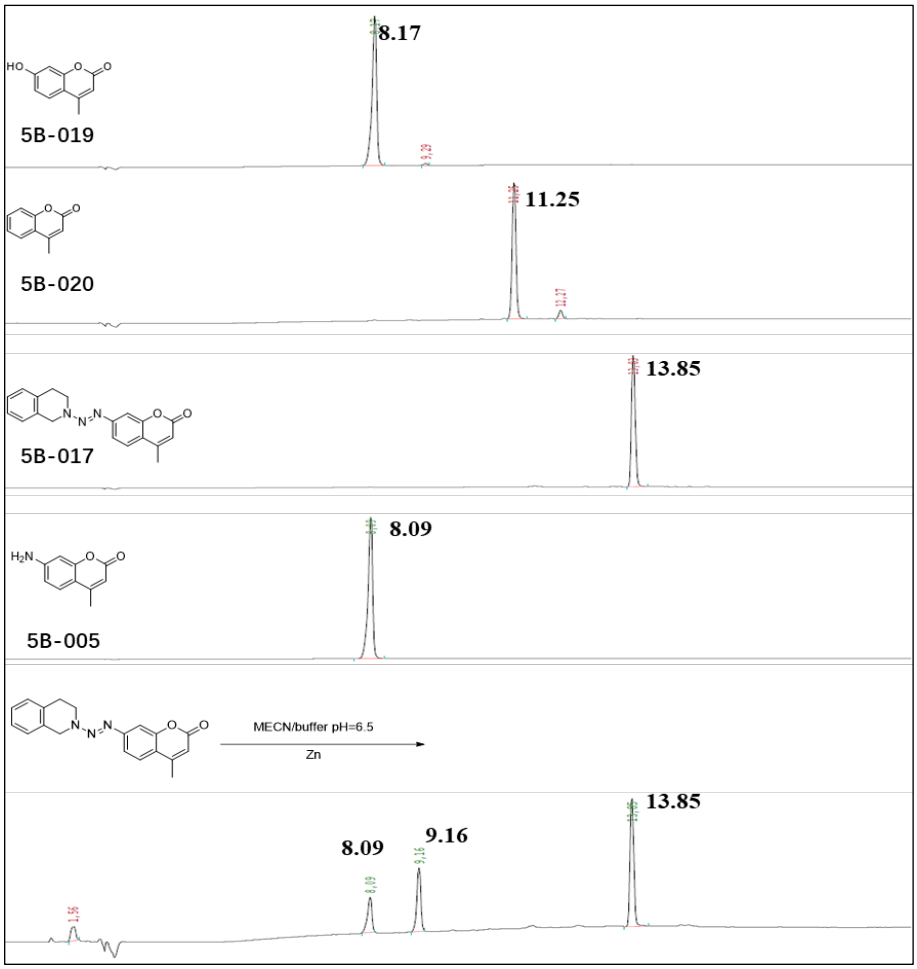

Figure 5B-07 HPLC spectrum. Chromatographic column: C_{18}, mobile phase: CH_3CN/H_2O (10/90-90/10) flow rate: 0.8ml/min column temperature: room temperature, detection wavelength: 350nm, injection volume: 10μL.

As the retention times of compounds **5B-019** and **5B-005** were very close, the released compound **5B-017** could not be distinguished by the analytical methods described above. In this case, we attempted to combining compounds **5B-019** and **5B-005,** and analyzing them again under the same chromatographic conditions. Although the two compounds could not be completely separated, the two peaks could be identified as containing two compounds. In **Figure 5B-08 A**, the two compounds are sampled at concentration (5B-019/5B-005 = 1/9) so that, Rt=8.41 and Rt=8.48 are

thought to correspond to compounds **5B-005** and **5B-019**, respectively. In the same way, 10% of compound **5B-019** is added to test C. As a result, Rt=8.39 and Rt=8.47 are thought to correspond to compounds **5B-005** and **5B-017**, respectively. However, we cannot explain the nature of the compound at Rt=9.41 (**Figure 5B-08 C**).

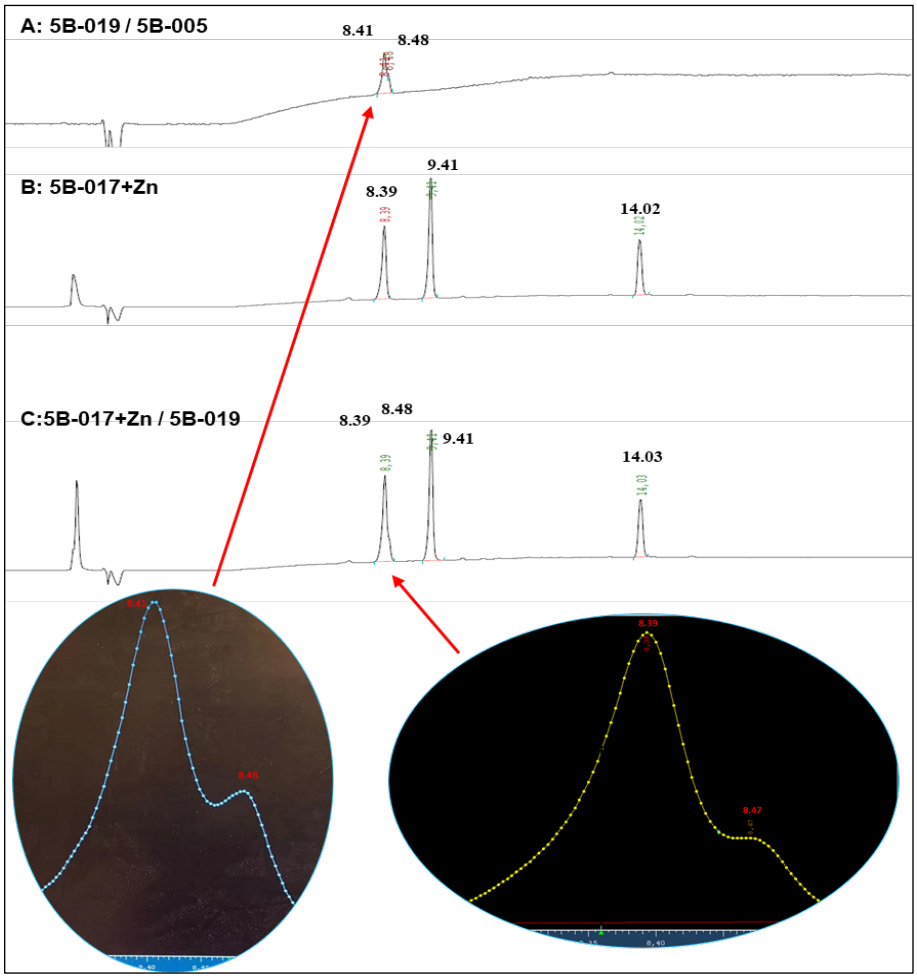

Figure 5B-08 HPLC spectrum. Chromatographic column: C_{18}, mobile phase: CH_3CN/H_2O (10/90-90/10) flow rate: 0.8ml/min column temperature: room temperature, detection wavelength: 350nm, injection volume: 10µL.

2.1.3.3. Triazene probe B5-017 LC-MS study

Next, to confirm the structures of the released product of compound **5B-017**, we used LC-MS to determine the compound's molecular weight. First in **Figure 5B-09 A,** we examined the stability of compound **5B-017** in solution. After 16 hours, the analysis showed that compound **5B-017** was stable in solution and no decomposition was observed. The results in **Figure 5B-09 B** show that compound **5B-017** release the three products under weak acid reductive conditions, of which peak 2, peak 3 and peak 4 have response at detection wavelength 350 nm, while peak 1 was only detectable in the mass spectrum.

A: B5-017 (CH_3CN/buffer pH6.5)

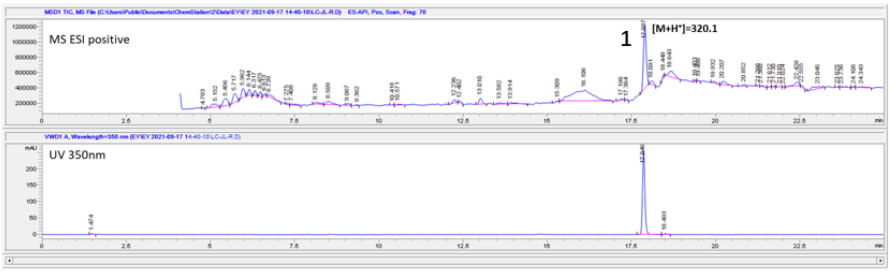

B: B5-017 (CH_3CN/buffer pH6.5+Zn)

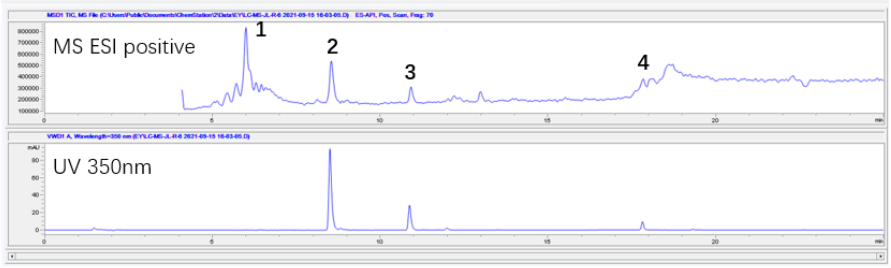

Figure 5B-09 LC-MS spectrum for 5B-017. Chromatographic column: C_{18}, mobile phase: CH_3CN/H_2O (10/90-90/10) flow rate: 1.0ml/min column temperature: room temperature, detection wavelength: 350nm, injection volume: 20μL.

Comprehensive analysis, the retention times, m/z and possible structures of them are shown in **Table 5B-01**.

Table 5B-01 LC-MS analysis results for 5B-017

	Peak	Mode	Rt (min)	Fragments (m/z)	Structure
A	1	[ESI$^+$]	17.85	[M+H$^+$]=320.1	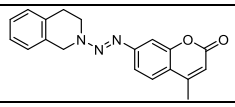
B	1	[ESI$^+$]	5.96	[M+H$^+$]=134.1	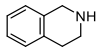
	2	[ESI$^+$]	8.55	[M+H$^+$]=176.1	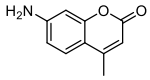
	3	[ESI$^+$]	10.92	[M+H$^+$]=203.1	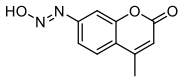
	4	[ESI$^+$]	17.85	[M+H$^+$]=320.1	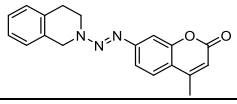

2.1.3.4. Triazene probe B5-018 fluorescence study

The same method was used to analyze compound **5B-018**. The fluorescence results showed a faster release than with compound **5B-017** before 20 mins, under the same conditions, possibly influenced by the structure of the compound (**Figure 5B-10**).

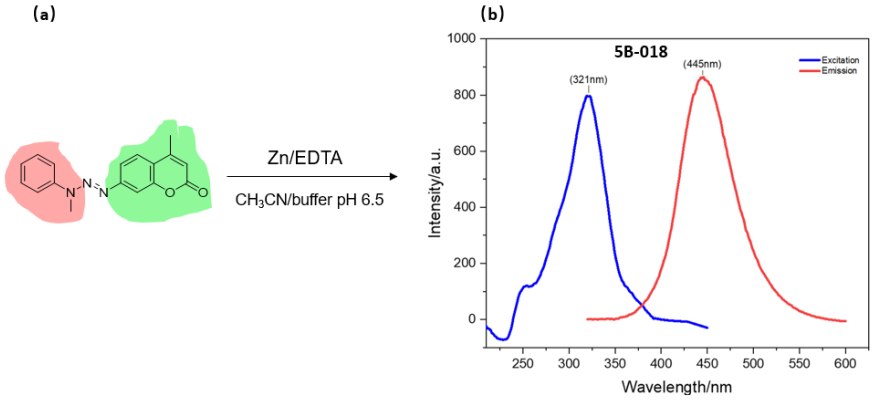

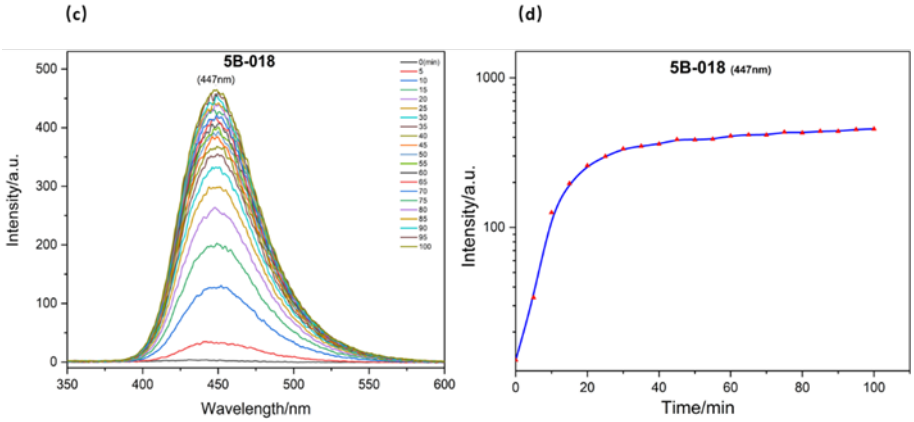

Figure 5B-10 Fluorescence spectrum of compound B5-018. (a) reaction **5B-018** at 1 mmol/L in Tris-HCl buffer pH=6.5, 10 mmol/L EDTA, 4 mg/mL Zn 10% acetonitrile t=2h. (**b**) Absorption (blue) and emission (red) spectra of **5B-018** at 1 mmol/L in Tris-HCl buffer pH=6.5 containing 10 % acetonitrile as a cosolvent. Excitation wavelength for fluorescence spectra was 321 nm. (**c**) Emission spectra of **5B-018** (1 mmol/L), upon treatment with Zn (4 mg/mL) in Tris-HCl buffer pH=6.5, 10 mmol/L EDTA 10% acetonitrile at 25 °C for 0-100 min. (**d**) Relative fluorescence intensity at 447 nm at 0-100 min.

2.1.3.5. Triazene probe B5-018 LC-MS study

We used LC-MS to study the compound's molecular weight. In **Figure 5B-11 A**, we examined the stability of compound **5B-018** in solution. After 16 hours, the analysis showed that compound **5B-018** was stable in solution and no decomposition was observed. The results in **Figure 5B-11 B** show that compound **5B-018** release the three products under weak acid reductive conditions, the results show in **Table 5B-02**.

A: B5-018 (CH_3CN/buffer pH6.5)

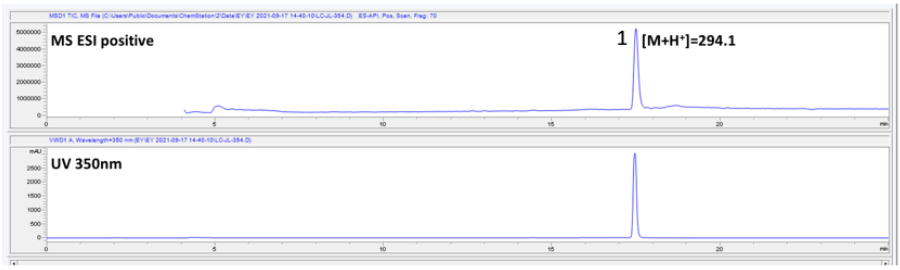

B: B5-018 (CH_3CN/buffer pH6.5+Zn)

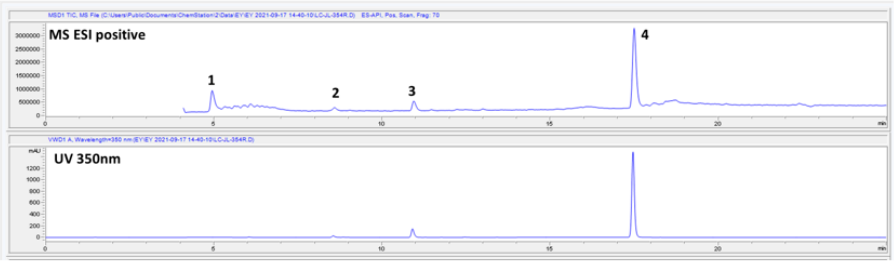

Figure 5B-11 LC-MS spectrum for 5B-018. Chromatographic column: C_{18}, mobile phase: CH_3CN/H_2O (10/90-90/10) flow rate: 1.0ml/min column temperature: room temperature, detection wavelength: 350nm, injection volume: 20μL.

Table 5B-02 LC-MS analysis results for **5B-018**

	Peak	Mode	Rt (min)	Fragments (m/z)	Structure
A	1	[ESI$^+$]	17.49	[M+H$^+$]=294.1	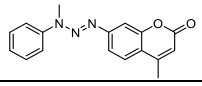
B	1	[ESI$^+$]	4.95	[M+H$^+$]=108.1	
	2	[ESI$^+$]	8.57	[M+H$^+$]=176.1	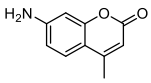
	3	[ESI$^+$]	10.94	[M+H$^+$]=203.1	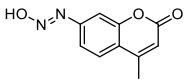
	4	[ESI$^+$]	17.53	[M+H$^+$]=294.1	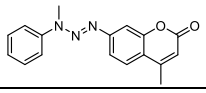

2.1.4. Possible release mechanisms of the triazene

According to the above experimental results, we hypothesize the possible reaction mechanism of the triazene compound in a weakly acidic chemical reduction environment. The compound is protonated in an acidic environment, followed by heterolytic cleavage of the N-N bond and, resulting in the formation of secondary amines and coumarin diazonium ion. The coumarin

diazonium ion reacts with water to give 7-(hydroxydiazenyl)-4-methyl-coumarin, after which the hydroxydiazenyl group is further reduced to form 7-amino-coumarin **5B-005** (**Figure 5B-12**).

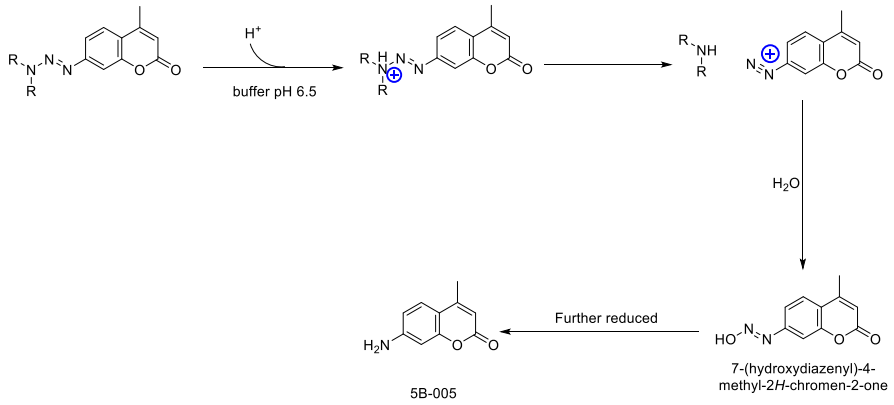

Figure 5B-12 Possible release mechanisms of the triazene under chemically reducing conditions

In the mechanism study, we found no evidence of free radical formation by single electron transfer during chemical reduction environment. we speculate that there is a difference in the reaction mechanism between the release of triazene fluorescent probe during chemical reduction and *in vivo* enzyme-catalyzed reduction of triazene probe. Additional study using biological enzymes that catalyze processes more akin to those observed in the human tumor microenvironment is needed to better understand metabolic release mechanisms *in vivo*. These enzymes include nitroreductases, azo reductases (AzoR), and hepatic cytochrome P450 systems (CYP450)[11, 74, 75]. Among others, while also taking the pH of the reaction medium into consideration.

2.2.1. Design triazene diclofenac prodrug

To prepare diclofenac prodrug containing the triazene moiety, two synthetic strategies were designed. In the first case, the most convenient way is to directly use nitrate diclofenac as a substrate, then reduce the nitro group before producing diclofenac with a triazene moiety. The second strategy is to use cheap and easily available *o*,*o'*-dichloroaniline or *o*-substituted bromobenzene as starting materials. First prepared *m*-nitro-dichloroaniline by nitration reaction. Then, the aniline and bromobenzene are coupled to obtain *m*-nitro-diclofenac. Finally, nitro group is reduced and diazotized to prepare diclofenac prodrug containing the triazene moiety (**Scheme 5B-07**).

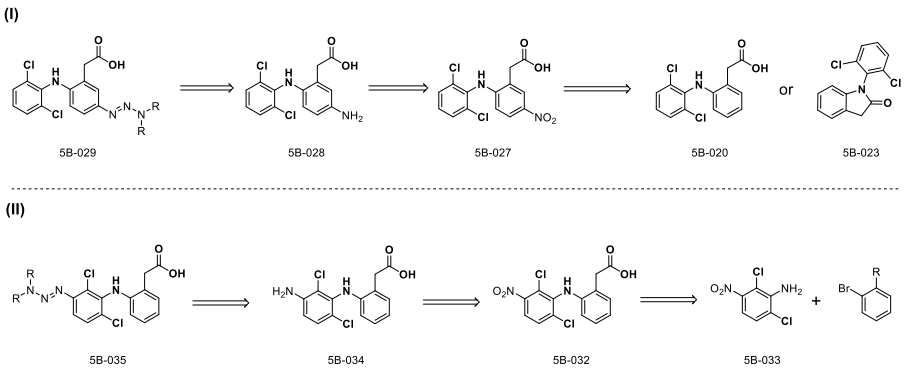

Scheme 5B-07 design synthetic route of triazene-diclofenac

2.2.2. Synthesis triazene diclofenac prodrug

Firstly, we used diclofenac ethyl ester **5B-020** as the starting material, because diclofenac is susceptible to intramolecular amination and cyclization in sulfuric acid to generate lactam compounds[76]. We used a direct nitration method in which we slowly added one equivalent nitric/sulfuric acid solution at a time while maintaining the temperature at 0^{o}C. It was found that the nitro group **5B-021** was introduced into both benzene rings of diclofenac (**Scheme 5B-08 I**) in a 24% yield. This indicates that the nitrogen atom of diclofenac has an activating effect on both aromatic rings.

Next, we attempted to find a way to reduce the effect of the nitrogen atom of diclofenac on the aromatic ring. The best solution was to amidate the nitrogen atom form the lactam compound **5B-023**[77]. Here, **5B-023** was obtained by treatment with thionyl chloride in an 96% yield. We tried direct nitration of **5B-023**, the results showed that mononitrification products were easily obtained **5B-024**, the compound **5B-024** by simply wash it with water without further purification, obtaining an excellent yield of 75%, the yield which was higher than the literature reported 52%[77]. Then, we tried to reduce the nitro group to amino group and prepared triazene according to the standard method described above. Unfortunately, we did not obtain the expected triazene derivative **5B-026** (**Scheme 5B-08 II**). Similarly, we tried to hydrolyze **5B-023** to open the ring, followed by the reduction nitro group of **5B-027** using Pd/C, H_2 to obtain amino **5B-028**. The same method was used to prepare the triazene derivatives, but the target compound **5B-029** was not obtained by silica gel chromatography (**Scheme 5B-08 III**).

I:

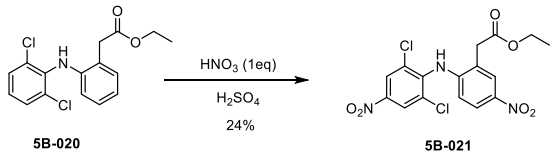

5B-020 **5B-021**

II:

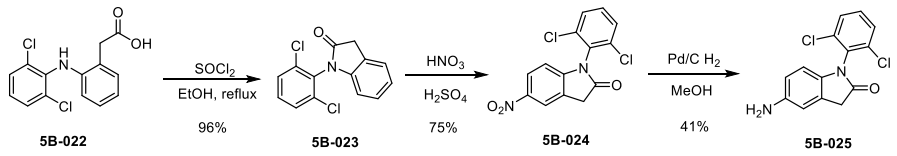

5B-022 **5B-023** **5B-024** **5B-025**

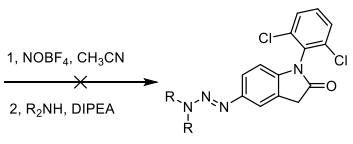

5B-026

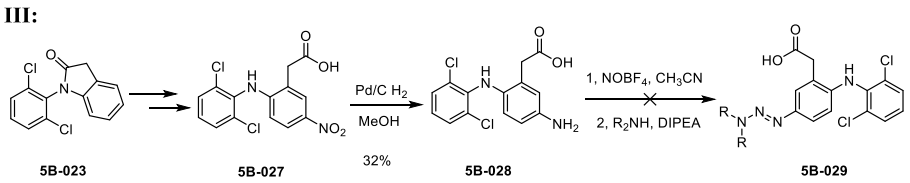

Scheme 5B-08 Synthetic route of the diclofenac triazene

Triazene derivatives cannot be synthesized by amino-diclofenac **5B-030a**. It's possible that the amino group is at the *p*-position of the nitrogen atom of diclofenac, causing tautomer to generate species such as the bis-iminoquinone **5B-030b** (**Scheme 5B-09-I**). Those species can easily polymerize, and indeed, during those experiments, we always observed the formation of deep brown mixtures over time and decomposition. Because of the above challenge in the preparation of triazene derivatives upon amino group introduction, we next attempted to add a nitro group at the diclofenac's *m*-position to prevent the formation of the tautomer described before (**Scheme 5B-09-II**).

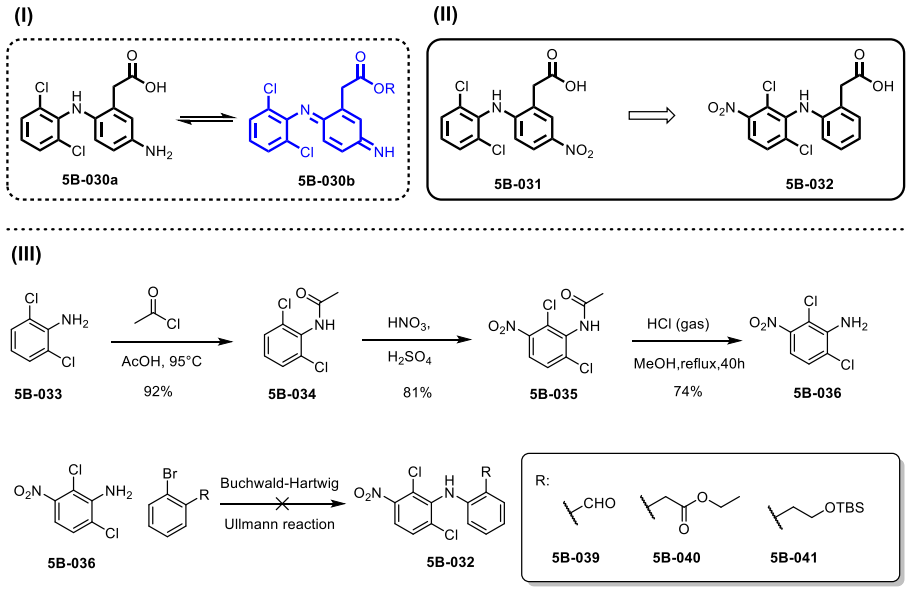

Scheme 5B-09 Synthetic route of the diclofenac triazene

The direct nitration solution is not possible when the nitro group is introduced at the meta position of the nitrogen atom of diclofenac. In this study, we

attempted to obtain the desired diclofenac derivatives by combining the nitro-containing aromatic compound **5B-036** with the *o*-substituted bromobenzene. Using the inexpensive dichloroaniline **5B-033** as a starting material, a three-step procedure can be used to synthesize *m*-nitro-dichloroaniline **5B-036**. The amino group was first acetylated to obtain the amide compound **5B-034**, which was then nitrated to give the *m*-nitro-phenylacetamide **5B-035**.

In the synthesis of amide, the conventional procedure was not used. Instead, **5B-034** was made by glacial acetic acid at a high temperature. It can be seen that the amination reaction was limited by the two chlorine atoms in the ortho position of the substrate **5B-033**. Direct nitration was used to introduce nitro in the *m*-position of the phenylamide to obtain **5B-035**. Next, **5B-035** was dissolved in methanol fed with an overdose of hydrogen chloride gas and refluxed for 40h to obtain the *m*-nitro-dichloroaniline **5B-036**[78] (**Scheme 5B-09-III**). Transition metal catalysis was used to couple the *m*-nitro-dichloroaniline **5B-036** and *o*-substituted bromo-benzene derivatives. To couple **5B-036** with bromobenzene (**5B-039**, **5B-040**, and **5B-041**), the palladium-catalyzed Buchwald-Hartwig reaction was firstly considered. All experiments were carried out by the variation of reaction parameters in sealed tubes and representative examples were presented in (**Table 5B-03**). We did not obtain the target product by silica gel chromatography separation and purification. So, we tried the Ullmman reaction at a higher temperature catalyzed by copper, but the reaction did not occur (**Table 5B-03**). The failure of the reaction above may be caused by the introduction of a nitro group in **5B-036**. In part A, compounds **5B-033** and **5B-039** can be synthesized smoothly under high-temperature sealing conditions, while compound **5B-036** is affected not only by the two chlorine atoms at the ortho position, but also by the meta-nitro group with a passivation effect on the benzene ring. Therefore, this the reaction did not occur.

Table 5B-03 Screening reaction conditions

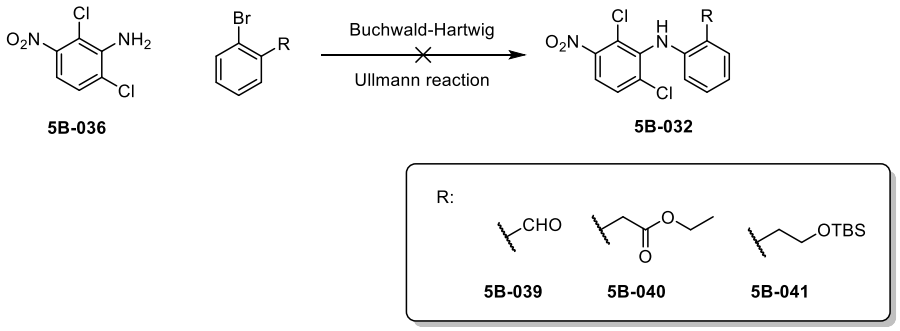

Entry	Reagents and Conditions	Result
1	$Pd_2(dba)_3$, BINAP, *t*-BuONa, Tol, 130 °C, 16h, Sealed tube	N.D.
2	$Pd_2(dba)_3$, BINAP, *t*-BuONa, dioxane, 130 °C, 24h, Sealed tube	N.D.
3	CuI, KI, K_2CO_3, DMF, 165 °C, 36h, Sealed tube	N.D.

Considering the time restrictions, the synthesis of triazene-diclofenac had to be stopped.

3. Conclusion

In part B of this chapter, we successfully synthesized triazene probes containing fluorescent groups through several phases of rational design and optimization, and solved the problem of triazene probe stability. Then, we investigated the release mechanism of triazene under chemical reduction conditions. Under chemical reduction conditions, unfortunately we could not observe the production of a single electron transfer product. This, led us to speculate that the reduction mechanism does not occur by radical homogeneous cleavage, which is probably very different from what is occurring in biological organisms. Further optimization is thus needed to mimic the *in vivo* reduction process *in vitro* through bioreductase catalysis and to investigate the mechanism of its release by modern analytical methods. Finally, while the two alternative synthetic strategies for the production of

diclofenac prodrugs containing the triazene moiety failed, our results provide support for further research.

4. References

1. Sharma, A.; Arambula, J. F.; Koo, S.; Kumar, R., et al., Hypoxia-targeted drug delivery. Chem Soc Rev 2019, 48 (3), 771-813.
2. Zhu, R.; He, H.; Liu, Y.; Cao, D., et al., Cancer-Selective Bioreductive Chemotherapy Mediated by Dual Hypoxia-Responsive Nanomedicine upon Photodynamic Therapy-Induced Hypoxia Aggravation. Biomacromolecules 2019, 20 (7), 2649-2656.
3. McKeown, S. R., Defining normoxia, physoxia and hypoxia in tumours-implications for treatment response. Br J Radiol 2014, 87 (1035), 20130676.
4. Mansoori, B.; Mohammadi, A.; Davudian, S.; Shirjang, S., et al., The Different Mechanisms of Cancer Drug Resistance: A Brief Review. Adv Pharm Bull 2017, 7 (3), 339-348.
5. O'Connor, L. J.; Cazares-Korner, C.; Saha, J.; Evans, C. N., et al., Design, synthesis and evaluation of molecularly targeted hypoxia-activated prodrugs. Nat Protoc 2016, 11 (4), 781-794.
6. Anduran, E.; Dubois, L. J.; Lambin, P.; Winum, J.-Y., Hypoxia-activated prodrug derivatives of anti-cancer drugs: a patent review 2006–2021. Expert Opin Ther Pat 2021, 1-12.
7. Mistry, I. N.; Thomas, M.; Calder, E. D. D.; Conway, S. J., et al., Clinical Advances of Hypoxia-Activated Prodrugs in Combination With Radiation Therapy. Int J Radiat Oncol Biol Phys 2017, 98 (5), 1183-1196.
8. Wilson, W. R.; Hay, M. P., Targeting hypoxia in cancer therapy. Nat Rev Cancer 2011, 11 (6), 393-410.
9. Wardman, P., Some reactions and properties of nitro radical-anions important in biology and medicine. Environmental Health Perspectives 1985, 64, 309-320.
10. Zhou, Y.; Maiti, M.; Sharma, A.; Won, M., et al., Azo-based small molecular hypoxia responsive theranostic for tumor-specific imaging and therapy. J Control Release 2018, 288, 14-22.
11. Kumari, R.; Sunil, D.; Ningthoujam, R. S.; Kumar, N. A., Azodyes as markers for tumor hypoxia imaging and therapy: An up-to-date review. Chem Biol Interact 2019, 307, 91-104.
12. Sun, L.; Li, G.; Chen, X.; Chen, Y., et al., Azo-Based Iridium(III) Complexes as Multicolor Phosphorescent Probes to Detect Hypoxia in 3D Multicellular Tumor Spheroids. Sci Rep 2015, 5, 14837.
13. Contreras-Baeza, Y.; Sandoval, P. Y.; Alarcon, R.; Galaz, A., et al., Monocarboxylate transporter 4 (MCT4) is a high affinity transporter capable of exporting lactate in high-lactate microenvironments. J Biol Chem 2019, 294 (52), 20135-20147.
14. Sasaki, S.; Futagi, Y.; Ideno, M.; Kobayashi, M., et al., Effect of diclofenac on SLC16A3/MCT4 by the Caco-2 cell line. Drug Metab Pharmacokinet 2016, 31 (3), 218-223.
15. Vander Linden, C.; Corbet, C.; Bastien, E.; Martherus, R., et al., Therapy-induced DNA methylation inactivates MCT1 and renders tumor cells vulnerable to MCT4 inhibition. Cell Rep 2021, 35 (9), 109202.
16. Todd, P. A.; Sorkin, E. M., Diclofenac sodium. A reappraisal of its pharmacodynamic and pharmacokinetic properties, and therapeutic efficacy. Drugs 1988, 35 (3), 244-285.
17. Huang, Y. T.; Cheng, Y. R.; Lin, H. C.; Chen, S. M., et al., Haemodynamic effects of chronic octreotide and tetrandrine administration in portal hypertensive rats. J Gastroenterol Hepatol 1998, 13 (3), 266-272.
18. Bhagya, N.; Chandrashekar, K., Tetrandrine–A molecule of wide bioactivity. Phytochemistry 2016, 125, 5-13.
19. Lan, J.; Huang, L.; Lou, H.; Chen, C., et al., Design and synthesis of novel C14-urea-tetrandrine derivatives with potent anti-cancer activity. Eur J Med Chem 2018, 143, 1968-1980.
20. Lan, J.; Wang, N.; Huang, L.; Liu, Y., et al., Design and synthesis of novel tetrandrine derivatives as potential anti-tumor agents against human hepatocellular carcinoma. Eur.J.Med.Chem 2017, 127, 554-566.

21. Heister, P.; Poston, R., Tetrandrine as a Therapeutic Agent for COVID-19. Authorea Preprints 2020, 1-6.
22. Heister, P. M.; Poston, R. N., Pharmacological hypothesis: TPC2 antagonist tetrandrine as a potential therapeutic agent for COVID-19. Pharmacol. Res. Perspect. 2020, 8 (5), e00653.
23. Wang, G.; Lemos, J., Tetrandrine: A new ligand to block voltage-dependent Ca2+ and Ca2+-activated K+ channels. Life Sci 1994, 56 (5), 295-306.
24. Li, Y.; Li, D.; Wang, P.; Zhu, W., et al., Tetrandrine partially reverses multidrug resistance of human laryngeal cancer cells. J Int Med Res 2020, 48 (8), 1-9.
25. Li, F.; Dong, Y. Z.; Zhang, D.; Zhang, X. M., et al., Molecular mechanisms involved in drug-induced liver injury caused by urate-lowering Chinese herbs: A network pharmacology study and biology experiments. PLoS One 2019, 14 (5), e0216948.
26. Schutz, R.; Muller, M.; Geisslinger, F.; Vollmar, A., et al., Synthesis, biological evaluation and toxicity of novel tetrandrine analogues. Eur J Med Chem 2020, 207, 112810.
27. Tian, Y.; Shen, S.; Jiang, Y.; Shen, Q., et al., CYP3A5 mediates bioactivation and cytotoxicity of tetrandrine. Arch Toxicol 2016, 90 (7), 1737-1748.
28. Cao, Z.; Li, W.; Liu, R.; Li, X., et al., pH- and enzyme-triggered drug release as an important process in the design of anti-tumor drug delivery systems. Biomed Pharmacother 2019, 118, 109340.
29. Mahato, R.; Tai, W.; Cheng, K., Prodrugs for improving tumor targetability and efficiency. Adv Drug Deliv Rev 2011, 63 (8), 659-670.
30. Thurow, S.; Fernandes, A. A. G.; Quevedo-Acosta, Y.; de Oliveira, M. F., et al., Preparation of Organic Nitrates from Aryldiazoacetates and Fe(NO3)3.9H2O. Org Lett 2019, 21 (17), 6909-6913.
31. Zare, H.; Ghanbari, M. M.; Jamali, M.; Aboodi, A., A novel and efficient strategy for the synthesis of various carbamates using carbamoyl chlorides under solvent-free and grinding conditions using microwave irradiation. Chin Chem Lett 2012, 23 (8), 883-886.
32. Kondoh, A.; Odaira, K.; Terada, M., Ring expansion of epoxides under Bronsted base catalysis: formal [3+2] cycloaddition of beta,gamma-epoxy esters with imines providing 2,4,5-trisubstituted 1,3-oxazolidines. Angew Chem Int Ed Engl 2015, 54 (38), 11240-11244.
33. Ostrowski, S.; Wolniewicz, A. M., An approach to fused pyrimidine derivativesvia Schiff bases of aromaticortho-nitrocarbaldehydes. An investigation of substituent effects on the reaction course. Chem Heterocycl Compd 2000, 36 (6), 705-713.
34. Kumar, A.; Bansal, D.; Bajaj, K.; Sharma, S., et al., Synthesis of some newer derivatives of 2-amino benzoic acid as potent anti-inflammatory and analgesic agents. Bioorg. Med. Chem. 2003, 11 (23), 5281-5291.
35. Takale, B. S.; Feng, X.; Lu, Y.; Bao, M., et al., Unsupported Nanoporous Gold Catalyst for Chemoselective Hydrogenation Reactions under Low Pressure: Effect of Residual Silver on the Reaction. J Am Chem Soc 2016, 138 (32), 10356-10364.
36. Wei, C.; Han, B.; Zheng, D.; Zheng, Q., et al., Aluminum Complexes Bearing Bidentate Amido–Phosphine Ligands for Ring-Opening Polymerization of ε-Caprolactone: Steric Effect on Coordination Chemistry and Reactivity. Organometallics 2019, 38 (19), 3816-3823.
37. Ishibashi, K.; Tsue, H.; Tokita, S.; Matsui, K., et al., Regioselectively N-methylated azacalix[8]arene octamethyl ether prepared by catalytic aryl amination reaction using a temporal N-silylation protocol. Org Lett 2006, 8 (26), 5991-5994.
38. Boyd, R. E.; Carson, J. R.; Codd, E. E.; Gauthier, A. D., et al., Synthesis and binding affinities of 4-diarylaminotropanes, a new class of delta opioid agonists. Bioorg. Med. Chem Lett 2000, 10 (10), 1109-1111.
39. Wakuluk-Machado, A.-M.; Dewez, D. F.; Baguia, H.; Imbratta, M., et al., Pd(OH)2/C, a Practical and Efficient Catalyst for the Carboxylation of Benzylic Bromides with Carbon Monoxide. Org Process Res Dev. 2019, 24 (5), 713-723.
40. Tsuchihashi, G.; Ogura, K.; Sakoda, R.; Hashiba, I., et al. O-(N-Allyl-2, 6-dichloroanilino) phenylacetic acid Derivative and a Process for Preparing the Same. 1980.

41. Prousek, J., The course of reaction of 4-nitrobenzyl bromide and 5-nitrofurfuryl bromide with bases: Operation of anion-radical mechanism. Collect. Czech. Chem. Commun. 1982, 47 (5), 1334-1338.
42. Li, B. S.; Wang, Y.; Proctor, R. S.; Zhang, Y., et al., Carbene-catalysed reductive coupling of nitrobenzyl bromides and activated ketones or imines via single-electron-transfer process. Nat Commun 2016, 7, 12933.
43. Lim, T.; Ryoo, J. Y.; Han, M. S., Transition-Metal-Free Borylation of Aryl Bromide Using a Simple Diboron Source. J Org Chem 2020, 85 (16), 10966-10972.
44. Zernickel, A.; Du, W.; Ghorpade, S. A.; Sawant, D. N., et al., Bedford-Type Palladacycle-Catalyzed Miyaura Borylation of Aryl Halides with Tetrahydroxydiboron in Water. J Org Chem 2018, 83 (4), 1842-1851.
45. Zhang, K.; Budinska, A.; Passera, A.; Katayev, D., N-Nitroheterocycles: Bench-Stable Organic Reagents for Catalytic Ipso-Nitration of Aryl- and Heteroarylboronic Acids. Org Lett 2020, 22 (7), 2714-2719.
46. Calvo, R.; Zhang, K.; Passera, A.; Katayev, D., Facile access to nitroarenes and nitroheteroarenes using N-nitrosaccharin. Nat Commun 2019, 10 (1), 3410.
47. Branstetter, B.; Breitenbucher, J.; Lebsack, A.; Liu, J., et al. Preparation of Imidazolo-, Oxazolo-, and Thiazolopyrimidine Compounds as Modulators of Transient Receptor Potential Protein Vanilloid Receptor 1 (TRPV1) Activity. 2009.
48. Murakami, K.; Yorimitsu, H.; Osuka, A., Two-Step, Practical, and Diversity-Oriented Synthesis of Multisubstituted Benzofurans from Phenols through Pummerer Annulation Followed by Cross-coupling. Bull. Chem. Soc. Jpn. 2014, 87 (12), 1349-1366.
49. Kirchberg, S.; Fröhlich, R.; Studer, A., Stereoselective Palladium-Catalyzed Carboaminoxylations of Indoles with Arylboronic Acids and TEMPO. Angew. Chem. Int. Ed. Engl. 2009, 48 (23), 4235-4238.
50. Galisteo, A.; Jannus, F.; Garcia-Garcia, A.; Aheget, H., et al., Diclofenac N-Derivatives as Therapeutic Agents with Anti-Inflammatory and Anti-Cancer Effect. Int J Mol Sci 2021, 22 (10), 5067.
51. Dounay, A. B.; Overman, L. E., The asymmetric intramolecular Heck reaction in natural product total synthesis. Chem Rev 2003, 103 (8), 2945-2964.
52. Hirotaki, K.; Hanamoto, T., Mizoroki-Heck reaction of (1-fluorovinyl)methyldiphenylsilane with aryl iodides. J Org Chem 2011, 76 (20), 8564-8568.
53. Cushman, D. W.; Ondetti, M. A. Hydroxycarbamoylalkylacylpipecolic acid compounds. 1979 patent.
54. Carnell, A. J.; Kirk, R.; Smith, M.; McKenna, S., et al., Inhibition of human alpha-methylacyl CoA racemase (AMACR): a target for prostate cancer. ChemMedChem 2013, 8 (10), 1643-1647.
55. Merabet-Khelassi, M.; Houiene, Z.; Aribi-Zouioueche, L.; Riant, O., Green methodology for enzymatic hydrolysis of acetates in non-aqueous media via carbonate salts. Tetrahedron: Asymmetry 2012, 23 (11-12), 828-833.
56. Sikora, A.; Chełminiak-Dudkiewicz, D.; Siódmiak, T.; Tarczykowska, A., et al., Enantioselective acetylation of (R , S)-atenolol: The use of Candida rugosa lipases immobilized onto magnetic chitosan nanoparticles in enzyme-catalyzed biotransformation. J. Mol. Catal. 2016, 134, 43-50.
57. Poojari, Y.; Clarson, S. J., Thermal stability of Candida antarctica lipase B immobilized on macroporous acrylic resin particles in organic media. Biocatal. Agric. Biotechnol. 2013, 2 (1), 7-11.
58. Bosshart, P. D.; Kalbermatter, D.; Bonetti, S.; Fotiadis, D., Mechanistic basis of L-lactate transport in the SLC16 solute carrier family. Nat Commun 2019, 10 (1), 2649.
59. Wang, N.; Jiang, X.; Zhang, S.; Zhu, A., et al., Structural basis of human monocarboxylate transporter 1 inhibition by anti-cancer drug candidates. Cell 2021, 184 (2), 370-383 e313.
60. Li, C.; Li, W.-H.; Dong, L., Efficient synthesis of N-butadiene substituted oxindole derivatives. Org. Chem. Front. 2018, 5 (23), 3460-3463.

61. Harrell, M. L.; Malinski, T.; Torres-Lopez, C.; Gonzalez, K., et al., Alternatives for Conventional Alkane Solvents. J Am Chem Soc 2016, 138 (44), 14650-14657.
62. Ghodsinia, S. S. E.; Akhlaghinia, B., A high-yielding, expeditious, and multicomponent synthesis of urea and carbamate derivatives by using triphenylphosphine/trichloroisocyanuric acid system. Phosphorus Sulfur Silicon Relat Elem 2016, 191 (1), 1-7.
63. Saleem, A.; Brown, G. D.; Brady, F.; Aboagye, E. O., et al., Metabolic activation of temozolomide measured in vivo using positron emission tomography. Cancer res. 2003, 63 (10), 2409-2415.
64. Baker, S. D.; Wirth, M.; Statkevich, P.; Reidenberg, P., et al., Absorption, metabolism, and excretion of 14C-temozolomide following oral administration to patients with advanced cancer. Clin Cancer Res 1999, 5 (2), 309-317.
65. Mizoi, K.; Hosono, M.; Kojima, H.; Ogihara, T., Establishment of a primary human hepatocyte spheroid system for evaluating metabolic toxicity using dacarbazine under conditions of CYP1A2 induction. Drug Metab Pharmacokinet 2020, 35 (2), 201-206.
66. Reid, J. M.; Kuffel, M. J.; Miller, J. K.; Rios, R., et al., Metabolic activation of dacarbazine by human cytochromes P450: the role of CYP1A1, CYP1A2, and CYP2E1. Clin Cancer Res 1999, 5 (8), 2192-2197.
67. Kadiiska, M. B.; De Costa, K. S.; Mason, R. P.; Mathews, J. M., Reduction of 1,3-diphenyl-1-triazene by rat hepatic microsomes, by cecal microflora, and in rats generates the phenyl radical metabolite: nn ESR spin-trapping investigation. Chem Res Toxicol 2000, 13 (11), 1082-1086.
68. Murray, J. B.; Roughley, S. D.; Matassova, N.; Brough, P. A., Off-rate screening (ORS) by surface plasmon resonance. An efficient method to kinetically sample hit to lead chemical space from unpurified reaction products. J Med Chem 2014, 57 (7), 2845-2850.
69. Patel, A. S.; Jain, V.; Rao, V. N.; Lin, Y. W., et al., Design, synthesis and antitumour evaluation of pyrrolo[1,2-f]-phenanthridine and dibenzo[f,h]pyrrolo[1,2-b]isoquinoline derivatives. Eur J Med Chem 2020, 202, 112516.
70. Rachid, Z.; Brahimi, F.; Qiu, Q.; Williams, C., et al., Novel nitrogen mustard-armed combi-molecules for the selective targeting of epidermal growth factor receptor overexperessing solid tumors: discovery of an unusual structure-activity relationship. J Med Chem 2007, 50 (11), 2605-2608.
71. Zhu, R.; Liu, M. C.; Luo, M. Z.; Penketh, P. G., et al., 4-nitrobenzyloxycarbonyl derivatives of O(6)-benzylguanine as hypoxia-activated prodrug inhibitors of O(6)-alkylguanine-DNA alkyltransferase (AGT), which produces resistance to agents targeting the O-6 position of DNA guanine. J Med Chem 2011, 54 (21), 7720-7728.
72. Soleimani, E.; Khodaei, M. M.; Batooie, N.; Samadi, S., Tetrakis(acetonitrile)copper(I) hexafluorophosphate catalyzed coumarin synthesis via pechmann condensation under solvent-free condition. J Heterocycl Chem. 2012, 49 (2), 409-412.
73. Wiedemann, T.; Voit, G.; Tchernook, A.; Roesle, P., et al., Monofunctional hyperbranched ethylene oligomers. J Am Chem Soc 2014, 136 (5), 2078-2085.
74. Piao, W.; Tsuda, S.; Tanaka, Y.; Maeda, S., et al., Development of azo-based fluorescent probes to detect different levels of hypoxia. Angew Chem Int Ed Engl 2013, 52 (49), 13028-13032.
75. Guo, T.; Cui, L.; Shen, J.; Zhu, W., et al., A highly sensitive long-wavelength fluorescence probe for nitroreductase and hypoxia: selective detection and quantification. Chem Commun (Camb) 2013, 49 (92), 10820-10822.
76. Somashekar, P.; PAI, P. S.; RAO, G., Synthesis and Characterization of Specified Impurities of Aceclofenac. Chem. Eng. Trans. 2013, 2 (3), 813-820.
77. Isakovich, I.; Ryabova, S. Y.; Alekseeva, L.; Granik, V., Synthesis of 5-substituted 1-(2′, 6′-dichlorophenyl)-3-aminomethylene-2-indolinones. Pharm. Chem. J. 1995, 29 (12), 856-860.
78. Campbell, J. E.; Duncan, K. W.; Mills, J. E. J.; Munchhof, M. J. Amine-substituted heterocyclic compounds as ehmt2 inhibitors and derivatives thereof. 2020 patent.

Conclusion and perspectives

In this PhD thesis, we worked on tumor metabolism-related targets for which we designed and synthesized inhibitory compounds, including in the form of prodrugs to be selectively release in the tumor microenvironment to minimize potential adverse effects. We also had at heart to evaluate the biological activity of these compounds in *in vitro* culture assays to determine their efficacy.

In the first part of our research, we focused on tumor mitochondrial OXPHOS complex I, recently highlighted as an attractive anticancer target. Firstly, we developed and synthesized 28 derivatives of 5-amine-1,2,3-triazol-4-carboxamide CAI and employed a three-step bioactivity screening procedure to study the inhibitory activity of Complex I. The results showed significant activities of 12 derivatives endowed with complex I inhibitory activity. 3D tumor spheroid experiments were used to better mimic the *in vivo* microenvironment, and four potential compounds were further selected as attractive hits, of which **3-049** was considered as the most promising compound (**Figure 6-01**). We also provided a preliminary structure-activity relationship study that will help further development of Complex I inhibitors. (see Chapter I Part A)

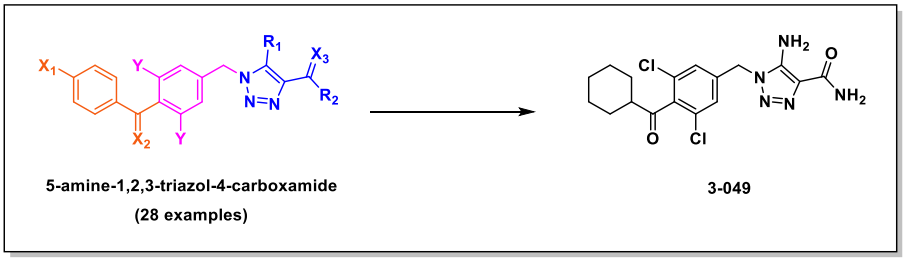

Figure 6-01 CAI derivatives

Following that, we continued to develop compounds containing 1,2,3-triazol-5-amine, 4-(1,2,4-oxadiazol-5-yl)-1,2,3-triazol-5-amine, and 5-(5-methyl-1,2,4-triazol-3-yl)-1,2,4-oxadiazole groups. By using Seahorse technology, the inhibitory activity of the compound against Complex I was evaluated. Preliminary results indicated that the compound containing 5-(5-methyl-1,2,4-triazol-3-yl)-1,2,4-oxadiazole group is associated with the preservation of the inhibitory activity of Complex I (**Figure 6-02**). (see Chapter I Part B and Part C)

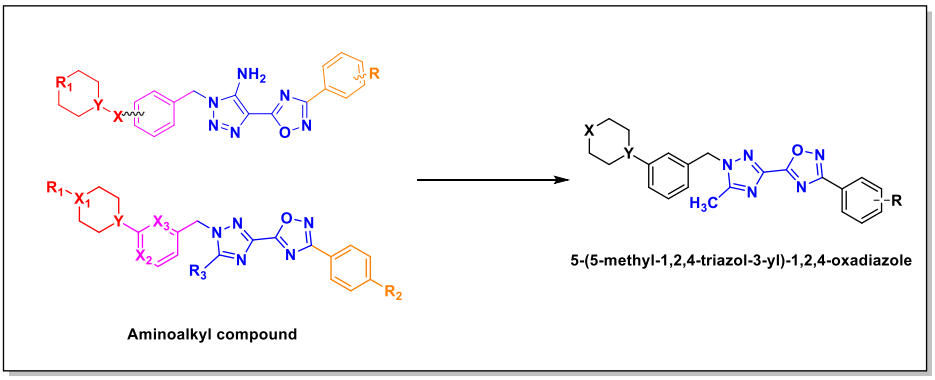

Figure 6-02 Aminoalkyl derivatives

The second part of our research is about the tumor drug delivery systems. Tumor tissues exhibit an acidic microenvironment and we therefore used pH low insertion peptide (pHLIP) to generate conjugates aiming to improve the delivery of drugs into tumors (and thereby to avoid unnecessary side effects).

We aimed to design and synthesize pHLIP conjugates with previously reported drug molecules that target fatty acid metabolism in tumor cells (CPT1 inhibitor Etomoxir **4-010** and DGAT1 inhibitor T863 **4-029**). The pH-sensitivity of the conjugate drug delivery system and its effect on fatty acid metabolism were evaluated in tumor cells *in vitro*.

We successfully designed and synthesized drug fragments **4-010** and **4-029** and used disulfide bonds to link the pHLIP. Following that, interactions between the conjugate and POPC vesicles at different pH conditions were studied, showing that conjugate **4-020*d*** could be successfully inserted into the POPC vesicles. *In vitro* cellular study however revealed that the pH-sensitive etomoxir conjugates **4-020*d*** had no effect on the increase of DHA-induced ferroptotic cell death. One reason for this could be that the conjugate is not inserted into the tumor cell, meaning that the amino acid sequence of pHLIP needs to be further designed and optimized. (see Chapter II).

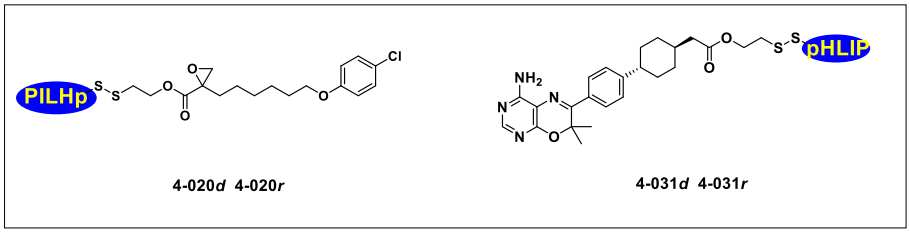

Figure 6-03 pH sensitive conjugates

The third part of our research is about the hypoxia activated prodrugs (HAPs). We prepared a prodrug by combining the hypoxia-sensitive nitro moiety with diclofenac. This prodrug has the potential to overcome the side effects associated with systemic inhibition of cyclooxygenase (COX). Bioreductive fragments 4-nitrobenzyl, 1-methyl-2-nitroimidazolyl and azo group were grafted onto tetrandrine to prepare prodrugs for comparison of the properties of hypoxia sensitive moiety. We successfully synthesized three diclofenac prodrugs with nitro moieties by trying different synthesis strategies, and

successfully grafted 4-nitrobenzyl, 1-methyl-2-nitroimidazolyl, and azo groups onto tetrandrine (**Figure 6-04**). (see Chapter III part A)

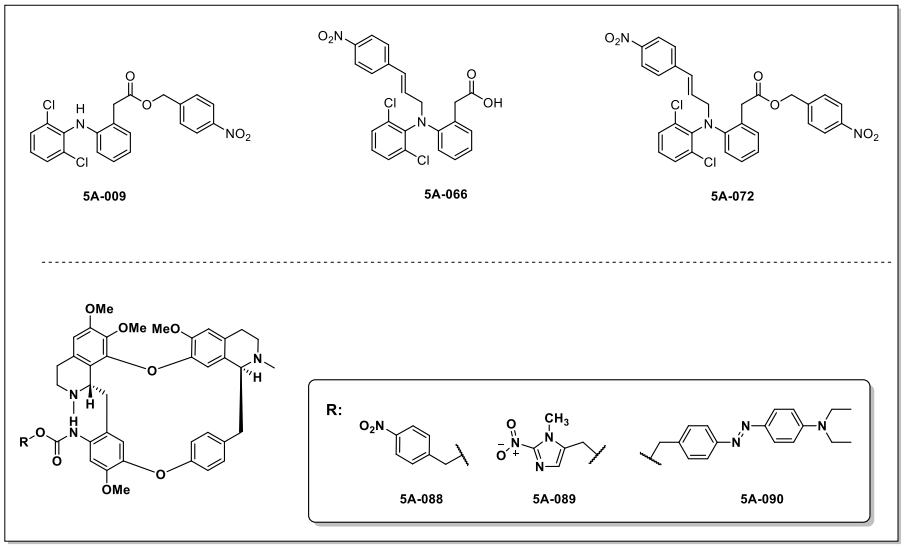

Figure 6-04 hypoxia-activated prodrugs

The third part of our research also focused on the design and synthesis of a novel type of bioreduced triazene probe. We optimized the structure of the triazene probe until we obtained the stable triazene probes (**5B-016**, **5B-017, 5B-018**) (**Figure 6-05**). The release of the triazene probe was studied using chemical reduction conditions, indicating that the probe can be released under weak acid reduction conditions, but not via the free radical formation by single electron transfer. It will be critical in the future to assess the reaction mechanism in a simulated *in vivo* environment recapitulating the low oxygen tumor environment. (see Chapter III part B)

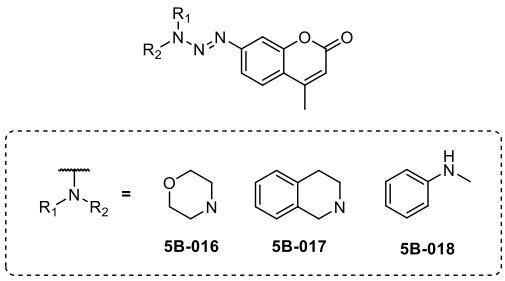

Figure 6-05 Triazene probes

In conclusion, our work provides new insights for the development of compounds targeting tumor metabolism-related targets including through the harnessing of peculiarities of the tumor microenvironment to generate acidic pH or hypoxia-sensitive prodrugs. This study was envisioned as a systematic effort that required collaborations with different research groups to accomplish this ambitious goal. The main part of my work was to apply medicinal chemistry methods to design and synthesize related compounds or prodrugs. The design and synthesis schemes were carried out as planned and target compounds were obtained for each part. Main objectives of this thesis were thus reached, and even if more work is needed to optimize and validate new chemical entities *in vivo*, our work have paved the way for future research.

Perspectives

Although the overall goal has been accomplished, there are still many areas that can be improved and further optimized.

For example, there is a need to optimize compounds containing 5-(5-methyl-1,2,4-triazol-3-yl)-1,2,4-oxadiazole group, and establish the corresponding structure-activity relationship (**Scheme 6-01**).

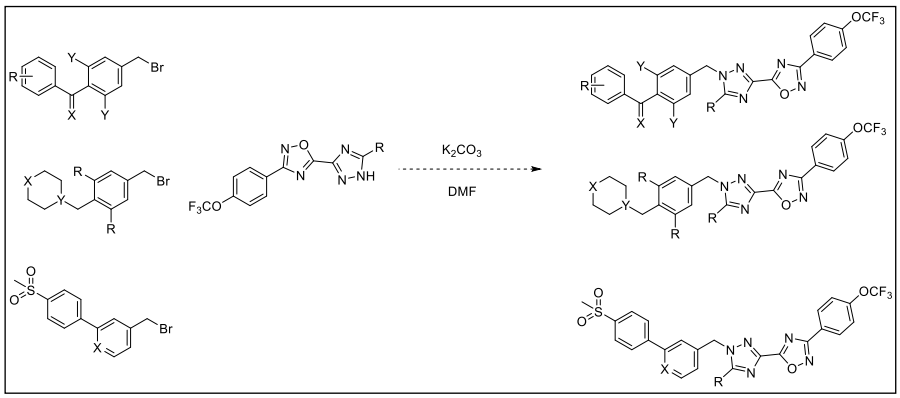

Scheme 6-01 Synthetic routes of aminoalkyl derivatives

For etomoxir, the chirality exists in the ethylene oxide of the compound. According to the literature, some studies have concluded that (*R*)-compound was superior to racemic-compound[4]. Therefore, two synthetic routes for chiral compound should be designed. The difference in the biological activities of both (*R*)-compound and racemic-compound should be analysed. (**Scheme 6-02**).

[4] Ceccarelli, S. M.; Chomienne, O.; Gubler, M.; Arduini, A., Carnitine palmitoyltransferase (CPT) modulators: a medicinal chemistry perspective on 35 years of research. *J Med Chem* **2011,** *54* (9), 3109-3152

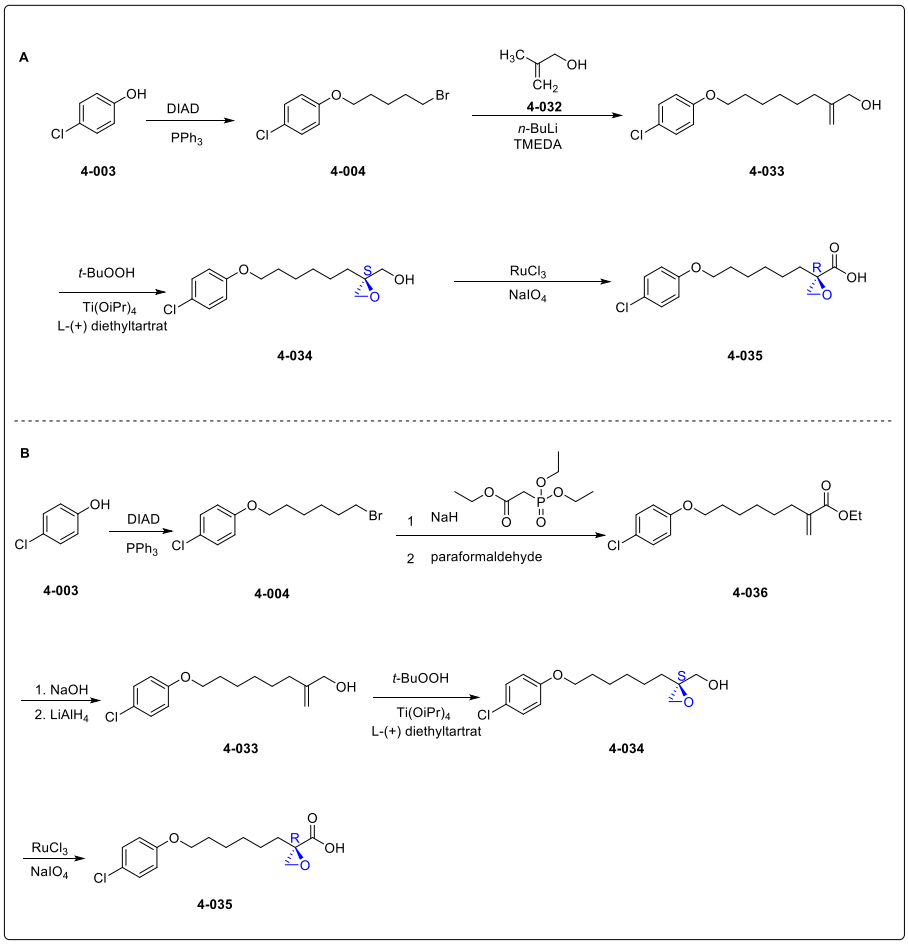

Scheme 6-02 Preparation of *S*-Etomoxir for CPT1 inhibitor

When we used a variety of synthetic schemes to study the synthesis of diclofenac prodrugs with nitro moiety, we unexpectedly discovered three cyclized compounds (**5A-051**, **5A-065, 5A-067**) (**Figure 6-06**), establishing a new synthetic strategy for studying analogous compounds in the future. *N*-substituted tetrahydroindole and *N*-substituted tetrahydroquinoline exhibit a diverse range of biological activities that would certainly warrant further investigations.

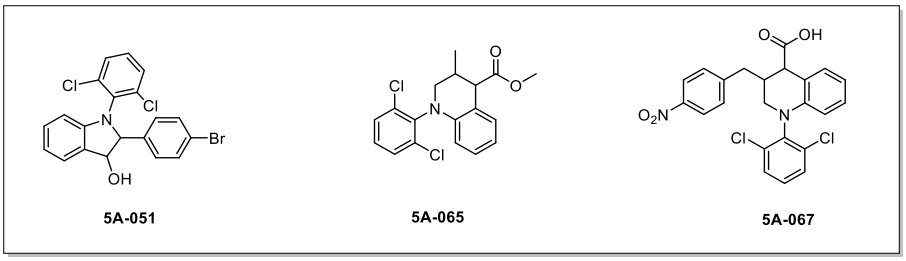

Figure 6-06 three new cyclized compounds

In the future, using enzyme-catalyzed prodrug release experiments *in vitro* and a variety of detection methods, we should be able to infer the mechanism of prodrug release associated with single electron transfer (**Figure 6-07**). We will be able to use this information to optimize the conditions of prodrug release and obtain relevant metabolic kinetic information.

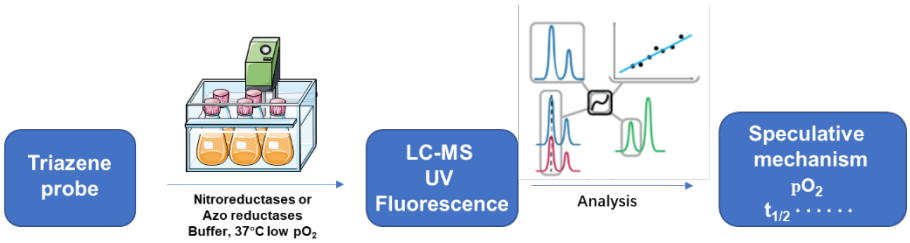

Figure 6-07 Enzyme-catalyzed prodrug release studies

More specifically, we could create a cellular hypoxia gradient by placing a coverslip on top of the cells thereby gradually decreasing the oxygen concentration from the perimeter of the coverslip to the center[5]. Fluorescence microscopy could then be used to examine the fluorescence intensity caused by the release of triazene probes (**Figure 6-08**); another option could be to exploit the spontaneous hypoxia gradient generated within 3D tumor spheroid models.

[5] Piao, W.; Tsuda, S.; Tanaka, Y.; Maeda, S., et al., Development of azo-based fluorescent probes to detect different levels of hypoxia. *Angew Chem Int Ed* 2013, 52 (49), 13028-13032.

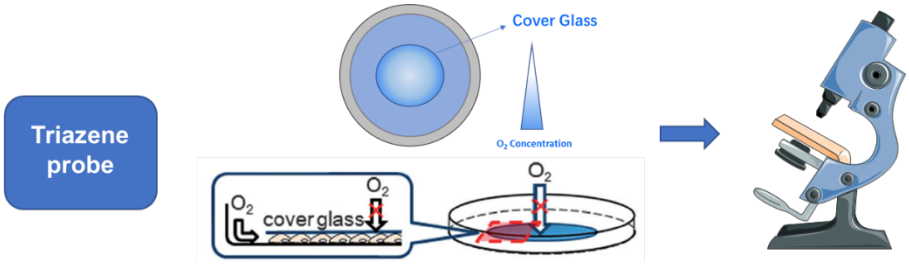

Figure 6-08 Fluorescence intensity of triazene probes at different oxygen concentrations observed by inverted fluorescence microscopy

Regarding diclofenac, functional group conversion may be used to add the nitro group, and prepare triazene derivative as in **Scheme 6-03**.

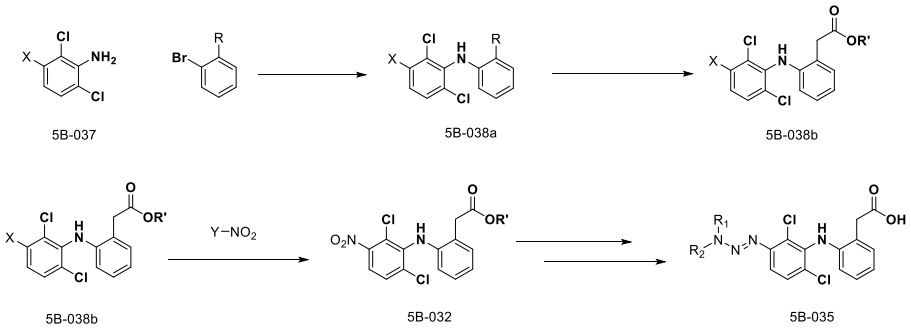

Scheme 6-03 Synthetic routes of triazene diclofenac

Experiment part

General

Unless otherwise mentioned, reagents were purchased from commercial sources (Sigma Aldrich, TCI, Acros, FluoroChem) and used without further purification. All solvents were dried from Na or CaH_2 and purified by distillation before being used. NMR spectra were recorded at room temperature on a Bruker Avance UltraShield instrument operating at a frequency of 300 MHz for ^{1}H and 75 MHz for ^{13}C. Chemical shifts (δ) are reported in ppm relative to $CDCl_3$ (δ = 7.26 ppm) and DMSO-d_6 (δ = 2.50 ppm) for ^{1}H NMR and $CDCl_3$ (δ = 77.2 ppm) and DMSO-d_6 (δ = 39.52 ppm) for ^{13}C NMR multiplicity (s = singlet, d = doublet, t = triplet, m = multiplet, q = quartet, br = broad). Column chromatography was performed over ROCC Silica gel 60 (40-63 μm). Thin layer chromatography was performed on prepared thin layers precoated plates: Silica gel Merck 60 F254. The visualization of spots on TLC plates was done by UV light (254nm or 365 nm) or $KMnO_4$ solution staining. High Resolution Mass Spectra were obtained from a Thermo Scientific Qexactive with accurate mass reported for the molecular ion or suitable fragment ions.

Chapter I:

Experimental protocols and analyses

Part A

General procedure for preparation of benzene azidomethyl

Synthesis of (4-(azidomethyl)-2,6-dichlorophenyl)(phenyl)methanone

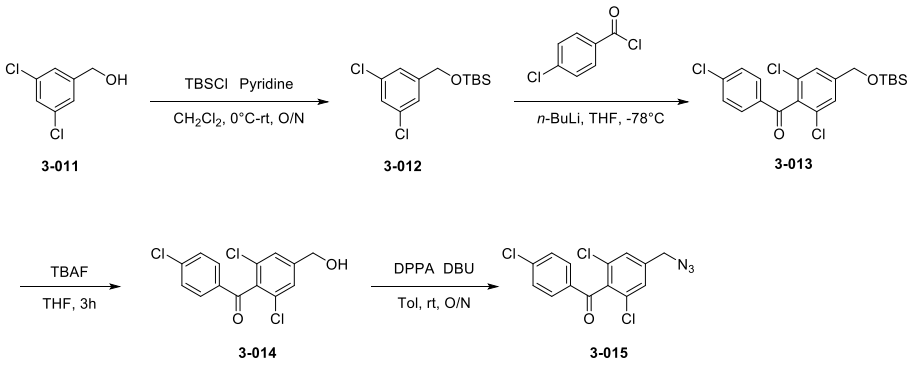

The compound (3,5-dichlorophenyl) methanol (5.0 g, 28.24 mmol) in dichloromethane (30 ml) solution of *tert*-butyidimethylsilyl chloride (5.4 ml, 31.07 mmol), pyridine (2.7 ml, 33.89 mmol) was added under argon at 0°C. After stirring overnight at room temperature and after completion of the reaction, the mixture was washed with HCl aq (1M) and brine by extraction with CH_2Cl_2, dried over anhydrous sodium sulfate, filtered and concentrated under reduced pressure to give a colorless oil. The residue was purified by silica gel column chromatography (petroleum ether/ ethyl acetate 100/1) to give the compound *tert*-butyl ((3,5-dichlorobenzyl) oxy) dimethylsilane as a colorless oil (7.5 g, 89.0%).**^{1}H-NMR** (300MHz, $CDCl_3$): ppm δ 7.23-7.19 (m, 3H), 4.68 (s, 2H), 0.91 (s, 9H), 0.11(s, 6H).

To a solution of *tert*-butyl ((3,5-dichlorobenzyl)oxy) dimethylsilane **3-012** (1.0 g, 3.43 mmol) was dissolved in anhydrous THF (7.0 mL) followed the addition of *n*-BuLi (2.5 M solution in hexane, 1.4 mL, 3.4 mmol) dropwise at -78 °C. The resulting solution was stirred at -78 °C for 60 min followed by the addition of 4-chlorobenzoyl chloride (460 µL, 3.43 mmol). The reaction was stirred at -78 °C to room temperature for 3 h then quenched with HCl aq (1M). The extractions were performed with ethyl acetate and the combined organic layers were dried over $MgSO_4$, filtered and concentrated under reduced pressure to give a pale-yellow oil. The crude product was used for next step without further purification. The crude product in THF (5 mL)

was added TBAF (1.0 M solution in THF, 8.6 mL, 8.58 mmol) at room temperature and stirred at room temperature for 3 h then quenched with aqueous saturated NH_4Cl solution. The extractions were performed with ethyl acetate and the combined organic layers were dried over $MgSO_4$ followed by concentrated under reduced pressure to give a brown powder. The residue was purified by silica gel column chromatography (CH_2Cl_2/ MeOH 50/1-30/1) to give the compound (4-chlorophenyl)(2,6-dichloro-4-(hydroxymethyl)phenyl) methanone **3-014** as an off-white solid (776 mg, 70 %).**^{1}H-NMR** (300MHz, DMSO-d_6): ppm δ 7.77 (d, J= 6.0 Hz, 2H), 7.67 (d, J= 6.0 Hz, 2H), 7.56 (s, 2H), 5.57 (t, J= 6.0 Hz, 1H), 4.60 (d, J= 6.0 Hz, 2H). **^{13}C-NMR** (75MHz, DMSO-d_6): ppm δ191.60, 148.36, 140.42, 134.84, 133.99, 131.46, 130.78, 130.23, 126.46, 61.83.

To a solution of (4-chlorophenyl) (2,6-dichloro-4-(hydroxymethyl) phenyl) methanone **3-014** (200 mg, 0.63 mmol) dissolved in THF 8.0 mL was treated dropwise 1,8-diazabicyclo [5.4.0]undec-7-ene DBU (115 µL, 0.76 mmol), after 5 min added the diphenylphosphoryl azide DPPA (206 µL, 0.95 mmol) at room temperature. Stirring the mixture for overnight at the same temperature, the mixture was added aqueous saturated ammonium chloride. The mixture was extracted with ethyl acetate, and the combined organic extract was washed with brine, dried over $MgSO_4$ followed by concentrated under reduced pressure. The residue was purified by silica gel column chromatography (petroleum ether/ ethyl acetate 30/1-10/1) to give the compound (4-(azidomethyl)-2,6-dichlorophenyl)(4-chlorophenyl)methanone **3-015** as a light yellow oil (162 mg, 75 %). **^{1}H-NMR** (300MHz, $CDCl_3$): ppm δ 7.76 (d, J= 9.0 Hz, 2H), 7.76 (d, J= 9.0 Hz, 2H), 7.56 (s, 2H), 4.60 (s, 2H).**^{13}C-NMR** (75MHz, $CDCl_3$): ppm δ 191.02, 141.09, 139.50, 136.86, 133.72, 132.36, 130.93, 129.45, 127.38, 53.26.

Synthesis of 5-(azidomethyl)-1,3-dichloro-2-(4-chlorobenzyl)benzene

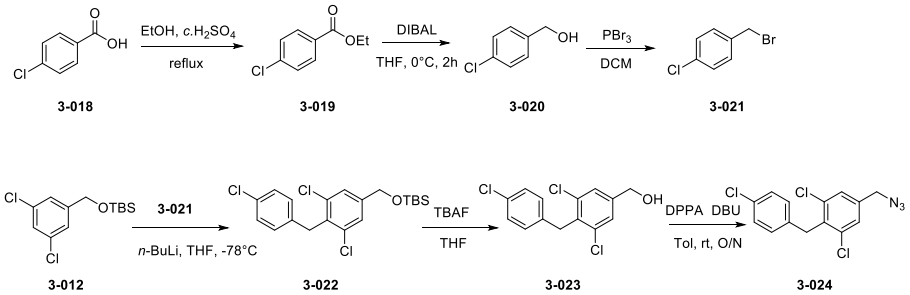

To a solution of 4-chlorobenzoic acid **3-018** (1.0 g, 3.39 mmol) dissolved in EtOH 15 mL was treated dropwise concentrated sulfuric acid (90 µL, 1.60 mmol), the mixture was heated at reflux for overnight. The mixture was cooled, concentrated under reduced pressure and diluted

with water. The aqueous layer was extracted with ethyl acetate, and the combined organic extract was washed with brine, dried over $MgSO_4$ followed by concentrated under reduced pressure to afford crude ethyl 4-chlorobenzoate as a yellow solid. The crude compound was not purified to the next step. To a solution of ethyl 4-chlorobenzoate **3-019** dissolved in THF 15 mL was cooled to 0°C. The diisobutylaluminium hydride (1M solution in THF, 12.8 ml, 12.78 mmol) was added to dropwise at 0°C, it was them stirred at 0°C 2h which is was quenched with 10% Rochelle's salt solution. The mixture was then stirred for more 1h until the organic layer separates out. The mixture was extracted with ethyl acetate, and the combined organic extract was washed with brine, dried over $MgSO_4$ followed by concentrated under reduced pressure. The residue was purified by silica gel column chromatography (petroleum ether/ ethyl acetate 5/1-3/1) to give the compound (4-chlorophenyl)methanol **3-020** as a light yellow solid (675 mg, 74 %). **^{1}H-NMR** (300MHz, $CDCl_3$): ppm δ 7.50-7.20 (m, 4H), 4.45 (s, 2H), 2.80 (s, 1H).

To a solution of (4-chlorophenyl)methanol **3-020** (500 mg, 3.51 mmol) in dry CH_2Cl_2 7 mL was slowly added phosphorus tribromide (335 µL, 3.51 mmol) at 0°C, and the mixture was stirred at room temperature for 3 h. The mixture was cooled at 0°C, and quenched with water. The mixture was extracted with ethyl acetate and washed with water, before dried over $MgSO_4$. The residue was purified by silica gel column chromatography (petroleum ether/ ethyl acetate 50/1) to give the compound 4-chlorobenzyl bromide **3-021** as a colorless solid (667 mg, 93 %). **^{1}H-NMR** (300MHz, $CDCl_3$): ppm δ 7.50-7.20 (m, 4H), 4.46 (s, 2H).

The next step according to the method of (4-(azidomethyl)-2,6-dichlorophenyl)(4-chlorophenyl)methanone to give 5-(azidomethyl)-1,3-dichloro-2-(4-chlorobenzyl)benzene **3-024** (153 mg, 71 %) as a yellow oil. **^{1}H-NMR** (300MHz, $CDCl_3$): ppm δ 7.59 (s, 2H), 7.43 (d, J= 9.0 Hz, 2H), 7.29 (d, J= 9.0 Hz, 2H), 4.56 (s, 2H), 4.51 (s, 2H).

Synthesis of 4-(4-(azidomethyl)-2,6-dichlorobenzyl) morpholine

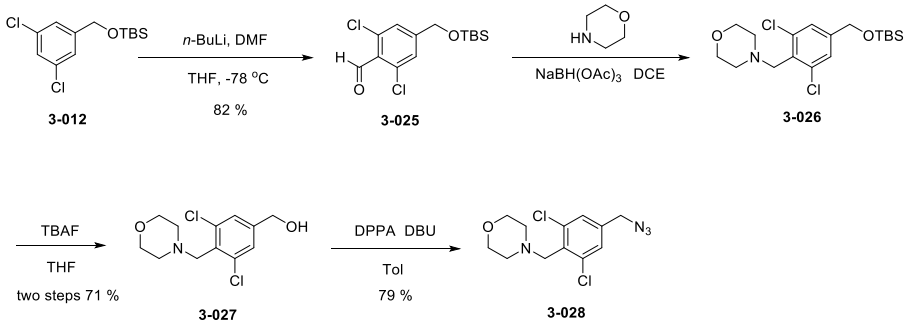

To a solution of *tert*-butyl((3,5-dichlorobenzyl)oxy)dimethylsilane **3-012** (2.0 g, 6.87 mmol) in anhydrous THF at -78 °C, under Ar atmosphere, was added dropwise *n*-BuLi (2.9 mL of 2.50 M solution in hexane, 7.21 mmol). After 40 min, anhydrous DMF (640 µL, 8.24 mmol) was added slowly dropwise to the solution. After the addition, the solution was stirred at -78 °C for 2 h then quenched with 1M HCl. The extractions were performed with ethyl acetate and the combined organic layers was washed with water, brine, dried with $MgSO_4$ and filtered. The solvent was removed under reduced pressure to give residue product, the residue was purified by silica gel column chromatography (petroleum ether/ ethyl acetate 50/1) to give the compound 4-(((*tert*-butyldimethylsilyl)oxy)methyl)-2,6-dichlorobenzaldehyde **3-025**, as a colorless solid (1.8 g, 82 %). **^{1}H-NMR** (300MHz, DMSO-d_6): ppm δ 10.34 (s, 1H), 7.48 (s, 2H), 4.79 (s, 2H), 0.91 (s, 9H), 0.10 (s, 6H).

Preparation $NaBH(OAc)_3$ triacetoxyborohydride

To a solution of sodium borohydride (590 mg, 15.66 mmol) in the anhydrous dichloroethane the temperature was kept between 15 and 20 °C, then added the dropwise glacial acetic acid (2.9 g, 50.11 mmol). After addition of acetic acid was completed, the mixture was warmed to ambient temperature and stirred for 3-4 h.

To a solution of 4-(((*tert*-butyldimethylsilyl)oxy)methyl)-2,6-dichlorobenzaldehyde **3-025** (1.0 g, 3.13 mmol) and the morpholine (1.4 ml, 15.66 mmol) in the dichloroethane 10 ml was added dropwise in the triacetoxyborohydride (above solution), and the mixture was stirred and allowed to warm room temperature 24 h under Argon. The solution was quenched by added aqueous saturated $NaHCO_3$, the extractions were performed with CH_2Cl_2 and the combined organic layers was washed with water, brine, dried with $MgSO_4$ and filtered. The solvent was removed under reduced pressure to give the crude compound. The residue was purified by silica gel column chromatography (CH_2Cl_2/ MeOH 50/1-30/1) to give the compound 4-(4-(((*tert*-butyldimethylsilyl)oxy)methyl)- 2,6-dichlorobenzyl)morpholine as a crude yellow oil. The crude compound was not purified to the next step. The crude 4-(4-(((*tert*-butyldimethylsilyl)oxy)methyl) -2,6- dichlorobenzyl) morpholine in THF (8 mL) was added TBAF (1.0 M solution in THF, 7.7 mL, 7.68 mmol) at room temperature and stirred at room temperature for 4 h then quenched with aqueous saturated NH_4Cl solution. The extractions were performed with ethyl acetate and the combined organic layers were dried over $MgSO_4$ followed by concentrated under reduced pressure to give a brown solid. The residue was purified by silica gel column chromatography (CH_2Cl_2/ MeOH 50/1-40/1) to give the compound (3,5-dichloro-4- (morpholinomethyl) phenyl) methanol **3-026** as a light yellow solid (610 mg, 71 %). **^{1}H-NMR** (300MHz, $CDCl_3$): ppm δ 7.31 (s, 2H), 5.30 (s, 1H), 4.65 (s, 2H), 3.73 (s, 2H), 3.64 (dd,

J= 9.0 Hz, 3.0 Hz, 4H), 2.57 (dd, *J*= 9.0 Hz, 3.0 Hz, 4H). **^{13}C-NMR** (75MHz, $CDCl_3$): ppm δ 140.69, 135.39, 131.25, 124.81, 65.46, 62.02, 55.00, 51.80.

The next step according to the method of synthesis **3-015** to give the compound (4-(azidomethyl) -2,6-dichlorophenyl) (4-(trifluoromethyl)phenyl)methanone **3-028** as a light yellow oil (431 mg, 79 %).**^{1}H-NMR** (300MHz, $CDCl_3$): ppm δ 7.27 (s, 2H), 4.31 (s, 2H), 3.74 (s, 2H), 3.65 (dd, *J*= 3.0, 9.0 Hz, 4H), 2.56 (dd, *J*= 3.0, 9.0 Hz, 4H). **^{13}C-NMR** (75MHz, $CDCl_3$): ppm δ 140.69, 135.39, 131.25, 124.81, 65.46, 62.02, 55.00, 51.80.

Synthesis of *N*-(4-(azidomethyl)phenyl)-4-(trifluoromethyl)benzamide

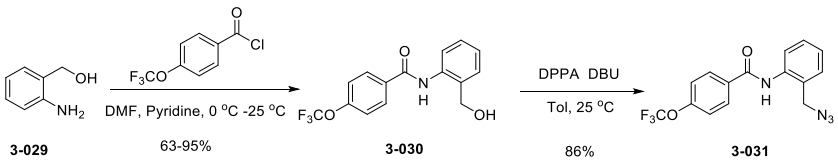

3-029 63-95% **3-030** 86% **3-031**

To a solution of (2-aminophenyl)methanol **3-029** (1.0 g, 8.12 mmol) in the DMF at 0 °C was treated dropwise with TEA (1.2 ml, 8.53 mmol) and 4-(trifluoromethoxy)benzoyl chloride (1.3 ml, 8.12 mmol). The mixture was stirred and allowed to 50°C 4h under Argon. The solution was quenched by adding saturation NH_4Cl (aq). The solution extractions were performed with CH_2Cl_2 and the combined organic layers was washed with water, brine, dried with $MgSO_4$ and filtered. The solvent was removed under reduced pressure to give the crude compound. The residue was purified by silica gel column chromatography (CH_2Cl_2/ MeOH 50/1) to give the compound *N*-(2-(hydroxymethyl)phenyl)-4-(trifluoromethoxy)benzamide **3-030** as a yellow powder (1.8 g, 70 %). **^{1}H-NMR** (300MHz, DMSO-d_6): ppm δ 10.17 (s, 1H), 8.06 (d, *J*= 9.0 Hz, 2H), 7.68 (dd, *J*= 1.5, 7.1 Hz, 1H), 7.55 (d, *J*= 9.0 Hz, 2H), 7.45 (dd, *J*= 1.5, 7.1 Hz, 1H), 7.30 (t, *J*= 6.0 Hz, 1H), 7.21 (t, *J*= 6.0 Hz, 1H), 5.54 (t, *J*= 6.0 Hz, 1H), 4.59 (d, *J*= 6.0 Hz, 2H).

The next step according to the method of synthesis **3-015** to give the compound *N*-(2-(azidomethyl)phenyl)-4-(trifluoromethoxy)benzamide **3-031**, as a yellow oil (186 mg, 86 %).**^{1}H-NMR** (300MHz, DMSO-d_6): ppm δ 10.20 (s, 1H), 8.11 (dd, *J*= 3.0, 6.0 Hz, 2H), 7.55 (dd, *J*= 3.0 Hz, 6.0 Hz, 1H), 7.47 (dd, *J*= 3.0, 6.0 Hz, 2H), 7.43-7.30 (m, 2H), 4.52 (s, 2H). **^{13}C-NMR** (75MHz, DMSO-d_6): ppm δ 164.57, 150.57, 135.97, 133.43, 131.44, 130.44, 130.12, 129.49, 50.63.

Synthesis of 4-(2-(azidomethyl)phenyl)morpholine

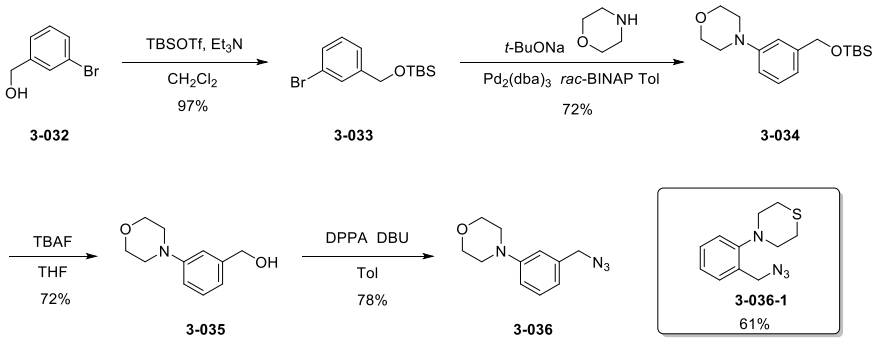

The compound (3-bromophenyl)methanol **3-032** (2.0 g, 10.69 mmol) in dichloromethane (10 ml) solution of *tert*-butyldimethylsilyl trifluoromethanesulfonate TBSOTf (2.5 ml, 10.69 mmol), triethylamine (1.8 ml, 12.83 mmol) was added under argon at 0°C. After stirring 3h at room temperature and after completion of the reaction, the mixture was washed with HCl aq (1M) and brine by extraction with CH_2Cl_2, dried over anhydrous sodium sulfate, filtered and concentrated under reduced pressure to give a colorless oil. The residue was purified by silica gel column chromatography (Petroleum ether/ ethyl acetate 50/1) to give the compound ((3-bromobenzyl)oxy)(*tert*-butyl)dimethylsilane **3-033** as a colorless oil (3.11 g, 97%). **^{1}H-NMR** (300MHz, DMSO-d_6): 7.49-7.48 (m, 1H), 7.46-7.42 (m, 1H), 7.32-7.30 (m, 2H), 4.71 (s, 2H), 0.90 (s, 9H), 0.08 (s, 6H).

The following reaction procedure is a slightly modified reported procedure[6]. A mixture of tris -(dibenzylideneacetone) dipalladium $Pd_2(dba)_3$ (19 mg, 0.02 mmol), the ligand 2-dicyclohexylphosphino -2′,6′- dimethoxybiphenyl *rac*-BINAP (37 mg, 0.06 mmol, 9 mol %) and 10 mL of anhydrous toluene was added into an oven dried flask with argon in room temperature. Then, ((3-bromobenzyl)oxy)(*tert*-butyl)dimethylsilane **3-033** (200 mg, 0.66 mmol), morpholine (325 µL, 3.32 mmol) and *t*-BuONa (83 mg, 0.86 mmol) were sequentially added to the reaction mixture. Then the reaction mixture was heated to 100 °C for 12 h. After completion of the reaction, the resulting reaction mixture was slowly brought to room temperature, and then quenched by adding water and extracted with ethyl acetate. The organic layer was dried over sodium sulphate and concentrated under reduced pressure to give the crude compound. The crude product used for next step without further purification. The crude compound in THF (8 mL) was added TBAF (1.0 M solution in THF, 2.0 mL, 1.98 mmol) at room temperature and stirred at room temperature for 4 h then quenched with aqueous saturated NH_4Cl solution. The extractions were performed with ethyl acetate and the combined organic

[6] a. M. D. Charles, P. Schultz and S. L. Buchwald, Org. Lett.,2005, 7, 3965. b. Mudithanapelli C, Kim M. Org & Biomolecular Chem, 2020.

layers were dried over $MgSO_4$ followed by concentrated under reduced pressure to give a brown solid. The residue was purified by silica gel column chromatography (CH_2Cl_2/ MeOH 50/1-30/1) to give the compound (3-morpholinophenyl) methanol **3-035** as a light yellow solid (92 mg, 72 %).

The next step according to the method of synthesis **3-015** to give the compound 4-(3-(azidomethyl)phenyl) morpholine **3-016** (176 mg, 78 %) as a yellow solid. **^{1}H-NMR** (300MHz, $CDCl_3$): ppm δ 7.30-7.22 (m, 1H), 6.94-6.91 (m, 2H), 6.81-6.78 (m, 1H), 4.36 (s, 2H), 3.74 (t, *J*=3.0 Hz, 4H), 3.12 (t, *J*=3.0 Hz, 4H). **^{13}C-NMR** (75MHz, $CDCl_3$): ppm δ 151.76, 136.69, 129.79, 119.50, 115.48, 115.20, 66.52, 54.46, 48.73.

Synthesis of *tert*-butyl 4-((2-(azidomethyl)phenyl)amino)piperidine-1-carboxylate

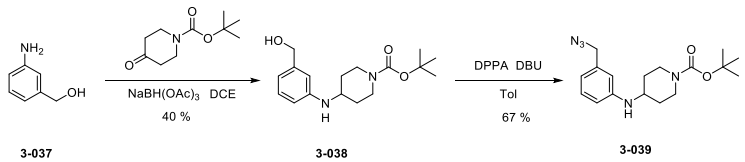

3-037 **3-038** **3-039**

To a solution of (2-aminophenyl)methanol **3-037** (1.2 g, 9.74 mmol) and the *tert*-butyl 4-oxopiperidine-1-carboxylate (2.5 g, 12.67 mmol) in the dichloroethane 10ml was added triacetoxyborohydride (6.2 g, 29.23 mmol) in the dichloroethane, and the mixture was stirred and allowed to warm room temperature 24h under Argon. The solution was quenched by added aqueous saturated $NaHCO_3$, the extractions were performed with CH_2Cl_2 and the combined organic layers was washed with water, brine, dried with $MgSO_4$ and filtered. The solvent was removed under reduced pressure to give the crude compound. The residue was purified by silica gel column chromatography (CH_2Cl_2/ MeOH 50/1) to give the compound *tert*-butyl 4-((2-(hydroxymethyl)phenyl)amino) piperidine- 1-carboxylate **3-038** as a yellow solid (1.2 g, 40 %). **^{1}H-NMR** (300MHz, DMSO-d_6): ppm δ 7.11-7.04 (m, 2H), 7.64. (d, *J*=9.0 Hz, 1H), 6.54 (t, *J*=9.0 Hz, 1H), 5.12 (t, *J*=6.0 Hz, 1H), 4.91 (d, *J*=6.0 Hz, 1H), 4.40 (d, *J*=6.0 Hz, 2H), 3.86-3.82 (m, 2H), 3.53-3.45 (m, 1H), 3.02-3.29 (m, 2H), 1.95-1.86 (m, 2H), 1.40 (s, 9H), 1.31-1.24 (m, 2H).

The next step according to the method of synthesis **3-015** to give the compound *tert*-butyl 4-((2-(azidomethyl)phenyl)amino)piperidine-1-carboxylate **3-039** (361 mg, 67 %) as a yellow oil. **^{1}H-NMR** (300MHz, $CDCl_3$): ppm δ 7.17 (t, *J*=6.0 Hz, 1H), 6.65-6.52 (m, 3H), 4.25 (s, 2H), 4.08-4.01 (m, 2H), 3.47-3.41 (m, 1H), 2.07-2.01 (m, 2H),1.47 (s, 9H), 1.37-1.30 (m, 2H).

Synthesis of *N*-allyl-2-cyanoacetamide

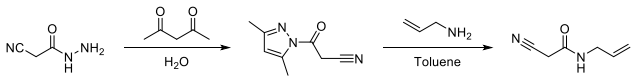

To a solution of 2-cyanoacetohydrazide (6.0 g, 60.55 mmol) in the water was added HCl (Catalytic amount) and pentane-2,4-dione (6.3 ml, 60.55 mmol). The mixture was stirred at room temperature for 2h. The precipitate was filtered, washed with water and dried to obtain a white solid as the pure product 3-(3,5-dimethyl-1*H*-pyrazol-1-yl)-3-oxopropanenitrile as a white solid (9.7 g, 98 %)**.** **^{1}H-NMR** (300MHz, $CDCl_3$): ppm δ 6.03 (s, 1H), 4.28 (s, 2H), 2.55 (s, 3H), 2.22 (s, 3H).**^{13}C-NMR** (75MHz, $CDCl_3$): ppm δ 162.45, 153.88, 144.73, 113.44, 112.46, 30.95, 26.89, 14.06, 13.77.

To a solution of 3-(3,5-dimethyl-1*H*-pyrazol-1-yl)-3-oxopropanenitrile (1.0 g, 6.13 mmol) in the toluene, was added the allylamine (460 µL, 6.13 mmol). The mixture was refluxed for 30 min and then cooled room temperature. The precipitate was filtered, washed with *n*-hexane and dried to obtain a colorless solid as the pure product *N*-allyl-2-cyanoacetamide (649 mg, 85 %) as a off-white solid**.** **^{1}H-NMR** (300MHz, DMSO-d_6): ppm δ 8.38 (s, 1H), 5.84-5.73 (m, 1H), 5.19-5.16 (m, 1H), 3.72 (t, *J*= 3.0 Hz, 2H), 3.65 (s, 2H). **^{13}C-NMR** (75MHz, DMSO-d_6): ppm δ 162.39, 134.94, 116.62, 116.03, 103.62, 41.78, 25.69.

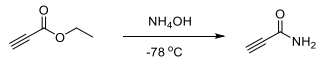

Ethyl propiolate (1ml g, 11.51 mmol) was added to the stirred aqueous ammonia (25 %, 9 ml, 57.57 mmol) at -78°C. drop wise over 5 mins. The resulting mixture was stirred under -78°C. for 1 h and was allowed to room temperature 3 h and after completion of the reaction. The reaction mixture was concentrated under *vacuo*. The residue was purified by silica gel column chromatography (Petroleum ether/ ethyl acetate 5/1 – 3/1) to give the compound propynoic acid amide as a light yellow solid (678 mg, 85 %). **^{1}H-NMR** (300MHz, DMSO-d_6): ppm δ 8.06 (s, 1H), 7.60 (s, 1H), 4.06 (s, 1H).

Synthesis of CAI derivatives 3-040 to 3-056 and 3-063 to 3-068

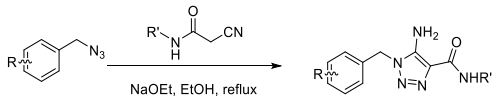

5-amino-1-(3,5-dichloro-4-(4-chlorobenzoyl)benzyl)-*1H*-1,2,3-triazole-4-carboxamide **(3-040)**

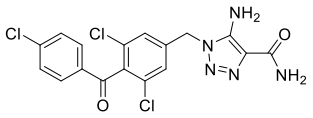

A stirred solution of sodium ethoxide (120 mg, 1.76 mmol) in EtOH (8 mL) at 0 °C was treated dropwise with 2-cyanoacetamide (148 mg, 1.76 mmol). After 10 min a solution of (4-(azidomethyl)-2,6-dichlorophenyl) (4-chlorophenyl)methanone (200 mg, 0.59 mmol) in EtOH 1 mL was added dropwise and the reaction was allowed to warm to room temperature before heating to reflux for 3 h. After cooling to room temperature, the reaction was diluted by addition of water and EtOAc, the organic phase separated, the aqueous layer was extracted with EtOAc and the organic phase washed with brine, dried over anhydrous $MgSO_4$, filtered and concentrated. The residue was purified by silica gel column chromatography (CH_2Cl_2/ MeOH 50/1 to 20/1) to give the below compound 5-amino-1-(3,5-dichloro-4-(4-chlorobenzoyl)benzyl)-*1H*-1,2,3-triazole-4- carboxamide **(3-040)**. (84 mg, 34 %) as a brownish yellow powder. **Chemical Formula:** $C_{17}H_{12}Cl_3N_5O_2$, **Molecular weight:** 424.6660, **^{1}H-NMR** (300MHz, $CDCl_3$): ppm δ 7.74 (dd, *J*=2.0 Hz, 7.2 Hz, 2H), 7.45 (dd, *J*=2.0 Hz, 7.2 Hz, 2H), 7.26 (s, 2H), 6.86 (s, 1H), 5.72 (s, 1H), 5.41 (s, 2H), 5.30 (s, 2H). **^{13}C-NMR** (75MHz, $CDCl_3$): ppm δ 190.92, 164.42, 144.46, 141.33, 137.60, 133.41, 132.84, 130.92, 129.50, 126.85, 123.05, 109.98, 50.87. **HRMS** ($APCI^+$): calculated for $C_{17}H_{13}Cl_3N_5O_2$ $[M+H]^+$:424.0130, found: 424.0127.

5-amino-1-(4-benzoyl-3,5-dichlorobenzyl)-*1H*-1,2,3-triazole-4-carboxamide **(3-041)**

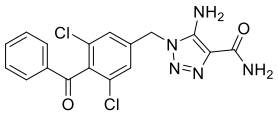

According to the method **3-040**, to give the compound 5-amino-1-(4-benzoyl-3,5-dichlorobenzyl)-*1H*-1,2,3-triazole-4-carboxamide (**3-041**) (83 mg, 25 %) as a yellow solid. **Chemical Formula:** $C_{17}H_{13}Cl_2N_5O_2$, **Molecular weight:** 390.2240, **^{1}H-NMR** (300MHz, DMSO-d_6): ppm δ 7.77-7.73 (m, 3H), 7.62-7.55 (m, 2H), 7.51 (s, 1H), 7.39 (d, *J*=8.1 Hz, 2H), 6.53 (s, 2H), 5.52 (s, 2H). **^{13}C-NMR** (75MHz, DMSO-d_6): ppm δ 192.24, 164.58, 145.39, 140.89, 136.67, 135.52, 135.01, 131.21, 130.03, 129.67, 127.93, 122.25, 47.51. **HRMS** ($APCI^+$): calculated for $C_{17}H_{14}Cl_2N_5O_2$ $[M+H]^+$:390.0519, found: 309.0519.

5-amino-1-(3,5-dichloro-4-(4-methylbenzoyl)benzyl)-*1H*-1,2,3-triazole-4-carboxamide **(3-042)**

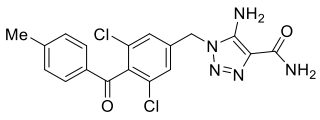

According to the method **3-040**, to give the compound 5-amino-1-(3,5-dichloro-4-(4-methylbenzoyl)benzyl)-*1H*-1,2,3- triazole-4-carboxamide (**3-042**) (105 mg, 42 %) as a yellow powder. **Chemical Formula:** $C_{18}H_{15}Cl_2N_5O_2$, **Molecular weight:** 404.2510, **^{1}H-NMR** (300MHz, DMSO-d_6): ppm δ 7.64 (d, *J*=8.6 Hz, 2H), 7.51 (s, 1H), 7.43 (s, 2H), 7.39 (d, *J*=8.1 Hz, 2H), 7.16 (s, 1H), 6.53 (s, 2H), 5.52 (s, 2H), 2.39 (s, 3H). **^{13}C-NMR** (75MHz, DMSO-d_6):

ppm δ 191.65, 164.56, 146.40, 145.36, 140.72, 136.84, 132.64, 131.19, 130.56, 129.80, 127.86, 122.22, 47.50, 21.84. **HRMS** (APCI$^+$): calculated for $C_{18}H_{16}Cl_2N_5O_2$ $[M+H]^+$:404.0676, found: 404.0675.

5-amino-1-(3,5-dichloro-4-(3-methylbenzoyl)benzyl)-*1H*-1,2,3-triazole-4-carboxamide **(3-043)**

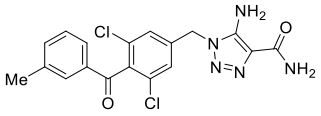

According to the method **3-040**, to give the compound 5-amino-1-(3,5-dichloro-4-(3-methylbenzoyl)benzyl)-*1H*-1,2,3- triazole-4-carboxamide (**3-043**) (94 mg, 27 %) as a yellow solid. **Chemical Formula:** $C_{18}H_{15}Cl_2N_5O_2$, **Molecular weight:** 404.2510, **^{1}H-NMR** (300MHz, DMSO-d_6): ppm δ 7.62-7.60 (m, 1H), 7.58-7.54 (m, 1H), 7.52-7.46 (m, 3H), 7.43 (s, 2H), 7.15 (s, 1H), 6.52 (s, 2H), 5.52 (s, 2H), 2.37 (s, 3H).**^{13}C-NMR** (75MHz, DMSO-d_6): ppm δ 192.29, 164.63, 145.42, 140.79, 139.58, 136.82, 136.20, 135.12, 131.23, 129.86, 129.51, 127.89, 127.27, 122.26, 47.55, 21.23. **HRMS** (APCI$^+$): calculated for $C_{18}H_{16}Cl_2N_5O_2$ $[M+H]^+$:404.0676, found: 404.0673.

5-amino-1-(3,5-dichloro-4-(4-methoxybenzoyl)benzyl)-1H-1,2,3-triazole-4-carboxamide **(3-044)**

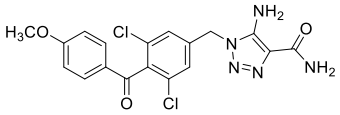

According to the method **3-040**, to give the compound 5-amino-1-(3,5-dichloro-4-(4-methoxybenzoyl)benzyl)-*1H*-1,2,3- triazole-4-carboxamide (**3-044**) (88 mg, 35 %) as a yellow solid. **Chemical Formula:** $C_{18}H_{15}Cl_2N_5O_3$, **Molecular weight:** 420.2500, **^{1}H-NMR** (300MHz, DMSO-d_6): ppm δ 7.70 (d, J=9.0 Hz, 2H), 7.50 (s, 1H), 7.43 (s, 2H), 7.10 (d, J=9.0 Hz, 2H), 6.77 (s, 2H), 6.52 (s, 1H), 5.52 (s, 2H), 3.85 (s, 3H). **^{13}C-NMR** (75MHz, DMSO-d_6): ppm δ 190.36, 164.98, 162.33, 146.83, 140.33, 137.05, 132.20, 131.25, 128.05, 127.85, 115.31, 56.25, 51.35, 47.60. **HRMS** (APCI$^+$): calculated for $C_{18}H_{16}Cl_2N_5O_3$ $[M+H]^+$: 420.0625, found: 420.0629.

5-amino-1-(3,5-dichloro-4-(4-(trifluoromethoxy)benzoyl)benzyl)-*1H*-1,2,3-triazole-4-carboxamide **(3-045)**

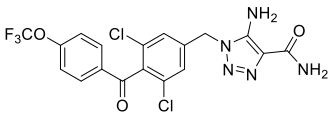

According to the method **3-040**, to give the compound 5-amino-1-(3,5-dichloro-4-(4-(trifluoromethoxy)benzoyl) benzyl)- *1H*-1,2,3-triazole-4-carboxamide (**3-045**) (101 mg, 42 %) as a yellow powder. **Chemical Formula:** $C_{18}H_{12}Cl_2F_3N_5O_3$, **Molecular weight:** 474.2212, **^{1}H-NMR** (300MHz, DMSO-d_6): ppm δ 7.91 (dd, J=2.0 Hz, 6.8 Hz, 2H), 7.52 (s, 1H), 7.57 (dd, J=1.2 Hz, 9.0 Hz, 2H), 7.48 (s, 2H), 7.17 (s, 1H), 6.54 (s, 2H), 5.53 (s, 2H). **^{13}C-**

NMR (75MHz, DMSO-d_6): ppm δ 190.53, 164.12, 152.74, 144.92, 140.73, 135.65, 133.19, 131.86, 130.73, 127.60, 121.78, 121.44, 47.05. **HRMS** ($APCI^+$): calculated for $C_{18}H_{13}Cl_2F_3N_5O_3$ $[M+H]^+$: 474.0342, found:474.0344.

5-amino-1-(3,5-dichloro-4-(4-(trifluoromethyl)benzoyl)benzyl)-*1H*-1,2,3-triazole-4-carboxamide **(3-046)**

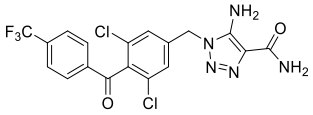

According to the method **3-040**, to give the compound 5-amino-1-(3,5-dichloro-4-(4-(trifluoromethyl)benzoyl) benzyl) -*1H*-1,2,3-triazole-4- carboxamide (**3-046**) (87 mg, 36 %) as a yellow solid. **Chemical Formula:** $C_{18}H_{12}Cl_2F_3N_5O_2$, **Molecular weight:** 458.2222, **^{1}H-NMR** (300MHz, DMSO-d_6): ppm δ 7.98 (s, 4H), 7.51 (s, 1H), 7.49 (s, 2H), 7.15 (s, 1H), 6.53 (s, 2H), 5.54 (s, 2H). **^{13}C-NMR** (75MHz, DMSO-d_6): ppm δ 164.55, 145.37, 137.89, 135.85, 134.69, 131.20, 130.55, 130.49, 128.09, 126.70, 122.22, 121.91, 121.56, 58.06, 47.50. **HRMS** ($APCI^+$): calculated for $C_{18}H_{13}Cl_2F_3N_5O_2$ $[M+H]^+$: 458.0393, found: 458.0394.

1-(4-(2-naphthoyl)-3,5-dichlorobenzyl)-5-amino-*1H*-1,2,3-triazole-4-carboxamide **(3-047)**

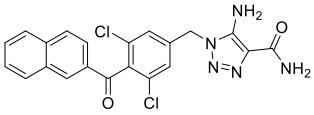

According to the method **3-040**, to give the compound 1-(4-(2-naphthoyl)-3,5-dichlorobenzyl)-5-amino-*1H*-1,2,3-triazole -4-carboxamide **(3-047)** (91 mg, 24 %) as a yellow solid. **Chemical Formula:** $C_{21}H_{15}Cl_2N_5O_2$, **Molecular weight:** 440.2840, **^{1}H-NMR** (300MHz, $CDCl_3$): ppm δ 8.31 (d, *J*=3.0 Hz, 1H) 8.16-8.10 (t, *J*= 9.0 Hz, 2H), 8.04 (d, *J*=6.0 Hz, 1H), 7.93 (dd, *J*=3.0, 9.0 Hz, 1H), 7.75-7.70 (m, 1H), 7.65-7.60 (m, 1H), 7.51 (s, 1H), 7.49 (s, 2H), 7.16 (s, 1H), 6.55 (s, 2H), 5.56 (s, 2H). **^{13}C-NMR** (75MHz, $CDCl_3$): ppm δ 192.62, 164.79, 144.88, 137.95, 137.71, 136.35, 132.84, 132.73, 132.50, 132.44, 129.90, 129.43, 129.21, 127.92, 127.10, 126.93, 123.84, 122.74, 48.43. **HRMS** ($APCI^+$): calculated for $C_{21}H_{16}Cl_2N_5O_2$ $[M+H]^+$: 440.0676, found:440.0676.

5-amino-1-(3,5-dichloro-4-(morpholinomethyl)benzyl)-*1H*-1,2,3-triazole-4-carboxamide **(3-048)**

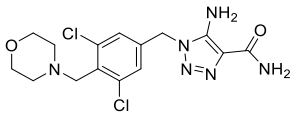

According to the method **3-040**, to give the compound 5-amino-1-(3,5-dichloro-4-(morpholinomethyl)benzyl)-*1H*-1,2,3- triazole-4-carboxamide (**3-048**) (84 mg, 33 %) as a yellow solid. **Chemical Formula:** $C_{15}H_{18}Cl_2N_6O_2$, **Molecular weight:** 385.2490, **^{1}H-NMR** (300MHz, DMSO-d_6): ppm δ 7.50 (s, 1H), 7.28 (s, 2H), 7.13 (s, 1H), 6.48 (s ,2H), 5.42 (s, 2H), 3.63 (s, 2H), 3.49 (t, *J*=4.5 Hz, 4H), 2.43 (t, *J*=4.5 Hz, 4H). **^{13}C-NMR** (75MHz, DMSO-d_6): ppm δ 164.55, 145.25, 138.54, 136.60, 133.28, 127.86, 122.15, 66.66, 56.58, 53.58, 47.34.

HRMS (APCI$^+$): calculated for $C_{15}H_{19}Cl_2N_6O_2$ $[M+H]^+$: 385.0941, found: 385.0943.

5-amino-1-(3,5-dichloro-4-(cyclohexanecarbonyl)benzyl)-*1H*-1,2,3-triazole-4-carboxamide **(3-049)**

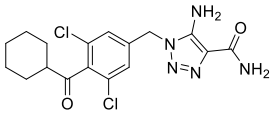

According to the method **3-040**, to give the compound 5-amino-1-(3,5-dichloro-4-(cyclohexanecarbonyl)benzyl)-*1H*-1,2,3-triazole-4-carboxamide (**3-049**) (76 mg, 23 %) as a yellow solid. **Chemical Formula:** $C_{17}H_{19}Cl_2N_5O_2$, **Molecular weight:** 396.2720, **^{1}H-NMR** (300MHz, DMSO-d_6): ppm δ 7.48 (s, 1H), 7.35 (s, 2H), 7.13 (s, 1H), 6.48 (s, 2H), 5.45 (s, 2H), 1.88-1.57 (m, 5H), 1.41-1.11 (m, 6H). **^{13}C-NMR** (75MHz, DMSO-d_6): ppm δ 204.37, 164.13, 144.84, 140.02, 134.26, 129.97, 127.46, 126.27, 121.76, 50.52, 47.18, 27.59, 25.00. **HRMS** (APCI$^+$): calculated for $C_{17}H_{19}Cl_2N_5O_2$ $[M+H]^+$: 396.0989, found: 396.0989.

N-allyl-5-amino-1-(3,5-dichloro-4-(4-(trifluoromethyl)benzoyl)benzyl)-*1H*-1,2,3-triazole-4-carboxamide **(3-050)**

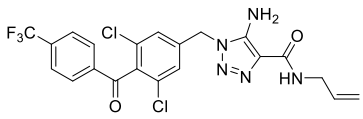

A solution of *N*-allyl-2-cyanoacetamide (154 mg, 0.80 mmol) in methanol (6.0 mL) at room temperature was treated with sodium ethoxide (56 mg, 0.83 mmol) followed by (4-(azidomethyl)-2,6-dichlorophenyl) (4-(trifluoromethyl)phenyl)methanone (200 mg, 0.53 mmol). The reaction was then stirred for 2h at 50 °C. After cooling to room temperature the reaction was diluted by addition of water and EtOAc, the organic phase separated, the aqueous layer was extracted with EtOAc and the organic phase washed with brine, dried over anhydrous $MgSO_4$, filtered and concentrated. The residue was purified by silica gel column chromatography (CH_2Cl_2/ EtOAc 10/1) to give the compound to give the title compound *N*-allyl-5-amino-1-(3,5-dichloro-4-(4- (trifluoromethyl)benzoyl)benzyl)-1*H*-1,2,3-triazole-4- carboxamide (**3-050**) (108 mg, 36 %) as a yellow solid. **Chemical Formula:** $C_{21}H_{16}Cl_2F_3N_5O_2$, **Molecular weight:** 498.2872, **^{1}H-NMR** (300MHz, DMSO-d_6): ppm δ 8.30 (t, *J*=6.2 Hz, 1H), 7.98 (s, 4H), 7.50 (s, 2H), 6.54 (s, 2H), 5.91-5.80 (m, 1H), 5.55 (s, 2H), 5.16-5.02 (m ,2H), 3.85 (t, *J*=6.2 Hz, 2H). **^{13}C-NMR** (75MHz, DMSO-d_6): ppm δ 191.68, 162.27, 145.18, 141.34, 137.88, 136.21, 135.86, 134.71, 134.29, 131.21, 130.48, 128.10, 127.13, 122.19, 115.36, 47.54, 46.13. **HRMS** (APCI$^+$): calculated for $C_{21}H_{17}Cl_2F_3N_5O_2$ $[M+H]^+$:498.0706, found: 498.0705.

5-amino-1-(3,5-dichloro-4-(4-(trifluoromethyl)benzyl)benzyl)-*1H*-1,2,3-triazole-4-carboxamide **(3-051)**

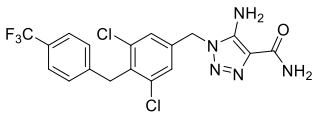

According to the method **3-040**, to give the compound 5-amino-1-(3,5-dichloro-4-(4-(trifluoromethyl)benzyl)benzyl) -*1H*-1,2,3-triazole-4-carboxamide (**3-051**) (91 mg, 24 %) as a yellow solid. **Chemical Formula:** $C_{18}H_{14}Cl_2F_3N_5O$, **Molecular weight:** 444.2392, **^{1}H-NMR** (300MHz, DMSO-d_6): ppm δ 7.65 (d, J=8.3 Hz, 2H), 7.50 (s, 1H), 7.38 (s, 2H), 7.31 (d, J=8.3 Hz, 2H), 7.15 (s, 2H), 6.48 (s, 2H), 5.43 (2H), 4.23 (s, 2H). **^{13}C-NMR** (75MHz, DMSO-d_6): ppm δ 164.59, 145.29, 142.86, 138.33, 135.71, 134.96, 134.71, 129.10, 128.09, 126.72, 125.92, 122.19, 47.35, 36.11. **HRMS** (APCI$^+$): calculated for $C_{18}H_{15}Cl_2F_3N_5O$ $[M+H]^+$: 444.0601, found:444.0599.

5-amino-1-(3,5-dichloro-4-(4-chlorobenzyl)benzyl)-*1H*-1,2,3-triazole-4-carboxamide **(3-052)**

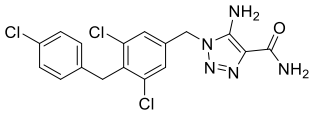

According to the method **3-040**, 5-amino-1-(3,5-dichloro-4-(4-chlorobenzyl)benzyl)-*1H*-1,2,3-triazole-4-carboxamide (**3-052**) (88 mg, 25 %) as a yellow solid. **Chemical Formula:** $C_{17}H_{14}Cl_3N_5O$, **Molecular weight:** 410.6830, **^{1}H-NMR** (300MHz, DMSO-d_6): ppm δ 7.50 (s, 1H), 7.36-7.31 (m, 4H), 7.14-7.10 (m, 3H), 6.48 (s, 2H). 5.43 (s, 2H), 4.23 (s, 2H). **^{13}C-NMR** (75MHz, DMSO-d_6): ppm δ 164.59, 145.28, 138.15, 136.95, 135.63, 135.40, 131.47, 130.17, 128.93, 128.05, 122.18, 47.35, 35.60. **HRMS** (APCI$^+$): calculated for $C_{17}H_{15}Cl_3N_5O$ $[M+H]^+$: 410.0337, found: 410.0338.

5-amino-1-(4-(4-chlorobenzoyl)-3,5-difluorobenzyl)-*1H*-1,2,3-triazole-4-carboxamide **(3-053)**

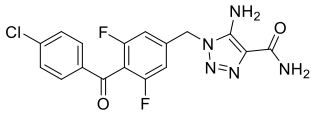

According to the method **3-040**, to give the compound 5-amino-1-(4-(4-chlorobenzoyl)-3,5-difluorobenzyl)-*1H*-1,2,3- triazole-4-carboxamide (**3-053**) (76 mg, 23 %) as a yellow solid. **Chemical Formula:** $C_{17}H_{14}ClF_2N_5O$, **Molecular weight:** 377.7798, **^{1}H-NMR** (300MHz, DMSO-d_6): ppm δ 7.82 (d, J= 8.6 Hz, 2H), 7.65 (d, J= 8.7 Hz, 2H), 7.50 (s,1H), 7.37 (s, 2H), 7.15-7.10 (m ,3H), 6.51 (s, 2H), 5.55 (s, 2H). **^{13}C-NMR** (75MHz, DMSO-d_6): ppm δ 187.53, 164.57, 145.44, 140.43, 135.12, 131.58, 130.00, 129.82, 122.22, 112.02, 111.70, 56.83, 47.87. **HRMS** (APCI$^+$): calculated for $C_{17}H_{13}ClF_2N_5O_2$ $[M+H]^+$: 392.0721, found: 392.0714.

1-(4-acetyl-3,5-dichlorobenzyl)-5-amino-*1H*-1,2,3-triazole-4-carboxamide **(3-054)**

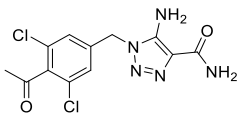

According to the method **3-040**, to give the compound 1-(4-acetyl-3,5-dichlorobenzyl)-5-amino-*1H*-1,2,3-triazole -4-carboxamide (**3-054**) (81 mg, 29 %) as a yellow solid. **Chemical Formula:** $C_{12}H_{11}Cl_2N_5O_2$, **Molecular weight:** 328.1530, **^{1}H-NMR** (300MHz, DMSO-d_6): ppm δ 7.49 (s, 1H), 7.37 (s, 2H), 7.14 (s, 1H), 6.49 (s, 2H). 5.46 (s, 2H), 2.53 (s, 3H). **^{13}C-NMR** (75MHz,

DMSO-d_6): ppm δ 200.03, 164.53, 145.30, 140.40, 139.07, 129.60, 127.85, 122.20, 47.43, 31.45. **HRMS** (APCI$^+$): calculated for $C_{12}H_{12}Cl_2N_5O_2$ $[M+H]^+$: 328.0363, found: 328.0362.

5-amino-1-(3,5-dimethylbenzyl)-*1H*-1,2,3-triazole-4-carboxamide **(3-055)**

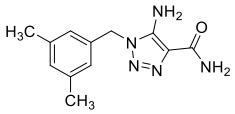

According to the method **3-040**, to give the compound **5**-amino-1-(3,5-dimethylbenzyl)-*1H*-1,2,3-triazole-4-carboxamide (**3-055**) (57 mg, 27 %) as a yellow solid. **Chemical Formula:** $C_{12}H_{15}N_5O$, **Molecular weight:** 245.2860, **^{1}H-NMR** (300MHz, DMSO-d_6): ppm δ 7.44 (s, 1H), 7.09 (s, 1H), 6.93 (s, 1H), 6.82 (s, 2H), 6.35 (s, 2H), 5.32 (s, 2H). 2.23 (s, 6H). **^{13}C-NMR** (75MHz, DMSO-d_6): ppm δ 164.72, 145.15, 138.08, 136.25, 129.52, 125.53, 124.68, 122.10, 48.67, 21.35. **HRMS** (APCI$^+$): calculated for $C_{12}H_{16}N_5O$ $[M+H]^+$: 246.1350, found: 246.1355.

5-amino-1-(3,5-dichlorobenzyl)-*1H*-1,2,3-triazole-4-carboxamide **(3-056)**

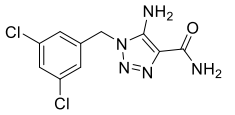

According to the method **3-040**, to give the compound 5-amino-1-(3,5-dichlorobenzyl)-*1H*-1,2,3-triazole-4-carboxamide (**3-056**) (71 mg, 25 %) as a yellow solid. **Chemical Formula:** $C_{10}H_9Cl_2N_5O$, **Molecular weight:** 286.1160, **^{1}H-NMR** (300MHz, DMSO-d_6): ppm δ 7.59 (t, J= 2.4 Hz,1H), 7.48 (s, 1H), 7.25 (d, J= 2.4 Hz, 2H), 7.13 (s, 1H). 6.47 (s, 2H), 5.44 (s, 2H). **^{13}C-NMR** (75MHz, DMSO-d_6): ppm δ 164.56, 145.28, 140.47, 134.70, 127.96, 126.71, 122.17, 47.62. **HRMS** (APCI$^+$): calculated for $C_{10}H_{10}Cl_2N_5O$ $[M+H]^+$: 286.0257, found: 286.0255.

5-amino-1-(4-(4-chlorobenzamido)benzyl)-*1H*-1,2,3-triazole-4-carboxamide **(3-063)**

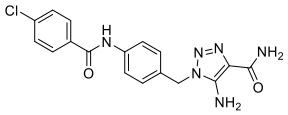

According to the method **3-040**, to give the compound 5-amino-1-(4-(4-chlorobenzamido)benzyl)-*1H*-1,2,3-triazole-4-carboxamide (**3-063**) (76 mg, 27 %) as a yellow solid. **Chemical Formula:** $C_{17}H_{15}ClN_6O_2$, **Molecular weight:** 555.9022, **^{1}H-NMR** (300MHz, DMSO-d_6): ppm δ 10.36 (s, 1H), 7.97 (d, J=8.4 Hz, 2H), 7.74 (d, J=8.4 Hz, 2H), 7.61 (d, J=8.6 Hz, 2H), 7.47 (s, 1H), 7.22 (d, J=8.6 Hz, 2H), 7.10 (s, 1H), 6.39 (s, 2H), 5.38 (s, 2H). **^{13}C-NMR** (75MHz, DMSO-d_6): ppm δ 164.29, 144.70, 138.50, 136.46, 131.21, 130.01, 129.64, 129.01, 128.47, 127.88, 121.73, 120.53, 48.00. **HRMS** (APCI$^+$): calculated for $C_{17}H_{16}ClN_6O_2$ $[M+H]^+$:371.1018, found: 371.1018.

5-amino-1-(3-(4-(trifluoromethoxy)benzamido)benzyl)-*1H*-1,2,3-triazole-4-carboxamide **(3-064)**

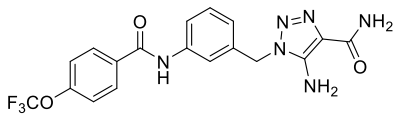

According to the method **3-040**, to give the compound 5-amino-1-(3-(4-(trifluoromethoxy) benzamido)benzyl)-*1H*-1,2,3-triazole-4-carboxamide (**3-064**) (81 mg, 32 %) as a yellow solid. **Chemical Formula:** $C_{18}H_{15}F_3N_6O_3$, **Molecular weight:** 420.3522, **^{1}H-NMR** (300MHz, DMSO-d_6): ppm δ 10.43 (s, 1H), 8.11-8.08 (m 2H), 7.54 (s, 1H), 7.52-7.49 (m, 2H), 7.42-7.32 (m, 2H), 7.16 (s, 1H), 6.40 (s, 2H), 5.43 (s, 2H), 4.47 (s, 2H). **^{13}C-NMR** (75MHz, DMSO-d_6): ppm δ 165.01, 151.07, 145.44, 139.94, 137.11, 136.78, 134.57, 130.69, 129.65, 124.39, 123.45, 122.28, 121.27, 120.63, 119.65, 54.27. **HRMS** (APCI$^+$): calculated for $C_{18}H_{16}F_3N_6O_3$ $[M+H]^+$:421.1231, found: 421.1231.

Tert-butyl 4-((3-((5-amino-4-carbamoyl-*1H*-1,2,3-triazol-1-yl)methyl)phenyl)amino) piperidine -1-carboxylate **(3-065)**

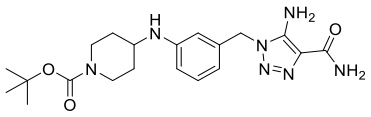

According to the method **3-040**, to give the compound *tert*-butyl 4-((3-((5-amino-4-carbamoyl-*1H*-1,2,3-triazol-1-yl)methyl) phenyl)amino) piperidine-1-carboxylate (**3-065**) 61mg, 24 %) as a yellow solid. **Chemical Formula:** $C_{20}H_{29}N_7O_3$, **Molecular weight:** 415.4980, **^{1}H-NMR** (300MHz, DMSO-d_6): ppm δ 7.44 (s, 1H), 7.11-6.97 (m, 2H), 6.51 (d, J= 6.0 Hz, 1H), 6.41-6.30 (m, 4H), 5.60 (d, J= 8.4 Hz, 2H)， 5.28 (s, 2H), 4.41 (q, J= 6.8, 14.0 Hz, 1H), 3.86 (d, J= 13.2 Hz, 2H), 3.40-3.29 (m, 2H), 2.95-2.85 (m, 2H), 1.90-1.79 (m, 2H), 1.40 (s, 9H). **^{13}C-NMR** (75MHz, DMSO-d_6): ppm δ 164.33, 153.92, 147.85, 144.79, 136.60, 129.16, 121.64, 114.36, 111.38, 111.29, 54.88, 48.59, 31.42, 28.08. **HRMS** (APCI$^+$): calculated for $C_{20}H_{30}N_7O_3$ $[M+H]^+$:416.2405, found:416.2404.

5-amino-1-(3-morpholinobenzyl)-*1H*-1,2,3-triazole-4-carboxamide **(3-066)**

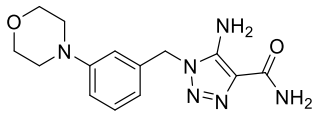

According to the method **3-040**, to give the compound 5-amino-1-(3-morpholinobenzyl)-*1H*-1,2,3-triazole-4-carboxamide (**3-066**) (83 mg, 30 %) as a yellow solid. **Chemical Formula:** $C_{14}H_{18}N_6O_2$, **Molecular weight:** 302.3380, **^{1}H-NMR** (300MHz, DMSO-d_6): ppm δ 7.44 (s, 1H), 7.19 (t, J=7.4 Hz, 1H), 7.08 (s,1H), 6.89 (s, 2H), 6.60 (d, J=8.4 Hz, 1H), 6.36 (s, 2H), 5.33 (s, 2H), 3.73(t, J=5.0 Hz, 4H), 3.07(t, J=5.0 Hz, 4H). **^{13}C-NMR** (75MHz, DMSO-d_6): ppm δ 164.71, 151.64, 145.14, 137.06, 129.70, 122.05, 118.51, 114.84, 114.68, 66.49, 49.08, 48.76. **HRMS** (APCI$^+$): calculated for $C_{14}H_{19}N_6O_2$ $[M+H]^+$:303.1564, found: 303.1564.

5-amino-1-(2-(4-(trifluoromethoxy)benzamido)benzyl)-*1H*-1,2,3-triazole-4-carboxamide **(3-067)**

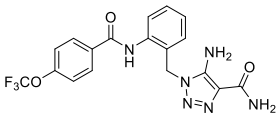

According to the method **3-040**, to give the compound 5-amino-1-(2-(4-(trifluoromethoxy)benzamido)benzyl)-*1H*-1,2,3-triazole-4-carboxamide (**3-067**) (77 mg, 24 %) as a yellow solid. **Chemical Formula:** $C_{18}H_{15}F_3N_6O_3$, **Molecular weight:** 420.3522, **^{1}H-NMR** (300MHz, DMSO-d_6): ppm δ 10.30 (s, 1H), 8.16 (dd, *J*=1.9, 6.8 Hz, 2H), 7.56 (d, *J*=8.0 Hz, 2H), 7.50 (d, *J*=6.7 Hz, 2H), 7.37 (t, *J*=7.9 Hz, 1H), 7.24 (t, *J*=7.6 Hz,1H), 7.12 (s, 1H), 6.92 (d, *J*=7.7 Hz, 1H), 6.34(s, 2H), 5.46 (s, 2H). **^{13}C-NMR** (75MHz, DMSO-d_6): ppm δ 164.93, 164.65, 145.43, 135.85, 133.94, 131.32, 130.65, 128.61, 128.03, 126.96, 126.73, 122.31, 121.24, 45.88. **HRMS** (APCI$^+$): calculated for $C_{18}H_{16}F_3N_6O_3$ $[M+H]^+$:421.1231, found:421.1129.

5-amino-1-(2-thiomorpholinobenzyl)-*1H*-1,2,3-triazole-4-carboxamide **(3-068)**

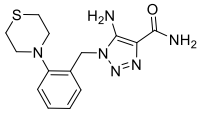

According to the method **3-040**, to give the compound 5-amino-1-(2-thiomorpholinobenzyl)-*1H*-1,2,3-triazole-4- carboxamide (**3-068**) (64 mg, 23 %) as a yellow solid. **Chemical Formula:** $C_{14}H_{18}N_6OS$, **Molecular weight:** 318.3990, **^{1}H-NMR** (300MHz, DMSO-d_6): ppm δ 7.47 (s, 1H),7.29-7.19 (m, 2H), 7.12-7.03 (m, 2H), 6.65 (d, *J*=7.4 Hz, 1H), 6.37 (s, 2H), 5.39 (s, 2H), 3.12-3.07 (m, 4H), 2.82-2.77 (m, 4H). **^{13}C-NMR** (75MHz, DMSO-d_6): ppm δ 164.71, 152.13, 145.70, 131.47, 129.01, 127.86, 124.80, 122.02, 121.66, 55.11, 49.06, 28.05. **HRMS** (APCI$^+$): calculated for $C_{14}H_{19}N_6OS$ $[M+H]^+$:319.1336, found: 319.1334.

Synthesis of CAI derivatives 3-057-3-062

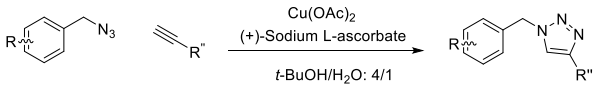

3-057-3-062

1-(3,5-dichloro-4-(4-chlorobenzoyl)benzyl)-*1H*-1,2,3-triazole-4-carboxylic acid **(3-057)**

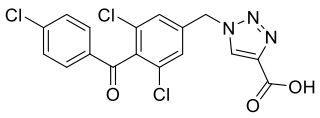

To a solution of propiolic acid (38 µL, 0.62 mmol) and (4-(azidomethyl)-2,6-dichlorophenyl) (4-chlorophenyl) methanone (200 mg, 0.59 mmol) in a *tert*-Butanol/water (5 mL, 4/1) mixture, $Cu(OAc)_2$ (11 mg, 0.06 mmol) and sodium L-ascorbate (23 mg, 0.12 mmol) were added. After stirring for overnight at room temperature, the reaction mixture was diluted with water and extracted with EtOAc, the organic phase separated, the aqueous layer was extracted with EtOAc and the organic phase washed with brine, dried over anhydrous $MgSO_4$, filtered and concentrated in *vacuo*. After the residue was purified by silica gel column chromatography (CH_2Cl_2/ MeOH 50/1, 0.5 % HOAc) to give the compound to give the compound 1-(3,5-dichloro-4-(4-chlorobenzoyl)benzyl)-*1H*-1,2,3-triazole-4-carboxylic acid (**3-**

057) (173 mg, 72 %) as a light yellow solid. **Chemical Formula:** $C_{17}H_{10}Cl_3N_3O_3$, **Molecular weight:** 410.6350, **^{1}H-NMR** (300MHz, DMSO-d_6): ppm δ 13.16 (br s, 1H), 8.88 (s, 1H), 7.78 (dd, J= 3.0, 6.0 Hz, 2H), 7.68-7.65 (m, 4H), 5.76 (s, 2H).**^{13}C-NMR** (75MHz, DMSO-d_6): ppm δ 191.23, 162.03, 140.62, 140.39, 133.69, 131.54, 131.30, 130.27, 129.99, 128.93, 51.99. **HRMS** (APCI$^+$): calculated for $C_{17}H_{11}Cl_3N_3O_3$ $[M+H]^+$: 409.9861, found: 409.9858.

1-(3,5-dichloro-4-(4-chlorobenzoyl)benzyl)-*1H*-1,2,3-triazole-4-carboxamide **(3-058)**

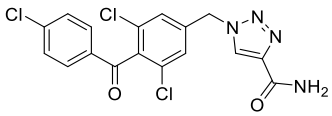

According to the method of (**3-057**), to give the compound 1-(3,5-dichloro-4-(4-chlorobenzoyl)benzyl)-*1H*-1,2,3-triazole-4-carboxamide (**3-058**) (174 mg, 72 %) as a yellow solid. **Chemical Formula:** $C_{17}H_{11}Cl_3N_4O_2$, **Molecular weight:** 409.6510, **^{1}H-NMR** (300MHz, DMSO-d_6): ppm δ 8.73 (s, 1H), 7.89 (s, 1H), 7.79 (dd, J= 3.0, 6.0 Hz, 2H), 7.67-7.64 (m, 4H), 7.51 (s, 1H), 5.76 (s, 2H). **^{13}C-NMR** (75MHz, DMSO-d_6): ppm δ 191.22, 161.84, 143.78, 140.62, 140.53, 136.63, 133.69, 131.54, 131.31, 130.27, 128.88, 127.67, 51.99. **HRMS** (APCI$^+$): calculated for $C_{17}H_{12}Cl_3N_4O_2$ $[M+H]^+$: 409.0021, found: 409.0018.

(4-((4-(aminomethyl)-*1H*-1,2,3-triazol-1-yl)methyl)-2,6-dichlorophenyl)(4-chlorophenyl) methanone **(3-059)**

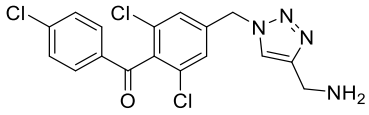

According to the method of (**3-057**), to give the compound (4-((4-(aminomethyl)-*1H*-1,2,3-triazol-1-yl)methyl)-2,6-dichlorophenyl) (4-chlorophenyl) methanone (**3-059**) (165 mg, 71 %) as a yellow solid. **Chemical Formula:** $C_{17}H_{13}Cl_3N_4O$, **Molecular weight:** 395.6680, **^{1}H-NMR** (300MHz, DMSO-d_6): ppm δ 8.22 (s, 1H), 7.77 (dd, J= 3.0, 6.0 Hz, 2H), 7.67 (dd, J= 3.0, 6.0 Hz, 2H), 7.61 (s, 2H), 5.74 (s, 2H), 3.97 (s, 2H), 1.01 (t, J= 6.8 Hz, 2H). **^{13}C-NMR** (75MHz, DMSO-d_6): ppm δ 191.23, 141.17, 140.64, 136.44, 133.66, 131.50, 131.26, 130.29, 129.43, 128.62, 124.45, 51.63, 35.82. **HRMS** (APCI$^+$): calculated for $C_{17}H_{14}Cl_3N_4O$ $[M+H]^+$: 395.0228, found: 395.0228.

methyl 1-(3,5-dichloro-4-(4-chlorobenzoyl)benzyl)-*1H*-1,2,3-triazole-4-carboxylate **(3-060)**

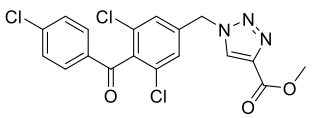

According to the method of (**3-057**), to give the compound methyl 1-(3,5-dichloro-4-(4-chlorobenzoyl)benzyl)-*1H*-1,2,3-triazole-4-carboxylate (**3-060**) (177 mg, 71 %) as a yellow solid. **Chemical Formula:** $C_{18}H_{12}Cl_3N_3O_3$, **Molecular weight:** 424.6620, **^{1}H-NMR** (300MHz, DMSO-d_6): ppm δ 8.99 (s, 1H), 7.78 (dd, J= 3.0, 6.0 Hz, 2H), 7.68-7.64 (m, 4H), 5.78 (s, 2H), 3.85 (s, 3H). **^{13}C-NMR** (75MHz, $CDCl_3$): ppm δ 191.22, 161.07, 140.63, 140.25,

139.43, 136.68, 133.68, 131.53, 131.31, 130.26, 128.94, 52.31, 52.08. **HRMS** (APCI$^+$): calculated for $C_{18}H_{13}Cl_3N_3O_3$ $[M+H]^+$: 424.0017, found: 424.0014.

(4-chlorophenyl)(2,6-dichloro-4-((4-(hydroxymethyl)-*1H*-1,2,3-triazol-1-yl)methyl) phenyl) methanone **(3-061)**

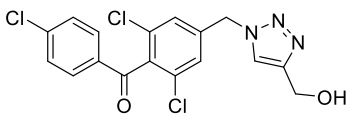

According to the method of (**3-057**), to give the compound (4-chlorophenyl)(2,6-dichloro-4-((4-(hydroxymethyl)-*1H*-1,2,3-triazol-1-yl) methyl)phenyl) methanone (**3-061**) (154 mg, 66 %) as a yellow solid. **Chemical Formula:** $C_{17}H_{12}Cl_3N_3O_2$, **Molecular weight:** 396.6520, **^{1}H-NMR** (300MHz, DMSO-d_6): ppm δ 8.17 (s, 1H), 7.77 (dd, *J*= 3.0, 6.0 Hz, 2H), 7.67 (dd, *J*= 3.0 6.0 Hz, 2H), 7.60 (s, 2H), 5.70 (s, 2H), 5.20 (t, *J*= 6.0 Hz, 1H), 4.54 (d, *J*= 6.0 Hz, 2H). **^{13}C-NMR** (75MHz, $CDCl_3$): ppm δ 191.23, 149.03, 141.27, 140.61, 136.43, 133.69, 131.51, 131.25, 130.29, 128.59, 123.80, 55.51, 51.60. **HRMS** (APCI$^+$): calculated for $C_{17}H_{13}Cl_3N_3O_2$ $[M+H]^+$: 396.0068, found: 396.0065.

1-(4-(4-chlorobenzoyl)-3,5-difluorobenzyl)-*1H*-1,2,3-triazole-4-carboxamide **(3-062)**

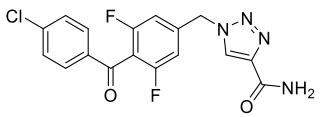

According to the method of (**3-057**), to give the compound 1-(4-(4-chlorobenzoyl)-3,5-difluorobenzyl)-*1H*-1,2,3-triazole-4-carboxamide (**3-062**) (167 mg, 68 %) as a yellow solid. **Chemical Formula:** $C_{17}H_{11}ClF_2N_4O_2$, **Molecular weight:** 376.7478, **^{1}H-NMR** (300MHz, DMSO-d_6): ppm δ 8.71 (s, 1H), 7.90 (s, 1H), 7.85 (dd, *J*= 3.0, 6.0 Hz, 2H), 7.67 (dd, *J*= 3.0, 6.0 Hz, 2H). 7.52 (s, 1H), 7.32 (d, *J*= 9.0 Hz, 2H), 5.78 (s, 2H). **^{13}C-NMR** (75MHz, $CDCl_3$): ppm δ 187.53, 164.62, 161.02, 160.91, 157.70, 145.47, 142.87, 140.44, 135.15, 131.55, 129.97, 122.26, 112.03, 111.70, 47.90. **HRMS** (APCI$^+$): calculated for $C_{17}H_{12}ClF_2N_4O_2$ $[M+H]^+$: 377.0612, found: 377.0608.

Part B

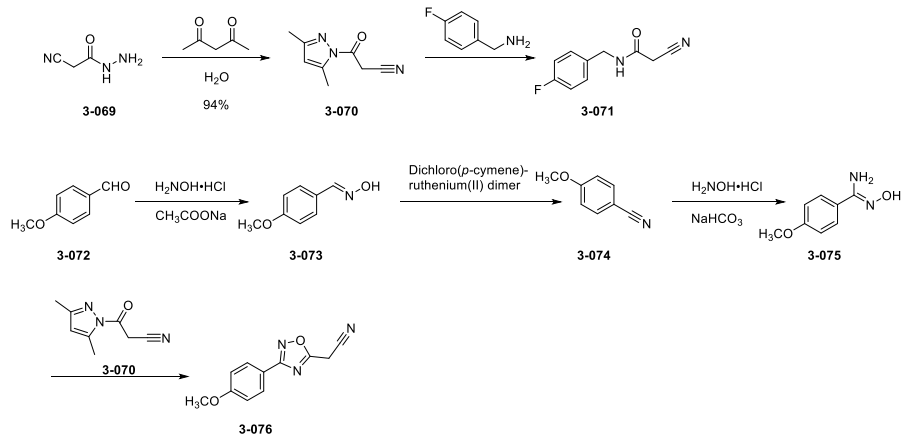

Synthesis of 2-cyano-*N*-(4-fluorobenzyl) acetamide **(3-071)**

To a solution of 2-cyanoacetohydrazide **3-069** (6.0 g, 60.55 mmol) in the water was added HCl (Catalytic amount) and pentane-2,4-dione (6.25 ml, 60.55 mmol). The mixture was stirred at room temperature for 2h. The precipitate was filtered, washed with water and dried to obtain a white solid as the pure product 3-(3,5-dimethyl-1*H*-pyrazol-1-yl)-3-oxopropanenitrile **3-070** as a white solid (9.7 g, 98 %)**.** **^{1}H-NMR** (300MHz, $CDCl_3$): ppm δ 6.03 (s, 1H), 4.28 (s, 2H), 2.55 (s, 3H), 2.22 (s, 3H).**^{13}C-NMR** (75MHz, $CDCl_3$): ppm δ 162.45, 153.88, 144.73, 113.44, 112.46, 30.95, 26.89, 14.06, 13.77.

To a solution of 3-(3,5-dimethyl-1*H*-pyrazol-1-yl)-3-oxopropanenitrile **3-070** (1.0 g, 6.13 mmol) in the toluene and (4-fluorophenyl)methanamine (767 mg, 6.13 mmol). The mixture was refluxed for 30 min and then cooled to room temperature. The precipitate was filtered, washed with *n*-hexane and dried to obtain a colorless solid as the pure product 2-cyano-*N*-(4-fluorobenzyl)acetamide **3-071** (1.1 g, 96%)**.** **^{1}H-NMR** (300MHz, DMSO-d_6): ppm δ 8.72 (s, 1H), 7.30 (dd, *J*= 6.0 Hz, 3.0 Hz, 2H), 7.15 (t, *J*= 9.0 Hz, 2H), 4.27 (d, *J*= 6.0 Hz, 2H), 3.69 (s, 2H). **^{13}C-NMR** (75MHz, DMSO-d_6): ppm δ 166.51, 165.83, 163.30, 138.45, 138.41, 133.07, 132.96, 119.79, 118.84, 118.56, 45.55, 28.93.

Synthesis of 2-(3-(4-methoxyphenyl)-1,2,4-oxadiazol-5-yl) acetonitrile **(3-076)**

To a solution of 4-methoxybenzaldehyde **3-072** (2.0 g, 14.69 mmol) in the EtOH (90%) was added hydroxylamine hydrochloride (1.12 g, 16.16 mmol) and sodium acetate (2.41 g, 29.38 mmol). The mixture was stirring at *rt* for 30 min and then refluxed for 1 h, the mixture was then cooled to *rt*. The EtOH was removed in *vacuo*. The residue was added with water and extracted with ethyl acetate, washed with brine, dried over anhydrous $MgSO_4$, filtered and concentrated.

The residue was purified by silica gel column chromatography (Petroleum ether/ CH_2Cl_2 3/2) to give the below compound 4-methylbenzaldehyde oxime **3-073** as a white solid (1.80 g, 91 %).**^{1}H-NMR** (300MHz, $CDCl_3$): ppm δ 8.11 (s,1H), 7.51 (dd, *J*=9.0 Hz, 3.0 Hz, 2H), 6.91 (dd, *J*=9.0 Hz, 3.0 Hz, 2H), 3.83 (s, 3H).**^{13}C-NMR** (75MHz, $CDCl_3$): ppm δ 161.63, 150.34, 133.54, 129.07, 125.06, 114.81, 55.90.

To a solution of 4-methylbenzaldehyde oxime **3-073** (1.50 g, 9.92 mmol) in acetonitrile was added Dichloro(*p*-cymene) ruthenium (II) dimer $[Ru_2(p\text{-}PriC_6H_4Me)_2(\text{-}Cl)Cl]_2$ (182 mg, 0.3mmol, 3mol %) and refluxed for 4 h. The mixture was filtered, and the filtrate was concentrated in *vacuo*. The residue was subjected to silica gel chromatography with (petroleum ether/CH_2Cl_2 2:1) to give the compound 4-methoxybenzonitrile **3-074** (1.06 g, 80 %). To a solution of 4-methoxybenzonitrile **3-074** (1.0 g, 7.51 mmol) in the EtOH was added hydroxylamine hydrochloride (2.61 g, 37.55 mmol) and sodium bicarbonate (3.79 g, 45.06 mmol). The mixture was stirring at *rt* for 30 min and then refluxed for 3 h, the mixture was then cooled to *rt*. The inorganic solids were removed by filtration and the solvent was removed in *vacuum* to give crude product as a light yellow solid. The residue was purified by silica gel column chromatography (CH_2Cl_2/ MeOH 20/1) to give the compound *N*′-hydroxy-4-methoxybenzimidamide **3-075** as a white solid (980 mg, 79 %)**.**

To a solution of *N*′-hydroxy-4-methoxybenzimidamide **3-075** (800 mg, 4.81 mmol) in the 1,4-dioxane was added 3-(3,5-dimethyl-1*H*-pyrazol-1-yl)-3-oxopropanenitrile **3-070** (786 mg, 4.81 mmol). The mixture was refluxed for overnight, then the mixture was cooled to *rt*. The 1,4-dioxane was removed in *vacuo*. The residue was added with water and extracted with CH_2Cl_2, washed with brine, dried over anhydrous $MgSO_4$, filtered and concentrated. The residue was purified by silica gel column chromatography (CH_2Cl_2/ MeOH 50/1) to give the compound 2-(3-(4-methoxyphenyl)-1,2,4-oxadiazol-5-yl) acetonitrile **3-076** as a brownish yellow solid (841 mg, 81 %)**. ^{1}H-NMR** (300MHz, $CDCl_3$): ppm δ 8.02 (dd, *J*=6.8 Hz, 2.0 Hz, 2H), 7.00 (dd, *J*=6.8 Hz, 2.0 Hz, 2H), 4.11 (s, 2H), 3.88 (s, 3H). **^{13}C-NMR** (75MHz, $CDCl_3$): ppm δ 168.78, 168.55, 162.36, 129.22, 118.08, 114.41, 111.95, 67.09, 55.44.

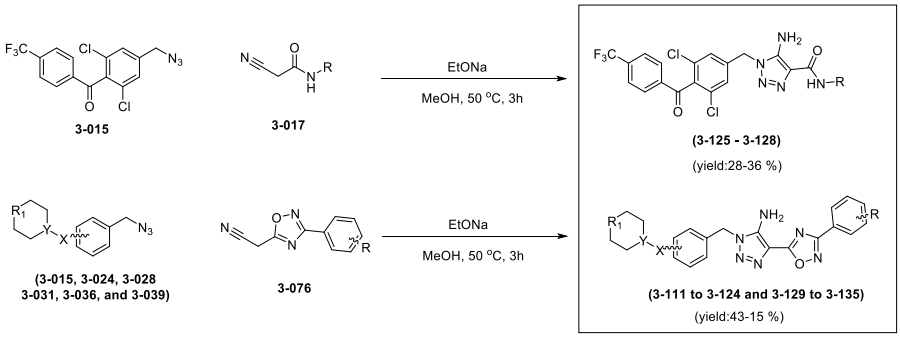

(4-((5-amino-4-(3-(4-methoxyphenyl)-1,2,4-oxadiazol-5-yl)-1*H*-1,2,3-triazol-1-yl)methyl)-2,6-dichlorophenyl)(*p*-tolyl)methanone **(3-111)**

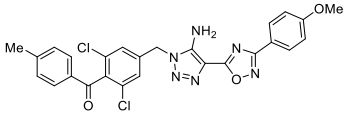

A solution of 2-(3-(4-methoxyphenyl)-1,2,4-oxadiazol-5-yl)acetonitrile (148 mg, 0.69 mmol) in methanol (5.0 mL) at *rt* was treated with sodium ethoxide (47 mg, 0.69 mmol) followed by (4-(azidomethyl)-2,6-dichlorophenyl)(*p*-tolyl)methanone (200 mg, 0.62 mmol). The reaction was then stirred for 3h at 50 °C. After cooling a light yellow precipitate was formed, which was removed by filtration, washed with ice-cold EtOH, then dried *in* vacuo to give the compound **3-111** (74 mg, 22 %) as a light yellow solid. **Chemical Formula:** $C_{26}H_{20}Cl_2N_6O_3$. **Molecular weight:** 535.3850. **^{1}H-NMR** (300MHz, DMSO-d_6): ppm δ 8.13 (dd, *J*=2.0, 7.0 Hz, 2H), 7.65 (d, *J*=8.2 Hz, 2H), 7.53 (s, 2H), 7.39 (d, *J*=8.2 Hz, 2H), 7.10 (dd, *J*=2.0, 7.0 Hz, 2H), 7.08 (s, 2H), 5.67 (s, 2H), 3.85 (s, 3H), 2.39 (s, 3H). **^{13}C-NMR** (75MHz, DMSO-d_6): ppm δ 191.66, 169.32, 167.44, 162.21, 146.43, 145.38, 140.30, 137.00, 132.66, 131.29, 130.57, 129.81, 129.56, 127.98, 118.98, 115.39, 114.96, 55.88, 47.93, 21.82. **HRMS** (APCI$^+$): calculated for $C_{26}H_{21}Cl_2N_6O_3$ $[M+H]^+$:535.1047, found: 535.1047.

(4-((5-amino-4-(3-(4-methoxyphenyl)-1,2,4-oxadiazol-5-yl)-1*H*-1,2,3-triazol-1-yl)methyl)-2,6-dichlorophenyl)(4-chlorophenyl)methanone **(3-112)**

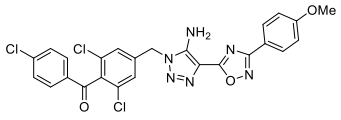

According to the method of **3-111**, to give the compound **3-112** (91 mg, 28%) as a yellow solid. **Chemical Formula:** $C_{25}H_{17}Cl_3N_6O_3$. **Molecular weight:** 555.8000. **^{1}H-NMR** (300MHz, DMSO-d_6): ppm δ 8.12 (d, *J*=9.0 Hz, 2H), 7.77 (d, *J*=8.4 Hz, 2H), 7.67 (d, *J*=8.4 Hz, 2H), 7.55 (s, 2H), 7.12 (d, *J*=8.4 Hz, 2H), 7.08 (s, 2H), 5.66 (s, 2H), 3.85 (s, 3H). **^{13}C-NMR** (75MHz, DMSO-d_6): ppm δ 191.22, 169.32, 167.44, 162.21, 145.39, 140.70, 136.30, 133.69, 131.50, 131.28, 130.29, 129.56, 128.12, 118.98, 115.38, 114.96, 55.89, 47.93. **HRMS** (APCI$^+$): calculated for $C_{25}H_{18}Cl_3N_6O_3$ $[M+H]^+$:555.0501, found: 555.0503.

(4-((5-amino-4-(3-(2-bromophenyl)-1,2,4-oxadiazol-5-yl)-1*H*-1,2,3-triazol-1-yl)methyl)-2,6-dichlorophenyl)(4-(trifluoromethyl)phenyl)methanone **(3-113)**

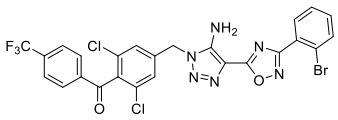

According to the method of **3-111**, to give the compound **3-113** (70 mg, 15%) as a yellow solid. **Chemical Formula:** $C_{25}H_{14}BrCl_2F_3N_6O_2$. **Molecular weight:** 638.2262. **^{1}H-NMR** (300MHz, DMSO-d_6): ppm δ 8.02 (d, J=7.6 Hz, 1H),7.97 (s, 4H), 7.87(d, J=7.6 Hz, 1H), 7.62-7.57 (m, 3H), 7.53 (d, J=8.0 Hz, 1H), 7.08(s, 2H), 5.68 (s, 2H). **^{13}C-NMR** (75MHz, DMSO-d_6): ppm δ 191.67, 169.24, 167.50, 145.50, 140.93, 137.93, 136.04, 134.75, 134.37, 133.05, 132.75, 131.32, 130.49, 128.44, 128.23, 127.16, 121.92, 115.17, 47.94. **HRMS** (APCI$^+$): calculated for $C_{25}H_{15}BrCl_2F_3N_6O_2$ $[M+H]^+$:636.9764, found: 636.9764.

(4-((5-amino-4-(3-(4-methoxyphenyl)-1,2,4-oxadiazol-5-yl)-1*H*-1,2,3-triazol-1-yl)methyl)-2,6-dichlorophenyl)(4-(trifluoromethyl)phenyl)methanone **(3-114)**

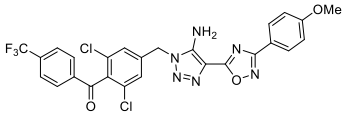

According to the method of **3-111**, to give the compound **3-114** (76 mg, 24%) as a yellow solid. **Chemical Formula:** $C_{26}H_{17}Cl_2F_3N_6O_3$. **Molecular weight:** 589.3562. **^{1}H-NMR** (300MHz, DMSO-d_6): ppm δ 8.12 (d, J=8.6 Hz, 2H), 7.98 (s, 4H), 7.58 (s, 2H), 7.13(d, J=9.0 Hz, 2H), 7.09(s, 2H), 5.67 (s, 2H), 3.85(s, 3H). **^{13}C-NMR** (75MHz, DMSO-d_6): ppm δ 221.51, 191.69, 167.44, 162.21, 145.41, 140.99, 137.92, 136.00, 131.30, 130.49, 129.55, 128.19, 127.19, 118.97, 114.96, 110.00, 55.89, 47.93. **HRMS** (APCI$^+$): calculated for $C_{26}H_{18}Cl_2F_3N_6O_3$ $[M+H]^+$:589.0764, found: 589.0768.

(4-((5-amino-4-(3-(4-(trifluoromethoxy)phenyl)-1,2,4-oxadiazol-5-yl)-1*H*-1,2,3-triazol-1-yl)methyl)-2,6-dichlorophenyl)(4-chlorophenyl)methanone **(3-115)**

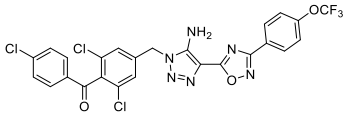

According to the method of **3-111**, to give the compound **3-115** (61 mg, 17%) as a yellow solid. **Chemical Formula:** $C_{25}H_{14}Cl_3F_3N_6O_3$. **Molecular weight:** 609.7712. **^{1}H-NMR** (300MHz, DMSO-d_6): ppm δ 8.33 (dd, J=2.0 7.2 Hz, 2H), 7.77 (dd, J=2.2, 6.4 Hz, 2H), 7.68 (dd, J=2.2, 6.4 Hz, 2H), 7.59 (d, J=7.2 Hz, 2H), 7.55 (s, 2H), 7.13 (s, 2H), 5.67 (s, 2H). **^{13}C-NMR** (75MHz, DMSO-d_6): ppm δ 191.21, 169.85, 166.81, 150.94, 145.58, 140.66, 136.33, 133.73, 131.49, 131.31, 130.28, 130.12, 128.13, 125.95, 122.00, 115.25, 47.95. **HRMS** (APCI$^+$): calculated for $C_{25}H_{15}Cl_3F_3N_6O_3$ $[M+H]^+$:609.0218, found: 609.0215.

(4-((5-amino-4-(3-(4-(trifluoromethoxy)phenyl)-1,2,4-oxadiazol-5-yl)-1*H*-1,2,3-triazol-1-yl)methyl)-2,6-dichlorophenyl)(*p*-tolyl)methanone **(3-116)**

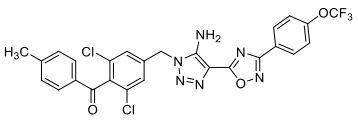

According to the method of **3-111**, to give the compound **3-116** (59 mg, 16%) as a yellow solid. **Chemical Formula:** $C_{26}H_{17}Cl_2F_3N_6O_3$. **Molecular weight:** 589.3562. **^{1}H-NMR** (300MHz, DMSO-d_6): ppm δ 8.33 (dd, J=2.1. 6.8 Hz, 2H), 7.66 (dd, J=1.8. 8.2 Hz, 2H), 7.58 (d, J=8.0 Hz, 2H), 7.53 (s, 2H), 7.39 (d, J=8.4 Hz, 2H), 7.13(s, 2H), 5.66 (s, 2H), 2.39 (s, 3H). **^{13}C-NMR** (75MHz, DMSO-d_6): ppm δ 191.62, 169.81, 166.76, 146.39, 145.53, 140.24, 137.00, 132.65, 131.28, 130.53, 130.09, 129.78, 127.96, 125.92, 121.98, 115.20, 47.93, 21.81. **HRMS** (APCI$^+$): calculated for $C_{26}H_{18}Cl_2F_3N_6O_3$ $[M+H]^+$:589.0764, found: 58.0767.

(4-((5-amino-4-(3-(4-(trifluoromethoxy)phenyl)-1,2,4-oxadiazol-5-yl)-1*H*-1,2,3-triazol-1-yl)methyl)-2,6-dichlorophenyl)(4-(trifluoromethyl)phenyl)methanone **(3-117)**

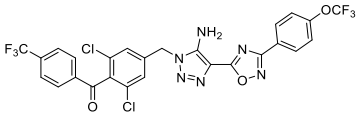

According to the method of **3-111**, to give the compound**3-117** (76 mg, 22%) as a yellow solid. **Chemical Formula:** $C_{26}H_{14}Cl_2F_6N_6O_3$. **Molecular weight:** 643.3274. **^{1}H-NMR** (300MHz, DMSO-d_6): ppm δ 8.33 (dd, J=2.0, 6.8 Hz, 2H), 7.99 (s, 4H), 7.61-7.58 (m, 4H), 7.14 (s, 2H), 5.68 (s, 2H). **^{13}C-NMR** (75MHz, DMSO-d_6): ppm δ 191.67, 169.84, 166.80, 150.91, 145.59, 140.95, 137.94, 136.03, 131.31, 130.48, 130.11, 128.19, 127.13, 125.94, 122.00, 115.23, 105.85, 47.95. **HRMS** (APCI$^+$): calculated for $C_{26}H_{15}Cl_2F_6N_6O_3$ $[M+H]^+$:643.0482, found: 643.0476.

tert-butyl 4-(4-((5-amino-4-(3-(4-(trifluoromethoxy)phenyl)-1,2,4-oxadiazol-5-yl)-1*H*-1,2,3-triazol-1-yl)methyl)-2,6-dichlorobenzyl)piperazine-1-carboxylate **(3-118)**

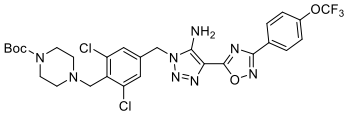

According to the method of **3-111**, to give the compound **3-118** (71 mg, 21%) as a yellow solid. **Chemical Formula:** $C_{28}H_{29}Cl_2F_3N_8O_4$. **Molecular weight:** 669.4872. **^{1}H-NMR** (300MHz, DMSO-d_6): ppm δ 8.32 (dd, J=2.0, 6.8 Hz, 2H), 7.60 (d, J=8.5 Hz, 2H), 7.37 (s, 2H), 7.09 (s, 2H), 5.56 (s, 2H), 3.65 (s, 2H), 3.24 (t, J=3.0 Hz, 4H), 2.39 (t, J=3.0 Hz, 4H), 1.30(s, 9H). **^{13}C-NMR** (75MHz, DMSO-d_6): ppm δ 169.79, 166.76, 154.12, 150.89, 145.43, 138.12, 136.71, 133.56, 130.10, 127.99, 125.92, 121.98, 115.12, 79.22, 56.21, 52.88, 47.77, 28.50. **HRMS** (APCI$^+$): calculated for $C_{28}H_{30}Cl_2F_3N_8O_4$ $[M+H]^+$: 669.1714, found: 669.1718.

(4-((5-amino-4-(3-(4-(trifluoromethoxy)phenyl)-1,2,4-oxadiazol-5-yl)-1*H*-1,2,3-triazol-1-yl)methyl)-2,6-dichlorophenyl)(4-methoxyphenyl)methanone **(3-119)**

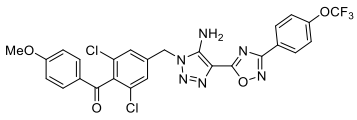

According to the method of **3-111**, to give the compound **3-119** (62 mg, 17%) as a yellow solid. **Chemical Formula:** $C_{26}H_{17}Cl_2F_3N_6O_4$. **Molecular weight:** 605.3552. **^{1}H-NMR** (300MHz, DMSO-d_6): ppm δ 8.33 (d, J=9.0 Hz, 2H), 7.70 (d, J=9.0 Hz, 2H), 7.60 (d, J=8.0 Hz, 2H), 7.52 (s, 2H),7.13-7.08 (m, 4H), 5.66 (s, 2H), 3.86 (s, 3H). **^{13}C-NMR** (75MHz, DMSO-d_6): ppm δ 190.36, 165.00, 145.55, 140.11, 137.18, 132.19, 131.33, 130.12, 130.05, 128.09, 127.98, 125.94, 125.27, 122.01, 115.31, 56.25, 47.95. **HRMS** (APCI$^+$): calculated for $C_{26}H_{18}Cl_2F_3N_6O_4$ $[M+H]^+$:605.0713, found: 605.0715.

1-(3,5-dichloro-4-(morpholinomethyl)benzyl)-4-(3-(4-(trifluoromethoxy)phenyl)-1,2,4-oxadiazol-5-yl)-1*H*-1,2,3-triazol-5-amine **(3-120)**

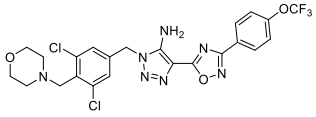

According to the method of **3-111**, to give the compound **3-120** (133 mg, 35%) as a yellow solid. **Chemical Formula:** $C_{23}H_{20}Cl_2F_3N_7O_3$. **Molecular weight:** 570.3542. **^{1}H-NMR** (300MHz, DMSO-d_6): ppm δ 8.32 (dd, J=2.1. 6.8 Hz, 2H), 7.57 (d, J=6.0 Hz, 2H), 7.37 (s, 2H), 7.09 (s,2H), 5.56 (s, 2H), 3.64 (s, 2H), 3.49 (t, J=4.3 Hz, 4H), 2.43 (t, J=4.3 Hz, 4H). **^{13}C-NMR** (75MHz, DMSO-d_6): ppm δ 169.78, 166.75, 150.88, 145.42, 138.06, 136.69, 133.48, 130.09, 127.97, 125.92, 121.97, 115.12, 109.98, 66.66, 56.57, 53.57, 47.77. **HRMS** (APCI$^+$): calculated for $C_{23}H_{21}Cl_2F_3N_7O_3$ $[M+H]^+$:570.1030, found: 570.1029.

1-(3,5-dichloro-4-(piperidin-1-ylmethyl)benzyl)-4-(3-(4-(trifluoromethoxy)phenyl)-1,2,4-oxadiazol-5-yl)-1*H*-1,2,3-triazol-5-amine **(3-121)**

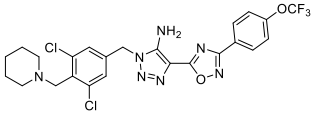

According to the method of **3-111**, to give the compound **3-121** (110 mg, 29%) as a yellow solid. **Chemical Formula:** $C_{24}H_{22}Cl_2F_3N_7O_2$. **Molecular weight:** 568.3822. **^{1}H-NMR** (300MHz, DMSO-d_6): ppm δ 8.32 (d, J=9.0 Hz, 2H), 7.58 (d, J=6.0 Hz, 2H), 7.35 (s, 2H), 7.09 (s, 2H), 5.55 (s, 2H), 3.57 (s, 2H), 2.39 (s, 4H), 1.39 (s, 6H). **^{13}C-NMR** (75MHz, DMSO-d_6): ppm δ 169.80, 166.75, 150.88, 145.42, 137.82, 136.68, 134.22, 130.09, 127.89, 125.93, 121.97, 115.12, 56.96, 54.36, 47.78, 26.03, 24.25. **HRMS** (APCI$^+$): calculated for $C_{24}H_{23}Cl_2F_3N_7O_2$ $[M+H]^+$:568.1237, found: 568.1237.

1-(3,5-dichloro-4-(pyrrolidin-1-ylmethyl)benzyl)-4-(3-(4-(trifluoromethoxy)phenyl)-1,2,4-oxadiazol-5-yl)-1*H*-1,2,3-triazol-5-amine **(3-122)**

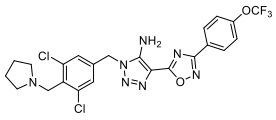

According to the method of **3-111**, to give the compound **3-122** (116 mg, 29%) as a yellow solid. **Chemical Formula:** $C_{23}H_{20}Cl_2F_3N_7O_2$. **Molecular weight:** 554.3552. **^{1}H-NMR** (300MHz, DMSO-d_6): ppm δ 8.32 (d, J=2.2. 7.8 Hz, 2H), 7.58 (d, J=6.0 Hz, 2H), 7.36 (s, 2H), 7.09 (s, 2H), 5.55 (s, 2H), 3.78 (s, 2H), 2.62-2.58 (m, 2H), 1.65-1.61 (m, 4H). **^{13}C-NMR** (75MHz, DMSO-d_6): ppm δ 169.79, 166.75, 150.88, 145.41, 137.72, 136.23, 134.65, 130.08, 127.97, 125.92, 121.96, 118.74, 115.11, 53.86, 53.24, 47.77, 23.57. **HRMS** (APCI$^+$): calculated for $C_{23}H_{21}Cl_2F_3N_7O_2$ $[M+H]^+$:554.1081, found: 554.1082.

4-(3-(2-bromophenyl)-1,2,4-oxadiazol-5-yl)-1-(3,5-dichloro-4-(piperidin-1-ylmethyl) benzyl) -1*H*-1,2,3-triazol-5-amine **(3-123)**

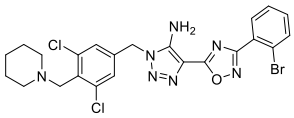

According to the method of **3-111**, to give the compound **3-123** (101 mg, 27%) as a yellow solid. **Chemical Formula:** $C_{23}H_{22}BrCl_2N_7O$. **Molecular weight:** 563.2810. **^{1}H-NMR** (300MHz, DMSO-d_6): ppm δ 8.01 (dd, J=2.0, 7.7 Hz, 1H), 7.86 (dd, J=1.4. 7.6 Hz, 1H), 7.62-7.35 (m, 2H), 7.35 (s, 2H), 7.01 (s, 2H), 5.55 (s, 2H), 3.58 (s, 2H), 2.39 (s, 4H), 1.41-1.36 (m, 6H). **^{13}C-NMR** (75MHz, DMSO-d_6): ppm δ 169.19, 167.45, 145.32, 137.79, 136.68, 134.34, 134.23, 133.03, 132.73, 129.53, 128.43, 128.21, 127.91, 121.89, 115.05, 56.97, 54.37, 47.76, 26.03, 24.26. **HRMS** (APCI$^+$): calculated for $C_{23}H_{23}BrCl_2N_7O$ $[M+H]^+$:562.0519, found: 562.0520.

4-(3-(2-bromophenyl)-1,2,4-oxadiazol-5-yl)-1-(3,5-dichloro-4-(morpholinomethyl)benzyl) -1*H*-1,2,3-triazol-5-amine **(3-124)**

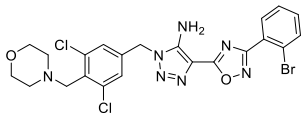

According to the method of **3-111**, to give the compound **3-124** (109 mg, 29%) as a yellow solid. **Chemical Formula:** $C_{22}H_{20}BrCl_2N_7O_2$. **Molecular weight:** 565.2530. **^{1}H-NMR** (300MHz, DMSO-d_6): ppm δ 8.02 (dd, J=2.0, 7.6 Hz, 1H), 7.87 (dd, J=1.2, 7.8 Hz, 1H), 7.62-7.52 (m, 2H), 7.37 (s, 2H), 7.01(s, 2H), 5.56 (s, 2H), 3.65 (s, 2H), 3.49 (t, J= 6.0 Hz, 4H), 2.44 (t, J= 6.0 Hz, 4H). **^{13}C-NMR** (75MHz, DMSO-d_6): ppm δ 169.19, 145.33, 138.06, 136.69, 134.34, 133.49, 133.04, 132.73, 129.54, 128.43, 127.99, 121.89, 97.02, 66.66, 56.58, 53.58, 47.76. **HRMS** (APCI$^+$): calculated for $C_{22}H_{21}BrCl_2N_7O_2$ $[M+H]^+$:564.0312, found: 564.0312.

5-amino-1-(3,5-dichloro-4-(4-(trifluoromethyl)benzoyl)benzyl)-*N*-(4-fluorobenzyl)-1*H*-1,2,3-triazole-4-carboxamide **(3-125)**

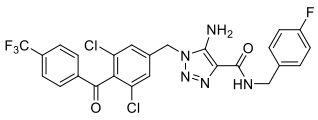

A solution of 2-cyano-*N*-(4-fluorobenzyl)acetamide (154 mg, 0.801 mmol) in methanol (6.0 mL) at room temperature, sodium ethoxide (56 mg, 0.828 mmol) followed by (4-(azidomethyl)-2,6-dichlorophenyl)(4-(trifluoromethyl)phenyl)methanone (200 mg, 0.534 mmol). The reaction was then stirred for 3h at 50 °C. After cooling to room temperature the reaction was diluted by addition of water and EtOAc, the organic phase separated, the aqueous layer was extracted with EtOAc and the organic phase washed with brine, dried over anhydrous $MgSO_4$, filtered and concentrated. The residue was purified by silica gel column chromatography (CH_2Cl_2/ EtOAc 10/1) to give the compound to give the title compound **3-125** (108 mg, 36 %) as a yellow solid. **Chemical Formula:** $C_{25}H_{17}Cl_2F_4N_5O_2$. **Molecular weight:** 566.3376. **^{1}H-NMR** (300MHz, DMSO-d_6): ppm δ 8.78 (t, J=6.0 Hz, 1H), 7.97 (s, 4H), 7.51 (s, 2H), 7.36 (q, J=5.4, 8.6 Hz, 2H), 7.13 (t, J=9.0 Hz, 2H), 6.56 (s, 2H), 5.54 (s, 2H), 4.38 (d, J=6.0 Hz, 2H). **^{13}C-NMR** (75MHz, DMSO-d_6): ppm δ 191.68, 162.42, 145.25, 141.31, 137.90, 136.79, 135.89, 134.72, 134.29, 131.21, 130.50, 129.83, 129.72, 128.17, 127.18, 122.10, 115.46, 115.18, 47.54. **HRMS** (APCI$^+$): calculated for $C_{25}H_{18}Cl_2F_4N_5O_2$ $[M+H]^+$:566.0768, found:566.0771.

5-amino-*N*-(3,5-bis(trifluoromethyl)benzyl)-1-(3,5-dichloro-4-(4-(trifluoromethyl) benzoyl) benzyl) -1*H*-1,2,3-triazole-4-carboxamide **(3-126)**

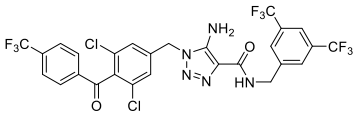

According to the method of **3-125**, to give the compound **3-126** (104 mg, 28.43%) as a yellow solid. **Chemical Formula:** $C_{27}H_{16}Cl_2F_9N_5O_2$. **Molecular weight:** 684.3436. **^{1}H-NMR** (300MHz, DMSO-d_6): ppm δ 8.99 (t, J=6.0 Hz, 1H), 8.02 (s, 2H), 7.99 (s, 1H), 7.97 (s, 4H), 7.51 (s, 2H), 6.60 (s, 2H), 5.55 (s, 2H), 4.58 (d, J=6.0 Hz, 2H). **^{13}C-NMR** (75MHz, DMSO-d_6): ppm δ 191.67, 162.68, 145.38, 144.19, 141.26, 137.90, 135.90, 134.72, 134.29, 131.21, 130.75, 130.48, 130.32, 128.77, 128.18, 127.15, 125.65, 122.03, 121.82, 121.04, 47.55. **HRMS** (APCI$^+$): calculated for $C_{27}H_{17}Cl_2F_9N_5O_2$ $[M+H]^+$:684.0610, found:684.0608.

5-amino-*N*-(2-chloro-5-(trifluoromethyl)benzyl)-1-(3,5-dichloro-4-(4-(trifluoromethyl) benzoyl) benzyl) -1*H*-1,2,3-triazole-4-carboxamide **(3-127)**

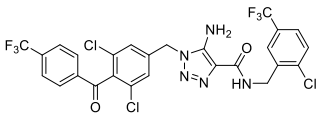

According to the method of **3-125**, to give the compound **3-127** (98 mg, 28%) as a yellow solid. **Chemical Formula:** $C_{26}H_{16}Cl_3F_6N_5O_2$. **Molecular weight:** 650.7874. **^{1}H-NMR** (300MHz, DMSO-d_6): ppm δ 8.92 (t, J=6.0 Hz, 1H), 7.96 (s, 4H), 7.74-7.64 (m, 3H), 7.53 (s,

2H), 6.62 (s, 2H), 5.57 (s, 2H), 4.56 (d, *J*=6.0 Hz, 2H). **^{13}C-NMR** (75MHz, DMSO-d_6): ppm δ 191.65, 162.73, 145.44, 141.26, 139.01, 137.90, 136.65, 135.91, 134.72, 131.23, 130.67, 130.48, 128.42, 128.17, 127.99, 127.09, 125.67, 121.82, 47.58. **HRMS** (APCI$^+$): calculated for $C_{26}H_{17}Cl_3F_6N_5O_2$ $[M+H]^+$:650.0347, found: 650.0347.

5-amino-1-(3,5-dichloro-4-(4-(trifluoromethyl)benzoyl)benzyl)-*N*-(4-fluorophenethyl)-1*H*-1,2,3-triazole-4-carboxamide **(3-128)**

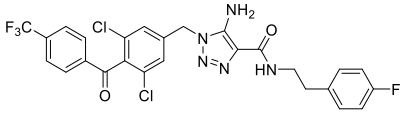

According to the method of **3-125**, to give the compound **3-128** (31 %) as a yellow solid. **Chemical Formula:** $C_{26}H_{19}Cl_2F_4N_5O_2$. **Molecular weight:** 580.3646. **^{1}H-NMR** (300MHz, DMSO-d_6): ppm δ 8.92 (t, *J*=6.0 Hz, 1H), 7.96 (s, 4H), 7.49 (s, 2H), 7.25 (q, *J*=6.0, 9.0 Hz, 2H), 7.10 (t, *J*=9.0 Hz, 2H), 6.54 (s, 2H), 5.54 (s, 2H), 3.45 (q, *J*=6.0, 12.0 Hz, 2H), 2.82 (t, *J*=6.0 Hz, 2H). **^{13}C-NMR** (75MHz, DMSO-d_6): ppm δ 191.66, 162.84, 162.39, 159.63, 145.13, 141.35, 137.89, 136.11, 135.87, 134.71, 134.29, 131.21, 130.85, 130.75, 130.49, 128.11, 127.12, 122.23, 115.58, 115.30, 47.53, 34.97. **HRMS** (APCI$^+$): calculated for $C_{26}H_{20}Cl_2F_4N_5O_2$ $[M+H]^+$:580.0925, found: 580.0928.

1-(2-morpholinobenzyl)-4-(3-(4-(trifluoromethoxy)phenyl)-1,2,4-oxadiazol-5-yl)-1*H*-1,2,3-triazol-5-amine **(3-129)**

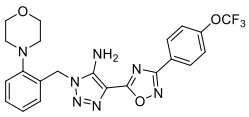

According to the method of **3-111**, to give the compound **3-129** (126 mg, 28%) as a yellow solid. **Chemical Formula:** $C_{22}H_{20}F_3N_7O_3$. **Molecular weight:** 487.4432. **^{1}H-NMR** (300MHz, DMSO-d_6): ppm δ 8.33 (d, *J*=9.0 Hz, 2H), 7.60 (d, *J*=9.0 Hz, 2H), 7.37-7.27 (m, 2H), 7.13-7.07 (m, 2H), 6.84 (d, *J*=6.0 Hz, 2H), 5.56 (s, 2H), 3.79 (s, 4H), 2.89 (s, 4H). **^{13}C-NMR** (75MHz, DMSO-d_6): ppm δ 222.68, 197.22, 169.98, 166.80, 152.88, 151.04, 145.94, 131.04, 130.13, 129.36, 128.29, 124.95, 122.04, 121.22, 114.82, 66.96, 53.20, 45.66. **HRMS** (APCI$^+$): calculated for $C_{22}H_{21}F_3N_7O_3$ $[M+H]^+$: 488.1653, found: 488.1657.

1-(3-morpholinobenzyl)-4-(3-(4-(trifluoromethoxy)phenyl)-1,2,4-oxadiazol-5-yl)-1*H*-1,2,3-triazol-5-amine **(3-130)**

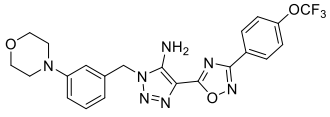

According to the method of **3-111**, to give the compound **3-130** (111 mg, 25%) as a yellow solid. **Chemical Formula:** $C_{22}H_{20}F_3N_7O_3$. **Molecular weight:** 487.4432. **^{1}H-NMR** (300MHz, DMSO-d_6): ppm δ 8.32 (dd, *J*=3.0, 9.0 Hz, 2H), 7.59 (d, *J*=9.0 Hz, 2H), 7.21 (t, *J*=9.0 Hz, 1H), 7.04-6.96 (m, 3H), 6.90 (d, *J*=6.0 Hz, 1H), 6.68 (d, *J*=6.0 Hz, 1H), 5.48

(s, 2H), 3.79 (t, *J*=3.0 Hz, 4H), 3.09 (t, *J*=3.0 Hz, 4H). **^{13}C-NMR** (75MHz, DMSO-d_6): ppm δ 169.89, 166.73, 151.70, 145.35, 136.67, 130.10, 129.82, 125.95, 121.99, 118.47, 114.97, 114.72, 66.49, 49.48, 48.73. **HRMS** (APCI$^+$): calculated for $C_{22}H_{21}F_3N_7O_3$ [M+H]$^+$: 488.1653, found: 488.1653.

N-(2-((5-amino-4-(3-(4-(trifluoromethoxy)phenyl)-1,2,4-oxadiazol-5-yl)-1*H*-1,2,3-triazol-1-yl)methyl)phenyl)-4-(trifluoromethoxy)benzamide **(3-131)**

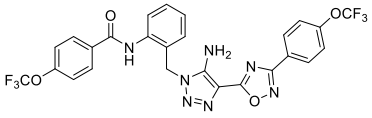

According to the method of **3-111**, to give the compound **3-131** (94 mg, 21%) as a yellow solid. **Chemical Formula:** $C_{26}H_{17}F_6N_7O_4$. **Molecular weight:** 605.4574. **^{1}H-NMR** (300MHz, DMSO-d_6): ppm δ 10.33 (s, 1H), 8.32 (d, *J*=9.0 Hz, 2H), 8.15 (d, *J*=9.0 Hz, 2H), 7.57 (t, *J*=6.0 Hz, 4H), 7.46 (d, *J*=6.0 Hz, 1H), 7.39 (t, *J*=6.0 Hz, 1H), 7.26 (t, *J*=6.0 Hz, 1H), 6.97-6.95 (m, 3H), 5.59 (s, 2H). **^{13}C-NMR** (75MHz, DMSO-d_6): ppm δ 169.85, 166.75, 165.04, 151.07, 145.68, 135.87, 133.81, 131.38, 130.67, 130.11, 128.75, 127.94, 127.39, 127.00, 125.94, 122.01, 121.21, 115.10, 46.48. **HRMS** (APCI$^+$): calculated for $C_{26}H_{18}F_6N_7O_4$ [M+H]$^+$: 606.1319, found: 606.1318.

N-(3-((5-amino-4-(3-(4-(trifluoromethoxy)phenyl)-1,2,4-oxadiazol-5-yl)-1*H*-1,2,3-triazol-1-yl)methyl)phenyl)-4-(trifluoromethoxy)benzamide **(3-132)**

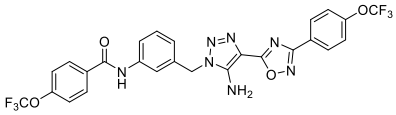

According to the method of **3-111**, to give the compound **3-132** (77 mg, 21%) as a yellow solid. **Chemical Formula:** $C_{26}H_{17}F_6N_7O_4$. **Molecular weight:** 605.4574. **^{1}H-NMR** (300MHz, DMSO-d_6): ppm δ 10.41 (s, 1H), 8.33 (d, *J*=9.0 Hz, 2H), 8.05 (d, *J*=9.0 Hz, 2H), 7.75 (d, *J*=6.0 Hz, 1H), 7.64 (s, 2H), 7.58 (d, *J*=6.0 Hz, 2H), 7.50 (d, *J*=6.0 Hz, 2H), 7.37 (t, *J*=6.0 Hz, 1H), 7.06-7.04 (m, 2H), 5.59 (s, 2H). **^{13}C-NMR** (75MHz, DMSO-d_6): ppm δ 169.92, 166.75, 164.86, 150.89, 145.51, 139.84, 136.57, 134.40, 130.53, 130.10, 129.44, 125.95, 123.27, 122.00, 121.13, 120.19, 119.33, 114.97, 49.08. **HRMS** (APCI$^+$): calculated for $C_{26}H_{18}F_6N_7O_4$ [M+H]$^+$: 606.1369, found: 606.1319.

N-(4-((5-amino-4-(3-(4-(trifluoromethoxy)phenyl)-1,2,4-oxadiazol-5-yl)-1*H*-1,2,3-triazol-1-yl)methyl)phenyl)-4-chlorobenzamide **(3-133)**

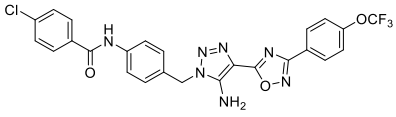

According to the method of **3-111**, to give the compound **3-133**(71 mg, 17%) as a yellow solid. **Chemical Formula:** $C_{25}H_{17}ClF_3N_7O_3$. **Molecular weight:** 555.9022. **^{1}H-NMR** (300MHz, DMSO-d_6): ppm δ 10.34 (s, 1H), 8.16 (d, *J*=9.0 Hz,

2H), 7.97 (d, *J*=9.0 Hz, 2H), 7.75 (d, *J*=9.0 Hz, 2H), 7.64-7.58 (m, 4H), 7.30 (d, *J*=9.0 Hz, 2H), 7.04 (s, 2H), 5.46 (t, *J*=6.0 Hz, 2H). **^{13}C-NMR** (75MHz, DMSO-d_6): ppm δ 174.74, 167.43, 164.88, 151.15, 138.83, 136.87, 134.02, 131.02, 130.07, 129.95, 128.93, 125.05, 122.23, 120.94, 116.71, 109.99, 35.99, 32.58. **HRMS** (APCI$^+$): calculated for $C_{25}H_{18}ClF_3N_7O_3$ $[M+H]^+$: 556.1106, found: 556.1101.

(4-((5-amino-4-(3-(4-(dimethylamino)phenyl)-1,2,4-oxadiazol-5-yl)-1*H*-1,2,3-triazol-1-yl)methyl)-2,6-dichlorophenyl)(4-chlorophenyl)methanone **(3-135)**

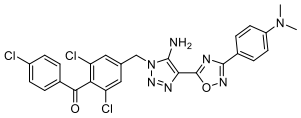

According to the method of **3-111**, to give the compound **3-135** (144 mg, 43%) as a yellow solid. **Chemical Formula:** $C_{26}H_{20}Cl_3N_7O_2$. **Molecular weight:** 568.8430. **^{1}H-NMR** (300MHz, DMSO-d_6): ppm δ 7.98 (d, *J*=9.0 Hz, 2H), 7.77 (d, *J*=6.0 Hz, 2H), 7.67 (d, *J*=6.0 Hz, 2H), 7.55 (s, 2H), 7.04 (s, 2H), 6.85 (d, *J*=9.0 Hz, 2H), 5.66 (s, 2H), 3.01 (s, 6H). **^{13}C-NMR** (75MHz, DMSO-d_6): ppm δ 191.22, 168.85, 167.81, 152.60, 145.24, 140.71, 140.61, 136.27, 133.67, 131.50, 131.26, 130.29, 128.96, 128.11, 115.52, 113.26, 112.09, 109.99, 47.92. **HRMS** (APCI$^+$): calculated for $C_{26}H_{21}Cl_3N_7O_2$ $[M+H]^+$:568.0817, found: 568.0814.

Part C

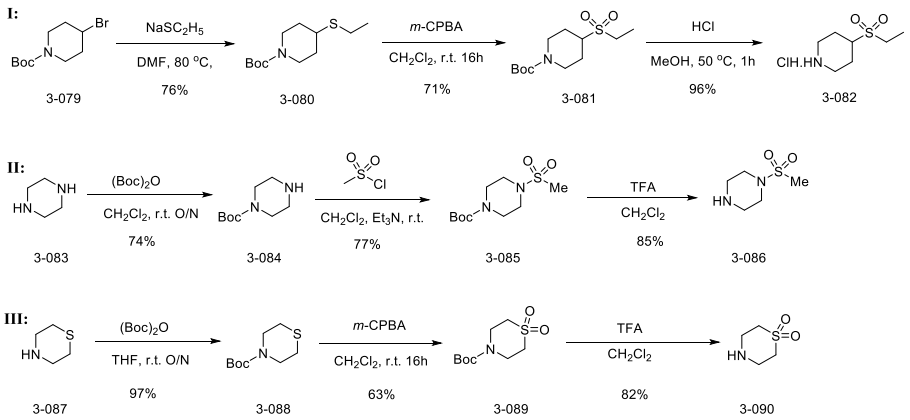

Synthesis of 4-(ethylsulfonyl)piperidine hydrochloride **(3-082)**

To a solution of 1-Boc-4-bromopiperidine (3.0 g, 11.36 mmol), sodium ethanethiolate (1.2 g, 136.3 mmol) in DMF is stirred at 80^{o}C for 20h. The reaction mixture is allowed to cool to room temperature and poured into ice-water. The resultant mixture is extracted with EtOAc. The combined organic extracts are washed with brine, dried ($MgSO_4$) and concentrated *in vacuo*

yielding the crude product. The residue was purified by silica gel column chromatography (petroleum ether/ ethyl acetate 10/1) to give the compound *tert*-butyl 4-(ethylthio)piperidine-1-carboxylate **3-080** as a brownish yellow solid (2.1 g, 76 %)**.** **^{1}H-NMR** (300MHz, $CDCl_3$): ppm δ 4.10-3.98 (m, 2H), 3.35-3.28 (m, 2H), 3.11-3.12 (m, 2H), 2.86-2.70 (m, 2H), 2.02-1.92 (m, 3H), 1.40 (s, 9H), 1.21 (t, *J*=3.0 Hz, 3H).

To a solution of *tert*-butyl 4-(ethylthio)piperidine-1-carboxylate **3-080** (2.0 g, 8.15 mmol) in CH_2Cl_2 is stirred at 0°C, *m*-CPBA (6.7 g, 16.30 mmol) was added in one portion, and the mixture was stirred at rt for the 16h. The reaction mixture was diluted with ethyl acetate, washed with 2.0 M aqueous NaOH and brine, dried over anhydrous $MgSO_4$, filtered and concentrated. The residue was purified by silica gel column chromatography (petroleum ether/ ethyl acetate 3/1) to give the compound *tert*-butyl 4-(ethylsulfonyl)piperidine-1-carboxylate **3-081** as a brownish yellow solid (1.6 g, 71 %)**.** **^{1}H-NMR** (300MHz, $CDCl_3$): ppm δ 4.37-4.21 (m, 2H), 3.00-2.91 (m, 3H), 2.81-2.65 (m, 2H), 2.10-2.00 (m, 2H), 2.02-1.92 (m, 3H), 1.46 (s, 9H), 1.40 (t, *J*=3.0 Hz, 3H).

To a solution of *tert*-butyl 4-(ethylsulfonyl)piperidine-1-carboxylate **3-081** (1.0 g, 3.61 mmol) in fresh HCl methanol solution (1.5 M, 15ml) is stirred at 50°C for 1h. After the mixture was concentrated *in vacuo*. The residue was suspended with cool methanol and the precipitate was collected by filtration to afford 4-(ethylsulfonyl)piperidine hydrochloride **3-082** (740 mg, 96%) as a white solid. **^{1}H-NMR** (300MHz, DMSO-d_6): ppm δ 9.82 (s, 1H), 8.86 (s, 1H), 3.51-3.37 (m, 2H), 3.12 (q, *J*=6.0, 12.0 Hz, 2H), 2.99-2.82 (m, 2H), 2.19-2.09 (m, 2H), 1.91-1.75 (m, 2H), 1.22 (t, *J*=6.0 Hz, 3H). **^{13}C-NMR** (75MHz, DMSO-d_6): ppm δ 53.36, 43.59, 41.67, 21.10, 5.84.

Synthesis of 1-(methylsulfonyl)piperazine **(3-086)**

To a solution of piperazine **3-083** (4.0 g, 46.44 mmol) in CH_2Cl_2 is stirred at 0°C. The solution of di-*tert*-butyldicarbonate (5.1 g, 23.22 mmol) in CH_2Cl_2 was slowly added in the reaction, and the reaction was kept under stirring at room temperature overnight. The white solid was filtered off. The filtrate was concentrated *in vacuo* and diluted in water and the white solid was filtered off again. The filtrate was saturated with K_2CO_3 and extracted with CH_2Cl_2. dried over anhydrous $MgSO_4$, filtered and concentrated to afford the compound **3-084** as a white solid (6.4 g, 74%). **^{1}H-NMR** (300MHz, $CDCl_3$): ppm δ 3.20 (t, *J* = 6.0 Hz, 4H,), 2.60 (t, *J* = 6.0 Hz, 4H), 2.29-2.39 (m, 1H), 1.38 (s, 9H).

To a solution of Boc-piperazine **3-084** (3.0 g, 16.11 mmol) in CH_2Cl_2 was added triethylamine (3.3 ml, 24.16 mmol) is stirred at 0°C. The solution of methanesulfonyl chloride (1.3 ml, 16.91 mmol) in CH_2Cl_2 was slowly added in the reaction. The resulting mixture was stirred at ambient

temperature for 2 h. The mixture was then washed with 1.0 M HCl, saturated $NaHCO_3$, and brine, dried over anhydrous $MgSO_4$, filtered and concentrated to afford the compound **3-085** as a white solid (3.3 g, 77%).**^{1}H-NMR** (300MHz, $CDCl_3$): ppm δ 3.70-3.64 (m, 4H), 3.16-3.14 (m, 4H), 2.70 (s, 3H), 1.44 (s, 9H).

To a solution of *tert*-butyl 4-(methylsulfonyl)piperazine-1-carboxylate **3-085** (1.0 g, 3.78 mmol) in CH_2Cl_2, TFA (0.5 ml) was added in the reaction and the mixture was stirred at rt for 3h. After the mixture was concentrated *in vacuo*. The residue was suspended with cool ether and the precipitate was collected by filtration to afford 1-(methylsulfonyl)piperazine **3-086** (525 mg, 85%) as a light yellow solid. **^{1}H-NMR** (300MHz, DMSO-d_6): ppm δ 9.30 (s, 1H), 3.37-3.34 (m, 4H), 3.19-3.14 (m, 4H), 2.86 (s, 3H).

Synthesis of thiomorpholine 1,1-dioxide **(3-090)**

Compounds thiomorpholine 1,1-dioxide **3-090** were prepared according to the methods of (**I**) and (**II**) described in above. As a light yellow solid (475 mg, 82%). **^{1}H-NMR** (300MHz, D_2O): ppm δ 3.85-3.79 (m, 4H), 3.66-3.60 (m, 4H). **^{13}C-NMR** (75MHz, D_2O): 48.05, 43.04.

Synthesis of 5-(5-ethyl-1-(3-(4-(methylsulfonyl) piperidin-1-yl)benzyl)-1*H*-1,2,4-triazol-3-yl)-3-(4-(trifluoromethoxy) phenyl) -1,2,4-oxadiazole (**3-101**)

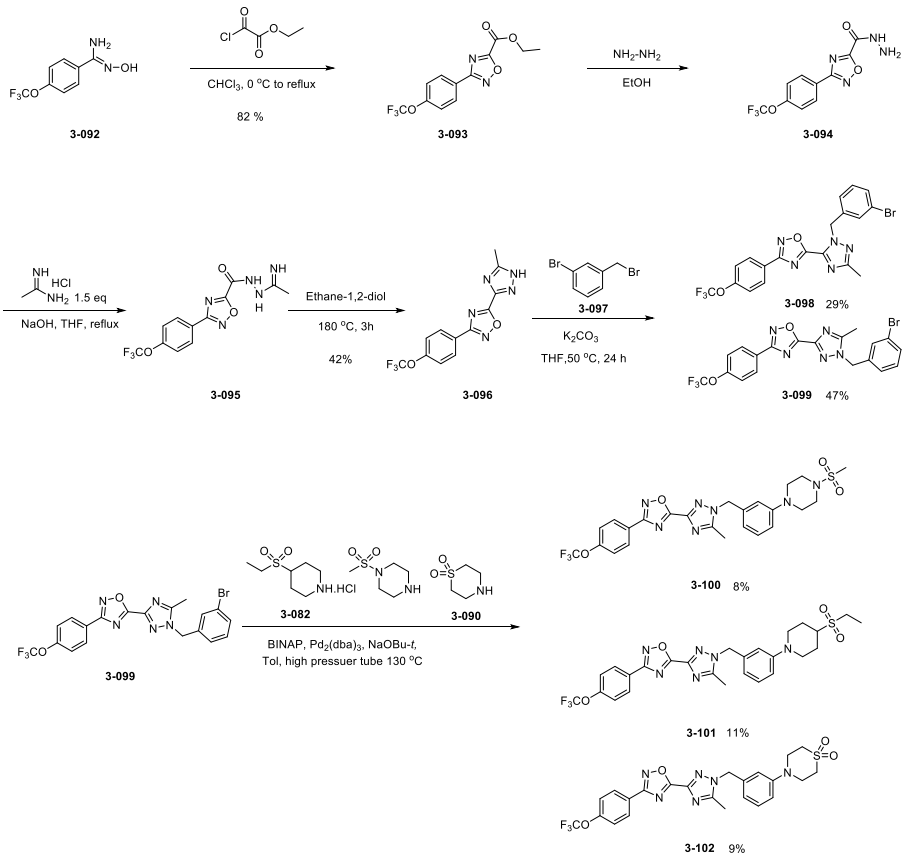

To a solution of 4-(trifluoromethoxy)benzamidoxime **3-092** (4.0 g, 18.17 mmol) in anhydrous chloroform is stirred at 0°C. The anhydrous pyridine (2.2 ml, 27.25 mmol) and ethyl chloroglyoxylate (2.3 mL, 21.80 mmol) were added under nitrogen atmosphere, and the mixture was heated under reflux for 1.5 h. The reaction mixture was cooled to rt, quenched with water, extracted with dichloromethane, washed with 1.0 M aqueous HCl and water, and dried ($MgSO_4$) and concentrated *in vacuo* yielding the crude product. The residue was purified by silica gel column chromatography (petroleum ether/ ethyl acetate 3/1) to give the compound ethyl 3-(4-(trifluoromethoxy)phenyl)-1,2,4-oxadiazole-5-carboxylate **3-093** as a white solid (4.3 g, 82 %). **^{1}H-NMR** (300MHz, $CDCl_3$): ppm δ 8.21 (dd, *J*=2.0, 6.9 Hz, 2H), 7.35 (dd, *J*=1.1, 9.0 Hz, 2H), 4.58 (q, *J*=7.2, 14.4 Hz, 2H), 1.5 (t, *J*=7.0 Hz, 3H). **^{13}C-NMR** (75MHz, $CDCl_3$): ppm δ 168.58, 166.98, 154.17, 151.92, 129.64, 124.33, 121.31, 64.25, 14.18.

To a solution of (trifluoromethoxy)phenyl)-1,2,4-oxadiazole-5-carboxylate **3-093** (4.0 g, 13.98 mmol) in ethanol, hydrazine monohydrate (3.42 mL, 69.88 mmol) was added, and the mixture was stirred at rt for 16 h. The resulting mixture was concentrated *in vacuo* to afford crude 3-(4-

(Trifluoromethoxy)phenyl)-1,2,4-oxadiazole-5-carbohydrazide **3-094** as a yellow solid, which was used for the next step without further purification. To a solution of **3-094** (crude product, < 13.95 mmol) and acetamidine hydrochloride (2.0 g, 20.92 mmol) in anhydrous THF, NaOH (837 mg, 20.92 mmol) was added at rt under argon atmosphere, and the mixture was heated under reflux for 15 h. Then, the solvent was removed *in vacuo*, and the residue was dissolved in ethylene glycol. The mixture was further stirred at 180 °C for 2 h. The reaction mixture was diluted with water, extracted with ethyl acetate, washed with water and then brine, and dried ($MgSO_4$) and concentrated *in vacuo* yielding the crude product. The residue was purified by silica gel column chromatography (petroleum ether/ ethyl acetate 2/1) to give the compound 5-(5-Methyl-1*H*-1,2,4-triazol-3-yl) -3-(4- (trifluoromethoxy) phenyl) -1,2,4-oxadiazole **3-096** as a light yellow solid (1.9 g, 42 %). **^{1}H-NMR** (300MHz, DMSO-d_6): ppm δ 8.20 (dd, *J*=2.6, 7.4 Hz, 2H), 7.59 (dd, *J*=2.8, 6.9 Hz, 2H), 2.49 (s, 3H). **^{13}C-NMR** (75MHz, DMSO-d_6): ppm δ 169.47, 167.23, 155.48, 150.56, 149.21, 129.43, 125.06, 121.68, 11.59.

The solution of 5-(5-methyl-1*H*-1,2,4-triazol-3-yl) -3-(4- (trifluoromethoxy) phenyl) -1,2,4-oxadiazole **3-096** (2.0g, 6.43 mmol) in anhydrous THF was added K_2CO_3 (1.3 g, 9.64 mmol) in the reaction at rt under argon atmosphere, and the mixture was stirred at 50 °C for 5 min, followed by the addition of 3-bromobenzyl bromide (1.8 mg, 7.07 mmol). After stirring at 50 ^{o}C for 24 h. the reaction mixture was quenched with water, extracted with ethyl acetate, washed water and brine, and dried ($MgSO_4$) and concentrated *in vacuo* yielding the crude product. The residue was purified by silica gel column chromatography (petroleum ether/ ethyl acetate 1/1) to give the compound 5-(1-(3-Bromobenzyl)-5-methyl-1*H*-1,2,4-triazol-3-yl)-3-(4-(trifluoromethoxy)phenyl)-1,2,4-oxadiazole **3-098** as a yellow solid (890 mg, 29 %) and 5-(1-(3-bromobenzyl) -3-methyl-1*H*- 1,2,4-triazol-5-yl) -3-(4- (trifluoromethoxy) phenyl) -1,2,4-oxadiazole **3-099** as a yellow solid (1450 mg, 47 %). **^{1}H-NMR** (300MHz, DMSO-d_6): ppm δ 8.21z (dd, *J*=2.4, 7.4 Hz, 2H), 7.61-7.35 (m,4H), 7.37 (t, *J*=4.2 Hz, 1H), 7.31 (d, *J*=6.2 Hz, 1H), 5.58 (s, 2H), 2.59 (s, 3H). **^{13}C-NMR** (75MHz, DMSO-d_6): ppm δ 168.99, 167.28, 155.46, 150.60, 148.28, 137.90, 131.10, 131.07, 130.62, 129.49, 126.96, 124.99, 121.96, 121.72, 51.17, 11.70.

The solution of **3-099** (150 mg, 0.31 mmol) and **3-082** (133 mg, 0.62 mmol) in anhydrous toluene was added *t*-BuONa (75 mg, 0.78 mmol), BINAP (18 mg, 0.028 mmol), Pd_2dba_3 (9 mg, 0.09 mmol) under argon atmosphere in the sealed tube, and the mixture was heated under 130 ^{o}C for 36 h. The reaction mixture was diluted with ethyl acetate, filtered through a pad of Celite, and concentrated *in vacuo*. The crude product was purified by silica gel column chromatography (CH_2Cl_2/ CH_3OH v/v 50/1) to give the compound 5-(5-ethyl-1-(3-(4-(methylsulfonyl) piperidin-1-yl)benzyl)-1*H*-1,2,4-triazol-3-yl)-3-(4-(trifluoromethoxy) phenyl)

-1,2,4-oxadiazole **3-101** as a brownish yellow solid (20 mg, 11 %). **Chemical Formula:** $C_{26}H_{27}F_3N_6O_4S$. **Molecular weight:** 576.5952. **^{1}H-NMR** (300MHz, DMSO-d_6): ppm δ 8.22 (dd, J=3.0, 6.0 Hz, 2H), 7.61 (dd, J=3.0, 6.0 Hz, 2H), 7.21 (t, J=9.0 Hz, 1H), 6.95 (m, 2H), 6.63 (d, J=9.0 Hz, 1H), 5.49 (s, 2H), 3.85 (d, J=9.0 Hz, 2H), 3.08 (q, J=6.0, 9.0 Hz, 2H), 2.83-2.72 (m, 2H), 2.58 (s, 3H), 2.05 (d, J=9.0 Hz, 2H), 1.75-1.58 (m, 2H), 1.25-1.15 (m, 4H). **HRMS** (APCI$^+$): calculated for $C_{26}H_{27}F_3N_6O_4S$ $[M+H]^+$:577.1845, found: 577.1839.

5-(5-methyl-1-(3-(4-(methylsulfonyl)piperazin-1-yl)benzyl)-1H-1,2,4-triazol-3-yl)-3-(4-(trifluoromethoxy)phenyl)-1,2,4-oxadiazole **(3-100)**

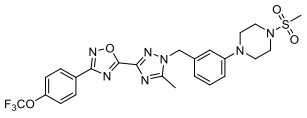

According to the method of **3-101**, to give the compound **3-100** (14 mg, 8%) as a brownish yellow solid. **Chemical Formula:** $C_{24}H_{24}F_3N_7O_4S$. **Molecular weight:** 563.5562. **^{1}H-NMR** (300MHz, DMSO-d_6): ppm δ 8.21 (d, J=9.2 Hz, 2H), 7.61 (d, J=6.5 Hz, 2H), 7.27-7.20 (m, 1H), 7.00-6.91 (m, 2H), 6.68 (d, J=6.2 Hz, 1H), 5.48 (s, 2H), 3.28-3.19 (m, 8H), 2.91 (s, 3H), 2.57 (s, 3H). **^{13}C-NMR** (75MHz, DMSO-d_6): ppm δ 191.22, 168.85, 167.81, 152.60, 145.24, 140.71, 140.61, 136.27, 133.67, 131.50, 131.26, 130.29, 128.96, 128.11, 115.52, 113.26, 112.09, 109.99, 47.92. **HRMS** (APCI$^+$): calculated for $C_{26}H_{21}Cl_3N_7O_2$ $[M+H]^+$:564.1641, found: 564.1635.

4-(3-((5-methyl-3-(3-(4-(trifluoromethoxy)phenyl)-1,2,4-oxadiazol-5-yl)-1H-1,2,4-triazol-1-yl)methyl)phenyl)thiomorpholine 1,1-dioxide **(102)**

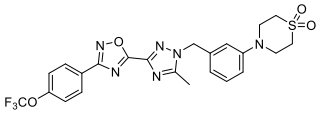

According to the method of **3-101**, to give the compound **3-102** (15 mg, 9%) as a brownish yellow solid. **Chemical Formula:** $C_{23}H_{21}F_3N_6O_4S$. **Molecular weight:** 534.5142. **^{1}H-NMR** (300MHz, DMSO-d_6): ppm δ 8.22 (d, J=8.9 Hz, 2H), 7.60 (d, J=6.4 Hz, 2H), 7.25-7.21 (m, 1H), 7.05-6.98 (m, 2H), 6.67 (d, J=6.4 Hz, 1H), 5.49 (s, 2H), 3.82-3.74 (m ,4H), 3.16-3.09 (m, 4H), 2.57 (s, 3H). **^{13}C-NMR** (75MHz, DMSO-d_6): ppm δ 191.22, 168.85, 167.81, 152.60, 145.24, 140.71, 136.27, 133.67, 131.50, 130.29, 128.96, 128.11, 115.52, 113.26, 112.09, 109.99, 47.93. **HRMS** (APCI$^+$): calculated for $C_{26}H_{21}Cl_3N_7O_2$ $[M+H]^+$:535.1375, found: 535.1370.

Synthesis of 5-(5-methyl-1-((2-thiomorpholinopyridin-4-yl) methyl)-1*H*-1,2,4-triazol-3-yl)-3-(4-(trifluoromethoxy) phenyl)-1,2,4-oxadiazole (**3-109**)

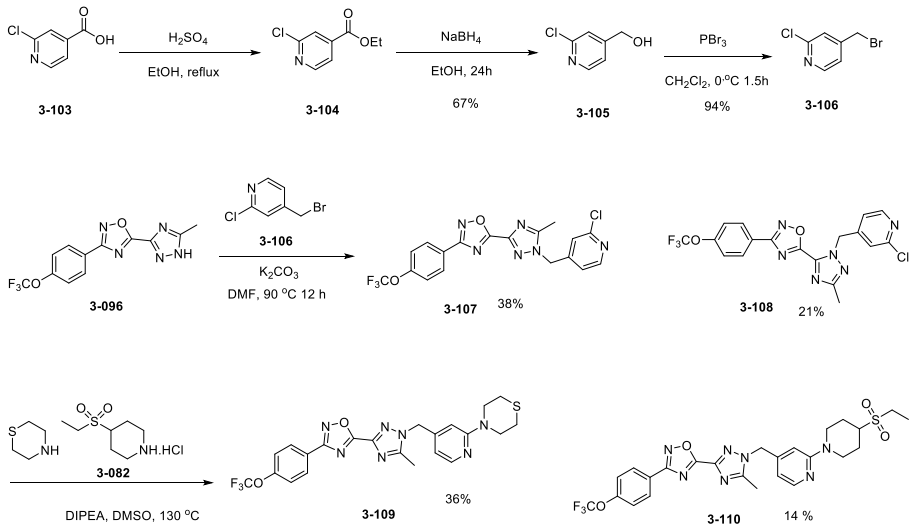

To a solution of 2-chloroisonicotinic acid **3-103** (4.0 g, 25.39 mmol) dissolved in EtOH was treated dropwise concentrated sulfuric acid (270 μL, 5.08 mmol), the mixture was heated at reflux for overnight. The mixture was cooled, concentrated under reduced pressure and diluted with water. The aqueous layer was extracted with ethyl acetate, and the combined organic extract was washed with brine, dried over $MgSO_4$ followed by concentrated under reduced pressure to afford crude ethyl ethyl 2-chloroisonicotinate **3-104** as a yellow solid. The crude compound was not purified to the next step. To a solution of ethyl 2-chloroisonicotinate **3-104** dissolved in EtOH was cooled to 0ºC, the $NaBH_4$ (2.45 g, 64.65 mmol) was added in the reaction. The reaction mixture is refluxed with stirring for 3h and then concentrated *in vacuo.* The mixture was extracted with ethyl acetate, and the combined organic extract was washed with brine, dried over $MgSO_4$ followed by concentrated under reduced pressure. The residue was purified by silica gel column chromatography (petroleum ether/ ethyl acetate 5/1-3/1) to give the compound (2-chloropyridin-4-yl) methanol **3-105** as a colorless solid (2.1 g, 67 %). **^{1}H-NMR** (300MHz, DMSO-d_6): ppm δ 8.32 (d, J=6.4 Hz,1H), 7.41-7.39 (m, 1H), 7.34-7.31 (m, 1H), 5.54 (br, 1H), 4.55 (s, 2H). **^{13}C-NMR** (75MHz, DMSO-d_6): ppm δ 156.65, 150.90, 150.15, 121.72, 121.08, 61.59.

To a solution of (2-chloropyridin-4-yl)methanol **3-105** (800 mg, 5.57 mmol) in dry CH_2Cl_2 was slowly added phosphorus tribromide (635 μL, 6.69 mmol) at 0°C, and the mixture was stirred at room temperature for 3 h. The mixture was cooled at 0°C, and quenched with water. The mixture was extracted with ethyl acetate and washed with water, before dried over $MgSO_4$. The residue was purified by silica gel column chromatography (petroleum ether/ ethyl acetate 50/1) to give the compound 4-(bromomethyl)-2-chloropyridine **3-106** as a colorless solid (1080 mg,

94 %). **^{1}H-NMR** (300MHz, $CDCl_3$): ppm δ 8.37 (d, *J*=4.2 Hz,1H), 7.35 (s, 1H), 7.23 (s, *J*=2.8 Hz,1H), 4.35 (s, 1H).

The solution of 5-(5-methyl-1*H*-1,2,4-triazol-3-yl) -3-(4- (trifluoromethoxy) phenyl) -1,2,4-oxadiazole **3-096** (2.0 g, 6.43 mmol) in anhydrous THF was added K_2CO_3 (1.3 g, 9.64 mmol) in the reaction at rt under argon atmosphere, and the mixture was stirred at 50 °C for 5 min, followed by the addition of 4-(bromomethyl)-2-chloropyridine **3-106** (1.5 g, 7.07 mmol). After stirring at 50 ºC for 24 h. the reaction mixture was quenched with water, extracted with ethyl acetate, washed water and brine, and dried ($MgSO_4$) and concentrated *in vacuo* yielding the crude product. The residue was purified by silica gel column chromatography (petroleum ether/ ethyl acetate 2/1) to give the compound 5-(1-((2-chloropyridin-4-yl) methyl)-5-methyl-1*H*-1,2,4-triazol-3-yl)-3-(4-(trifluoromethoxy) phenyl)-1,2,4-oxadiazole **3-107** as a yellow solid (1070 mg, 38 %). **3-107 ^{1}H-NMR** (300MHz, DMSO-d_6): ppm δ 8.42 (d, *J*=7.4 Hz, 1H), 8.21 (d, *J*=6.7 Hz, 2H), 7.60 (d, *J*=7.3 Hz, 2H), 7.45 (s, 1H), 7.27 (s, *J*=6.5 Hz, 1H), 5.68 (s, 2H), 2.58 (s, 3H). **^{13}C-NMR** (75MHz, DMSO-d_6): ppm δ 174.70, 172.44, 161.22, 160.57, 155.78, 155.67, 154.54, 153.35, 134.65, 130.26, 128.04, 127.05, 126.91, 55.43, 16.76.

The solution of **3-107** (150 mg, 0.343 mmol) and **3-082** (345 µL, 3.43 mmol) in anhydrous DMSO was added DIPEA (845 µL, 4.58 mmol) under argon atmosphere, and the mixture was heated under 130 ºC for 24 h. The reaction mixture was diluted with water, extracted with ethyl acetate, washed with water and then brine, and dried ($MgSO_4$) and concentrated *in vacuo* yielding the crude product. The residue was purified by silica gel column chromatography (CH_2Cl_2/ CH_3OH v/v 50/1) to give the compound 5-(5-methyl-1-((2-thiomorpholinopyridin-4-yl) methyl)-1*H*-1,2,4-triazol-3-yl)-3-(4-(trifluoromethoxy) phenyl)-1,2,4-oxadiazole **3-109** as a brownish yellow solid (24 mg, 14 %). **Chemical Formula:** $C_{25}H_{26}F_3N_7O_4S$. **Molecular weight:** 577.5832. **^{1}H-NMR** (300MHz, DMSO-d_6): ppm δ 8.22 (d, *J*=9.6 Hz, 2H), 8.08 (d, *J*=4.2 Hz, 1H), 7.61 (d, *J*=6.6 Hz, 2H), 6.85 (s, 1H), 6.40 (d, *J*=3.0 Hz, 1H), 5.50 (s, 2H), 4.44 (d, *J*=10.4 Hz, 2H), 3.51-3.39 (m, 1H), 3.12-3.03 (m, 2H), 2.96-2.84 (m, 2H), 2.57 (s, 3H), 2.08-1.98 (m, 2H), 1.62-1.48 (m, 2H), 1.22 (t, *J*=6.0 Hz, 3H). **^{13}C-NMR** (75MHz, DMSO-d_6): ppm δ 191.22, 168.85, 167.81, 152.60, 145.24, 140.71, 136.27, 133.67, 131.50, 130.29, 128.96, 128.11, 115.52, 113.26, 112.09, 109.99, 47.92. **HRMS** (APCI$^+$): calculated for $C_{26}H_{21}Cl_3N_7O_2$ $[M+H]^+$:578.1797, found: 578.1792.

5-(5-methyl-1-((2-thiomorpholinopyridin-4-yl)methyl)-1*H*-1,2,4-triazol-3-yl)-3-(4-(trifluoromethoxy) phenyl)-1,2,4-oxadiazole **(3-110)**

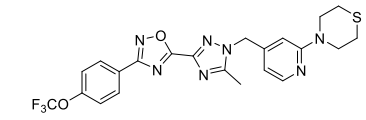

According to the method of **3-110**, to give the compound **3-109** (62 mg, 36 %) as a brownish yellow solid. **Chemical Formula:** $C_{22}H_{20}F_3N_7O_2S$. **Molecular weight:** 503.5042. **^{1}H-NMR** (300MHz, DMSO-d_6): ppm δ 8.21 (d, J=6.0 Hz, 2H), 8.07 (d, J=3.0 Hz, 1H), 7.61 (d, J=9.0 Hz, 2H), 6.81 (s, 1H), 6.37 (d, J=3.0 Hz, 1H), 5.50 (s, 2H), 3.93-3.88 (m, 4H), 2.61-2.55 (m, 7H). **^{13}C-NMR** (75MHz, DMSO-d_6): ppm δ 191.22, 168.85, 167.81, 152.60, 145.24, 140.71, 136.27, 133.67, 131.50, 131.26, 130.29, 128.96, 128.11, 115.52, 113.26, 112.09, 109.99, 47.92. **HRMS** (APCI$^+$): calculated for $C_{26}H_{21}Cl_3N_7O_2$ $[M+H]^+$:504.1429, found: 504.1424.

Chapter II:

Experimental protocols and analysis

Synthesis of 6-bromohexan-1-ol **(4-002)**

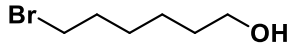

To a solution of hexane-1,6-diol **4-001** (10.0 g, 84.62 mol) in toluene, was added dropwise hydrobromic acid (48% in water, 9.6 mL, 84.62 mol) at room temperature. The mixture was stirred and heated at reflux overnight, TLC analysis indicated that substantial amounts of hexane-1,6-diol still remained. Thus, a further quantity of hydrobromic acid (2.0 mL) was added, and the mixture was heated at reflux 6 h, at which time TLC monitor showed full conversion. The reaction mixture was allowed to cool to room temperature, and the organic layer were separated. The organic layer was diluted with ethyl ether and washed with 1M NaOH and brine. Drying over anhydrous $MgSO_4$ and concentration of the organic layer in *vacuo* give a yellow oil. The oil was purified by silica gel column chromatography (petroleum ether/ ethyl acetate *v/v* = 5/1) to give the compound 6-bromohexan-1-ol **4-002** as a colorless oil (13.9 g, 90 %).**Chemical Formula:** $C_6H_{13}BrO$, **Molecular weight:** 181.0730. **^{1}H-NMR** (300MHz, $CDCl_3$): ppm δ 3.64 (t, J =5.8 Hz, 2H), 3.40 (t, J =8.7 Hz, 2H), 2.09 - 2.00 (m**,** 1H), 1.93 - 1.80 (m, 2H), 1.62 - 1.53 (m, 2H), 1.49-1.35 (m, 4H). **HRMS** ($APCI^+$)**:** Calculated for $C_6H_{12}Br$ $[M\text{-}OH]^-$ 163.0117, found: 163.0117.

Synthesis of 1-((6-bromohexyl)oxy)-4-chlorobenzene **(4-004)**

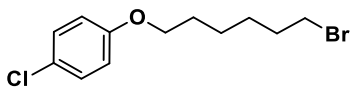

The 1-((6-bromohexyl) oxy)-4-chlorobenzene **4-004** was prepared following a procedure previously reported by M.Sc. Dominik Gärtner et al.[7].To a solution of triphenylphosphine (7.1 g, 27.06 mmol), 6-bromohexan-1-ol **4-002** (5.0 g, 27.06 mmol) and 4-chlorophenol **4-003** (3.5 g, 27.06 mmol,) in anhydrous THF, was added dropwise diisopropyl azodicarboxylate DIAD (6.24 mL, 29.77 mmol, 94% purity) dropwise at 0°C. After addition, the reaction mixture was stirred overnight at room temperature. The mixture was concentrated under *vacuo* and the residue was diluted with ethyl ether and washed with water and brine. Drying over anhydrous $MgSO_4$ and concentration of the organic layer in *vacuo* give a yellow oil. The oil was purified by silica gel column chromatography (petroleum ether/ ethyl acetate v/v 20/1) to give the compound 1-((6-bromohexyl)oxy)-4-chlorobenzene **4-004** as a colorless oil (6.7 g, 85 %).**Chemical Formula:** $C_{12}H_{16}BrClO$, **Molecular weight:** 291.6130. **^{1}H-NMR**

[7] Gärtner D, Stein A L, Grupe S, et al. Iron-Catalyzed Cross-Coupling of Alkenyl Acetates[*J*]. Angewandte Chemie International Edition, 2015, 54(36): 10545-10549.

(300MHz, $CDCl_3$): ppm δ 7.22 (d, J = 9.0 Hz, 2H), 6.81 (d, J = 9.0 Hz, 2H), 3.92 (t, J = 6.0 Hz, 2H), 3.44 (t, J = 6.0 Hz, 2H), 1.94-1.74 (m, 4H), 1.56-1.48 (m, 4H). **^{13}C-NMR** (75MHz, $CDCl_3$): ppm δ 157.67, 129.29, 125.37, 115.75, 68.03, 33.81, 32.67, 29.03, 27.92, 25.28. **HRMS** ($APCI^+$)**:** Calculated for $C_{12}H_{17}BrClO$ $[M+H]^+$ 291.0146, found: 291.0146.

Synthesis of diethyl 2-(6-(4-chlorophenoxy)hexyl)malonate **(4-006)**

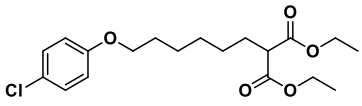

The diethyl 2-(6-(4-chlorophenoxy)hexyl)malonate **4-006** was prepared following a procedure previously reported by Guowei Kang et al.[8] The NaH (60% NaH in mineral oil, 760 mg, 18.86 mmol) was added in portions to a solution of dimethyl malonate (3.2 ml, 18.86 mmol) in 40 mL THF at 0 °C, and the resulting suspension was stirred for 0.5 h. The 1-((6-bromohexyl)oxy)-4-chlorobenzene **4-004** (5.0 g, 17.15 mmol) was then added in the mixture at room temperature. After the reaction was completed as checked by TLC about 4 h, the solvent was removed by rotary evaporation and added saturated aqueous NH_4Cl. The aqueous phase was then extracted with CH_2Cl_2. The combined organic extracts and washed with water and brine. Drying over anhydrous $MgSO_4$ and concentration of the organic layer in *vacuo* give a brownish yellow oil. The oil was purified by silica gel column chromatography (petroleum ether/ ethyl acetate v/v 20/1-10/1) to give the compound diethyl 2-(6-(4-chlorophenoxy)hexyl)malonate **4-006** as a light yellow oil (3.9 g, 61 %). **Chemical Formula:** $C_{19}H_{27}ClO_5$, **Molecular weight:** 370.8700. **^{1}H-NMR** (300MHz, $CDCl_3$): ppm δ 7.23 (d, J = 9.0 Hz, 2H), 6.82 (d, J = 9.0 Hz, 2H), 4.25-4.18 (q, J = 9.0 Hz, 4H), 3.92 (t, J = 6.0 Hz, 2H), 3.33 (t, J = 6.0 Hz, 1H), 1.96-1.88 (m, 2H), 1.80-1.75 (m, 2H), 1.40-1.32 (m, 6H), 1.28 (t, J = 6.0 Hz, 6H). **^{13}C-NMR** (75MHz, $CDCl_3$): ppm δ 169.52, 157.67, 129.24, 125.30, 115.73, 68.15, 61.29, 61.00, 53.42, 52.03, 29.05, 28.96, 28.64, 27.23, 25.73, 14.10. **HRMS** (ESI^+)**:** Calculated for $C_{19}H_{28}ClO_5$ $[M+H]^+$ 371.1620, found: 371.1620.

Synthesis of 8-(4-chlorophenoxy)-2-(ethoxycarbonyl)octanoic acid **(4-007)**

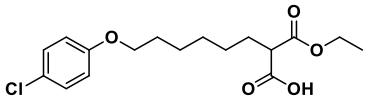

The diethyl 2-(6-(4-chlorophenoxy)hexyl)malonate **4-006** (3.0 g, 8.09 mmol) was added to a solution of KOH (455 mg, 8.09 mmol) in EtOH at room temperature and the solution was stirred overnight, and the reaction completion was monitored by TLC. The solvent was concentrated under *vacuo* and the residue was dissolved in 1M HCl and washed with ethyl acetate, the aqueous layer was acidified and extracted with ethyl acetate

[8] Kang G, Yamagami M, Vellalath S, et al. Enantioselective Synthesis of Medium-Sized Lactams via Chiral α, β-Unsaturated Acylammonium Salts[J]. Angewandte Chemie, 2018, 130(22): 6637-6641.

three times. The combined organic layers were washed with water and brine. Drying over anhydrous $MgSO_4$ and concentration of the organic layer in *vacuo* give the residue. The residue was purified by silica gel column chromatography (CH_2Cl_2/ MeOH v/v 50/1 0.5 % AcOH) to give the compound 8-(4-chlorophenoxy)-2-(ethoxycarbonyl)octanoic acid **4-007** as a light yellow solid (2.3 g, 83 %). **Chemical Formula:** $C_{17}H_{23}ClO_5$ **Molecular weight:** 342.8160. **^{1}H-NMR** (300MHz, $CDCl_3$): ppm δ 7.21 (d, J = 9.0 Hz, 2H), 6.80 (d, J = 9.0 Hz, 2H,), 4.22 (q, J = 9.0 Hz, 2H), 3.90 (t, J = 6.0 Hz, 2H), 3.38 (t, J = 6.0 Hz, 1H), 1.94-1.92 (m, 2H), 1.80-1.71 (m, 2H), 1.48-1.38 (m, 6H), 1.28 (t, J = 6.0 Hz, 3H). **^{13}C-NMR** (75MHz, $CDCl_3$): ppm δ 174.77, 169.49, 157.65, 129.24, 125.32, 115.73, 68.12, 61.74, 51.57, 29.03, 28.91, 28.82, 27.13, 25.70, 14.05.

Synthesis of ethyl 8-(4-chlorophenoxy)-2-methyleneoctanoate **(4-008)**

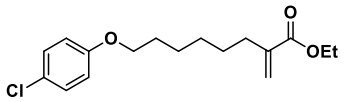

To a solution of 8-(4-chlorophenoxy)-2-(ethoxycarbonyl)octanoic acid **4-007** (4.0 g, 11.67 mmol) is added diethylamine (1.2 mL, 11.67 mmol) and paraformaldehyde (550 mg, 17.50mmol) in the CH_2Cl_2 at 0° C. The mixture was refluxed overnight. The reaction mixture was allowed to cool to room temperature, diluted with more CH_2Cl_2, and washed with 10% aqueous citric acid solution and brine. Drying over anhydrous $MgSO_4$ and concentration of the organic layer in *vacuo* give the residue. The residue was purified by silica gel column chromatography (petroleum ether/ ethyl acetate v/v 10/1) to give the compound ethyl 8-(4-chlorophenoxy)-2-methyleneoctanoate **4-008** as a yellow oil (2.8 g, 76 %) **Chemical Formula:** $C_{17}H_{23}ClO_3$, **Molecular weight:** 310.8180. **^{1}H-NMR** (300MHz, $CDCl_3$): ppm δ 7.19 (d, J = 9.0 Hz, 2H), 6.78 (d, J = 9.0 Hz, 2H,), 6.12 (d, J = 3.0 Hz, 1H), 5.49 (d, J = 3.0 Hz, 1H), 4.18 (q, J = 9.0 Hz, 2H), 3.87 (t, J = 6.0 Hz, 2H), 2.32-2.27 (m, 2H), 1.77-1.70 (m, 2H), 1.51-1.33 (m, 6H), 1.28 (t, J = 6.0 Hz, 3H). **^{13}C-NMR** (75MHz, $CDCl_3$): ppm δ 167.24, 157.72, 140.96, 129.21, 125.23, 124.24, 115.72, 68.15, 60.51, 31.78, 29.10, 28.91, 28.33, 25.79, 14.21.

Synthesis of ethyl 2-(6-(4-chlorophenoxy)hexyl)oxirane-2-carboxylate **(4-009)**

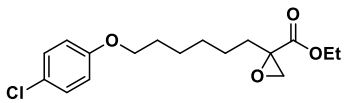

To a solution of ethyl 8-(4-chlorophenoxy)-2-methyleneoctanoate **4-008** (2.0 g, 6.43 mmol) in 1,2-dichloroethane was added *m*-CPBA (4.3 g, 19.30 mmol, 77 %) at 0° C, then the mixture was heated to reflux overnight. The reaction mixture was cooled to room temperature., diluted with CH_2Cl_2, the pH was adjusted to 8 with saturated aq. $NaHCO_3$. The mixture was extracted with CH_2Cl_2. The combined organic layers washed with water and

brine. Drying over anhydrous $MgSO_4$ and concentration of the organic layer in *vacuo* give a brownness oil. The residue was purified by silica gel column chromatography (petroleum ether/ ethyl acetate v/v 20/1-10/1) to give the compound ethyl 2-(6-(4-chlorophenoxy)hexyl)oxirane-2-carboxylate **4-009** as a light yellow oil (1.3 g, 63 %). **Chemical Formula:** $C_{17}H_{23}ClO_4$, **Molecular weight:** 326.8170. **^{1}H-NMR** (300MHz, $CDCl_3$): ppm δ 7.23(d, J = 9.0 Hz, 2H), 6.82 (d, J = 9.0 Hz, 2H), 4.32-4.14 (m, 2H), 3.92 (t, J = 9.0 Hz, 2H), 3.04 (d, J = 6.0 Hz, 1H), 2.79 (d, J = 6.0 Hz, 1H), 2.15-2.06 (m, 2H), 1.83-1.73 (m, 2H), 1.51-1.37 (m, 6H), 1.30 (t, J = 6.0 Hz, 3H). **^{13}C-NMR** (75MHz, $CDCl_3$): ppm δ 170.40, 157.68, 129.24, 125.30, 115.73, 68.15, 61.58, 57.00, 51.83, 31.17, 29.22, 29.03, 25.81, 24.71, 14.12. **HRMS** (ESI^+)**:** Calculated for $C_{17}H_{23}ClO_4Na$ $[M+Na]^+$ 349.1177, found: 349.1176.

Synthesis of 2-(6-(4-chlorophenoxy)hexyl)oxirane-2-carboxylic acid **(4-010)**

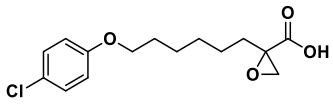

The ethyl 2-(6-(4-chlorophenoxy)hexyl)oxirane-2-carboxylate **4-009** (2.0 g, 6.12 mmol) was added to a solution of KOH (360 mg, 6.43 mmol) in aqueous EtOH (EtOH/H_2O v/v 9/1) at room temperature, and the reaction completion was monitored by TLC. The solvent was concentrated under *vacuo* and the resulting residue was dissolved in 1M HCl and washed with ethyl acetate, the aqueous layer was acidified and extracted with ethyl acetate. The combined organic layers were washed with water and brine. Drying over anhydrous $MgSO_4$ and concentration of the organic layer in *vacuo* give a yellow residue. The residue was purified by silica gel column chromatography (CH_2Cl_2/ MeOH v/v 50/1) to give the compound 2-(6-(4-chlorophenoxy)hexyl)oxirane-2-carboxylic acid **4-010** as a yellow solid (1.6 g, 88 %). **Chemical Formula:** $C_{15}H_{19}ClO_4$, **Molecular weight:** 298.7630. **^{1}H-NMR** (300MHz, $CDCl_3$): ppm δ 10.13 (br, 1H), 7.21(d, J = 9.0 Hz, 2H), 6.80 (d, J = 9.0 Hz, 2H), 3.90 (t, J = 9.0 Hz, 2H), 3.08 (d, J = 6.0 Hz, 1H), 2.87 (d, J = 6.0 Hz, 1H), 2.19-2.13 (m, 1H), 1.79-1.69 (m, 2H), 1.67-1.66 (m, 1H), 1.60-1.40 (m, 6H). **^{13}C-NMR** (75MHz, $CDCl_3$): ppm δ 174.24, 157.65, 129.25, 125.32, 115.73, 68.11, 57.18, 52.25, 30.52, 29.16, 29.01, 25.79, 24.59. **HRMS** (ESI^+)**:** Calculated for $C_{15}H_{19}ClO_4Na$ $[M+Na]^+$ 321.0861, found: 321.0864.

Synthesis of (2-hydroxyethyl)pyridyl disulfide **(4-018)**

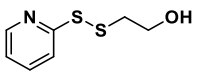

The (2-hydroxyethyl)pyridyl disulfide **4-018** was prepared following a procedure previously reported by Ryo Horikawa et al. [9] 2,2′-Dipyridyldisulfide **4-016** (1.5 g, 13.35 mmol) was dissolved in fresh MeOH 20 mL. AcOH 0.5

[9] Horikawa R, Sunayama H, Kitayama Y, et al. A programmable signaling molecular recognition nanocavity prepared by molecular imprinting and post-imprinting modifications[J]. Angewandte Chemie International Edition, 2016, 55(42): 13023-13027.

ml was then added at room temperature. To this mixture, a solution of 2-mercaptoethanol **4-017** (460 µL, 4.45 mmol) in MeOH 5 mL was added dropwise at room temperature over a 30 min period under continuous stirring. The reaction mixture was further stirred at room temperature overnight. The solvent was evaporated to give a yellow oil, which was then purified by silica gel column chromatography (petroleum ether/ ethyl acetate v/v 10/1) to give the compound (2-hydroxyethyl)pyridyl disulfide **4-018** as a light yellow oil (777 mg, 81 %). **Chemical Formula:** $C_7H_9NOS_2$, **Molecular weight:** 187.2750. **^{1}H-NMR** (300MHz, $CDCl_3$): ppm δ 8.51-8.49 (m, 1H), 7.61-7.55 (m, 1H), 7.41-7.38 (m, 1H), 7.17-7.12 (m, 1H), 5.74 (s, 1H), 3.80 (t, J = 9.0 Hz, 2H), 2.95 (t, J = 4.0 Hz, 2H)**, ^{13}C-NMR** (75MHz, $CDCl_3$): ppm δ 159.13, 149.79, 136.89, 121.82, 121.49, 58.30, 42.59. **HRMS** ($APCI^+$)**:** Calculated for $C_7H_{10}NOS_2$ $[M+H]^+$ 188.0198, found: 188.0199.

Synthesis of 2-(pyridin-2-yldisulfaneyl)ethyl-2-(6-(4-chlorophenoxy)hexyl)oxirane-2-carboxylate **(4-019)**

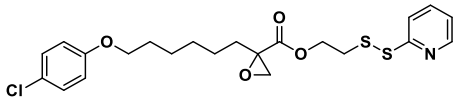

The Etomoxir **4-010** (200 mg, 0.670 mmol) and (2-hydroxyethyl)pyridyl disulfide **4-018** (131 mg, 0.736 mmol) were dissolved in CH_2Cl_2, followed by addition of DMAP (25 mg, 0.200 mmol), EDCI (193 mg, 1.00 mmol), HOBt (136 mg, 1.00 mmol) and DIPEA (166 µL, 1.00 mmol). The mixture was stirred at room temperature for overnight. After the mixture was diluted with CH_2Cl_2 and washed with water and brine. Drying over anhydrous $MgSO_4$ and concentration of the organic layer in *vacuo* give a yellow oil. The oil was purified by silica gel column chromatography (petroleum ether/ ethyl acetate v/v 10/1) to give the compound 2-(pyridin-2-yldisulfaneyl)ethyl 2-(6-(4-chlorophenoxy)hexyl)oxirane-2-carboxylate **4-019** as a yellow oil (224 mg, 71 %). **Chemical Formula:** $C_{22}H_{26}ClNO_4S_2$, **Molecular weight:** 468.0230. **^{1}H-NMR** (300MHz, $CDCl_3$): ppm δ 8.46-8.43 (m, 1H), 7.65-7.61 (m, 2H), 7.18 (dd, J = 3.0, 9.0 Hz, 2H), 7.10-7.05 (m, 1H), 6.78 (dd, J = 9.0 Hz, 2H), 4.48-4.31 (m, 2H), 3.88 (t, J = 6.0 Hz, 2H), 3.06-3.02 (m, 3H), 2.77 (d, J = 6.0 Hz, 1H), 2.10-2.02 (m, 1H), 1.76-1.59 (m, 3H), 1.52-1.35 (m, 6H). **^{13}C-NMR** (75MHz, $CDCl_3$): ppm δ 169.96, 159.09, 157.39, 149.56, 136.85, 129.00, 125.01, 120.77, 119.71, 115.50, 67.92, 62.83, 56.72, 51.75, 36.80, 30.89, 28.93, 25.63, 24.51. **HRMS** (ESI^+)**:** Calculated for $C_{22}H_{27}ClNO_4S_2$ $[M+H]^+$ 468.1065, found: 468.1065.

Synthesis of ethyl 2-(4-phenylcyclohexylidene) acetate **(4-023)**

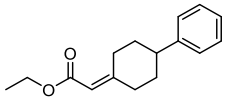

To the solution of sodium hydride NaH (60 wt % in mineral oil, 1.6 g, 36.16 mmol) was added in portions to a solution of triethyl

phosphonoacetate (7.6 mL, 36.16 mmol) in THF (25.0 mL) at 0°C. After the addition was complete the reaction mixture was stirred at ambient temperature for 30 minutes before added dropwise a solution of 4-phenylcyclohexanone (**59**) (6.0 g, 34.43 mmol) in THF (8.0 mL). After 30 minutes at ambient temperature the reaction as indicated by TLC, the reaction mixture was poured into 5% aq. $KHSO_4$ and extracted with diethyl ether. The organic layer was washed with water, brine, dried over $MgSO_4$, filtered and concentrated in *vacuo*. The residue was purified by silica gel column chromatography (petroleum ether/ ethyl acetate 100/1) to give the compound ethyl 2-(4-phenylcyclohexylidene) acetate **4-023** as a colorless oil (7.5 g, 89.0%). **Chemical Formula:** $C_{16}H_{20}O_2$, **Molecular weight:** 244.3340. **^{1}H-NMR** (300MHz, $CDCl_3$): ppm δ 7.20-7.16 (m, 5H), 5.68 (s, 1H), 4.12 (q, J = 6.0 Hz, 2H), 2.78-2.68 (m, 1H), 2.43-2.29 (m, 2H), 2.10-2.06 (m, 2H), 1.72-1.54 (m, 2H), 1.17-1.22 (m, 5H). **^{13}C-NMR** (75MHz, $CDCl_3$): ppm δ 166.70, 161.78, 146.00, 128.46, 126.79, 126.23, 113.81, 59.58, 44.10, 37.72, 35.62, 34.83, 29.77, 29.47, 14.38.

Synthesis of *trans* ethyl 2-(4-phenylcyclohexyl)acetate **(4-024*trans*)**

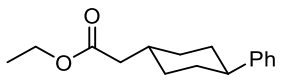

To a solution of ethyl 2-(4-phenylcyclohexylidene) acetate **4-023** (6.0 g, 24.56 mmol) in EtOH (50.0 mL) was added 10 % Pd/C (600 mg). The reaction mixture was stirred at ambient temperature for 3 h under an atmospheric pressure of hydrogen. The catalyst was removed by filtration and the filtrate was concentrated in vacuo to provide ethyl 2-(4-phenylcyclohexyl)acetate **4-024** as a cololess oil (5.9 g, 97 %) as a mixture of *cis* and *trans* isomers (*trans* /*cis*=2.8:1). The *trans* ethyl 2-(4-phenylcyclohexyl)acetate was prepared following a procedure previously reported by Vince S. C. Yeh et al.[10] To a solution of ethyl 2-(4- phenylcyclohexyl)acetate **4-024** (15.0 g, 60.89 mmol) in the ethanol, the aqueous solution of LiOH (10.0 g in 50 ml water) was added, and the resulting reaction mixture was warmed to 50 °C. After 1 h, the *trans* Li-carboxylate crystallized from the reaction mixture as a thick slurry, and additional water was added to facilitate mixing, which continued at 50 °C for an additional 6 h. The hydrolysis was complete by TLC, and the reaction mixture was cooled to room temperature. The *trans* Li salt was collected by filtration and washed with aqueous 5 % LiOH (2 × 30 ml). The wet cake was partitioned between ethyl acetate 100 ml and 6 M HCl 50 ml, and the suspension was mixed until all solids were dissolved. After separation of the layers, the ethyl acetate layer was concentrated by rotary evaporation, and the residue was treated with EtOH, which was then removed in the same manner, to give the *trans* 2-(4-

[10] Yeh V S C, Beno D W A, Brodjian S, et al. Identification and preliminary characterization of a potent, safe, and orally efficacious inhibitor of acyl-CoA: diacylglycerol acyltransferase 1[J]. Journal of medicinal chemistry, 2012, 55(4): 1751-1757.

phenylcyclohexyl)acetic acid **4-031*trans*** as a white solid, directly to the next step. The residue was dissolved in EtOH 100 ml and H_2SO_4 0.3 mL was added. The reaction mixture was heated to reflux and mixed overnight. The solution was cooled to room temperature. After the mixture was concentrated to a volume of approximately 10 mL by rotary evaporation, the water and ethyl acetate was added, the layers were separated, and the organic layer was washed with saturated aqueous $NaHCO_3$ and brine, dried over $MgSO_4$, filtered and concentrated in *vacuo*. The residue was purified by silica gel column chromatography (petroleum ether/ ethyl acetate 50/1-20/1) to give the compound *trans* ethyl 2-(4-phenylcyclohexylidene) acetate **4-024*trans*** as a colorless oil (4.9 g, 33 %, *trans* /*cis*=100:7). **Chemical Formula:** $C_{16}H_{22}O_2$, **Molecular weight:** 246.3500 **^{1}H-NMR** (300MHz, $CDCl_3$): ppm δ 7.34-7.17 (m, 5H), 4.16 (q, J = 6.0 Hz, 2H), 2.54-2.44 (m. 1H), 2.24 (d, J = 6.0 Hz, 2H), 1.94-1.81 (m, 5H), 1.59-1.44 (m, 2H), 1.27 (t, J = 6.0 Hz, 3H), 1.18-1.13 (m, 2H). **^{13}C-NMR** (75MHz, $CDCl_3$): ppm δ 173.06, 147.33, 128.32, 126.80, 125.92, 60.19, 44.09, 42.09, 34.59, 33.90, 33.22, 14.32.

Synthesis of *trans* ethyl 2-(4-(4-(2-bromo-2-methylpropanoyl)phenyl)cyclohexyl)acetate **(4-026)**

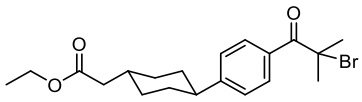

Anhydrous $AlCl_3$ (4.87 g, 36.53 mmol) was added in portions to a solution of *trans* ethyl 2-(4-phenylcyclohexylidene) acetate **4-024*trans*** (3.0g, 12.18 mmol) in CH_2Cl_2 at 0 °C followed by the drop wise addition of 2-bromo-2-methylpropanoyl bromide (1.6 mL, 13.40 mmol). After 1.5 h at 0 °C the reaction mixture was poured into ice water and extracted with $CHCl_3$. The combined organic layers were washed with saturated aq. $NaHCO_3$ and brine, dried over $MgSO_4$, filtered and concentrated in *vacuo*. The residue was purified by silica gel column chromatography (petroleum ether/ ethyl acetate 50/1-20/1) to give the compound *trans* ethyl 2-(4-(4-(2-bromo-2-methylpropanoyl)phenyl)cyclohexyl)acetate **4-026** as a light yellow oil (3.7 g, 76 %). **Chemical Formula:** $C_{20}H_{27}BrO_3$, **Molecular weight:** 395.3370. **^{1}H-NMR** (300MHz, $CDCl_3$): ppm δ 8.10 (dd, J = 3.0, 6.0 Hz, 2H), 7.27 (dd, J = 3.0, 6.0 Hz, 2H), 4.15 (q, J = 6.0 Hz, 2H), 2.57-2.49 (m, 1H), 2.24 (d, J = 9.0 Hz, 2H), 2.03 (s, 6H), 1.93-1.84 (m, 5H), 1.59-1.46 (m, 2H), 1.27 (t, J = 6.0 Hz, 3H), 1.19-1.14 (m, 2H). **^{13}C-NMR** (75MHz, $CDCl_3$): ppm δ 196.25, 172.98, 152.38, 132.34, 130.55, 126.61, 60.47, 60.24, 44.11, 41.98, 34.46, 33.53, 33.00, 31.70, 14.32.

Synthesis of *trans* ethyl 2-(4-(4-(4-amino-7,7-dimethyl-7*H*-pyrimido[4,5-b] [1,4]oxazin-6-yl)phenyl) cyclohexyl)acetate **(4-028)**

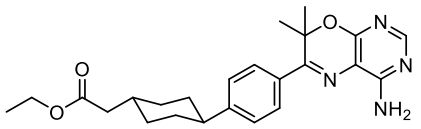

To a solution of 4 5,6-diaminopyrimidin-4(1*H*)-one (160 mg, 1.26 mmol), an appropriate *trans* ethyl 2-(4-(4-(2-bromo-2-methylpropanoyl)phenyl)cyclohexyl)acetate **4-026** (1.0 g, 2.53 mmol), and 1 M HCl (1.26 ml, 1.26mmol) in 50% aqueous EtOH was heated at reflux for overnight. After cooling to ambient temperature, the mixture was concentrated to half volume, diluted with ethyl acetate, and washed with aqueous 1 M NaOH three times and brine, dried over $MgSO_4$, and concentrated in *vacuo*. The residue was purified by silica gel column chromatography (CH_2Cl_2/ MeOH 50/1) to give the compound *trans* ethyl 2-(4-(4-(4-amino-7,7-dimethyl-7*H*-pyrimido[4,5-*b*][1,4]oxazin-6-yl)phenyl)cyclohexyl)acetate **4-028** as a light yellow solid (220 mg, 21 %). **Chemical Formula:** $C_{24}H_{30}N_4O_3$, **Molecular weight:** 422.5290. **^{1}H-NMR** (300MHz, $CDCl_3$): ppm δ 8.12 (s, 1H), 7.56 (d, J = 9.0 Hz, 2H), 7.25 (d, J = 9.0 Hz, 2H), 5.59 (s, 2H), 4.13 (q, J = 7.20 Hz, 2H), 2.56-2.48 (m, 1H), 2.24 (d, J = 6.8 Hz, 2H), 1.49-1.80 (m, 5H), 1.69 (s, 6H), 1.59-1.43 (m, 2H), 1.27 (t, J = 7.2 Hz, 3H), 1.21-1.13 (m, 2H). **^{13}C-NMR** (75MHz, $CDCl_3$): ppm δ 158.91, 149.86, 147.04, 137.20, 133.33, 132.88, 126.46, 121.18, 120.33, 115.82, 115.16, 66.29, 45.84, 36.64. **HRMS** (ESI^+)**:** Calculated for $C_{24}H_{31}N_4O_3$ $[M+H]^+$:423.2390, found: 423.2390.

Synthesis of *trans* 2-(4-(4- (4-amino-7, 7-dimethyl-7*H* -pyrimido [4,5-*b*] [1,4] oxazin-6-yl) phenyl) cyclohexyl) acetic acid **(4-029)**

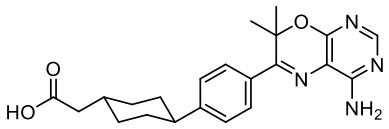

To the solution of *trans* ethyl 2-(4-(4-(4-amino-7,7-dimethyl-7H-pyrimido[4,5-b][1,4]oxazin-6-yl)phenyl)cyclohexyl)acetate **4-028** (400 mg, 0.946mmol) in ethanol and THF (*v*/*v*=6/4). was treated with 1 M NaOH in aqueous EtOH (EtOH/H_2O 90/10) at 50 °C for 1h. After this time, the solution was cooled to room temperature, and the volume was reduced by rotary evaporation to residue. The residue was added aqueous saturated ammonium chloride and the mixture was extracted with CH_2Cl_2, and the combined organic extract was washed with brine, dried over $MgSO_4$ followed by concentrated under reduced pressure. The residue was purified by silica gel column chromatography (CH_2Cl_2/MeOH 50/1-30/1) to give the below compound **4-029** (256 mg, 61 %). **Chemical Formula:** $C_{22}H_{26}N_4O_3$, **Molecular weight:** 394.4750. **^{1}H-NMR** (300MHz, $CDCl_3$): ppm δ 12.06 (s, 1H), 7.95 (s, 1H), 7.64 (d, J = 9.0 Hz, 2H), 7.30 (d, J = 9.0 Hz, 2H), 6.96 (s, 2H), 2.57-2.49 (m, 1H), 2.14 (d, J = 9.0 Hz, 2H), 1.83-1.70 (m, 5H), 1.60 (s, 6H), 1.55-1.42 (m, 2H), 1.18-1.06 (m, 2H). **^{13}C-NMR** (75MHz, $CDCl_3$): ppm δ 174.23, 162.37, 159.94, 157.72, 157.17, 149.59, 134.59, 128.79, 126.96, 108.57, 78.36, 43.65, 41.92, 34.30, 33.76, 32.98, 25.93.

Synthesis of 1*H*-benzo[*d*][1,2,3]triazol-1-yl (2-(pyridin-2-yldisulfaneyl)ethyl) carbonate **(4-032)**

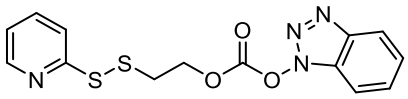

The 1*H*-benzo[*d*][1,2,3]triazol-1-yl (2-(pyridin-2-yldisulfanyl)ethyl) carbonate **4-032** was prepared following a procedure previously reported by Jyoti Roy *et al*.[11] (2-hydroxyethyl)pyridyl disulfide **4-018** (500 mg, 2.67 mmol) was dissolved in CH_2Cl_2 and Et_3N (375 μL, 2.67 mmol) and added dropwise to a solution of triphosgene (260 mg, 0.889 mmol) at 0 °C. The solution was stirred at room temperature for 1.5 h, followed by dropwise addition of a solution of hydroxybenzotriazole (360 mg, 2.67 mmol) in CH_2Cl_2 and Et_3N (375 μL, 2.67 mmol). The mixture was then stirred at room temperature for overnight and then diluted with $CHCl_3$ and washed with H_2O and brine. The organic layer was dried over anhydrous $MgSO_4$, filtered, and concentrated. The resulting yellow oil was triturated with hexane and filtered to provide the product 1*H*-benzo[*d*][1,2,3]triazol-1-yl (2-(pyridin-2-yldisulfanyl)ethyl) carbonate **4-032** as a light yellow solid (680 mg, 74%). **Chemical Formula:** $C_{14}H_{12}N_4O_3S_2$. **Molecular weight:** 348.3950. **^{1}H-NMR** (300MHz, DMSO-d_6): ppm δ 8.36 (d, J = 4.6 Hz, 1 H), 8.14 (d, J = 8.4 Hz, 1 H), 8.01 (d, J = 8.6 Hz, 1 H), 7.90 (t, J = 8.2 Hz, 1 H), 7.78–7.73(m, 2 H), 7.64 (t, J = 7.8 Hz, 1 H), 7.20 (m, 1 H), 4.71 (t, J = 5.8 Hz, 2 H), 3.39 (t, J = 6.2 Hz, 2 H). **HRMS** (ESI$^+$)**:** Calculated for $C_{14}H_{13}N_4O_3S_2$ $[M+H]^+$: 349.0424 found: 349.0422.

Synthesis of *trans* 2-(4-(4-(7,7-dimethyl-4-(((2-(pyridin-2-yldisulfaneyl)ethoxy)carbonyl) amino)-7*H*-pyrimido[4,5-b][1,4]oxazin-6-yl)phenyl)cyclohexyl)acetic acid **(4-030b)**

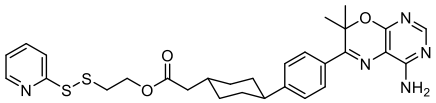

The *trans* ethyl 2-(4-(4-(4-amino-7,7-dimethyl-7*H*-pyrimido[4,5-*b*][1,4]oxazin-6-yl)phenyl) cyclohexyl) acetate **4-029** (200 mg, 0.507 mmol) was dissolved in CH_2Cl_2, followed by addition (2-hydroxyethyl)pyridyl disulfide **4-018** (114 mg, 0.608 mmol), DMAP (20 mg, 0.152 mmol), EDCI (145 mg, 0.760 mmol), HOBt (137 mg, 1.01mmol) and DIPEA (220 μl, 1.27 mmol). The mixture was stirred at room temperature for overnight and was then loaded directly onto a silica gel column and purified by flash column chromatography, eluting with 3% MeOH in $CHCl_3$, to provide the product *trans* 2-(pyridin-2-yldisulfanyl)ethyl 2-(4-(4-(4-amino-7,7-dimethyl-7*H*-pyrimido[4,5-*b*][1,4]oxazin-6-yl) phenyl) cyclohexyl) acetate **4-030b** as a brownish yellow solid (156 mg,

[11] Roy J, Nguyen T X, Kanduluru A K, et al. DUPA conjugation of a cytotoxic indenoisoquinoline topoisomerase i inhibitor for selective prostate cancer cell targeting[J]. Journal of medicinal chemistry, 2015, 58(7): 3094-3103.

54 %). **Chemical Formula:** $C_{29}H_{33}N_5O_3S_2$, **Molecular weight:** 563.7350, **^{1}H-NMR** (300MHz, $CDCl_3$): ppm δ 8.50-8.47 (m, 1H), 8.14 (s, 1H), 7.71-7.63 (m, 2H), 7.57 (d, J = 9.0 Hz, 2H), 7.26 (d, J = 9.0 Hz, 2H), 7.13-7.09 (m, 1H), 4.37 (t, J = 9.0 Hz, 2H), 3.07 (t, J = 6.0 Hz, 2H), 2.57-2.24 (m, 1H), 2.26 (d, J = 6.0 Hz, 2H), 1.98-1.84 (m, 5H), 1.75-1.64 (s, 7H), 1.58-1.47 (m, 2H), 1.28-1.12 (m, 2H). **^{13}C-NMR** (75MHz, $CDCl_3$): ppm δ 172.63, 163.55, 159.67, 159.17, 157.98, 157.10, 149.78, 149.66, 137.05, 134.36, 128.15, 126.81, 120.88, 119.82, 109.14, 79.00, 62.04, 43.88, 41.74, 37.43, 34.40, 33.66, 33.04, 26.25. **HRMS** (ESI^+)**:** Calculated for $C_{29}H_{34}N_5O_3S_2$ $[M+H]^+$:564.2098, found: 564.2094.

Chapter III:

Experimental protocols and analysis

Part A

Synthesis of 4-nitrobenzyl 2-(2-((2,6-dichlorophenyl) amino) phenyl) acetate (**5A-009**)

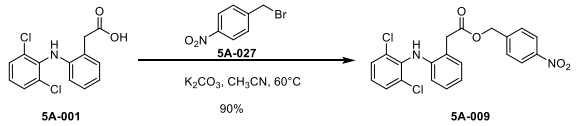

To a solution of diclofenac **5A-001** (200 mg, 84.62 mol) in acetonitrile, was added 1-(bromomethyl)-4-nitrobenzene **5A-027** at room temperature. The mixture was stirred and heated at 60 °C overnight. The reaction mixture was allowed to cool to room temperature and concentrated under reduced pressure, diluted with water and extracted with ethyl ether. The organic layer was dried anhydrous $MgSO_4$ and concentration of the organic layer in vacuum give the gray white solid. The oil was purified by silica gel column chromatography (petroleum ether/ ethyl acetate v/v = 10/1) to give the compound 4-nitrobenzyl 2-(2-((2,6-dichlorophenyl) amino) phenyl) acetate **5A-009** as a white solid (260 mg, 90 %). **Chemical Formula:** $C_{21}H_{16}Cl_2N_2O_4$, **Molecular weight:** 431.2690, **^{1}H-NMR** (300MHz, $CDCl_3$): ppm δ 8.18 (d, *J*= 9.0 Hz, 2H), 7.46 (d, *J*= 9.0 Hz, 2H), 7.33 (d, *J*= 6.0 Hz, 2H), 7.27-7.23 (m, 1H), 7.19-7.12 (m, 1H), 7.02-6.95 (m, 2H), 6.69 (s, 1H), 6.56 (d, *J*= 6.0 Hz, 1H), 5.27 (s, 2H), 3.90 (s, 2H). **^{13}C-NMR** (75MHz, $CDCl_3$): ppm δ 171.87, 147.87, 142.95, 142.75, 137.75, 131.05, 129.57, 129.04, 128.53, 128.42, 124.35, 123.96, 122.38, 118.58, 65.53, 38.61. **HRMS** (ESI^+): calculated for $C_{21}H_{17}Cl_2N_2O_4$ $[M+H]^+$:431.0565, found: 431.0560.

Synthesis of *N*-(2-(2-((*tert*-butyldimethylsilyl) oxy) ethyl) phenyl) -2,6-dichloroaniline (**5A-012**)

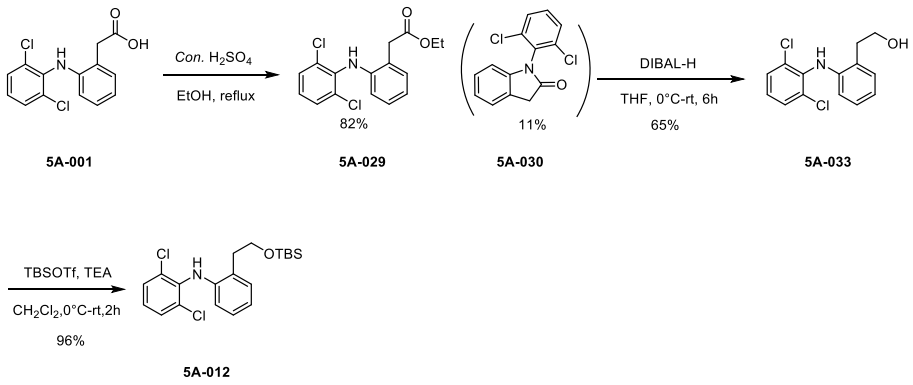

To a solution of diclofenac **5A-001** (1.0 g, 3.38 mol) dissolved in EtOH was treated dropwise concentrated sulfuric acid (45 µL, 0.84 mmol), the mixture was heated at reflux for overnight. The mixture was cooled, concentrated under reduced pressure and diluted with water. The aqueous layer was extracted with ethyl acetate, and the combined organic extract was washed with brine, dried over $MgSO_4$ followed by concentrated under reduced pressure to afford crude ethyl 2-(2-((2,6-dichlorophenyl)amino) phenyl) acetate as a yellow solid. The solid was purified by silica gel column chromatography (petroleum ether/ ethyl acetate v/v = 10/1) to give the compound 4 ethyl 2-(2-((2,6-dichlorophenyl) amino)phenyl) acetate **5A-029** as a white solid (890 mg, 82 %). **Chemical Formula:** $C_{16}H_{15}Cl_2NO_2$, **Molecular weight:** 324.2010, **^{1}H-NMR** (300MHz, $CDCl_3$): ppm δ 7.35 (d, *J*= 9.0 Hz, 2H), 7.25-7.22 (m, 1H), 7.16-7.09 (m, 1H), 7.01-6.92 (m, 2H), 6.56 (d, *J*= 6.0 Hz, 1H), 4.21 (q, *J*= 6.0, 12.0 Hz, 2H), 3.81 (s, 2H), 1.29 (t, *J*= 9.0 Hz, 3H).

To a solution of 4 ethyl 2-(2-((2,6-dichlorophenyl) amino)phenyl) acetate **5A-029** (800 mg, 2.47 mmol) dissolved in THF was cooled to -78 ºC. The diisobutylaluminium hydride DIBAL-H (1M solution in THF, 7.4 ml, 7.4 mmol) was added to dropwise at -78 ºC, it was them stirred at below 0ºC 2h which is was quenched with 10% Rochelle's salt solution. The mixture was then stirred for more 1h until the organic layer separates out. The mixture was extracted with ethyl acetate, and the combined organic extract was washed with brine, dried over $MgSO_4$ followed by concentrated under reduced pressure. The residue was purified by silica gel column chromatography (petroleum ether/ ethyl acetate 5/1-3/1) to give the compound 2-(2-((2,6-dichlorophenyl)amino)phenyl)ethan-1-ol **5A-033** as a yellow solid (452 mg, 65 %). **Chemical Formula:** $C_{14}H_{13}Cl_2NO$, **Molecular weight:** 282.1640, **^{1}H-NMR** (300MHz, DMSO-d_6): ppm δ 7.66 (s, 1H), 7.50 (d, *J*= 6.0 Hz, 2H), 7.19-7.13 (m, 2H), 7.01-6.95 (m, 1H), 6.82-6.76 (m, 1H), 6.18 (d, *J*= 9.0 Hz, 1H), 5.20 (t, *J*= 3.0 Hz, 1H), 3.75 (q, *J*= 3.0, 6.0 Hz, 2H), 2.85 (t, *J*= 6.0 Hz, 2H).**^{13}C-NMR** (75MHz, DMSO-d_6): ppm δ 173.97, 144.14, 132.34, 132.26, 131.43,

131.33, 131.01, 130.08, 129.91, 129.27, 127.13, 126.60, 122.95, 120.22, 109.73, 35.85.

The compound 2-(2-((2,6-dichlorophenyl)amino)phenyl)ethan-1-ol **5A-033** (400 mg, 28.24 mmol) in dichloromethane solution of *tert*-butyidimethylsilyl chloride (324 µL, 1.49 mmol), triethylamine (316 µL, 2.27 mmol) was added under argon at 0°C. After stirring overnight at room temperature and after completion of the reaction, the mixture was washed with HCl aq (1M) and brine by extraction with CH_2Cl_2, dried over anhydrous sodium sulfate, filtered and concentrated under reduced pressure to give a colorless oil. The residue was purified by silica gel column chromatography (petroleum ether/ ethyl acetate 50/1) to give the compound *N*-(2-(2-((*tert*-butyldimethylsilyl) oxy)ethyl)phenyl)-2,6-dichloroaniline **5A-012** as a colorless solid (450 mg, 96.0%). **Chemical Formula:** $C_{20}H_{27}Cl_2NOSi$, **Molecular weight:** 396.4270, **^{1}H-NMR** (300MHz, $CDCl_3$): ppm δ 7.54 (d, *J*= 8.0 Hz, 2H), 7.24 (t, *J*= 8.1 Hz, 1H), 7.13-7.08 (m, 1H), 6.98-6.89 (m, 2H), 6.75-6.69 (m, 1H), 6.08 (d, *J*= 7.6 Hz, 1H), 3.87 (t, *J*= 6.5 Hz, 2H), 2.91 (t, *J*= 6.3 Hz, 2H), 0.83 (s, 9H), 0.00 (s, 6H). **^{13}C-NMR** (75MHz, $CDCl_3$): ppm δ 150.67, 148.13, 142.51, 137.90, 137.05, 135.69, 135.25, 134.97, 133.95, 133.26, 131.31, 125.79, 119.25, 67.90, 39.72, 32.05, 23.40, 0.92.

Synthesis of 2,6-dichloro-*N*-(4-nitrobenzyl) aniline (**5A-018**)

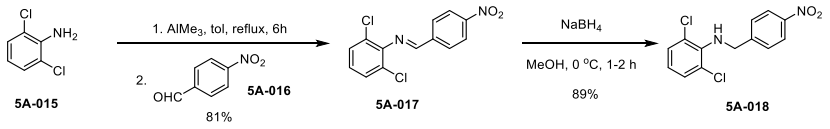

To a solution of 2,6-dichloroaniline **5A-015** (1.0 g, 6.17 mmol) dissolved in toluene was added trimethylaluminum (3.09 mL, 2.0 M in toluene, 6.17 mmol) slowly through a syringe at room temperature, and then the mixture was heated to reflux for 6 h. After the solution was cooled to room temperature, 4-nitrobenzaldehyde **5A-016** (933 mg, 6.17 mmol) was added. The mixture was heated to reflux for another 6 h. The reaction mixture was cooled to room temperature and hydrolyzed with 5% aqueous NaOH solution. The organic product was extracted with ethyl acetate and dried over $MgSO_4$ followed by concentrated under reduced pressure. The residue was purified by silica gel column chromatography (petroleum ether/ ethyl acetate 5/1-3/1) to give the compound *N*-(2,6-dichlorophenyl)-1-(4-nitrophenyl)methanimine **5A-017** as a yellow solid (1.47 g, 81 %). **Chemical Formula:** $C_{13}H_8Cl_2N_2O_2$, **Molecular weight:** 295.1190, **^{1}H-NMR** (300MHz, $CDCl_3$): ppm δ 8.76 (s, 1H), 8.41 (d, *J*= 8.7 Hz, 2H), 8.25 (d, *J*= 8.7 Hz, 2H), 7.57 (d, *J*= 8.2 Hz, 2H), 7.22 (d, *J*= 8.0 Hz, 1 H). **^{13}C-NMR** (75MHz, $CDCl_3$): ppm δ 166.90, 150.14, 146.81, 140.53, 130.48, 129.20, 126.79, 125.10, 124.71.

To a solution of *N*-(2,6-dichlorophenyl)-1-(4-nitrophenyl) methanimine **5A-017** (1.0 g, 3.39 mmol) dissolved in methanol was cooled to 0 °C, and $NaBH_4$ (128 mg, 3.39 mmol) was added to the reaction. The mixture stirring was heating to reflux for 3h. The reaction mixture was cooled to room temperature and concentrated under reduced pressure. The residue was purified by column chromatography (petroleum ether/ ethyl acetate 10/1) to give the compound 2,6-dichloro-*N*-(4-nitrobenzyl)aniline **5A-018** as a yellow solid (895 mg, 89 %). **Chemical Formula:** $C_{13}H_{10}Cl_2N_2O_2$, **Molecular weight:** 297.1350, **^{1}H-NMR** (300MHz, DMSO-d_6): ppm δ 8.16 (d, *J*= 8.7 Hz, 2H), 7.57 (d, *J*= 8.7 Hz, 2H), 7.28 (d, *J*= 8.0 Hz, 2H), 6.81 (t, *J*= 8.0 Hz, 2H), 5.20 (t, *J*= 8.0 Hz, 1H), 4.65 (d, *J*= 7.7 Hz, 1H).**^{13}C-NMR** (75MHz, DMSO-d_6): ppm δ 149.11, 147.04, 142.07, 129.85, 129.71, 129.21, 125.24, 123.94, 49.58.

Synthesis of 2-(4-bromophenyl)-1-(2,6-dichlorophenyl) indolin-3-ol (**5A-051**)

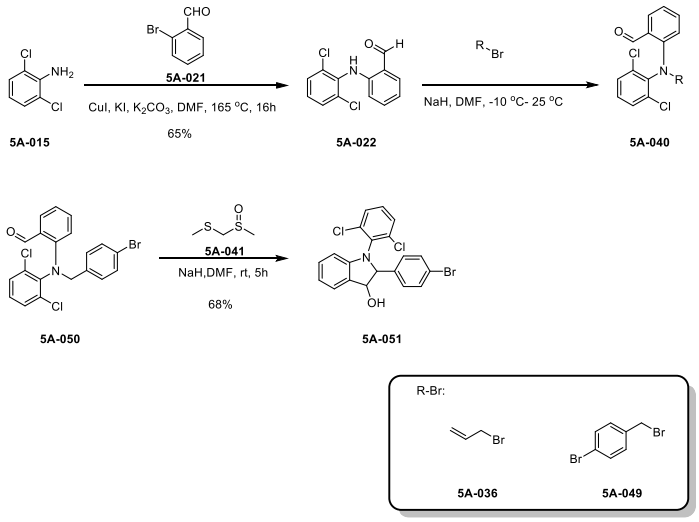

To a solution of 2,6-dichloroaniline (3.0 g, 18.52 mmol), 2-bromobenzaldehyde (723 µL, 6.17 mmol), copper(I) iodide (940 mg, 4.94 mmol), potassium iodide (1.0 g, 6.17 mmol), and potassium carbonate (1.7 g, 12.34 mmol) in the pressure tube. The pressure tube was evacuated under high vacuum and backfilled with argon, and then degassed *N*, *N*-dimethylformamide was added. The pressure tube was then sealed with a Teflon-coated screw cap and stirred for 16 h at 165 °C. The resulting dark mixture was cooled to room temperature and transferred into beaker. The ethyl acetate, ice water, and concentrated hydrochloric acid (10.0 mL) as well as charcoal and Celite were added, and the resulting slurry was vigorously stirred for 1 h. The mixture was filtered, the organic layer was dried with $MgSO_4$, filtered, and concentrated under reduced pressure. The residue was purified by silica gel column chromatography (petroleum

ether/ ethyl acetate 100/1-50/1) to give the compound 2-((2,6-dichlorophenyl) amino) benzaldehyde **5A-022** as a yellow solid (1065 mg, 65 %). **Chemical Formula:** $C_{13}H_9Cl_2NO$, **Molecular weight:** 266.1210, **^{1}H-NMR** (300MHz, $CDCl_3$): ppm δ 9.99 (s, 1H), 7.62 (dd, *J*= 1.7, 7.7 Hz, 2H), 7.42 (d, *J*= 8.1 Hz, 2H), 7.38-7.10 (m, 1H), 7.21-7.15 (m, 1H), 6.92-6.86 (m, 1H), 6.35 (d, *J*= 8.1 Hz, 1H). **^{13}C-NMR** (75MHz, $CDCl_3$): ppm δ 194.55, 147.07, 136.13, 135.33, 134.63, 134.39, 128.84, 127.76, 119.39, 117.79, 113.31, 110.00.

To a solution of 2-((2,6-dichlorophenyl) amino) benzaldehyde **5A-022** (200 mg, 0.75 mmol) dissolved in DMF was cooled to 0 °C. NaH (60% wt in mineral oil, 30 mg, 0.8 mmol) was gradually added to the reaction and stirring for 20 min at 0 °C. Then, allyl bromide (65 µL, 0.75 mmol) was added dropwise to the mixture and stirring for 2h at 0 °C. After the reaction is completed, the mixture was quenched with ice and extracted with ethyl acetate, and the combined organic extract was washed with brine, dried over $MgSO_4$ followed by concentrated under reduced pressure. The residue was purified by silica gel column chromatography (petroleum ether/ ethyl acetate 10/1) to give the compound 2-(allyl(2,6-dichlorophenyl) amino) benzaldehyde **5A-036** as an off-white solid (452 mg, 65 %). **Chemical Formula:** $C_{16}H_{13}Cl_2NO$, **Molecular weight:** 306.1860, **^{1}H-NMR** (300MHz, $CDCl_3$): ppm δ 7.65 (d, *J*= 7.7 Hz, 1H), 7.33-7.27 (m, 3H), 7.16 (d, *J*= 9.1 Hz, 1H), 7.06 (t, *J*= 8.1 Hz, 1H), 7.0-6.93 (m, 1H), 6.14-5.99 (m, 1H), 5.28-5.14 (m, 2H), 4.33 (d, *J*= 6.1 Hz, 2H). **^{13}C-NMR** (75MHz, $CDCl_3$): ppm δ 185.44, 147.21, 143.67, 140.15, 135.41, 134.40, 130.26, 129.70, 127.09, 124.56, 120.66, 119.45, 118.19, 55.25.

2-((4-bromobenzyl)(2,6-dichlorophenyl)amino)benzaldehyde (**5A-050**)

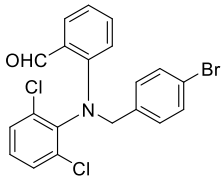

5B-050

According to the method **5A-040a**, to give the compound 2-((4-bromobenzyl)(2,6-dichlorophenyl)amino)benzaldehyde (**5A-050**) (265 mg, 83 %) as a yellow solid. **Chemical Formula:** $C_{20}H_{14}BrCl_2NO$, **Molecular weight:** 435.1420, **^{1}H-NMR** (300MHz, DMSO-d_6): ppm δ 9.85 (s, 1H, -CHO), 7.55-7.48 (m, 7H), 7.47-7.40 (m, 1H), 7.34-7.27 (m, 1H), 7.10-6.98 (m, 2H), 4.92 (s, 2H). **^{13}C-NMR** (75MHz, DMSO-d_6): ppm δ 190.73, 149.67, 145.52, 136.74, 134.67, 131.85, 130.97, 130.39, 129.73, 127.31, 127.11, 120.71, 54.91.

To a solution of 2-((4-bromobenzyl)(2,6-dichlorophenyl)amino)benzaldehyde **5A-050** (200 mg, 0.46 mmol) dissolved in DMF, and methyl((methylsulfinyl) methyl)sulfane (56 µL, 0.55 mmol), NaH (60% wt in mineral oil, 22 mg, 0.55 mmol) was added to the reaction and stirring for room temperature overnight. After the reaction was completed, the mixture was quenched with ice

and extracted with ethyl acetate, and the combined organic extract was washed with brine, dried over $MgSO_4$ followed by concentrated under reduced pressure. The residue was purified by silica gel column chromatography (petroleum ether/ ethyl acetate 10/1) to give the compound 2-(4-bromophenyl)-1-(2,6-dichlorophenyl)-1*H*-indole **5A-051** as a yellow solid (130 mg, 68 %). **Chemical Formula:** $C_{20}H_{14}BrCl_2NO$, **Molecular weight:** 435.1420, **^{1}H-NMR** (300MHz, DMSO-d_6): ppm δ 7.49-7.45 (m, 4H), 7.36-7.23 (m, 4H), 7.07 (t, *J*= 8.9 Hz, 1H), 6.80 (t, *J*= 6.7 Hz, 1H), 6.08 (d, *J*= 6.5 Hz, 1H), 5.97 (d, *J*= 8.0 Hz, 1H), 5.40-5.30 (m, 2H).**^{13}C-NMR** (75MHz, DMSO-d_6): ppm δ 147.05, 138.84, 136.24, 134.88, 134.04, 131.19, 130.40, 130.09, 129.94, 129.29, 128.79, 124.53, 121.16, 118.79, 107.08, 79.77, 75.68. **HRMS** (ESI^+): calculated for $C_{20}H_{14}BrCl_2NNaO$ $[M+Na]^+$:455.9534, found: 455.9528.

Synthesis of methyl 1-(2,6-dichlorophenyl)-3-methyl-1,2,3,4-tetrahydroquinoline -4-carboxylate **(5A-065)**

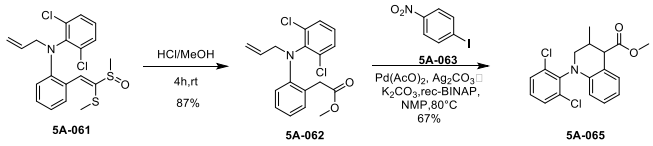

To a solution of *N*-allyl-2,6-dichloro-*N*-(2-(2-(methylsulfinyl)-2-(methylthio) vinyl) phenyl) aniline **5A-061** (150 mg, 0.36 mmol) dissolved in anhydrous methanol under argon, 5 mL fresh saturated hydrochloric methanol solution was added and the mixture was stirred for 24h at 60 °C. After the reaction was completed, and concentrated under reduced pressure. The residue was purified by silica gel column chromatography (petroleum ether/ ethyl acetate 10/1) to give the compound methyl 2-(2-(allyl(2,6-dichlorophenyl) amino) phenyl) acetate **5A-062** as a white solid (110 mg, 87 %). **Chemical Formula:** $C_{18}H_{17}Cl_2NO_2$, **Molecular weight:** 350.2390, **^{1}H-NMR** (300MHz, $CDCl_3$): ppm δ 7.32-7.21 (m, 5H), 7.13-6.96 (m, 3H), 6.08-5.93 (m, 1H), 5.26-5.10 (m, 2H), 4.34 (d, *J*= 6.1 Hz, 1H), 3.46 (s, 3H), 3.38 (s, 2H). **^{13}C-NMR** (75MHz, $CDCl_3$): ppm δ 171.49, 146.48, 142.55, 135.64, 134.91, 131.96, 129.68, 127.36, 126.78, 126.36, 122.49, 122.34, 117.76, 55.62, 51.63, 37.05.

To a solution of methyl 2-(2-(allyl(2,6-dichlorophenyl) amino) phenyl) acetate **5A-062** (150 mg, 0.43 mmol), 1-iodo-4-nitrobenzene (117 mg, 0.47 mmol), palladium acetate (II) (10 mg, 0.04 mmol), *rec*-BINAP (53 mg, 0.08 mmol), silver carbonate (236 mg, 0.86 mmol), and potassium carbonate (178 mg, 1.28 mmol) in the pressure tube. The pressure tube was evacuated under high vacuum and backfilled with argon, and then degassed *N*-Methyl-2-pyrrolidone NMP was added. The pressure tube was then sealed with a Teflon-coated screw cap and stirred for 14 h at 80 °C. The resulting dark mixture was cooled to room temperature

and the mixture dark solution was poured into $NaHCO_3$ and extracted with ethyl acetate, the organic layer was dried with $MgSO_4$, filtered, and concentrated under reduced pressure. The residue was purified by silica gel column chromatography (petroleum ether/ ethyl acetate 10/1) to give the compound methyl-1-(2,6-dichlorophenyl)-3-methyl-1,2,3,4-tetrahydroquinoline-4-carboxylate **5A-065** as an off-white solid (100 mg, 67 %). **Chemical Formula:** $C_{18}H_{17}Cl_2NO_2$, **Molecular weight:** 350.2390. **^{1}H-NMR** (300MHz, $CDCl_3$): ppm δ 7.44 (d, *J*= 8.1 Hz, 2H), 7.27-7.18 (m, 1H), 7.08 (d, *J*= 7.0 Hz, 1H), 6.98 (t, *J*= 7.7 Hz, 1H), 6.69 (t, *J*= 7.5 Hz, 1H), 5.98 (d, *J*= 8.3 Hz, 1H), 3.77 (s, 3H), 3.72-5.59 (m, 2H), 3.27-3.19 (m, 1H), 2.71-2.62 (m, 1H), 1.17 (d, *J*= 6.8 Hz, 3H). **^{13}C-NMR** (75MHz, $CDCl_3$): ppm δ 174.53, 142.17, 140.07, 137.16, 137.03, 129.75, 129.66, 129.44, 128.77, 128.30, 117.58, 117.15, 112.09, 52.16, 51.64, 50.59, 29.54, 18.36. **HRMS** (ESI^+): calculated for $C_{18}H_{18}Cl_2NO_2$ $[M+H]^+$: 350.0715, found: 350.0709.

Synthesis of methyl 2-(2-((2,6-dichlorophenyl) (3-(4-nitrophenyl) allyl) amino) phenyl) acetate (**5A-064**)

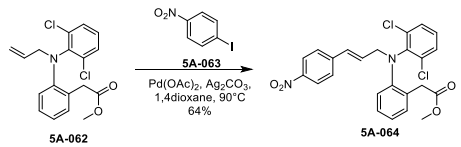

To a solution of methyl 2-(2-(allyl(2,6-dichlorophenyl) amino) phenyl) acetate **5A-062** (150 mg, 0.43 mmol), 1-iodo-4-nitrobenzene (213 mg, 0.85 mmol), palladium acetate (II) (10 mg, 0.04 mmol), and silver carbonate (354 mg, 1.28 mmol) in the pressure tube. The pressure tube was evacuated under high vacuum and backfilled with argon, and then degassed 1,4-dioxane was added. The pressure tube was then sealed with a Teflon-coated screw cap and stirred for 14 h at 90 °C. The resulting dark mixture was cooled to room temperature and the mixture dark solution was poured into $NaHCO_3$ and extracted with ethyl acetate, the organic layer was dried with $MgSO_4$, filtered, and concentrated under reduced pressure. The residue was purified by silica gel column chromatography (petroleum ether/ ethyl acetate 10/1-5/1) to give the compound 2-(2-((2,6-dichlorophenyl) (3-(4-nitrophenyl) allyl) amino) phenyl) acetate **5A-064** as a yellow solid (128 mg, 64 %). **Chemical Formula:** $C_{24}H_{20}Cl_2N_2O_4$, **Molecular weight:** 471.3340, **^{1}H-NMR** (300MHz, $CDCl_3$): ppm δ 8.13 (d, *J*= 8.8 Hz, 2H), 7.43 (d, *J*= 8.8 Hz, 2H), 7.32 (d, *J*= 8.0 Hz, 2H), 7.26-7.23 (m, 2H), 7.13-7.05 (m, 2H), 7.03-6.97 (m, 1H), 6.61-6.58 (m, 2H), 4.55 (d, *J*= 4.4 Hz, 2H), 3.47 (s, 3H), 3.39 (s, 2H). **^{13}C-NMR** (75MHz, $CDCl_3$): ppm δ 174.53, 142.17, 140.07, 137.16, 137.03, 129.75, 129.66, 129.44, 128.77, 128.30, 117.58, 117.15, 112.09, 52.16, 51.64, 50.59, 29.54, 18.36. **HRMS** (ESI^+): calculated for $C_{24}H_{21}Cl_2N_2O_4$ $[M+H]^+$: 471.0878, found: 471.0873.

Synthesis of 1-(2,6-dichlorophenyl)-3-(4-nitrobenzyl)-1,2,3,4-tetrahydroquinoline -4-carboxylic acid (**5A-067**)

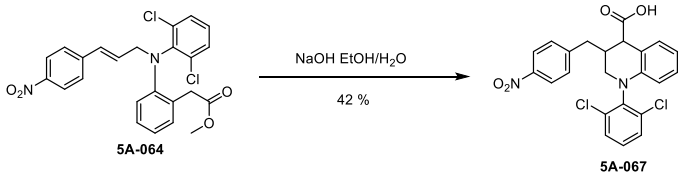

To a solution of 2-(2-((2,6-dichlorophenyl) (3-(4-nitrophenyl) allyl) amino) phenyl) acetate **5A-064** (100 mg, 0.21 mmol) dissolved in ethanol and NaOH (320 µL, 2M, 0.64 mmol) was added in the reaction stirring for 4h at 60 °C. After the reaction was completed, the mixture solution was poured into HCl (2M) and extracted with ethyl acetate, the organic layer was dried with $MgSO_4$, filtered, and concentrated under reduced pressure. The residue was purified by silica gel column chromatography (CH_2Cl_2/ Methanol 50/1-25/1 0.1% AcOH) to give the compound 1-(2,6-dichlorophenyl)-3-(4-nitrobenzyl)-1,2,3,4-tetrahydroquinoline-4-carboxylic acid **5A-067** as an off-white solid (40 mg, 42 %). **Chemical Formula:** $C_{23}H_{18}Cl_2N_2O_4$, **Molecular weight:** 457.3070, **^{1}H-NMR** (300MHz, DMSO-d_6): ppm δ 12.65 (s, 1H, -COOH), 8.18 (d, J= 8.7 Hz, 2H), 7.66-7.59 (m, 2H), 7.50-7.40 (m, 3H), 7.13 (d, J= 7.4 Hz, 1H), 6.96 (t, J= 8.0 Hz, 1H), 6.67 (t, J= 7.7 Hz, 1H), 5.84 (d, J= 8.4 Hz, 1H), 3.70 (dd, J= 3.3, 11.5 Hz, 1H), 3.48 (d, J= 3.9 Hz, 1H), 3.23 (dd, J= 3.3, 11.5 Hz, 1H), 3.02-2.75 (m, 3H).**^{13}C-NMR** (75MHz, DMSO-d_6): ppm δ 174.37, 147.99, 146.15, 141.62, 138.88, 135.87, 135.73, 130.60, 130.21, 130.07, 129.73, 128.06, 123.57, 117.40, 116.62, 111.23, 48.61, 46.31, 37.45, 34.77. **HRMS** (ESI^+): calculated for $C_{23}H_{17}Cl_2N_2O_4$ $[M-H]^-$: 455.0571, found: 455.0571.

Synthesis of 2-(2-((2,6-dichlorophenyl) (3-(4-nitrophenyl) allyl) amino) phenyl) acetic acid **(5A-066)**

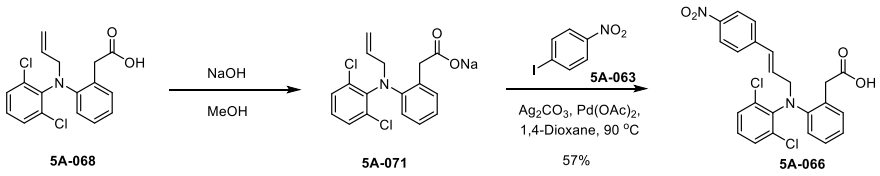

To a solution of 2-(2-(allyl(2,6-dichlorophenyl) amino) phenyl) acetic acid **5A-068** (150 mg, 0.45 mmol) dissolved in methanol and NaOH (18 mg, 0.45 mmol) was added in the reaction stirring for 1h at room temperature. After concentrated under vacuum for 12h. The mixture was used directly in the next step without purification. To a solution of sodium 2-(2-(allyl(2,6-

dichlorophenyl) amino) phenyl) acetate **5A-071**, 1-iodo-4-nitrobenzene (212 mg, 0.89 mmol), palladium acetate (II) (10 mg, 0.04 mmol), and silver carbonate (369 mg, 1.34 mmol) in the pressure tube. The pressure tube was evacuated under high vacuum and backfilled with argon, and then degassed 1,4-dioxane was added. The pressure tube was then sealed with a Teflon-coated screw cap and stirred for 14 h at 90 °C. The resulting dark mixture was cooled to room temperature and the mixture dark solution was poured into $NaHCO_3$ and extracted with ethyl acetate, the organic layer was dried with $MgSO_4$, filtered, and concentrated under reduced pressure. The residue was purified by silica gel column chromatography (CH_2Cl_2/ Methanol 50/1-25/1 0.1% AcOH) to give the compound 2-(2-((2,6-dichlorophenyl)(3-(4-nitrophenyl)allyl)amino)phenyl)acetic acid **5A-066** as a white solid (116 mg, 57 %). **Chemical Formula:** $C_{23}H_{18}Cl_2N_2O_4$, **Molecular weight:** 457.3070, **^{1}H-NMR** (300MHz, DMSO-*d_6*): ppm δ 12.00 (s, 1H, -COOH), 8.12 (d, *J*= 8.7 Hz, 2H), 7.57 (d, *J*= 8.7 Hz, 2H), 7.46-7.40 (m, 2H), 7.26-7.17 (m, 3H), 7.10 (d, *J*= 7.6 Hz, 2H), 6.97-6.90 (m, 1H), 6.72-6.66 (m, 1H), 4.50 (d, *J*= 5.3 Hz, 2H), 3.26 (s, 2H).**^{13}C-NMR** (75MHz, DMSO-*d_6*): ppm δ 172.52, 146.80, 146.42, 143.62, 142.21, 135.15, 132.55, 132.06, 130.80, 130.45, 128.40, 127.54, 127.36, 124.38, 122.52, 122.28, 54.74, 37.17, 21.48. **HRMS** (ESI^+): calculated for $C_{23}H_{17}Cl_2N_2O_4$ $[M-H]^-$: 455.0571, found: 455.0571.

ynthesis of 4-nitrobenzyl 2-(2-((2,6-dichlorophenyl) (3-(4-nitrophenyl) allyl) amino) phenyl) acetate (**5A-072**)

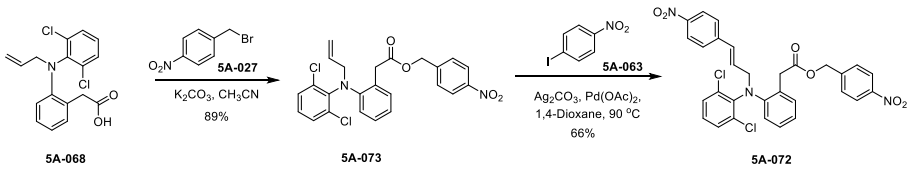

To a solution of 2-(2-(allyl(2,6-dichlorophenyl)amino)phenyl)acetic acid **5A-068** (200 mg, 0.59 mol) in acetonitrile, was added 1-(bromomethyl)-4-nitrobenzene **5A-027** (154 mg, 0.65 mol) at room temperature. The mixture was stirred and heated at 60 °C overnight. The reaction mixture was allowed to cool to room temperature and concentrated under reduced pressure, diluted with water and extracted with ethyl ether. The organic layer was dried anhydrous $MgSO_4$ and concentration of the organic layer in vacuum give the gray white solid. The solid was purified by silica gel column chromatography (petroleum ether/ ethyl acetate v/v = 5/1) to give the compound 4-nitrobenzyl 2-(2-(allyl(2,6-dichlorophenyl) amino) phenyl) acetate **5A-073** as a white solid (249 mg, 89 %). **Chemical Formula:** $C_{24}H_{20}Cl_2N_2O_4$, **Molecular weight:** 471.3340, **^{1}H-NMR** (300MHz, $CDCl_3$): ppm δ 8.19 (d, *J*= 8.8 Hz, 2H), 7.38 (d, *J*= 8.8 Hz, 2H), 7.27-7.22 (m, 4H), 7.12-7.07 (m, 2H), 7.02-6.96 (m, 2H), 6.06-5.91 (m, 1H), 5.26-5.08 (m, 2H), 4.95 (s,

2H), 4.33 (d, *J*= 6.0 Hz, 1H), 3.48 (s, 2H). **^{13}C-NMR** (75MHz, $CDCl_3$): ppm δ 170.67, 147.72, 146.66, 143.29, 142.74, 135.77, 132.13, 129.86, 128.17, 127.76, 126.96, 126.04, 123.82, 122.93, 122.60, 118.05, 64.81, 55.77, 37.19.

To a solution of methyl -nitrobenzyl 2-(2-(allyl(2,6-dichlorophenyl) amino) phenyl) acetate **5A-073** (200 mg, 0.42 mmol), 1-iodo-4-nitrobenzene (211 mg, 0.85 mmol), palladium acetate (II) (10 mg, 0.04 mmol), and silver carbonate (351 mg, 1.27 mmol) in the pressure tube. The pressure tube was evacuated under high vacuum and backfilled with argon, and then degassed 1,4-dioxane was added. The pressure tube was then sealed with a Teflon-coated screw cap and stirred for 14 h at 90 °C. The resulting dark mixture was cooled to room temperature and the mixture dark solution was poured into $NaHCO_3$ and extracted with ethyl acetate, the organic layer was dried with $MgSO_4$, filtered, and concentrated under reduced pressure. The residue was purified by silica gel column chromatography (petroleum ether/ ethyl acetate 5/1) to give the compound 2-(2-((2,6-dichlorophenyl) (3-(4-nitrophenyl) allyl) amino) phenyl) acetate **5A-072** as a yellow solid (165 mg, 66 %). **Chemical Formula:** $C_{30}H_{23}Cl_2N_3O_6$, **Molecular weight:** 592.4290, **^{1}H-NMR** (300MHz, $CDCl_3$): ppm δ 8.09 (d, *J*= 8.8 Hz, 2H), 8.02 (d, *J*= 8.8 Hz, 2H), 7.34-7.27 (m, 4H), 7.21-7.15 (m, 4H), 7.05-7.01 (m, 1H), 6.97-6.90 (m, 2H), 6.51-6.48 (m, 2H), 4.88 (s, 2H), 4.45 (d, *J*= 4.5 Hz, 2H), 3.40 (s, 2H). **^{13}C-NMR** (75MHz, $CDCl_3$): ppm δ 170.42, 147.61, 146.90, 146.42, 143.19, 143.09, 142.30, 135.60, 132.31, 131.51, 130.66, 129.89, 128.09, 127.86, 127.23, 126.88, 125.86, 123.92, 123.68, 122.73, 122.29, 64.74, 54.88, 37.09. **HRMS** (ESI^+): calculated for $C_{30}H_{24}Cl_2N_3O_6$ $[M+H]^+$: 592.1042, found: 592.1037.

Synthesis of (1-methyl-2-nitro-1*H*-imidazol-5-yl) methanol (**5A-081**)

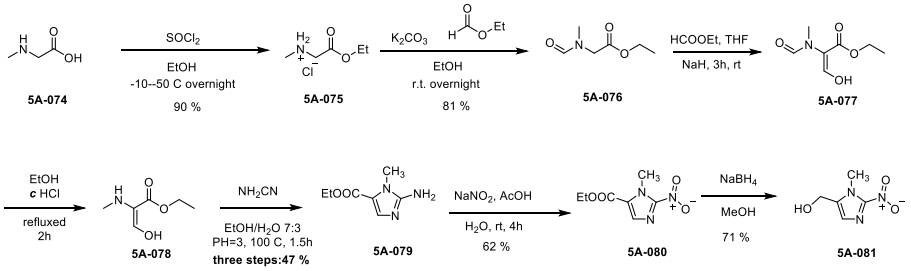

The thionyl chloride (26 mL, 360.00 mmol) was added dropwise under stirring to a solution of sarcosine (8.0 g, 90.00 mmol) in EtOH cooled in an ice-water bath, while maintaining temperature around to 10 ℃. Then the reaction mixture was gently heated at 55 ℃ overnight until the mixture became clear. Solvent and traces of thionyl chloride were removed by evaporation under reduced pressure and the solid residue was washed with Et_2O. The remaining solid was well dried under *vacuum* to afford compound 2-ethoxy-*N*-methyl-2-oxoethan-1-

aminium chloride **5A-075** (9.6 g, yield 90 %) as a white powder, which was used in the next step without further purification. **Chemical Formula:** $C_5H_{12}ClNO_2$, **Molecular weight:** 153.6055, **^{1}H-NMR** (300MHz, $CDCl_3$): ppm δ 9.68 (s, 2H), 4.22 (q, *J*= 6.9, 14.0 Hz, 2H), 3.83 (s, 2H), 2.79 (s, 3H), 1.25 (t, *J*=6.9 Hz, 3H).

The Ethyl *N*-methylglycinate hydrochloride salt **5A-074** (8.0 g, 52.43 mmol) was suspended in a mixture of EtOH and ethyl formate (v/v 8/5). Potassium carbonate (10.9 g, 78.64 mmol) was added under vigorous stirring and the suspension was stirred at rt overnight. The reaction mixture was then filtered and the precipitate was washed with EtOH. The filtrate was concentrated and dissolved in a minimum amount of water, followed by extraction with EtOAc the combined organic layers were dried over $MgSO_4$, filtered and concentrated under reduced pressure to afford compound Ethyl *N*-formyl-*N*-methylglycinate **5A-075** (6.1 g, Yield 81%) as a pale yellow liquid. To a solution of *N*-formyl sarcosine ethyl ester **5A-075** (5.0 g, 34.45 mmol) in an equal mixture of ethyl formate and THF, was added slowly NaH (60% wt in mineral oil, 2.1 g, 51.67 mmol) at ambient temperature. After the addition was completed and hydrogen release stopped and after this time a yellow suspension had formed, the reaction mixture was allowed to stirred during 3.5 h. The reaction mixture was concentrated under vacuum. The resulting solid was triturated with hexane, the hexane decanted, and the remaining solid dried *in vacuo*. EtOH and concentrated aqueous HCl were added to the solid, and the suspension heated under reflux for 2 h. The reaction mixture was filtered while hot, and the resulting colorless solid washed with boiling EtOH. The filtrate was concentrated *in vacuo* to leave an aqueous solution. The solid was diluted with EtOH and distilled water (v/v 7/3), the pH of the solution was adjusted to 3, using an aqueous 2 M solution of NaOH, and cyanamide (2.9 g, 68.89 mmol) was added. The resulting solution was heated under reflux for 90 min. After this time the solution was cooled to ambient temperature, then concentrated *in vacuo* to approximately less than the original volume. The pH was then adjusted to 8-9 using solid K_2CO_3, resulting in the formation of a precipitate. The solid was removed by filtration, washed with aqueous K_2CO_3 solution, H2O (a little), and dried *in vacuo*, to afford Ethyl 2-amino-1-methyl-1*H*-imidazole-5-carboxylate **5A-079** as a pale yellow solid (2.8 g, yield 47 %) **Chemical Formula:** $C_7H_{11}N_3O_2$, **Molecular weight:** 169.1840, **^{1}H-NMR** (300MHz, $CDCl_3$): ppm δ 7.42 (s, 1H), 4.74 (s, 2H), 4.27 (q, *J*=7.0, 14.0 Hz, 2H), 3.78 (s, 3H), 1.31 (t, *J*= 7.1 Hz, 3H), **^{13}C-NMR** (75MHz, $CDCl_3$): ppm δ 7.42, 4.74, 4.29, 3.78, 1.35, 1.30, 1.24.

To an aqueous solution of sodium nitrite (4.9g, 70.93 mmol), was added aminoimidazole **5A-079** (1.2 g, 7.09 mmol) in acetic acid in a drop wise manner. The solution was stirred at room temperature for 4 h, after this time no more nitrogen gas was evolved. the extractions were performed with CH_2Cl_2 and the combined organic layers was washed with brine, and a saturated

aqueous solution of Na_2SO_3, dried with $MgSO_4$ and filtered. The solvent was removed under reduced pressure to give the crude compound. The residue was purified by silica gel column chromatography (Petroleum ether/ EtOAc 10/1 to 5/1) to give the compound Ethyl 1-methyl-2-nitro-1*H*-imidazole-5-carboxylate **5A-080** as a light yellow solid (910 mg, 64 %): **Chemical Formula:** $C_7H_9N_3O_4$, **Molecular weight:** 199.1660, **^{1}H-NMR** (300MHz, $CDCl_3$): ppm δ 7.73 (s, 1H,), 4.39 (q, *J*= 7.3, 14.2 Hz, 2H), 4.34 (s, 3H), 1.40 (t, *J*= 7.2 Hz, 3H).

To a solution of nitroimidazole **5A-080** (400 mg, 2.01 mmol) in anhydrous THF and MeOH (v/v, 12/1) at 0 °C, was added sodium borohydride (228 mg, 6.03 mmol) portion wise. The reaction mixture was stirred at 0 °C for 45 min, and then at ambient temperature for 1 h. The reaction mixture was cooled to 0 °C, quenched by addition of ice and the pH adjusted to 7 using 1 M aqueous HCl. The aqueous mixture was saturated with solid NaCl, and the organic components extracted with ethyl acetate. The organic layers were combined, washed with saturated aqueous $NaHCO_3$ and brine, dried with $MgSO_4$ and filtered. The solvent was removed under reduced pressure to give the crude compound. The residue was purified by silica gel column chromatography (CH_2Cl_2/ MeOH 50/1-25/1) to give the compound (1-methyl-2-nitro-1H-imidazol-5-yl) methanol **5A-081** as a light yellow solid (226 mg, 71 %). **Chemical Formula:** $C_5H_7N_3O_3$, **Molecular weight:** 157.1290, **^{1}H-NMR** (300MHz, DMSO-d_6): ppm δ 7.11 (s, 1H), 5.49 (t, *J*= 5.4 Hz, 1H), 4.54 (d, *J*= 5.4 Hz, 2H), 3.91 (s, 3H).

Synthesis of (4-((4-(diethylamino) phenyl) diazenyl) phenyl) methanol (**5A-085**)

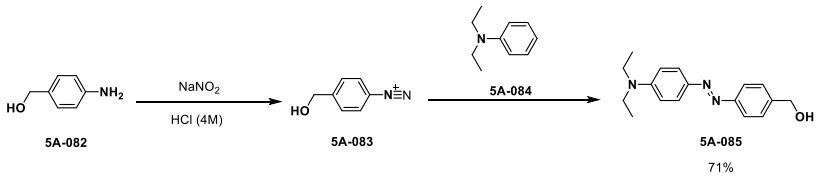

To a solution of (4-aminophenyl)methanol **5A-082** (500 mg, 4.06 mmol) dissolved in HCl (4M) was cooled 0 °C. and ice cooled aqueous solution of $NaNO_2$ (280 mg, 4.06 mmol) was added dropwise to the mixture. The mixture solution was stirring 30 min, and then the resulted diazonium solution was added to *N*,*N*-diethylaniline **5A-084** (650 µL, 4.06 mmol) keeping the temperature below 4 °C. The mixture was left under continuous stirring for 1 h, and then neutralized with saturated sodium acetate and extracted with ethyl ether. The organic layer was dried anhydrous $MgSO_4$ and concentration of the organic layer in vacuum to give the yellow solid. The solid was purified by silica gel column chromatography (CH_2Cl_2/ Methanol v/v = 50/1) to give the compound (4-((4-(diethylamino)phenyl)diazenyl)phenyl)methanol **5A-085** as a red solid (816 mg, 71 %). **Chemical Formula:** $C_{17}H_{21}N_3O$, **Molecular weight:** 283.3750,

[1]H-NMR (300MHz, $CDCl_3$): ppm δ 7.98-7.80 (m, 4H), 7.46 (d, J= 8.7 Hz, 2H), 6.72 (d, J= 8.7 Hz, 2H), 4.75 (s, 2H), 3.46 (q, J= 7.0, 14.0 Hz, 4H), 1.23 (t, J= 7.0 Hz, 6H). **[13]C-NMR** (75MHz, $CDCl_3$): ppm δ152.82, 150.15, 143.09, 141.80, 127.49, 125.32, 122.32, 110.97, 65.11, 44.72, 12.69.

Synthesis of C_{14}-substitute- tetrandrine (**5A-088**)

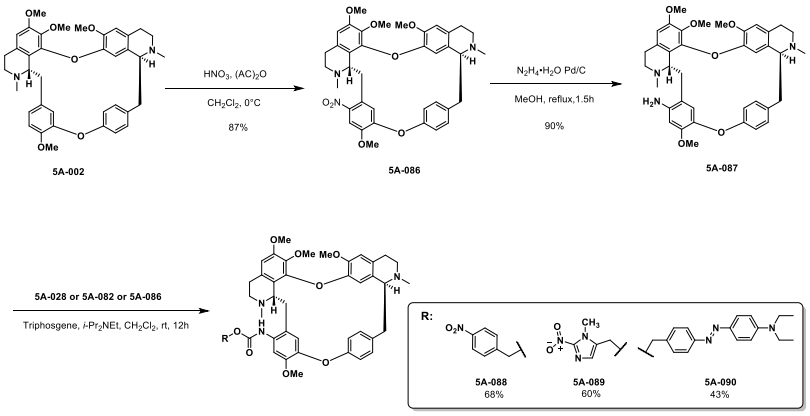

Under the protection of an argon atmosphere, concentrated HNO_3 (69%, 1.2 mL, 19.20 mmol) was slowly added dropwise to a solution of $(CH_3CO)_2O$ (3.0 mL, 32.00 mmol) at -10 °C. After 10 min, the reaction mixture was warmed up to room temperature, stirring was continued for 20 min and tetrandrine **5A-002** (1.0 g, 1.60 mmol) dissolved in dry CH_2Cl_2 was added dropwise. The reaction was monitored by thin layer chromatography. Upon completion, the reaction mixture was quenched with saturated aqueous solution of sodium bicarbonate, extracted with CH_2Cl_2, dried over anhydrous magnesium sulfate and filtered. The solvent was removed under reduced pressure. The residue was purified by silica gel chromatography from (CH_2Cl_2/MeOH 50/1 v/v, 0.1% TEA) to afford compound C_{14}-nitro-tetrandrine **5A-086** as a yellow solid (930 mg, 87 %). **Chemical Formula:** $C_{38}H_{41}N_3O_8$, **Molecular weight:** 667.7590, **[1]H-NMR** ($CDCl_3$, 400 MHz) ppm δ: 7.42 (s, 1H), 7.37 (dd, J = 4.0, 8.0 Hz, 1H), 7.12 (dd, J = 4.0, 8.0 Hz, 1H), 6.77 (dd, J = 4.0, 8.0 Hz, 1H), 6.54 (s, 1H), 6.52 (s, 1H), 6.30 (s, 1H), 6.28 (dd, J = 4.0, 8.0 Hz, 1H), 5.98 (s, 1H), 3.98 (s, 3H), 3.91 (dd, J = 4.0, 12.0 Hz, 1H), 3.75 (s, 3H), 3.69-3.63 (m, 1H), 3.52-3.49 (m, 2H), 3.38 (s, 3H), 3.30-3.25 (m, 1H), 3.18 (s, 3H), 2.96-2.73 (m, 7H), 2.63 (s, 3H), 2.53 (d, J = 12.0 Hz, 1H), 2.35 (m, 1H), 2.21 (s, 3H); **[13]C-NMR** ($CDCl_3$, 100 MHz) ppm δ: 152.3, 152.1, 151.5, 148.7, 148.2, 146.5, 144.2, 143.5, 137.5, 136.4, 133.1, 130.5, 130.4, 128.9, 128.1, 127.6, 121.6, 121.4, 121.3, 119.9, 117.2, 112.5, 108.2, 105.8, 63.6, 61.7, 60.3, 56.3, 55.8, 55.7, 45.3, 43.2, 42.8, 41.5, 37.9, 36.8, 25.3, 21.6.

The mixture of C_{14}-nitro-tetrandrine **5A-086** (1.0 g, 1.50 mmol) with palladium as a carbon hydrogenation catalyst (10%, 100 mg) was added to hydrazine hydrate (85%, 1.65 mL, 45.00 mmol) in methanol, and stirred at 80 °C. The reaction was completed in 2 h. The mixture was cooled down to room temperature and filtered to remove the catalyst. The filtrate was evaporated by rotary evaporation under reduced pressure. The residue was diluted with CH_2Cl_2, washed with water, dried over anhydrous magnesium sulfate and filtered. The solvent was removed under reduced pressure. The crude product was recrystallized from petroleum ether and acetone to give compound C_{14}-amino-tetrandrine **5A-087** as a light-yellow solid (860 mg, 90 %). **Chemical Formula:** $C_{38}H_{43}N_3O_6$, **Molecular weight:** 637.7770, **^{1}H-NMR** ($CDCl_3$, 400 MHz) ppm δ: 7.28 (dd, J = 4.0, 8.0 Hz, 1H), 7.18 (dd, J = 4.0, 8.0 Hz, 1H), 6.60 (dd, J = 4.0, 8.0 Hz, 1H), 6.50 (s, 1H), 6.46 (s, 1H), 6.31 (s, 1H), 6.29 (s, 1H), 6.12 (dd, J = 4.0, 8.0 Hz, 1H), 5.87 (s, 1H), 3.94 (d, J = 12.0 Hz, 1H), 3.87 (s, 3H), 3.80 (dd, J = 4.0, 12.0 Hz, 1H), 3.73 (s, 3H), 3.64 (m, 1H), 3.42 (m, 1H), 3.35 (s, 3H), 3.22 (dd, J = 4.0, 8.0 Hz, 1H), 3.11 (s, 3H), 2.88 (m, 7H), 2.61 (s, 3H), 2.42 (s, 3H), 2.35 (m, 2H); **^{13}C-NMR** ($CDCl_3$, 100 MHz) ppm δ: 156.6, 151.6, 149.4, 148.7, 148.5, 144.2, 142.0, 140.8, 138.0, 133.2, 132.6, 129.3, 128.0, 127.6, 127.4, 122.6, 122.1, 121.3, 120.9, 120.5, 120.2, 112.3, 105.8, 100.6, 64.2, 61.5, 59.9, 56.1, 55.6, 55.5, 44.9, 43.2, 42.3, 40.8, 40.0, 38.7, 24.6, 20.6.

To a solution of C_{14}-amino-tetrandrine **5A-087** (200 mg, 0.31 mmol) and triphosgene (46 mg, 0.15 mmol) in CH_2Cl_2, was added DIPEA (116 µL, 0.63 mmol) at room temperature. The mixture was stirred 30 min, and then **5A-028** (58 mg, 0.38 mol) added into the reaction for overnight at room temperature. After the reaction was completed and diluted with water and extracted with CH_2Cl_2. The organic layer was dried anhydrous $MgSO_4$ and concentration of the organic layer in vacuum give the brown solid. The solid was purified by silica gel column chromatography (CH_2Cl_2/ MeOH v/v = 50/1, 0.1% TEA) to give the compound C_{14}-4-nitrobenzyl carbamate-tetrandrine **5A-088** as a yellow solid (174 mg, 68 %). **Chemical Formula:** $C_{46}H_{48}N_4O_{10}$, **Molecular weight:** 816.9080, **^{1}H-NMR** ($CDCl_3$, 500 MHz) ppm δ 12.33 (br, 1H, -CONH-), 8.25 (d, J = 8.7 Hz, 2H), 7.66 (s, 1H), 7.57 (d, J = 8.7 Hz, 2H), 7.31 (dd, J = 2.4, 8.4 Hz, 1H), 7.21 (dd, J = 2.4, 8.4 Hz, 1H), 6.58 (dd, J = 2.5, 8.4 Hz, 1H), 6.52(s, 1H), 6.48 (s, 1H), 6.30 (s, 1H), 6.14 (dd, J = 2.5, 8.4 Hz, 1H), 5.31 (s, 2H), 3.95-3.91 (m, 4H), 3.85-3.81 (m, 4H), 3.74 (s, 3H), 3.65-3.46 (m, 2H), 3.36 (3H, s), 3.32-3.28 (m, 1H), 3.10 (s, 3H), 3.04-2.87 (m, 5H), 2.81-2.69 (m, 2H), 2.61 (s, 3H), 2.45 (s, 3H). **^{13}C-NMR** ($CDCl_3$, 125 MHz) ppm δ 156.58, 154.50, 152.52, 149.63, 149.17, 148.86, 147.92, 145.20, 144.98, 144.61, 138.55, 133.99, 133.27, 133.01, 130.07, 128.50, 128.19, 127.66, 127.33, 124.93, 124.21, 124.03, 121.66, 121.45, 121.18, 112.68, 106.27, 105.33, 65.06, 64.70, 64.12, 61.46, 60.51, 56.63, 56.15, 55.97, 53.86, 45.41, 43.09, 42.68, 40.88, 40.28, 39.31, 30.10, 24.93, 21.02. **HRMS** ($APCI^+$): calculated for $C_{46}H_{49}N_4O_{10}$ $[M+H]^+$: 817.3449, found: 817.3443.

C_{14}- (1-methyl-2-nitro-1*H*-imidazol-5-yl) methyl carbamate-tetrandrine (**5A-089**)

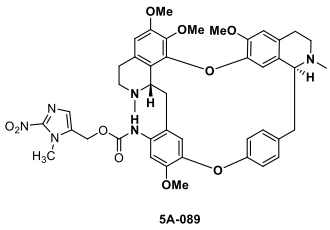

5A-089

According to the method **5A-088**, to give the compound C_{14}- (1-methyl-2-nitro-1*H*-imidazol-5-yl) methyl carbamate-tetrandrine (**5A-089**) (120 mg, 60 %) as a yellow solid. **Chemical Formula:** $C_{44}H_{48}N_6O_{10}$, **Molecular weight:** 820.9000, **^{1}H-NMR** ($CDCl_3$, 500 MHz) ppm δ 12.30 (br, 1H, -CONH-), 7.60 (s, 1H), 7.30 (dd, J = 2.4, 8.4 Hz, 1H), 7.27(s, 1H), 7.20 (dd, J = 2.4, 8.4 Hz, 1H), 7.07(s, 1H), 6.57 (dd, J = 2.5, 8.4 Hz, 1H), 6.13 (dd, J = 2.5, 8.4 Hz, 1H), 5.89 (s, 1H), 4.69 (s, 3H), 4.10 (s, 3H), 4.05 (m, 4H), 3.94 (s, 3H), 3.89 (d, J = 9.5 Hz, 1H), 3.84 (dd, J = 5.4, 11.0 Hz, 1H), 3.73 (s, 3H), 3.36 (s, 3H), 3.32-3.26 (m, 1H), 3.10 (s, 3H), 2.99-2.71 (m, 7H), 2.61 (s, 3H), 2.42 (s, 3H). **^{13}C-NMR** ($CDCl_3$, 125 MHz) ppm δ 156.50, 153.88, 152.54, 149.57, 149.20, 148.86, 146.51, 145.23, 144.60, 138.54, 137.11, 133.70, 133.28, 132.58, 130.09, 129.67, 127.81, 127.56, 125.12, 121.59, 121.51, 121.41, 121.22, 112.65, 106.28, 105.51, 64.61, 61.48, 60.51, 56.68, 56.14, 55.96, 55.44, 54.87, 45.30, 43.09, 42.59, 40.86, 40.15, 38.99, 34.80, 34.77, 24.91, 20.97. **HRMS** (APCI$^+$): calculated for $C_{44}H_{49}N_6O_{10}$ $[M+H]^+$: 821.3510, found: 821.3505.

C_{14}- 4-(diethylamino) phenyl) diazenyl) benzyl carbamate-tetrandrine (**5A-090**)

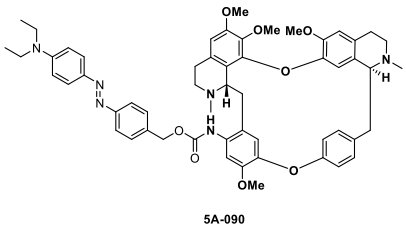

5A-090

According to the method **5A-088**, to give the compound C_{14}- 4-(diethylamino) phenyl) diazenyl) benzyl carbamate-tetrandrine (**5A-090**) (128 mg, 43 %) as a red solid. **Chemical Formula:** $C_{56}H_{62}N_6O_8$, **Molecular weight:** 947.1460, **^{1}H-NMR** ($CDCl_3$, 500 MHz) ppm δ 12.23 (br, 1H, -CONH-), 7.89-7.84 (m, 4H), 7.73 (s, 1H), 7.51 (d, J = 8.4 Hz, 2H), 7.30 (dd, J = 2.4, 8.4 Hz, 1H), 7.26(s, 1H), 7.20 (dd, J = 2.4, 8.4 Hz, 1H), 6.73 (d, J = 8.4 Hz, 2H), 6.61 (dd, J = 2.5, 8.4 Hz, 1H), 6.50 (s, 1H), 6.47 (s, 1H), 6.29 (s, 1H), 6.13 (dd, J = 2.5, 8.4 Hz, 1H), 5.89 (s, 1H), 5.26 (s, 2H),3.99-3.90 (m, 4H), 3.84-3.79 (m, 1H), 3.74 (s, 3H), 3.59-3.50 (m, 1H), 3.46 (q, J = 7.3, 14.5 Hz, 4H), 3.36 (s, 3H), 3.29-3.24 (m, 1H), 3.10 (s, 3H), 3.05-2.98 (s, 1H), 2.96-2.85 (m, 4H), 2.80-2.67 (m, 2H), 2.61 (s, 3H), 2.42 (s, 3H), 2.35 (m, 1H), 1.24 (t, J = 7.1 Hz, 6H); **^{13}C-NMR** ($CDCl_3$, 125 MHz) ppm δ 155.04, 153.35, 152.43, 150.62, 149.67, 149.10, 144.57, 143.50, 138.49, 134.47, 133.25, 130.01, 128.65, 125.76, 123.42, 122.61, 121.67, 121.45, 121.22, 112.68, 111.38, 106.24, 105.57, 64.67, 62.54, 60.51, 56.61, 56.14, 55.97, 52.34, 45.42, 45.13, 42.96, 42.74, 40.85, 40.31, 39.39, 25.05, 21.04, 14.62, 13.09. **HRMS** (APCI$^+$): calculated for $C_{56}H_{63}N_6O_8$ $[M+H]^+$: 947.4707, found: 947.4702.

Part B

Synthesis of (4-(3-(4-substitute phenyl) triaz-2-en-1-yl) phenyl) methanol (**5B-004**)

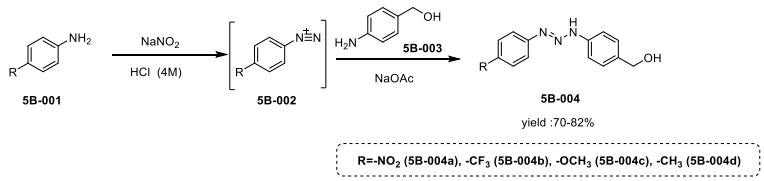

To a solution of 4-nitroaniline (500 mg, 3.62 mmol) dissolved in HCl (4M) was cooled 0 °C. After adding 2 g of crushed ice into it, and sodium nitrite in 2 mL cooled water was added dropwise for 3 min. keeping 0 °C for stirring 20 min. After (4-aminophenyl) methanol (445 mg, 3.62 mmol) was added into the reaction with constant stirring at 0 °C 5 min. Then sodium acetate (1.0 g, 12.67 mmol) in the cold water was added drop wise with constant stirring. The yellow precipitate begins to form immediately. After was stirring 1h, the precipitate was filtered and recrystallized (petroleum ether / ethyl acetate v/v 1/1) to give the compound (4-(3-(4-nitrophenyl) triaz-2-en-1-yl) phenyl) methanol **5B-004a** as a yellow solid (766 mg, 78 %). **Chemical Formula:** $C_{13}H_{12}N_4O_3$, **Molecular weight:** 272.2640, **^{1}H-NMR** (300MHz, DMSO-d_6): ppm δ 12.73 (br, 1H, -N=N-NH-), 8.54-8.32 (m, 8H), 5.23 (s, 1H), 4.49 (d, J= 6.0 Hz, 2H).**^{13}C-NMR** (75MHz, DMSO-d_6): ppm δ 154.29, 148.56, 128.78, 121.75, 65.01. **HRMS** (APCI$^+$): calculated for $C_{13}H_{13}N_4O_3$ $[M+H]^+$: 273.0988, found: 273.0985.

(4-(3-(4-(trifluoromethyl) phenyl) triaz-2-en-1-yl) phenyl) methanol (**5B-004b**)

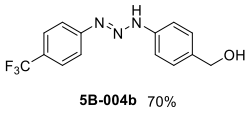

5B-004b 70%

According to the method **5B-004a**, to give the compound (4-(3-(4-(trifluoromethyl) phenyl) triaz-2-en-1-yl) phenyl) methanol (**5B-004b**) (128 mg, 70 %) as a yellow solid. **Chemical Formula:** $C_{14}H_{12}F_3N_3O$, **Molecular weight:** 295.2652, **^{1}H-NMR** (300MHz, DMSO-d_6): ppm δ 12.69 (br, 1H, -N=N-NH-), 7.71-7.31 (m, 8H), 5.28 (s, 1H), 4.52 (d, J= 6.0 Hz, 2H).**^{13}C-NMR** (75MHz, DMSO-d_6): ppm δ 127.74, 127.10, 121.24, 114.32, 63.03. **HRMS** (APCI$^+$): calculated for $C_{14}H_{13}F_3N_3O$ $[M+H]^+$: 296.1011, found: 296.1009.

(4-(3-(4-methoxyphenyl)triaz-2-en-1-yl)phenyl)methanol (**5B-004c**)

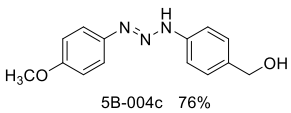

5B-004c 76%

According to the method **5B-004a**, to give the compound (4-(3-(4-methoxyphenyl)triaz-2-en-1-yl)phenyl)methanol (**5B-004c**) (146 mg, 76 %) as a yellow solid. **Chemical Formula:** $C_{14}H_{15}N_3O_2$, **Molecular weight:** 257.2930, **^{1}H-NMR** (300MHz, DMSO-d_6): ppm δ 12.77 (br,

1H, -N=N-NH-), 7.92-7.37 (m, 8H), 5.25 (s, 1H), 4.53 (d, *J*= 6.0 Hz, 2H), 3.85 (s, 3H). **^{13}C-NMR** (75MHz, DMSO-d_6): ppm δ 128.13, 114.94, 63.12, 55.78. **HRMS** (APCI$^+$): calculated for $C_{14}H_{16}N_3O_2$ $[M+H]^+$: 258.1243, found: 258.1247.

(4-(3-(*p*-tolyl)triaz-2-en-1-yl) phenyl) methanol (**5B-004d**)

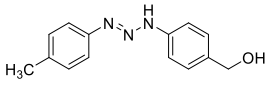

5B-004d 82%

According to the method **5B-004a**, to give the compound (4-(3-(*p*-tolyl)triaz-2-en-1-yl) phenyl) methanol (**5B-004d**) (184 mg, 82 %) as a yellow solid. **Chemical Formula:** $C_{14}H_{15}N_3O$, **Molecular weight:** 241.2940, **^{1}H-NMR** (300MHz, DMSO-d_6): ppm δ 12.75 (br, 1H, -N=N-NH-), 7.79-7.37 (m, 8H), 5.24 (s, 1H), 4.53 (d, *J*= 6.0 Hz, 2H), 2.43 (s, 3H).**^{13}C-NMR** (75MHz, DMSO-d_6): ppm δ 147.13, 121.94, 63.00, 63.12, 23.46. **HRMS** (APCI$^+$): calculated for $C_{14}H_{16}N_3O$ $[M+H]^+$: 242.1293, found: 242.1297.

Synthesis of 4-methyl-7-(3-(4-(trifluoromethyl) phenyl) triaz-2-en-1-yl)-2*H*-chromen-2-one (**5B-013**)

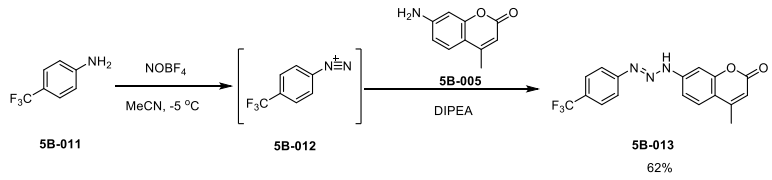

5B-011 5B-012 5B-005 DIPEA 5B-013 62%

To a solution of 4-(trifluoromethyl) aniline **5B-011** (0.3 mL, 2.38 mmol) dissolved in anhydrous acetonitrile under argon was cooled -5 °C. The nitrosonium tetrafluoroborate (556 mg, 4.77 mmol) was added to the reaction, and keeping stirred for 1h at -5 °C to formation of the diazonium salt. It was then added dropwise to another solution of ether, water, and Et_3N (0.6 mL) and 7-amino-4-methyl-chromen-2-one (626 mg, 3.57 mmol) at 0ºC. The mixture was stirred for 30 min followed by the subsequent extraction with ethyl acetate. The organic layer was dried anhydrous $MgSO_4$ and concentration of the organic layer in vacuum gives the yellow solid. The solid was purified by silica gel column chromatography (petroleum ether / ethyl acetate v/v 1/1) to give the compound 4-methyl-7-(3-(4-(trifluoromethyl)phenyl)triaz-2-en-1-yl)-2*H*-chromen-2-one **5B-013** as a yellow solid (512 mg, 62 %). **Chemical Formula:** $C_{17}H_{12}F_3N_3O_2$, **Molecular weight:** 347.2972, **^{1}H-NMR** (300MHz, DMSO-d_6): ppm δ 13.13 (br, 1H, -N=N-NH-), 7.87-7.28 (m, 7H), 6.42-6.22 (m, 1H), 2.43 (s, 3H). **^{13}C-NMR** (75MHz, DMSO-d_6): ppm δ 164.58, 153.46, 153.16, 127.54, 120.06, 117.38, 113.36, 106.43, 19.35.

Synthesis of 4-methyl-7-(morpholinodiazenyl)-2*H*-chromen-2-one (**5B-016**)

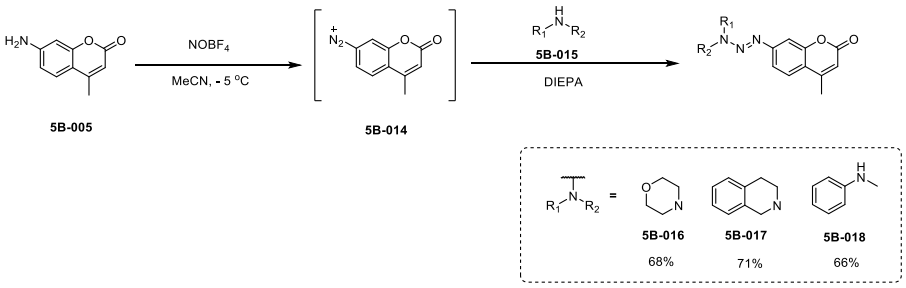

To a solution of 7-amino-4-methyl-coumarin **5B-005** (150 mg, 0.86 mmol) dissolved in anhydrous acetonitrile under argon was cooled -5 °C. The nitrosonium tetrafluoroborate (200 mg, 1.71 mmol) was added to the reaction, and keeping stirred for 1h at -5 °C to formation of the diazonium salt. It was then added dropwise to another solution of ether, water, and Et_3N (0.3 mL) and morpholine (0.3 mL, 3.42 mmol) at 0ºC. The mixture was stirred for 30 min followed by the subsequent extraction with ethyl acetate. The organic layer was dried anhydrous $MgSO_4$ and concentration of the organic layer in vacuum gives the yellow solid. The solid was purified by silica gel column chromatography (petroleum ether / ethyl acetate v/v 1/1) to give the compound 4-methyl-7-(morpholinodiazenyl)-2*H*-chromen-2-one **5B-016** as a yellow solid (160 mg, 68 %). **Chemical Formula:** $C_{14}H_{15}N_3O_3$, **Molecular weight:** 273.2920, **^{1}H-NMR** (300MHz, DMSO-d_6): ppm δ 7.76 (d, J= 9.0 Hz, 1H), 7.39 (dd, J= 3.0, 9.0 Hz, 1H), 7.28 (d, J= 3.0 Hz, 1H), 6.32-6.31 (m, 1H), 3.88-3.74 (m, 8H), 2.43 (d, J= 3.0 Hz, 3H).**^{13}C-NMR** (75MHz, DMSO-d_6): ppm δ 160.61, 154.51, 153.70, 153.40, 126.66, 117.89, 117.51, 113.49, 107.54, 18.71. **HRMS** (ESI^+): calculated for $C_{14}H_{16}N_3O_3$ $[M+H]^+$: 274.1192, found: 274.1186.

7-((3,4-dihydroisoquinolin-2(1*H*)-yl)diazenyl)-4-methyl-2*H*-chromen-2-one (**5B-017**)

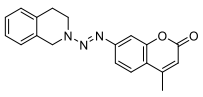
5B-017

According to the method **5B-016**, to give the compound 7-((3,4-dihydroisoquinolin-2(1*H*)-yl)diazenyl)-4-methyl-2*H*-chromen-2-one (**5B-017**) (260 mg, 71 %) as a yellow solid. **Chemical Formula:** $C_{19}H_{17}N_3O_2$, **Molecular weight:** 319.3640, **^{1}H-NMR** (300MHz, $CDCl_3$): ppm δ 7.55 (d, J= 9.0 Hz, 1H), 7.45-7.40 (m, 2H), 7.27-7.21 (m, 4H), 6.20 (s, 1H), 5.02 (s, 2H), 4.17 (s, 2H), 3.10 (t, J= 6.0 Hz, 2H), 2.43 (s, 3H).**^{13}C-NMR** (75MHz, $CDCl_3$): ppm δ 161.47, 154.56, 153.94, 152.42, 126.90, 124.93, 117.38, 113.36, 108.02, 26.92, 18.71. **HRMS** (ESI^+): calculated for $C_{19}H_{18}N_3O_2$ $[M+H]^+$: 320.1399, found: 320.1394.

4-methyl-7-(3-methyl-3-phenyltriaz-1-en-1-yl)-2*H*-chromen-2-one (**5B-018**)

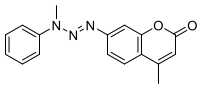

5B-018

According to the method **5B-016**, to give the compound 4-methyl-7-(3-methyl-3-phenyltriaz-1-en-1-yl)-2*H*-chromen-2-one (**5B-018**) (220 mg, 66 %) as a yellow solid. **Chemical Formula:** $C_{17}H_{15}N_3O_2$, **Molecular weight:** 294.3340, **^{1}H-NMR** (300MHz, DMSO-d_6): ppm δ 7.79 (d, J= 9.0 Hz, 1H), 7.63-7.58 (m, 2H), 7.53 (dd, J= 3.0, 9.0 Hz, 1H), 7.49-7.43 (m, 3H), 7.27-7.19 (m, 1H), 6.34-6.33 (m, 1H), 3.68 (s, 3H), 2.43 (s, 3H).**^{13}C-NMR** (75MHz, DMSO-d_6): ppm δ 161.11, 153.61, 150.75, 144.23, 128.45, 125.87, 119.82, 117.93, 113.56, 106.97, 36.95, 19.63. **HRMS** (ESI^+): calculated for $C_{17}H_{16}N_3O_2$ $[M+H]^+$: 294.1243, found: 294.1237.

Synthesis of ethyl 2-(2-((2,6-dichloro-4-nitrophenyl) amino)-5-nitrophenyl) acetate (**5B-021**)

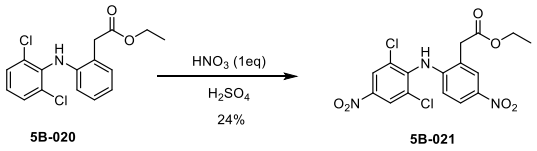

5B-020 5B-021

To a solution of ethyl 2-(2-((2,6-dichlorophenyl)amino)phenyl)acetate **5B-020** (1.0 g, 3.08 mol) dissolved in concentrated sulfuric acid at the 0 °C. The nitric acid (190 µL, 3.08 mol) is diluted in 2 ml of concentrated sulphuric acid and then slowly added dropwise to the reaction solution for approximately 7 minutes, and then keeping at 0 °C. TLC reveals that the reaction was complete after around 30 minutes. The reaction solution was progressively poured dropwise to a beaker containing ice cubes, and an off-white solid gradually precipitated, giving a crude product ethyl 2-(2-((2,6-dichloro-4-nitrophenyl)amino)-5-nitrophenyl)acetate. The solid was purified by silica gel column chromatography (petroleum ether/ ethyl acetate v/v = 5/1) to give the compound ethyl 2-(2-((2,6-dichloro-4-nitrophenyl) amino)-5-nitrophenyl) acetate **5B-021** as a white solid (336 mg, 24 %). **Chemical Formula:** $C_{16}H_{13}Cl_2N_3O_6$, **Molecular weight:** 414.1950, **^{1}H-NMR** (300MHz, $CDCl_3$): ppm δ 8.99 (s, 1H), 8.77 (s, 1H), 8.39 (s, 1H), 8.23 (s, 2H), 4.23 (q, J= 9.0, 12.0 Hz, 2H), 3.82 (s, 2H), 1.31 (t, J= 6.0 Hz, 3H). **^{13}C-NMR** (75MHz, $CDCl_3$): ppm δ 170.67, 143.02, 142.10, 141.16, 140.59, 131.34, 130.30, 127.09, 124.77, 121.15, 62.84, 39.16, 14.19.

Synthesis of 5-amino-1-(2,6-dichlorophenyl) indolin-2-one (**5B-025**)

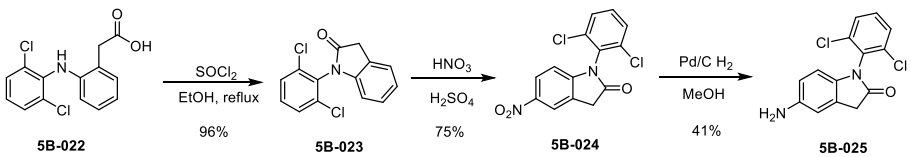

5B-022 5B-023 5B-024 5B-025

To a solution of diclofenac **5B-022** (1.0 g, 3.38 mol) dissolved in EtOH was treated dropwise thionyl chloride (250 µL, 3.38 mmol), the mixture was heated at reflux for overnight. The mixture was cooled, concentrated under reduced pressure and diluted with water. The aqueous layer was extracted with ethyl acetate, and the combined organic extract was washed with brine, dried over $MgSO_4$ followed by concentrated under reduced pressure to afford crude compound as a yellow solid. The solid was purified by silica gel column chromatography (petroleum ether/ ethyl acetate *v*/*v* = 10/1) to give the compound 1-(2,6-dichlorophenyl) indolin-2-one **5B-023** as a white solid (900 mg, 96 %). **Chemical Formula:** $C_{14}H_9Cl_2NO$, **Molecular weight:** 278.1320, **^{1}H-NMR** (300MHz, $CDCl_3$): ppm δ 7.53-7.50 (m, 2H), 7.40-7.33 (m, 2H), 7.24-7.18 (m, 1H), 7.12-7.07 (m, 1H), 6.41 (d, *J*= 9.0 Hz, 1H), 3.78 (s, 2H).

To a solution of 1-(2,6-dichlorophenyl) indolin-2-one **5B-023** (1.0 g, 3.60 mol) dissolved in concentrated sulfuric acid at the 0 °C. The nitric acid (210 µL, 3.60 mol) is diluted in 2 ml of concentrated sulphuric acid and then slowly added dropwise to the reaction solution for approximately 7 minutes, and then keeping at 0 °C. TLC reveals that the reaction was complete after around 30 minutes. The reaction solution was progressively poured dropwise to a beaker containing ice cubes, and an off-white solid gradually precipitated, giving a crude compound. The solid was purified by silica gel column chromatography (petroleum ether/ ethyl acetate v/v = 5/1) to give the compound 1-(2,6-dichlorophenyl)-5-nitroindolin-2-one **5B-024** as a yellow solid (870 mg, 75 %). **Chemical Formula:** $C_{14}H_8Cl_2N_2O_3$, **Molecular weight:** 323.1290, **^{1}H-NMR** (300MHz, DMSO-d_6): ppm δ 8.41 (d, *J*= 9.0 Hz, 1H), 8.33-8.31 (m, 1H), 8.20 (dd, *J*= 3.0, 9.0 Hz, 1H), 8.10 (d, *J*= 9.0 Hz, 1H), 6.95 (d, *J*= 9.0 Hz, 1H), 4.17 (s, 2H).**^{13}C-NMR** (75MHz, DMSO-d_6): ppm δ 173.81, 148.78, 143.69, 134.65, 133.02, 130.03, 129.34, 126.44, 125.52, 121.23, 109.31, 35.43.

To a solution of 1-(2,6-dichlorophenyl)-5-nitroindolin-2-one **5B-024** (500 mg, 1.55 mol) dissolved in methanol and the palladium on activated charcoal (10%, 164 mg, 0.15 mmol) was added in the reaction. Subsequently the flask was charged with hydrogen gas and the black suspension was stirred at room temperature for overnight. After the reaction was completed, and concentrated under reduced pressure. The residue was purified by silica gel column chromatography (CH_2Cl_2/methanol v/v 50/1) to give the compound 5-amino-1-(2,6-dichlorophenyl)indolin-2-one **5B-025** as a white solid (186 mg, 41 %). **Chemical Formula:** $C_{14}H_{10}Cl_2N_2O$, **Molecular weight:** 293.1470, **^{1}H-NMR** (300MHz, DMSO-d_6): ppm δ 7.72 (d, *J*= 6.0 Hz, 2H), 7.59-7.54 (m, 1H), 6.54 (d, *J*= 3.0 Hz, 1H), 6.38 (dd, *J*=3.0, 9.0 Hz, 2H), 6.05 (d, *J*= 9.0 Hz, 1H), 4.85 (s, 2H), 3.70 (s, 2H).**^{13}C-NMR** (75MHz, DMSO-d_6): ppm δ 173.97, 144.14, 132.34, 132.26, 131.43, 131.33, 131.01, 130.08, 129.91, 129.27, 127.13, 126.60, 122.95, 120.22, 109.73, 35.85.

Synthesis of 2,6-dichloro-3-nitroaniline (**5B-036**)

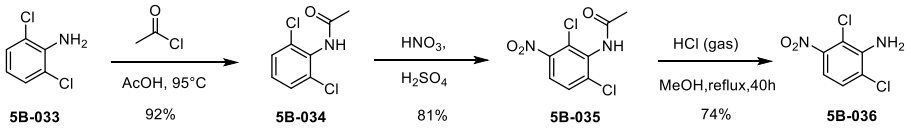

To a solution of 2,6-dichloroaniline **5B-033** (2.0 g, 12.34 mmol) dissolved in glacial acetic acid and the acetyl chloride (1.30 mL, 18.52 mmol) was added dropwise in the reaction. The mixture was heated at 90 °C for 30 min. The mixture was cooled, and the solution is poured into ice water, forming a white precipitate. The solids are filtered, washed with water and dried to give the compound *N*-(2,6-dichlorophenyl) acetamide **5B-034** as a white solid (2.3 g, 92 %). To a solution of *N*-(2,6-dichlorophenyl) acetamide **5B-034** (1.0 g, 4.90 mmol) dissolved in concentrated sulfuric acid at the 0 °C. The nitric acid (510 µL, 7.35 mmol) is diluted in 2 ml of concentrated sulphuric acid and then slowly added dropwise to the reaction solution for approximately 7 minutes, and then keeping at 0 °C. TLC reveals that the reaction was complete after around 30 minutes. The reaction solution was progressively poured dropwise to a beaker containing ice cubes, and an off-white solid gradually precipitated, giving a crude compound. The solid was purified by silica gel column chromatography (petroleum ether/ ethyl acetate v/v = 5/1) to give the compound *N*-(2,6-dichloro-3-nitrophenyl) acetamide **5B-035** as a yellow solid (988 mg, 81 %). **Chemical Formula:** $C_8H_6Cl_2N_2O_3$, **Molecular weight:** 249.0470, **^{1}H-NMR** (300MHz, DMSO-d_6): ppm δ 10.18 (s, 1H), 8.06 (d, J= 9.0 Hz, 1H), 7.84 (d, J= 9.0 Hz, 1H), 2.12 (s, 3H). **^{13}C-NMR** (75MHz, DMSO-d_6): ppm δ 169.27, 147.90, 129.46, 126.49, 124.74, 22.75.

To a solution of *N*-(2,6-dichloro-3-nitrophenyl) acetamide **5B-035** (3.0 g, 12.05 mmol) dissolved in 1,4-dioxane, the hydrogen chloride gas is passed into the reaction solution until it is saturated, and the tail gas is absorbed by sodium hydroxide. The resulting mixture was stirred for 48 h at 100 °C. The resulting mixture was concentrated under reduced pressure. The crude product was purified by silica gel column chromatography (petroleum ether/ ethyl acetate v/v = 3/1) to give the compound 2,6-dichloro-3-nitroaniline **5B-036** as a yellow solid (1.8 g, 74 %). **Chemical Formula:** $C_6H_4Cl_2N_2O_2$, **Molecular weight:** 207.0100, **^{1}H-NMR** (300MHz, DMSO-d_6): ppm δ 7.48 (d, J= 9.0 Hz, 1H), 7.19 (d, J= 9.0 Hz, 1H), 6.26 (s, 2H). **^{13}C-NMR** (75MHz, DMSO-d_6): ppm δ 148.25, 143.56, 128.61, 121.66, 111.80, 109.14.